Imperial College London

Department of Medicine

National Heart and Lung Institute

Role of KLF6 in endothelial pathology in pulmonary arterial hypertension

Thesis submitted in partial fulfilment of the requirements for the degree of Doctor of Philosophy in Clinical Medicine Research

By

Rehab Jameel Alharbi

2024

Declaration of Originality

I, Rehab Jameel Alharbi, declare that this thesis is my own work and has not been submitted in any form for another degree or diploma at any university or other institution of tertiary education. Information derived from the published or unpublished work of others has been acknowledged in the text and a list of references is given.

Rehab Jameel Alharbi

March 2024

Copyright Declaration

Acknowledgements

 , all praise is due to ALLAH S.W.T, the Most Beneficent and the Most Merciful, for his blessings upon me, and for helping me to carry on the research work even in times of stress and trouble.

First and foremost, my deepest gratitude goes to my primary supervisor, Professor Beata Wojciak-Stothard, for her invaluable advice, unprecedented support, constant guidance and encouragement throughout my PhD thesis. I would also like to express my gratitude to my co-supervisor, Dr Inês Cebola, for her guidance and support. Thanks also goes to Dr Graeme Birdsey and Dr Chris Rhodes for their constructive feedback and suggestions during my early and late-stage assessments.

Special thanks are also extended to all the former and current members of my group: Dr Adam Fellows, Salina Nicoleau, Maike Haensel, Thomas Coull, Venus Leung, Lucas Breuil, Katie Quigley, Aeman Ansari, Dr Régis Joulia, Dr Vanessa Ho, Dr Mai Alzaydi and Dr Alexander Ainscough.

To Eleni: How could I have done this without you? There are no words that can truly express how much your support has meant to me for the last three years. I could not be more grateful to have you as my friend.

A special acknowledgment goes to all the other members of the PH group: Dr Chien-Nien Chen, Chongyang Xie, Iyobel Kibreab, Dr Shanshan Song, Dr Ali Ashek, Dr Marili Niglas, Dr Farah Sabrin, Dr Merve Keles, Dr Chris Rhodes, Professor Lan Zhao, Professor Allan Lawrie and Professor Martin Wilkins.

My thanks also go to the Department of Medicine, NHLI and the faculty and its staff members, as well as all the colleagues who make our department an excellent research environment. Especially Charis Pericleous, for your help with the technical issues of the Quantstudio system, Daniela Pirri, for being my gym buddy, Dana Al-Ansari, for your enjoyable company and Noelle Pisacano for sharing your writing tips.

I am grateful to all the friends I met at Imperial College: Rean Mohammed, Jomana Khawandanah, Awatif Abdulmogith, Liliane Eleid, Lamia Aboelnasr, Deema Alassaf and Najd Aljadeed, who made my PhD life as enjoyable as possible.

A big thank you also goes to Steve Rothery from the FILM imaging facility for his assistance with ImageJ/FIJI macros and confocal microscopy.

I would like to gratefully acknowledge the University of Hafr Al Batin for funding this project and giving me the opportunity to pursue my PhD. Also, my sincere thanks go to the Ministry of Education and the Saudi Cultural Bureau in London for their support and assistance.

I would like to express my deepest gratitude to my ever-supportive friends, Eatedal and Fadiah. Your understanding and willingness to listen will never be forgotten. Thank you for being my sunshine – even on rainy days. Having you by my side has made this journey a truly remarkable one! I must also extend my thanks to Afrah; I cannot thank you enough for creating such unforgettable memories in London, and for exploring new places and trying new adventures. It was a time that I will always treasure.

Special thanks to Ghada Esheba, Professor of pathology at Umm al-Qura University, for her immeasurable advice and support throughout these years.

Finally, and most importantly, I am grateful beyond words to my dearest parents, Jameel and Mariam, and to all my brothers and sisters. Even though we were thousands of miles apart, without your comforting voices, your ongoing prayers and your constant support, completing my PhD would have remained a distant dream. I am incredibly grateful for your role in my success.

I am also grateful that I didn't have to travel this journey alone. I am particularly grateful to my sister Haneen, who currently pursuing her PhD at the University of Manchester, for being a constant source of support and a reminder of home. Special thanks to your wonderful sons, Mohammed and Ahmed, for being a source of comfort and joy on this journey.

Last but not least, I owe much to my constant silent friend, my laptop, for its reliability and performance during the countless hours through days and nights dedicated to data analysis and writing.

Dedication

I dedicate this PhD thesis to my beloved parents, and to my brothers and sisters. Your endless support and encouragement have been a constant source of strength that raised me up during my PhD journey.

Abstract

Background: Loss of endothelial homeostasis is a key contributor to vascular remodelling in PAH. PAH shares many characteristics with cancer, including increased cell proliferation and apoptosis resistance. Accumulating evidence suggests that Krüppel-like factor 6 (KLF6), a transcription factor implicated in the progression of cancer, may play a contributory role.

Hypothesis: Dysregulation of KLF6 signalling contributes to endothelial dysfunction in PAH.

Aims: (1) To study KLF6 expression in PAH; (2) To characterise KLF6 effects on endothelial transcriptome and function; (3) To compare KLF6 with KLF2 and KLF4, two closely related transcription factors that are implicated in PAH.

Methods: KLF6 expression was measured by qPCR in the lung tissues of hypoxic mice and MCT rats, ECFCs from PAH patients, and HPAECs exposed to hypoxia or TNF-α. Changes in the transcriptomic profile of KLF6-overexpressing HPAEC as well as lung tissues from patients with severe PAH were investigated. Changes in the transcriptional responses of HPAECs overexpressing KLF6 were compared with HPAECs overexpressing KLF2 or KLF4.

Results: *KLF6* expression was increased by hypoxic and inflammatory triggers in early preclinical PAH. *KLF6* expression in HPAECs was upregulated under the "double hit" condition of hypoxia combined with TNF-α, while the expression of *KLF2* and *KLF4* were reduced. RNA-seq analysis showed that KLF6 unlike KLF2 and KLF4, activates pro-angiogenic signalling and increases the expression of genes that regulate endothelial identity and survival, including *BMPR2*, *SOX17* and *ENG*. Spatial transcriptomic analysis revealed an increase in the expression of KLF6-regulated genes in the remodelled vessels. *KLF6* was upregulated in PAH ECFCs, and an accumulation of $KLF6^+$ ERG^+ vWF^+ cells was observed in plexiform lesions in human PAH.

Conclusion: KLF6 uniquely orchestrates endothelial repair, but its sustained activation in selected subsets of ECs in advanced PAH suggests its potential involvement in the exaggerated repair processes seen in human PAH.

Graphical abstract

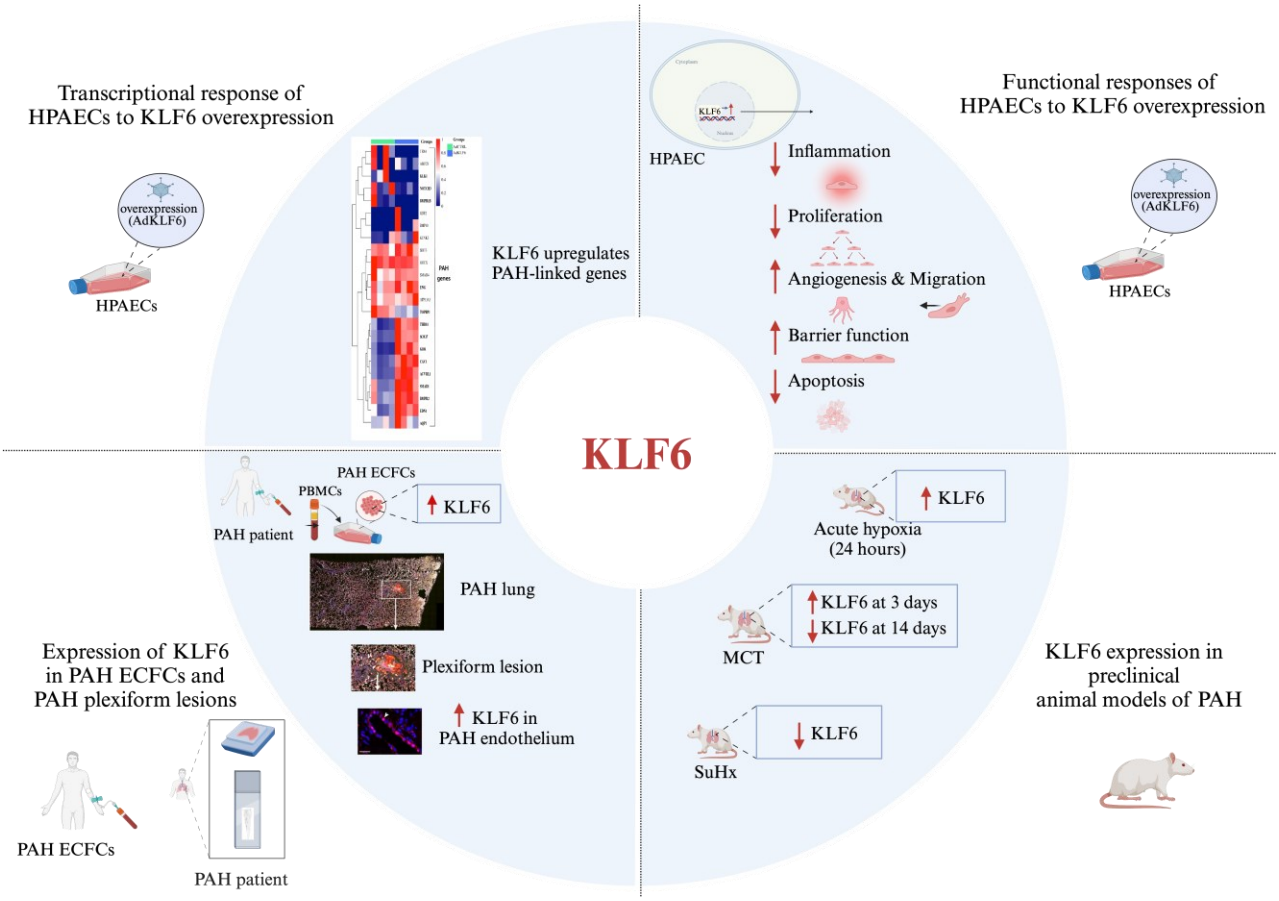

Figure 0.1 : Thesis graphical abstract.

Table of Contents

List of Figures

List of Tables

List of Abbreviations

5-HT	Serotonin/5-Hydroxytryptamine
5-LO	5-Lipoxygenase
ACTB	Actin Beta
Ad	Adenoviral
ALK1	Activin Receptor-Like Kinase 1
AMPK	AMP-Activated Protein Kinase
Ang II	Angiotensin II
ATP	Adenosine 5'-Triphosphate
B2M	Beta-2 Microglobulin
BCR	B Cell Receptor
BMP9	Bone Morphogenetic Protein 9
BMPR2	Bone morphogenetic protein receptor 2
BNIP3	Bcl 2/adenovirus E1B 19 kDa Interacting Protein 3
BOECs	Blood Outgrowth Endothelial Cells
BTSCs	Brain Tumour Stem Cells
cAMP	Cyclic Adenosine Monophosphate
CAV1	Caveolin-1
CBDL	Common Bile Duct Ligation
ccRCC	Clear Cell Renal Cell Carcinoma
cDNA	Complementary DNA
cGMP	Cyclic Guanosine Monophosphate
CLIC4	Chloride Intracellular Channel 4
CMap	Connectivity Map
COL1A1	Human Collagen Type I Alpha 1
CPBP	Core Promoter Binding Protein
DCs	Dendritic Cells
DEGs	Differentially Expressed Genes
DMSO	Dimethyl Sulfoxide
DO	Disease Ontology
ECFCs	Endothelial Colony Forming Cells
ECM	Extracellular Matrix
ECs	Endothelial Cells
EGM2	Endothelial Growth Medium 2
EndMT	Endothelial-Mesenchymal Transition
ENG	Endoglin
ENO1	Enolase 1
ERS	European Respiratory Society

ERα	Estrogen Receptors Alpha
ESC	European Society of Cardiology
ET-1	Endothelin-1
ET-1A	ET-1 Receptor A
ET-1B	ET-1 Receptor B
FAs	Focal Adhesions
FBS	Foetal Bovine Serum
FGF2	Fibroblast Growth Factor 2
FOXO	Forkhead box O
FSS	Fluid Shear Stress
FXR	Farnesoid X Receptor
GAGs	Glycosaminoglycans
GCX	Glycocalyx
GDF11	Growth Differentiation Factor 11
GFP	Green Fluorescent Protein
GO	Gene Ontology
GPCRs	G-Protein-Coupled Receptors
HA	Haemagglutinin
HDACI	Histone Deacetylase Inhibitor
HEK	Human Embryonic Kidney Cells
HIF-1α	Hypoxia-Inducible Factor 1 Alpha
HIF-1β	Hypoxia-Inducible Factor 1 Beta
HMGA1	High Mobility Group AT-hook 1
HPAECs	Human Pulmonary Artery Endothelial Cells
HPAH	Heritable PAH
HPH	Hypoxic Pulmonary Hypertension
HPS	Hepatopulmonary Syndrome
HREs	Hypoxia Response Elements
HRMECs	Human Retinal Microvascular Endothelial Cells
HRQOL	Health-Related Quality of Life
HUVECs	Human Umbilical Vein Endothelial Cells
ICAM-1	Intercellular Adhesion Molecule 1
IL-6	Interleukin 6
IPAH	Idiopathic PAH
IPF	Idiopathic Pulmonary Fibrosis
KLF2	Krüppel-Like Factor 2
KLF4	Krüppel-Like Factor 4
KLF6	Krüppel-Like Factor 6
KLFs	Krüppel-Like Factors
LDHA	Lactate Dehydrogenase A
lncRNAs	Long Non-Coding RNAs
Log_2FC	Log_2 Fold Change

LOH	Loss of Heterozygosity
LPS	Lipopolysaccharide
MCP-1	Monocyte Chemoattractant Protein-1
MCT	Monocrotaline
MEF2	Myocyte Enhancer Factor 2
miRNAs	MicroRNAs
MLECs	Mouse Lung Endothelial Cells
MMPs	Matrix Metalloproteinases
MOI	Multiplicity of Infection
mPAP	Mean Pulmonary Artery Pressure
MYH11	Myosin Heavy Chain 11
NF-κB	Nuclear Factor kappa-light-chain-enhancer of activated B cells
NFKBIA	Nuclear Factor-Kappa-B-Inhibitor Alpha
NFKBIB	Nuclear Factor-Kappa-B-Inhibitor Beta
NLS	Nuclear Localization Signal
NO	Nitric Oxide
NOS	Nitric Oxide Synthase
NSCLC	Non-Small Cell Lung Cancer
OSS	Oscillatory Shear Stress
PAECs	Pulmonary Artery Endothelial Cells
PAH	Pulmonary Arterial Hypertension
PASMCs	Pulmonary Artery Smooth Muscle Cells
PBMCs	Peripheral Blood Mononuclear Cells
PBS	Phosphate Buffered Saline
PDE5	Phosphodiesterase 5
PDK	Pyruvate Dehydrogenase Kinase
PECAM1	Platelet-Endothelial Cell Adhesion Molecule 1
PET	Polyethylene Terephthalate
PET	Polyethylene Terephthalate
PGI2	Prostaglandin I2
PGK1	Phosphoglycerate Kinase 1
PH	Pulmonary Hypertension
PHDs	Prolyl Hydroxylase Domain Proteins
PKA	Protein Kinase A
PLAU	Plasminogen Activator Urokinase
PMVEC	Pulmonary Microvascular Endothelial Cell
PTMs	Post Translational Modifications
PVR	Pulmonary Vascular Resistance
qPCR	Quantitative-PCR
RHC	Right Heart Catheterization
RNA-seq	RNA Sequencing
ROIs	Regions of Interest

ROS	Reactive Oxygen Species
RTKs	Receptor Tyrosine Kinases
RV	Right Ventricular
RVSP	Right Ventricular Systolic Pressure
scRNA-seq	Single Cell RNA Sequencing
SCs	Schwann Cells
sGC	Soluble Guanylate Cyclase
SHP	Small Heterodimer Partner
SLC2A1	Solute Carrier Family 2A1
SNP	Single Nucleotide Polymorphism
SOX17	SRY Box Transcription Factor 17
STS	Staurosporine
SuHx	Sugen/Hypoxia
TGF-β	Transforming Growth Factor Beta
TGF-βR	Transforming Growth Factor Beta Receptor
TNF-α	Tumour Necrosis Factor Alpha
VE-Cadherin	Vascular Endothelial Cadherin
VEGF	Vascular Endothelial Growth Factor
VEGFR2	Vascular Endothelial Growth Factor Receptor 2
VHL	Von Hippel-Lindau Protein
vWF	von Willebrand Factor
WHO	World Health Organization
WSPH	World Symposium on Pulmonary Hypertension
ZO-1	Zonula Occludens-1
α-SMA	Alpha-Smooth Muscle Actin

Chapter 1 : General introduction

1.1 Pulmonary vasculature: structure, function and development

The circulatory system, also known as the cardiovascular system, is composed of two main circuits, namely the systemic circulation and the pulmonary circulation. The systemic circulation is the longest of the two and distributes oxygenated blood and nutrients from the heart to the rest of the body through the aorta. The pulmonary circulation is a shorter circuit that facilitate the transport of deoxygenated blood from the heart to the lungs through the pulmonary arteries. Oxygenated blood is then circulated back to the heart from the lungs through the pulmonary veins.

Unlike the arteries in the systemic circulation, pulmonary arteries carry deoxygenated blood. The pulmonary circulation is composed of a network of arteries, veins, capillaries, and lymphatics that exchange blood and other tissue fluids between the heart and the lungs. The pulmonary circulation consists of three circuits: arterial circuit, venous circuit and lymphatic circuit (Jain, Bordes & Bhardwaj, 2023). The arterial circuit starts at the main pulmonary artery arising from the right ventricle of the heart, then divides into the left and right pulmonary arteries, and later into the network of small arteries, arterioles and finally tiny capillaries that surround the pulmonary alveoli. The venous circuit starts with venules that collect oxygenated blood from capillaries and combine to form smaller veins which then join together to deliver blood to the main pulmonary vein that carries the oxygenated blood from both lungs to the left atrium of the heart. The lymphatic circuit plays an important role in maintaining tissue fluid homeostasis by preventing the accumulation of interstitial fluid within the lung tissues. In addition to the pulmonary circulation, the bronchial circulation originates from the aorta and supplies oxygenated blood to the lung parenchyma and is made up of both superficial and deep systems. The superficial system drains into the hemiazygos and azygos veins, while the deep system drains into the pulmonary vein (Jain, Bordes & Bhardwaj, 2023; Sundjaja & Bordoni, 2023).

The walls of the pulmonary arteries are comparatively thinner and less muscular than those of similarly sized systemic arteries (Suresh & Shimoda, 2016). The arterial walls consist of three distinct layers: tunica intima, tunica media and tunica adventitia (Figure 1.1).

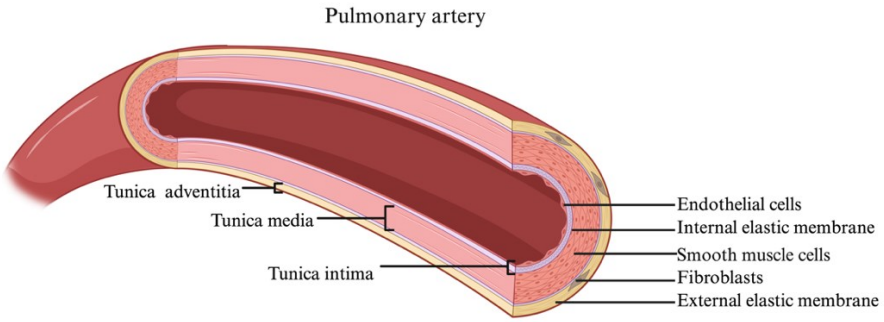

Figure 1.1: Structure of the pulmonary arterial wall.
The wall of the pulmonary artery comprises of three layers: the tunica intima, which consists of the endothelium and the internal elastic membrane; the tunica media, which consists of smooth muscle cells, and elastic fibres and the tunica externa, which consists of fibroblasts, connective tissue, and the external elastic membrane. Illustration created by the author using BioRender.com.

The tunica intima consists of a monolayer of squamous endothelial cells which is surrounded by a thin layer of connective tissue. The apical/luminal side of the vascular ECs is covered by the glycocalyx (GCX), a complex surface layer consisting of glycosaminoglycans (GAGs), glycoproteins, proteoglycans and glycolipids, as well as various growth factors such as vascular endothelial growth factor (VEGF) (Hu, Cano & D'Amore, 2021). The glycocalyx plays a crucial role in maintaining endothelial integrity and homeostasis by regulating vascular tone, permeability and mechanotransduction (Milusev, Rieben & Sorvillo, 2022). It exerts an anti-inflammatory and anti-thrombotic effect on the endothelial cell surface under healthy conditions (Hu, Cano & D'Amore, 2021). The basal/abluminal side of the endothelium is anchored to the basement membrane via multiprotein complexes known as focal adhesions (FAs), which link the intracellular cytoskeleton with the extracellular matrix (Arts et al., 2021; Legerstee et al., 2019). The ECs form a monolayer which acts as a semipermeable barrier, regulating the passage of fluids, blood cells and macromolecules through the vascular wall into the parenchymal tissue (Mironov et al., 2023). Endothelial junctional integrity and barrier function are largely regulated by adherens junction proteins such as vascular endothelial (VE)-cadherin and tight junction proteins such as occludin and zonula occludens (ZO)-1 (Claesson-Welsh, Dejana & McDonald, 2021).

The tunica media consists of concentric layers of vascular smooth muscle cells (VSMCs) and external elastic lamina. The VSMCs play a pivotal role in the blood vessel walls by providing structural support and regulating vascular tone and diameter (Chakraborty et al.,

2019). VSMCs are also key regulators of vasoconstriction, vasodilatation and extracellular matrix production (Basatemur et al., 2019) and exhibit phenotypic plasticity in response to changes in the surrounding environment as they can switch between two distinct states, known as “synthetic” and “contractile”, which are phenotypically and functionally different (Zha et al., 2020). Under normal physiological conditions, VSMCs show a contractile phenotype which is characterized by high expression levels of a variety of contractile proteins including α-smooth muscle actin (α-SMA), smooth muscle myosin heavy chain 11 (MYH11) and calponin (Cao et al., 2022). However, under pathological conditions, VSMCs switch from a differentiated “contractile” state to a de-differentiated “synthetic” state which is characterized by the reduced expression of contractile proteins and an increased production of matrix metalloproteinase (MMP) enzymes (Petsophonsakul et al., 2019).

The tunica adventitia, which is the outermost layer of the vessel wall, consists of ECM, fibroblasts, immune cells, lymphatic vessels, nerves and vasa vasorum (Tinajero & Gotlieb, 2020). Fibroblasts are critical for regulating the repair and remodelling processes following injury. They are responsible for producing ECM structural proteins (such as elastin and collagen), adhesive proteins (including laminin and fibronectin) and ground substances such as glycosaminoglycans (Kendall & Feghali-Bostwick, 2014). These proteins are crucial for maintaining the elasticity of healthy arteries. Imbalances in their relative proportions may contribute to the disease progression, as evidenced by the detection of elevated fibronectin expression in artery sections obtained from patients with pulmonary arterial hypertension (PAH) (Thenappan, Chan & Weir, 2018; Jones, Cowan & Rabinovitch, 1997).

The size and structure of blood vessels in the pulmonary vasculature vary according to their function. They are categorised as elastic, muscular, partially muscularized and non-muscularized vessels (Townsley, 2012). The large pulmonary arteries are classified as elastic arteries, and the tunica media (the middle layer) predominantly contains elastic fibres, interspersed with collagen fibres and vascular smooth muscle cells. As arterial diameter decreases, the number of elastic fibres in the tunica media also decreases, while the number of smooth muscle cells increases (Suresh & Shimoda, 2016). The smallest arteries, known as arterioles, have a single layer of smooth muscle cells which are proximal to capillaries. Capillaries are non-muscularised and consist of a single layer of endothelial cells. Changes in the structure of the pulmonary arteries and arterioles can lead to the development of PAH.

1.2 Definition and classification of pulmonary hypertension.

1.2.1 Pulmonary hypertension (PH)

Pulmonary hypertension (PH) is a severe and progressive lung disease which is associated with high morbidity and poor outcomes. It is defined as a resting mean pulmonary artery pressure (mPAP) >20 mmHg and is measured by right-heart catheterization (RHC) (Maron, 2023; Rajagopal et al., 2023; Humbert et al., 2022).

The classification of PH has been revised over the years, from the World Health Organization (WHO) symposium in 1973 to the 6th World Symposium on Pulmonary Hypertension (WSPH) in 2018 as well as the 2022 European Society of Cardiology (ESC)/European Respiratory Society (ERS) guidelines for the diagnosis and treatment of PH. PH is classified into five major groups based on pathological manifestations, haemodynamic characteristics, clinical presentations and treatment strategies. These are summarized in Table 1.1 below.

WHO Group	Clinical Group	Subgroups	Clinical Definition
1	Pulmonary Arterial Hypertension (PAH)	1.1 Idiopathic PAH 1.2 Heritable PAH 1.3 Drug- and toxin-induced PAH 1.4 PAH associated with: 1.4.1 Connective tissue disease 1.4.2 HIV infection 1.4.3 Portal hypertension 1.4.4 Congenital heart disease 1.4.5 Schistosomiasis 1.5 PAH long-term responders to CCB 1.6 PAH with overt features of PVOD/PCH 1.7 Persistent PH of the newborn	Pre-Capillary PH
2	PH due to left heart disease	2.1 PH due to heart failure with preserved LVEF 2.2 PH due to heart failure with reduced LVEF 2.3 Valvular heart disease 2.4 Congenital/acquired cardiovascular conditions leading to post-capillary PH	Post-Capillary PH
3	PH due to lung diseases and/or hypoxia	3.1 Obstructive lung disease 3.2 Restrictive lung disease 3.3 Other lung disease with mixed restrictive/obstructive pattern 3.4 Hypoxia without lung disease 3.5 Developmental lung disorders	Pre-Capillary PH

4	PH due to pulmonary artery obstructions	4.1 Chronic thromboembolic PH 4.2 Other pulmonary artery obstructions	Pre-Capillary PH
5	PH with unclear and/or multifactorial mechanisms	5.1 Haematological disorders 5.2 Systemic and metabolic disorders 5.3 Others 5.4 Complex congenital heart disease	Pre-Capillary PH Post-Capillary PH

Table 1.1: Clinical classification of pulmonary hypertension. Abbreviations: HIV, human immunodeficiency virus; CCB, calcium channel blockers; PVOD, pulmonary veno-occlusive disease; PCH, pulmonary capillary haemangiomatosis; LVEF, left ventricular ejection fraction. Adapted from (Sarah, Ashrith & Sandeep, 2021).

1.3 Pulmonary arterial hypertension (PAH)

This study focuses on PAH, which belongs to Group 1 of the five clinical subtypes of pulmonary hypertension according to World Health Organization (WHO) classification. PAH is a rare, progressive and incurable disease characterized by elevated blood pressure in the pulmonary arteries that may be either idiopathic or heritable or associated with other clinical conditions. PAH tends to occur three to five times more frequently in females than in males, with females between the ages of 30 and 60 years considered to be at the highest risk of developing PAH (Gorini et al., 2023). Early diagnosis of PAH is difficult, as its early stages can be asymptomatic or may be confused with other heart and lung conditions. Patients with early-stage PAH exhibit non-specific symptoms including dyspnoea, weakness, fatigue, chest pain and light-headedness or syncope (Kolton Schneider, Ali & Agnew, 2023). As PAH progresses, symptoms become more pronounced, with progressive right-sided heart failure that manifests as ascites, oedema and abdominal distension (Kolton Schneider, Ali & Agnew, 2023).

1.3.1 Pulmonary vascular remodelling in PAH

Pulmonary vascular remodelling is a key pathological feature of PAH, and results in the luminal narrowing of pulmonary arteries and an increased resistance to blood flow (Figure 1.2B).

The vascular remodelling involves alterations in apoptosis, angiogenesis, thrombosis, immune cell infiltration, inflammation and the phenotypic transformation of endothelial cells and smooth muscle cells, resulting in the stiffening of larger pulmonary arteries as well as

muscularization and narrowing of smaller normally non-muscular arteries due to hyperplasia of the arterial intimal and medial layers (Figure1.2C).

In severe cases of PAH, excessive proliferation, migration and apoptosis resistance, predominantly in endothelial cells, but also in smooth muscle cells, fibroblasts and inflammatory cells. This results in the formation of complex occlusive plexiform lesions (Figure1.2D) (Jia et al., 2023). These plexiform lesions are considered a histological hallmark of severe human (but not experimental) PAH. The exact initiating factors and molecular mechanisms that contribute to the formation of plexiform lesions are still unknown.

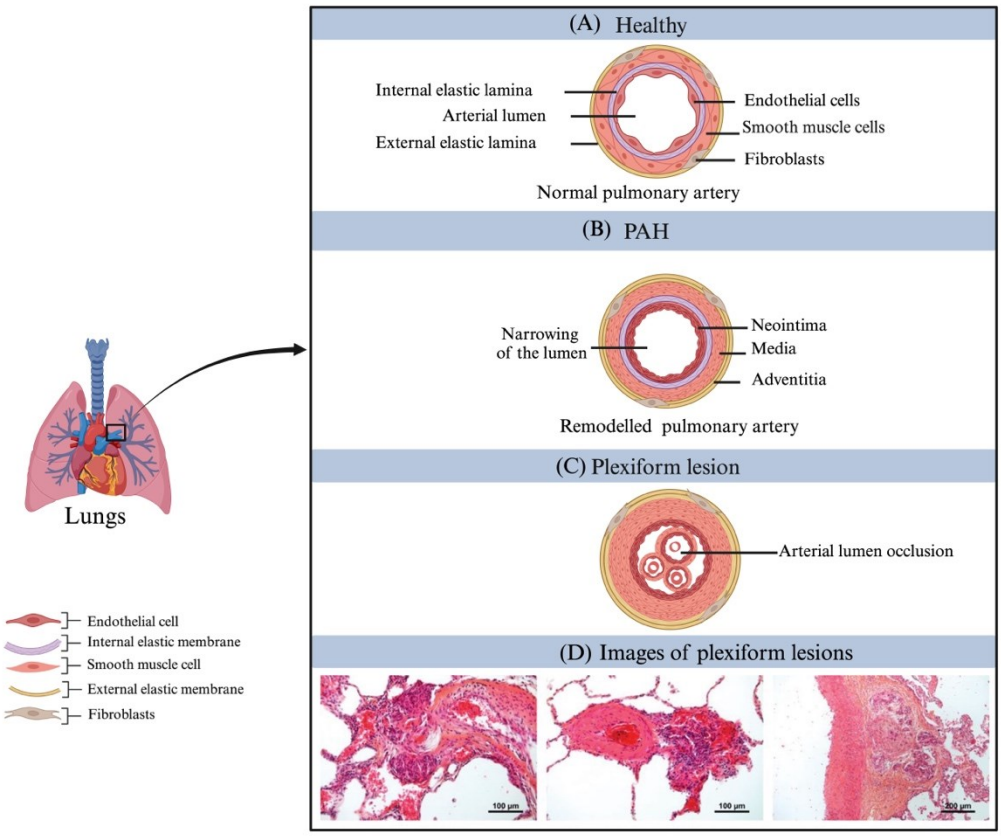

Figure 1.2: Pulmonary arterial changes in PAH.
(**A**) A normal pulmonary artery consists of three layers: the tunica intima, which is composed of endothelial cells, the tunica media, which consists of smooth muscle cells, and the tunica adventitia, which is composed of fibroblasts and connective tissue. The internal elastic lamina lies between ECs and SMCs and the external elastic lamina lies between SMCs and adventitia. (**B**) In severe PAH, the balance between vascular cell proliferation and apoptosis is disrupted, leading to hyperproliferation and resistance to apoptosis of pulmonary endothelial cells and smooth muscle cells. This causes progressive luminal narrowing and the remodelling of pulmonary arteries. (**C**) As the disease progresses, the remodelled artery becomes narrower, thicker and stiffer due to muscularisation, the thickening of the medial layer and the formation of obliterative plexiform lesions. (**D**) Representative haematoxylin and eosin (H&E) staining of plexiform lesions taken from a PAH patient. Images taken from (Humbert et al., 2019). Illustration created by the author using BioRender.com.

1.3.1.1 Intima: vascular endothelium

The intimal layer in a healthy pulmonary artery consists of a single layer of endothelial cells. Approximately 25% of patients with severe PAH exhibit a three-fold increase in intimal fractional thickness, resulting in 40-fold increase in pulmonary vascular resistance (PVR). The thickened intima is mainly composed of endothelial cells, but also contains smooth muscle cells, fibroblast-like cells, collagen, and mucin. Endothelial cells are a source of key regulators of vascular tone and vascular remodelling, including fibroblast growth factor 2 (FGF2), nitric oxide (NO), endothelin-1 (ET-1), prostaglandin I2 (PGI2), and serotonin/5-hydroxytryptamine (5-HT) (Tobal et al., 2021). Overproduction of these endothelium-derived paracrine mediators contributes to vasoconstriction and vascular remodelling (Tobal et al., 2021).

1.3.1.2 Media: vascular smooth muscle cells

The proliferation of medial vascular smooth muscle cells is the main pathological factor that contributes to vascular remodelling in PAH. Animal studies using either hypoxia or monocrotaline (MCT) models of PAH have provided insights into the course and anatomical location of PASMC proliferation (Tobal et al., 2021). In a hypoxic rat model of PAH, the onset of proliferation was observed in the hilar vessels, mainly in the intima and adventitia, with only slight changes in the medial layer (Tobal et al., 2021). Similar observations were obtained from a rat model of MCT (Tobal et al., 2021). However, a key finding was the reduction of PASMC proliferation in the hypoxic models of PAH after 4-5 weeks, indicating that active PASMC proliferation happens early in the disease. This was also observed in human tissue from patients with idiopathic PAH (IPAH) and hereditary PAH (HPAH), in which no active PASMC proliferation was observed in the end-stage PAH (Tobal et al., 2021). As noted in Section 1.3.1.1, endothelial cells are a significant contributor to PASMC proliferation. In addition to the PASMC proliferation seen in muscularised arteries and arterioles, the small pre-capillary arterioles also become muscularised in PAH. The increased muscularization of the arteriolar wall, together with neointima formation and chronic vasoconstriction, contribute to the reduction of vascular lumen and increased pulmonary vascular resistance in PAH.

1.3.1.3 Adventitia: fibroblasts

The adventitial layer is composed of various cell types, including fibroblasts, resident progenitor cells, immune modulatory cells and endothelial cells of the vasa-vasorum. Although structural changes in the adventitia have a more indirect effect on PVR rather than thickening

of the intima and media, the adventitia plays an important role in inflammatory signalling and facilitates feed-forward interactions between incoming macrophages and resident fibroblasts. The adventitial layer plays a key contributory role in vascular remodelling. Chazova *et al*. reported a 2- to 4-fold increase in adventitial thickening in the autopsies of 19 IPAH patients. In contrast, other investigators showed that the adventitial thickening in PAH is either mild or absent (Tobal et al., 2021).

1.3.1.4 Other cell types: pericytes and inflammatory cells

Pericytes are embedded in the basement membrane of microvessels such as precapillary arterioles, venules and capillaries, and closely associated with endothelial cells (Garrison et al., 2023) with a pericyte to endothelial cell ratio of between 1:7 and 1:9 (Li & Fan, 2023). Pericytes play an essential role in vascular homeostasis and remodelling, but their exact role of pericytes in pulmonary microvasculature are still not fully understood.

Ricard *et al*. demonstrated that increased pericyte coverage in distal pulmonary arteries in human PAH correlated well with arterial medial thickening induced by FGF2 and interleukin-6 (IL-6) signalling (Ricard et al., 2014). This study showed that transforming growth factor beta (TGF-β) promoted pericyte differentiation into contractile smooth muscle-like cells, thus leading to increased PVR and PAH (Ricard et al., 2014). Yuan *et al*. demonstrated that reduced pericyte-endothelial cell interaction causes pulmonary vascular remodelling, and is stimulated by pyruvate dehydrogenase kinase 4 (PDK4), which is a key regulator of mitochondrial metabolism and can influence the downstream effects of glycolysis (Yuan et al., 2016).

Vascular infiltration of inflammatory cells in PAH – including macrophages, neutrophils, mast cells, dendritic cells (DCs) and T- and B-lymphocytes – has been reported in several studies. Using flow cytometry, Marsh *et al*. showed that an increased number of activated plasmacytoid dendritic cells (pDCs), mast cells, macrophages, and gamma delta (δγ) T cells was observed in IPAH lung biopsies (Marsh et al., 2018). In IPAH patients, immature dendritic cells (DCs) accumulate in remodelled pulmonary arteries and could therefore be involved in PAH immunopathology (Perros et al., 2007). A recent study reported increased B cell receptor (BCR) signalling in circulating B cells in patients with IPAH (Heukels et al., 2021). This study also showed that a combination of pulmonary injury and increased activation of B cells is sufficient to promote PH symptoms in mice (Heukels et al., 2021). There is also a positive correlation between perivascular inflammation and intimal and medial fractional thickness,

suggesting that this inflammation may also be associated with the structural remodelling of the pulmonary vasculature (Stacher et al., 2012).

1.3.2 Disease mechanisms: contributory factors

1.3.2.1 Genetic and epigenetic factors

Dysregulation in transforming growth factor beta (TGF-β) signalling is a key contributory factor in the development of PAH (Rol et al., 2018). Mutations in bone morphogenetic protein receptor 2 (BMPR2), a member of TGF-β receptor family, have been identified in around 75% of heritable PAH (HPAH) patients (Machado et al., 2015; Soubrier et al., 2013) and between 11% and 40% of idiopathic PAH (IPAH) cases in adults (Koehler et al., 2004; Morisaki et al., 2004). These mutations also account for 50%-80% of HPAH and between 10% and 40% of IPAH cases in children (Abman et al., 2022; Haarman et al., 2020; Eyries et al., 2019; Zhu et al., 2019; Zhu et al., 2018a; Levy et al., 2016; Kerstjens-Frederikse et al., 2013). Mutations in the *BMPR2* gene are therefore considered the major genetic cause of PAH and the majority of HPAH cases. Mutations in other genes, including those from the TGF-β family of receptors and ligands, have also been found in PAH (Table 1.2).

Currently, several genes are associated with PAH with varying degrees of evidence. According to the PAH curation gene expert panel (https://clinicalgenome.org/affiliation/40071/), twelve out of 27 curated genes – including *BMPR2*, *CAV1*, *ACVRL1*, *ENG*, *KDR*, *SMAD9*, *ATP13A3*, *EIF2AK4*, *GDF2*, *KCNK3*, *TBX4* and *SOX17* – have been classified as definitive (Welch et al., 2023). There is some evidence linking *TET2*, *GGCX* and *ABCC8* with PAH, while other genes show limited evidence of their association with the disease, including *BMP10*, *PDGFD*, *FBLN2*, *KLF2*, *KLK1* and *AQP1* (Welch et al., 2023). The disputed panel of genes which show insufficient evidence includes *TOPBP1, SMAD1*, *SMAD4*, *BMPR1A, BMPR1B* and *NOTCH3* (Welch et al., 2023).

Gene symbol	Product name	References
BMPR2	BMPRII	(Deng et al., 2000; Lane et al., 2000)
SOX17	SOX17	(Gräf et al., 2018)
KLF2	KLF2	(Eichstaedt et al., 2017)
ACVRL1	ALK1	(Trembath et al., 2001)
BMPR1B	BMPR1B /ALK6	(Chida et al., 2012)
CAV1	Caveolin-1	(Austin et al., 2012)
ENG	Endoglin	(Harrison et al., 2005; Chaouat et al., 2004)
SMAD1	SMAD1	(Nasim et al., 2011)

SMAD4	SMAD4	(Nasim et al., 2011)
SMAD9	SMAD8	(Nasim et al., 2011; Shintani et al., 2009)
KDR	VEGFR2	(Eyries et al., 2020)
GDF2	BMP-9	(Wang et al., 2019a, 2016)
AQP1	Aquaporin-1	(Gräf et al., 2018)
TBX4	TBX4	(Kerstjens-Frederikse et al., 2013)
EIF2AK4	GCN2	(Best et al., 2017)
KCNK3	TASK-1	(Ma et al., 2013)
KCNA5	KCNA5	(Remillard et al., 2007)
ATP13A3	ATPase 13A3	(Gräf et al., 2018)
FIGN	Fidgetin	(Puigdevall et al., 2019)
ABCC8 (*SUR1*)	ABCC8	(Bohnen et al., 2018)
KLK1	Kallikrein-1	(Zhu et al., 2019)
GGCX	GGCX	(Zhu et al., 2019)

Table 1.2: List of genes affected by genetic variants associated with PAH.

1.3.2.2 Environmental Factors

1.3.2.2.1 Hypoxia

Oxygen (O_2) plays a crucial role in maintaining the intracellular adenosine 5'-triphosphate (ATP) levels that are required for many intracellular biochemical reactions. The oxygen levels in healthy human tissues vary between different organs (Table1.3), therefore the precise definition of hypoxia varies between different cell types. The oxygen level in the cell culture is maintained at ~21% O_2 and this differs from physiological level that the cell experiences *in vivo*. *In vitro,* most cell types are considered hypoxic at 1-5% O_2 (Wu & Yotnda, 2011).

Organ/Tissue	Physiological Oxygen (%)
Trachea	18%
Arterial blood	13%
Lungs	6%
Liver	5%
Brain	4-5%
Muscle	4%
Venous blood	5%
Pulmonary artery	1-5%

Table 1.3: Oxygen levels in various organs/tissues of the human body. Values obtained from (Gutierrez et al., 2007) for the pulmonary artery and (Carreau et al., 2011) for all other values.

Hypoxia activates hypoxia-inducible transcription factors (HIFs), which help cells to adapt to low O_2 levels by increasing the expression of genes involved in angiogenesis, cellular metabolism, proliferation and survival (Pullamsetti et al., 2020).

HIFs are heterodimeric proteins composed of an oxygen dependent α subunit (HIF-1α, HIF-2α or HIF-3α), and an oxygen independent β subunit (HIF-1β). The HIF response is regulated by prolyl hydroxylase domain proteins (PHDs), mainly PHD2, which are responsible for the regulation of HIF stability. The enzymatic activity of these enzymes requires molecular oxygen as a co-substrate.

Under normoxic conditions (physiological O_2 levels), PHD enzymes hydroxylate HIF-α subunits on proline residues, a process that leads to their ubiquitination and proteasomal degradation involving Von-Hippel-Lindau protein (VHL) (Strowitzki, Cummins & Taylor, 2019). In the absence of molecular oxygen, the hydrolytic activity of PHDs is inhibited and HIF-α remains stabilised, bypassing the ubiquitin-proteasome pathway. HIF-α then translocates into the nucleus, where it forms heterodimers with the HIF-1β subunit (Enescu et al., 2022). This heterodimeric complex then binds to hypoxia response elements (HREs) in the DNA, resulting in upregulation of hypoxia-responsive genes.

HIF-1α $^{+/-}$ mice exposed to chronic hypoxia (10% O_2 for 3 weeks) showed a delay in the onset of pulmonary vascular remodelling (Yu et al., 1999), while the inducible deletion of HIF-2α in the pulmonary endothelium protected against the development of PAH in mice exposed to chronic hypoxia (Cowburn et al., 2016). Meanwhile, mice with the inducible deletion of HIF-1α in SMCs attenuated pulmonary vascular remodelling and hypertrophy in PASMCs under chronic hypoxia (Ball et al., 2014).

The balance between proliferation and apoptosis of ECs, SMCs and fibroblasts is important in terms of maintaining the optimal thickness of the pulmonary arterial wall. Exposure to hypoxia induces HIFs which disrupt the balance between cell proliferation and apoptosis. Chronic exposure to hypoxia (>24 hours) induces the proliferation of pulmonary arterial ECs and SMCs *in vitro* and *in vivo*.

At high altitudes, the decrease in barometric pressure leads to a reduced level of O_2 in the air, which results in hypoxia (Witt & Huerta-Sánchez, 2019). People who live at high altitude have higher proximal pulmonary artery pressures and thicker medial and adventitial layers in their proximal pulmonary arteries than those who live at sea level (Sydykov et al., 2021a; Penaloza & Arias-Stella, 2007). Long term exposure to high altitude leads to the development of hypoxic pulmonary hypertension (HPH) (Sydykov et al., 2021b).

1.3.2.2.2 Shear Stress

Fluid shear stress (FSS) is the frictional force generated from blood flow, which is parallel to the blood vessel wall. It acts on the apical surface of the endothelium, and is a key regulator of endothelial function and vascular homeostasis. ECs have a variety of mechanosensors, particularly on their apical surfaces, including ion channels, integrins, receptor tyrosine kinases (RTKs) and G-protein-coupled receptors (GPCRs). These proteins can sense any change in shear stress and translate it into biochemical signals which result in alterations in EC gene expression and cell morphology, which are necessary for adapting to the flow (Davies, 2009).

Flow patterns, such as unidirectional laminar flow or disturbed flow, deferentially regulate the gene expression and functions of ECs (Chiu & Chien, 2011). High shear stress with unidirectional laminar flow is generally found in the straight and unbranched segments of the arteries, and is involved in maintaining the quiescence of ECs (Qin et al., 2010). Low shear stress with disturbed flow, which is found in the branches and curved points of the arteries, is associated with the activation of ECs, and leads to vascular inflammation and vascular remodelling (Wu et al., 2017).

ECs experiencing laminar flow are typically flattened and aligned within the direction of blood flow through the rearrangement of filamentous actin (F-actin) (Tzima et al., 2005). This cytoskeletal reorganization helps to minimise endothelial damage due to altered flow. In contrast, in the areas of disturbed flow, ECs are disorganized and poorly aligned (Hahn & Schwartz, 2009), which is correlated with increased endothelial permeability, thrombosis and leukocyte infiltration. Endothelial cell junctions have been shown to be involved in endothelial adaption to flow through the formation of a mechanosensory complex consisting of platelet-endothelial cell adhesion molecule 1 (PECAM1/CD31), VE-cadherin and vascular endothelial growth factor receptor 2 (VEGFR2). Disrupting any components of this mechanosensing complex will lead to the disruption of PECAM1/ VE-cadherin/ VEGFR2 complex and the suppression of actin cytoskeleton reorganization and cell alignment within the flow (Tzima et al., 2005).

Endothelial glycocalyx (GCX) is a thin layer with a mesh-like structure, composed of glycosaminoglycans (GAGs), glycoproteins, proteoglycans and plasma proteins that line the luminal surface of ECs (Aldecoa et al., 2020). The GCX is involved in the regulation of

vascular tone through the production of nitric oxide (NO) in response to physiological laminar flow (Mochizuki et al., 2003; Reitsma et al., 2007). Disturbed flow promotes GCX degradation leading to downregulation of NO production, resulting in a loss of vascular tone (Mitra et al., 2017). The degradation of GCX also prevents the necessary inter-endothelial communication required for vascular homeostasis (Ebong & DePaola, 2013).

1.3.2.2.3 Inflammation

Growing evidence shows that inflammation plays a crucial role in the initiation and progression of PAH (Figure 1.3). The accumulation of inflammatory cells – including dendritic cells (DCs), neutrophils, macrophages, mast cells, and lymphocytes (B and T cells) – has been found around pulmonary vessels in PAH patients and PH animals (Hu et al., 2020a). Inflammatory cell infiltrates have been observed around the remodelled pulmonary arteries, particularly in plexiform lesions, and are associated with excessive pulmonary vascular remodelling (PVR) and PAH severity (Ni et al., 2022; Klouda & Yuan, 2021; Hu et al., 2020b; Farha et al., 2012).

Elevated levels of pro-inflammatory cytokines and chemokines have been observed in preclinical and clinical PAH (Soon et al., 2010). The overproduction of inflammatory mediators, including tumour necrosis factor alpha (TNF-α), IL-1β, and IL-6, correlates with disease severity and survival in patients with PAH (Liang et al., 2021). All preclinical models of PAH – including Monocrotaline (MCT), chronic hypoxia and Sugen/hypoxia (SuHx) models – showed evidence of increased pro-inflammatory cytokines. IL-6 is consistently upregulated in preclinical animal models of PAH (Miyata et al., 2009; Bhargava et al., 1999). The overexpression of IL-6 is sufficient to develop PAH in transgenic mice, and its effects are augmented by chronic hypoxia (Steiner et al., 2009) while *IL6* knockout mice are protected from chronic hypoxia-induced PAH (Savale et al., 2009).

TNF-α is a major regulator of inflammatory responses in endothelial cells through the activation of nuclear factor-κB (NF-κB), which is a key driver of inflammation in PAH. Like IL-6, TNF-α was upregulated in MCT rats compared with control rats (Yang et al., 2018). MCT rats treated with a TNF-α blocker – recombinant TNF-α receptor II:IgG Fc fusion protein (rhTNFRFc) – were protected from development of PAH through inhibition of TNF-α induced NF-κB activation (Wang et al., 2013). Meanwhile, IL-1β was also increased in MCT and SuHx rat models of PAH (Li et al., 2021), and anti-IL-1 β treatment attenuated the development of PAH in MCT rats (Voelkel et al., 1994). Elevated levels of chemokines and

chemokine receptors including MCP-1/CCL2, CCL5, CX3CR1, CXCL10, CXCR4 and CCR2 have been implicated in PAH progression (Xu et al., 2021; Abid et al., 2019; El Chami & Hassoun, 2012; Heresi et al., 2010; Sanchez et al., 2007; Itoh et al., 2006; Dorfmüller et al., 2002). Some chemokines may serve as prognostic indicators of disease progression, and can be used to monitor patients' responses to therapies. For example, elevated monocyte chemoattractant protein-1 (MCP-1/CCL2) has been associated with beneficial effects of epoprostenol treatment on haemodynamic parameters, functional capacity in PAH patients (Damås et al., 2004). The upregulation of CXCL10 in PAH patients is also associated with improved survival (Heresi et al., 2010).

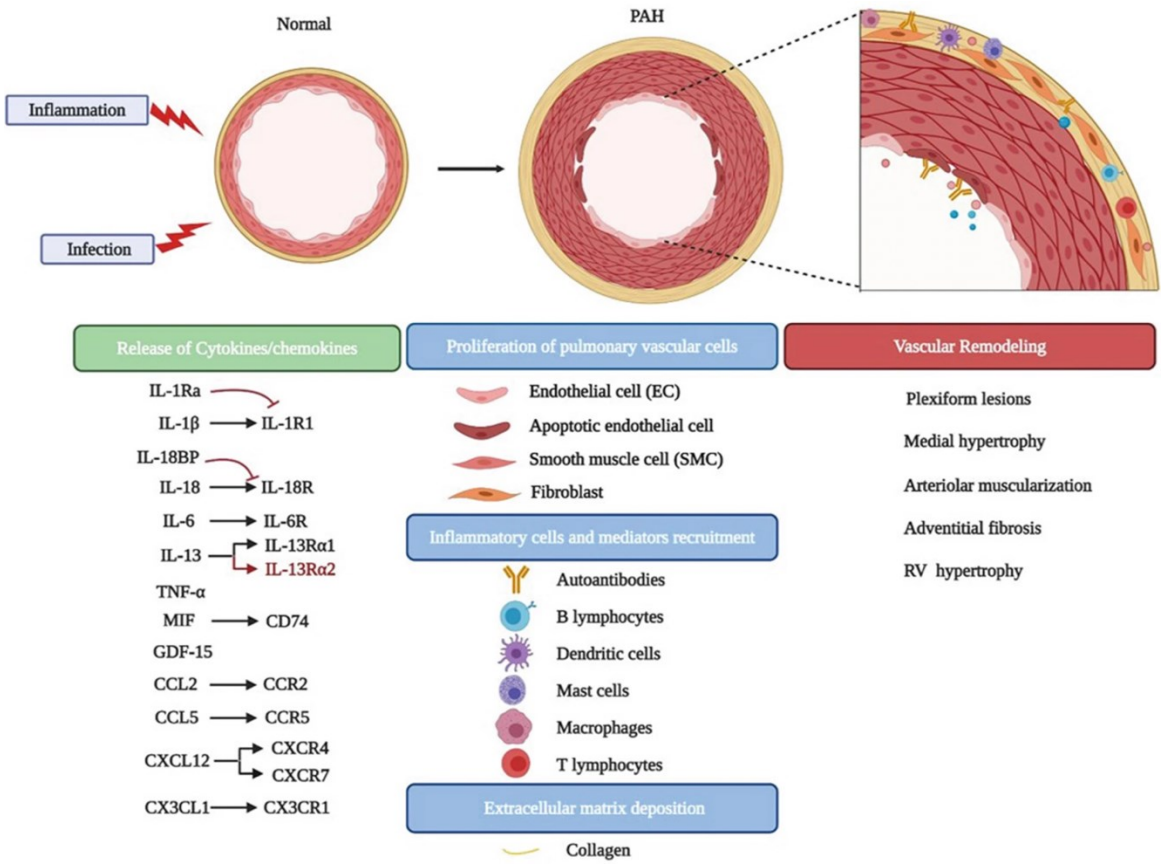

Figure 1.3: Inflammation-induced pulmonary vascular remodelling in PAH.
In response to vascular insults, cells in the pulmonary vasculature secrete pro-inflammatory cytokines and chemokines. The subsequent recruitment of inflammatory cells increases the levels of growth factors, cytokines, and chemokines, causing vascular remodelling. The progressive remodelling process leads to the muscularization of the pulmonary arteries and the formation of plexiform lesions. Illustration taken from (Liang et al., 2021).

1.4 Animal models of pulmonary arterial hypertension

1.4.1 *In vivo* models

To improve our understanding of the pathological mechanisms of PAH and to identify new therapeutic strategies, different animal models of PAH have been developed for preclinical studies, and various PAH models have been comprehensively described in recent reviews (Boucherat et al., 2022; Dignam et al., 2022; Wu et al., 2022). This chapter briefly describes the most frequently used rodent models that share key features of clinical PAH, including chronic hypoxia, Sugen/hypoxia (SuHx) and monocrotaline (MCT) models of PAH. However, none of the existing preclinical animal models of PAH can replicate the pathology of severe human PAH, particularly the formation of angio-proliferative plexiform lesions (Carman et al., 2019).

1.4.1.1 Chronic hypoxia model

Exposure to chronic hypoxia in a hypobaric chamber (10% O_2) for 3-4 weeks induces PH in mice and rats. Chronic hypoxia causes thickening and muscularisation of the small pulmonary arterioles, leading to pulmonary vascular remodelling as result of hypertrophy and hyperplasia of PASMCs (Stenmark et al., 2009). In rats, chronic hypoxia induces a moderate PH, which is characterized by increased mean PA pressure (mPAP), right ventricular (RV) hypertrophy, and the dysfunction and apoptosis of PAECs, leading to vascular remodelling (Pak et al., 2007). Mice develop only a mild PH with a slight increase in mPAP and a relatively low degree of pulmonary vascular remodelling (Maarman et al., 2013). Unlike human PAH, vascular remodelling in chronic hypoxia rodent models of PAH is fully reversible upon return to a normoxic environment.

1.4.1.2 Sugen 5416/hypoxia model

Sugen 5416/hypoxia (SuHx) models of PAH are generated by administering Sugen 5416 (SU5416), a vascular endothelial growth factor receptor 2 (VEGFR2) antagonist, in combination with chronic hypoxia, to recapitulate the pathological features of severe human PAH. Rats are subcutaneously injected with VEGFR2 inhibitor before being exposed to chronic hypoxia (10% O_2) for 3 weeks followed by normoxia for 10 weeks (Abe et al., 2010). VEGFR2 inhibitor treatment alone induces mild PAH in rats, while a combination of VEGFR2 inhibitor and chronic hypoxia causes severe and irreversible PAH associated with intimal cell proliferation and the formation of plexiform-like lesions, resembling to some extent the

pathology of human PAH (Abe et al., 2010; Taraseviciene-Stewart et al., 2001). One limitation of this model is that the SuHx model offers unpredictable results depending on strain and gender (Wu et al., 2022). Sugen/hypoxia mice show less severe symptoms than rats (Wu et al., 2022; Ciuclan et al., 2011; Taraseviciene-Stewart et al., 2001).

1.4.1.3 Monocrotaline model

Monocrotaline (MCT) is a pyrrolizidine alkaloid compound derived from the seeds or leaves of the *Crotalaria spectabilis* plant which are bioactivated to produce pyrrolic metabolites using the hepatic cytochrome P450 (CYP450) enzymes system (Roth & Reindel, 1991). The subcutaneous or intraperitoneal injection of MCT results in pulmonary arterial endothelial cell injury, which leads to PASMCs hyperplasia, hypertrophy and pulmonary arterial remodelling. This in turn leads to increased mean pulmonary arterial pressure (mPAP), right ventricular (RV) failure and death within 6 to 8 weeks (Ryan, Bloch & Archer, 2011). Although the precise mechanisms by which MCT induces PAH are unknown, endothelial dysfunction and perivascular inflammation are believed to play major roles in the development of MCT-PAH (Pak et al., 2007). MCT PAH is characterized by increased apoptosis of ECs, enhanced proliferation, and resistance to apoptosis in PASMCs, inflammatory cell infiltration and cytokine production followed by medial and adventitial thickening (Tang et al., 2021; Hill, Gillespie & McMurtry, 2017; Gomez-Arroyo et al., 2012). Although this model mimics many of the pathological characteristics of human PAH, the formation of plexiform lesions, which represents a typical histological feature of human disease, is not found here. As well as the absence of plexiform lesions, a further limitation of this model is that the response to MCT varies among species, strains and even individual animals due to differences in hepatic cytochrome P450 metabolism (Stenmark et al., 2009).

1.4.1.4 Other PAH models

1.4.1.4.1 BMPR2 model

There are several genetic models of PAH, of which the BMPR2 model is the best characterised. *BMPR2* is the main disease-causing gene in PAH, and mutations in this gene account for the majority of HPAH cases. *BMPR2* gene mutations can result from dominant negative effects or haploinsufficiency, leading to the appearance of disease phenotypes (Austin et al., 2009b; Machado et al., 2001). Impaired BMPR2 signalling due to loss of function mutations results in pulmonary ECs apoptosis, PASMCs hyperproliferation and perivascular inflammation

(Dannewitz Prosseda, Ali & Spiekerkoetter, 2020). To investigate the involvement of this pathway in the development and pathogenesis of PAH in more detail, monoallelic BMPR2$^{+/-}$ rats were developed, which remained phenotypically normal for up to 1 year. However, they developed severe PAH with vascular remodelling when exposed to a second vascular insult of either SU5416, SU5416 with chronic hypoxia, chronic hypoxia alone, monocrotaline, or adenovirus-expressing 5-lipoxygenase (5-LO) (Tian et al., 2019).

1.4.2 *In vitro* modelling: organ-on-chip models of PAH

Organs-on-chip models, also known as human microphysiological systems (hMPS) or tissue chips, are advanced *in vitro* microfluidic models that provide a potential alternative to *in vivo* animal models. Organ-on-chips enable researchers to accurately replicate key biological processes and responses of cells, tissues and organs *in vitro*. They represent novel tools for drug screening and personalized medicine that may help to bridge the gap between preclinical studies and clinical trials. The name “chips” comes from computer microchip fabrication technologies, which are also applied in the fabrication of organ-on-a-chip devices (Ingber, 2018).

Despite the promising name, in most cases, organs-on-chips cannot comprehensively reproduce the features of entire organs. Instead, the chips incorporate a small selection of organ-specific human cells cultured under physiological or disease-specific conditions of flow, pressure and oxygen tension (Leung et al., 2022).

Organs-on-chips can be generally divided into two different types based on the organ system: solid organ chips, which represent mesenchymal or parenchymal tissues, where cells are grown as a three-dimensional (3D) tissue mass, and barrier tissue chips, which represent epithelial and endothelial tissues, where cells are grown in two parallel channels separated by a porous membrane (Leung et al., 2022).

In the first published PAH-on-a-chip microfluidic model, Al-Hilal *et al*. cultured pulmonary arterial cells isolated from PAH lungs: PAECs, PASMCs and pulmonary artery adventitial cells were placed in parallel channels separated by trapezoidal pillars (Al-Hilal et al., 2020). The migration of PAECs or PASMCs into neighbouring channels was taken as a measure of intimal (or medial) thickening. The model facilitated direct microscopic observations of PAH cells but

was limited by poor accessibility to patient material and the inability to measure endothelial barrier function.

A more recent organ-on-chip microfluidic model of PAH as designed to mimic human PAEC-PASMC interactions in PAH by combining natural and induced BMPR2 disruption with hypoxia, a "double hit" condition known to induce PAH in preclinical models of the disease (Figure 1.4) (Ainscough et al., 2022a). This inducible model allowed researchers to study dynamic changes in functional and transcriptional cellular phenotype in response to physiological shear stress, as well as factors associated with PAH development such as hypoxia (2% O_2) and BMPR2 knockdown. The model also allowed the use of patient-derived endothelial cells, enabling personalized medicine applications. In this model, the RNA sequencing of human PAEC and PASMC cells as well as cells from PAH patients with *BMPR2* mutations revealed transcriptional signatures that were associated with PAH.

Organs-on-a-chips have great potential to replicate human organ-level physiology, provide insights into disease pathophysiology and accelerate drug development for personalized medicine. However, due to the complexity of the human system, several technical challenges remain (Danku et al., 2022; Tajeddin & Mustafaoglu, 2021).

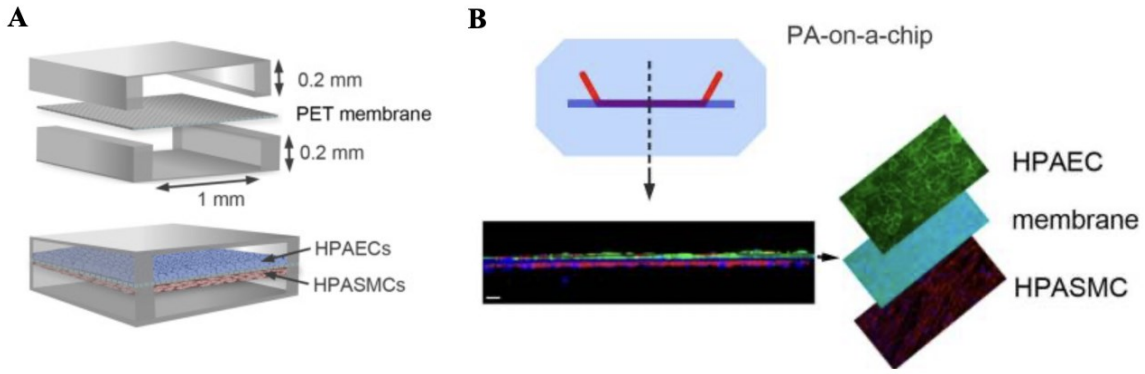

Figure 1.4: Organ-on-a-chip microfluidic model of PAH.
(A) Schematic illustration of the pulmonary artery-on-a-chip. **(B)** Confocal fluorescence Z-section image of the HPAEC-PASMC interface. HPAECs were stained with anti-VE-cadherin (green) and PASMCs with α-smooth muscle actin (red). Scale bar = 10 µm. Illustration taken from (Ainscough et al., 2022b).

1.5 Current therapies in pulmonary arterial hypertension

Despite numerous preclinical and clinical studies of PAH, the only curative option for PAH is lung transplantation. Current pharmacological treatments that are available for PAH focus primarily on targeting the pathways that affect vasoconstriction and cell proliferation (Sommer et al., 2021).

Three major pathophysiological pathways are implicated in the development and progression of PAH – nitric oxide (NO), prostacyclin (PGI2) and endothelin-1 (ET-1) pathways – have been used in targeted therapies for PAH (Figure 1.5) (Table 1.4). (Mandras et al., 2021). In PAH, vasodilators and anti-proliferative mediators such as NO and PGI2 are downregulated while vasoconstrictors and proliferation stimulants such as ET-1 are upregulated (Giaid & Saleh, 1995; Giaid et al., 1993; Christman et al., 1992). However, existing therapies can only offer symptomatic relief and cannot prevent or reverse pulmonary vascular remodelling (Deshwal, Weinstein & Sulica, 2021). Many of the current PAH therapies have limitations that are associated with adverse effects on the patients' health-related quality of life (HRQOL). Despite the recent advances in the treatment strategies, PAH remains a life-threatening condition with a poor prognosis. New individualized therapeutic approaches need to be developed.

1.5.1 Prostacyclin

Prostacyclin, also known as prostaglandin I2 (PGI2), is primarily produced by the pulmonary endothelium and acts as a ligand for the prostacyclin receptor (IP) expressed on pulmonary artery smooth muscle cells. The activation of the IP receptor promotes the production of cyclic adenosine monophosphate (cAMP), which induces protein kinase A (PKA) activity, resulting in vasodilatory and antiproliferative effects in PASMCs (Clapp et al., 2002). Circulating levels of PGI2 are decreased in PAH, leading to vasoconstriction and cell proliferation within the arterial wall. Compounds that target the prostacyclin pathway to compensate for the loss of PGI2 improve patient survival rates (Lang & Gaine, 2015; Jing et al., 2013; Simonneau et al., 2002).

1.5.2 Nitric oxide

NO is a vasodilator synthesised by nitric oxide synthase (NOS) from L-arginine in the pulmonary endothelium. NO diffuses to the underlying smooth muscle cells, where it induces cyclic guanosine monophosphate (cGMP) synthesis by activating soluble guanylate cyclase

(sGC), which leads to relaxation of the pulmonary smooth muscle cells. The effect of NO is inhibited by phosphodiesterase type 5 (PDE5), which degrades cGMP. PDE5 is primarily expressed in PASMCs, and is responsible for regulating the levels of cGMP. In PAH patients, NO synthase activity is reduced and PDE5 activity is increased, promoting vasoconstriction and PASMC proliferation (Galiè et al., 2005; Giaid & Saleh, 1995). Currently, drugs that target the NO pathway are divided into two groups, PDE5 inhibitors and sGC stimulators, based on their mechanism of action (Tettey et al., 2021). The independent administration of a PDE5 inhibitor and sGC stimulator has been shown to be effective in improving exercise capacity and quality of life in PAH patients, although combining the two therapies was poorly tolerated due to an increased risk of systemic hypotension (Galiè et al., 2015, 2009; Ghofrani et al., 2013).

1.5.3 Endothelin

Endothelin-1 is a potent mediator of vasoconstriction. It is produced predominantly by ECs and in smaller quantities by SMCs and fibroblasts. ET-1 binds to two receptor subtypes, ET-1 receptor A (ET-1A) and ET-1 receptor B (ET-1B). ET-1A and ET-1B are expressed in SMCs, while ECs express only ET-1B. The activation of ET-1A and ET-1B in SMCs induces vasoconstriction, while activating ET-1B in endothelial cells promotes vasorelaxation by activating PGI2 and NO pathways and functions as clearing receptor to remove a circulating ET-1 (Bremnes et al., 2000). ET-1 levels are upregulated in PAH patients (Giaid et al., 1993) and the inhibition of the ET-1 pathway by endothelin receptor antagonists has been shown to be beneficial in PAH patients. This inhibition can be a dual process for both ET-1A and ET-1B, or selective for ET-1A. The selective inhibition of the ET-1A receptor may be considered preferable to dual inhibition, as it allows ET-B receptors to preserve their specific functions (vasodilator and clearance) while inhibiting ET-A receptor-induced vasoconstriction and proliferation (Enevoldsen et al., 2020).

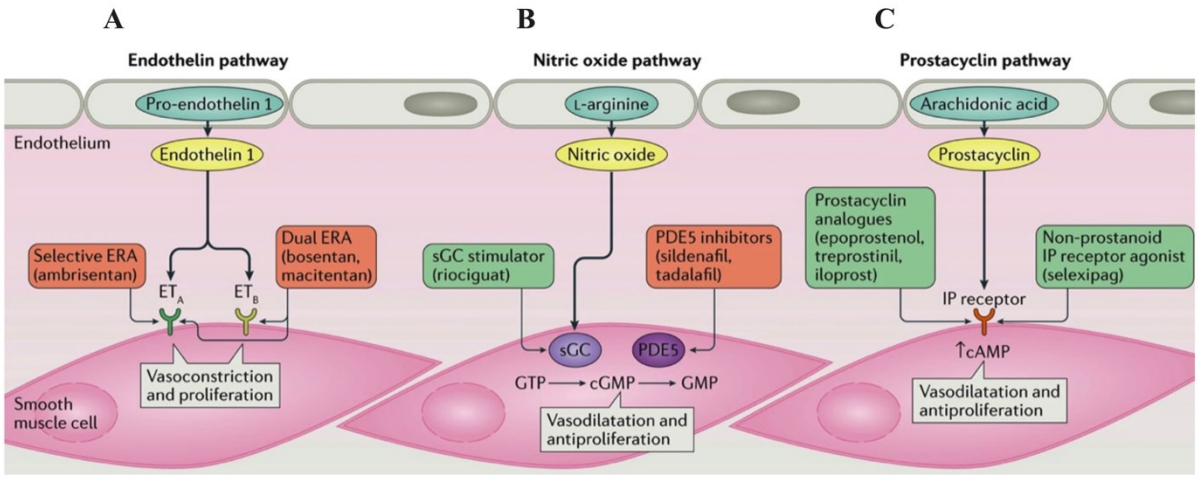

Figure 1.5: Pathways targeted in current PAH therapies.
(**A**) The endothelin signalling pathway causes vasoconstriction in pulmonary arteries due to constriction of SMCs and proliferation of ECs and SMCs. This pathway can be blocked by either selective or non-selective endothelin receptor antagonists. Endothelin (ET-1) is synthesised in ECs and activates two receptor subtypes: ET-1A and ET-1A. Both receptors are located on the surface of the SMCs. (**B**) The nitric oxide signalling pathway can be directly targeted by exogenous nitric oxide (NO) and phosphodiesterase type 5 (PDE5) inhibitors to prevent the degradation of cyclic guanosine monophosphate (cGMP) to guanosine monophosphate (GMP) or through soluble guanylate cyclase (sGC) stimulator. NO is synthesized in the pulmonary endothelium from L-arginine by NO synthase enzymes (NOS). The binding of NO to sGC leads to the formation of cGMP from GTP. PDE5 is an enzyme found mainly in SMCs which selectively degrades cGMP. (**C**) The prostacyclin signalling pathways can be targeted by either prostacyclin analogues or selective IP prostacyclin receptor agonists. Prostacyclin (PGI2) is synthesised in ECs by the conversion of arachidonic acid via prostacyclin synthase. PGI2 binds to the prostacyclin receptors (IP) on SMCs, causing an increase in cyclic adenosine monophosphate (cAMP) levels leading to pulmonary vasodilation. Illustration taken from (Lau et al., 2017).

Therapeutic Class	Drug Name	Route of Administration
Prostacyclin analogues	Epoprostenol	Intravenous
	Treprostinil	Intravenous Subcutaneous
	Iloprost	Inhalation
	Beraprost	Oral
Prostacyclin IP receptor agonist	Selexipag	Oral
Endothelin Receptor Antagonists	Bosentan	Oral
	Macitentan	Oral
	Ambrisentan	Oral
Phosphodiesterase-5 Inhibitors	Sildenafil	Oral
	Tadalafil	Oral
Soluble Guanylate Cyclase Stimulators	Riociguat	Oral

Table 1.4: Current approved drugs for PAH. Table adapted from (Kondo et al., 2019).

1.6 Endothelial dysfunction in PAH

Endothelial cells are quiescent and genetically stable under normal physiological conditions. However, they become activated in response to vascular injury or pathological stimuli such as genetic mutations, hypoxia, shear stress, and inflammation. Any prolonged activation of ECs will disrupt endothelial homeostasis, leading to endothelial dysfunction which precedes the development of PAH.

Endothelial dysfunction can be induced by genetic and environmental factors (see Section 1.3.2). It is manifested by changes in the regulatory functions of the endothelium, resulting in increased production of vasoconstrictors, pro-inflammatory, pro-angiogenic and pro-thrombotic mediators and decreased production of vasodilatory, anti-proliferative and anti-thrombotic mediators (Kurakula et al., 2021).

A key feature of endothelial dysfunction in PAH is an imbalance in the production of vasodilators and vasoconstrictors by the endothelium. Endothelial vascular tone is regulated by several EC-derived factors, including endothelin-1, nitric oxide, and prostacyclin. Increasing evidence shows that any imbalance between NO and ET-1 plays a critical role in the pathogenesis of PAH. Increases in the levels of ET-1 has been associated with the formation of plexiform lesions in PAH lungs (Giaid et al., 1993). NO is an important mediator of pulmonary vascular relaxation and is responsible for inhibiting the proliferation of PASMCs. The level of vasorelaxants and anti-proliferative factors NO and PGI2 are reduced in PAH (Christman et al., 1992). Their specific functions are described in Section 1.5.

EC apoptosis is thought to initiate PAH, and can be induced by various stimuli, including TNF-α or mechanical stress (Cracowski et al., 2014; Sakao et al., 2006). Following endothelial damage, clonal selection of apoptosis-resistant and hyperproliferative endothelial cells is thought to contribute to the formation of neointima and complex plexiform lesions in severe human PAH (Sakao, Tatsumi & Voelkel, 2009; Masri et al., 2007). In support of this view, VEGFR2 antagonist induces EC apoptosis in the SuHx rat model, which is followed by the increased proliferation of apoptosis-resistant endothelial cells and the formation of complex occlusive vascular lesions (Taraseviciene-Stewart et al., 2001). Distal pulmonary arteries from the lungs of IPAH patients show increased numbers of proliferating ECs and decreased numbers of apoptotic ECs (Tu et al., 2011). ECs isolated from IPAH lungs consistently show increased proliferation and reduced susceptibility to apoptosis (Tu et al., 2011).

Endothelial dysfunction is also characterised by a reduction in the integrity of the EC barrier, which exposes the underlying smooth muscle cells to growth factors and inflammatory cells from the blood, causing their proliferative activation (Burton et al., 2011). Mice with the endothelium-specific deletion of *BMPR2* show decreased endothelial barrier function, suggesting that BMPR2 plays an important role in maintaining EC barrier integrity (Hong et al., 2008; Beppu et al., 2004). Meanwhile, enhancing the BMPR2 signalling pathway by administering BMP9 improves barrier integrity in endothelial cells derived from PAH patients with *BMPR2* mutations (Long et al., 2015).

Uncontrolled EC proliferation and impaired angiogenesis are the main contributors to the formation of plexiform lesions. ECs from plexiform lesions express high levels of VEGF, VEGFR2 HIF-1α and HIF-1β, providing evidence for dysregulated angiogenesis in PAH (Tuder et al., 2001a; Hirose et al., 2000a). In addition, PAECs that are stimulated with hypoxia or treated with VEGF show an upregulation of growth differentiation factor 11 (GDF11), which is known to induce impaired proliferation and angiogenesis in PAH (Yu et al., 2018).

Endothelial cells can also undergo conversion to mesenchymal phenotype under pathological conditions through endothelial-to-mesenchymal transition (EndMT). The EndMT cells may directly contribute to endothelial dysfunction in PAH by transforming ECs into smooth muscle-like cells with higher proliferative and migratory capacity, or indirectly through paracrine effects on arterial intimal and medial proliferation (Suzuki et al., 2018). EndMT markers are seen in lung sections from BMPR2-deficient rats and PAH patients (Ranchoux et al., 2015). Another study has shown that BMPR2 silencing induces EndMT by increasing the expression of high mobility group AT-hook 1 (HMGA1) in PAECs. However, knocking down the HMGA1 or its target Slug has been shown to prevent BMPR2 silencing-induced EndMT (Hopper et al., 2016). Endothelial BMPR2 silencing increases the expression of EndMT markers Slug and Twist, leading to a cell junction protein switch from VE-cadherin to N-cadherin (Hiepen et al., 2019).

1.6.1 ECFCs in PAH

Endothelial colony forming cells (ECFCs) – also termed blood outgrowth endothelial cells (BOECs) or the late outgrowth endothelial colony forming cells – are rare circulating endothelial progenitor cells which can be isolated from human peripheral blood mononuclear cells (PBMCs) fractions and expanded exponentially *ex vivo*. Cultured ECFCs show key characteristics that are typical of endothelial cells, such as cobblestone morphology, and the expression of endothelial cell markers (CD144, CD31, CD146), and are negative for immune cell markers (CD45, CD14) (O'Neill et al., 2018). ECFCs demonstrate increased proliferative and angiogenic potential, and can promote vascular repair and *de novo* angiogenesis (Banno & Yoder, 2018). Although the phenotypic and functional properties of cultured ECFCs are well known, the origin and function of naïve ECFCs and their role in health and disease remain unclear. However, considering their potential for promoting *in vivo*/*in situ* endothelialisation and therapeutic angiogenesis, ECFCs have tremendous potential in regenerative medicine (Far,is et al., 2020; Avci-Adali, Ziemer & Wendel, 2010). ECFCs derived from PAH blood appear to harbour the characteristics of the disease and can be used as cellular models for studying the pathological mechanisms that underlie it.

The phenotypic characteristics of ECFCs isolated from PAH patients have been studied extensively in various laboratories (Melero-Martin, 2022; de Boer et al., 2020; Kutikhin et al., 2020; Paschalaki & Randi, 2018). PAH ECFCs exhibit a higher proliferative potential than control ECFCs, which suggests that these cells may contribute to the formation of angio-proliferative lesions in PAH (Duong et al., 2011). For example, ECFCs derived from PAH patients harbouring *BMPR2* mutations show a hyperproliferative phenotype and an impaired capacity to form vascularized networks (Toshner et al., 2009). In another study, PAH ECFCs with *BMPR2* mutations showed increased permeability in response to lipopolysaccharide (LPS), although this effect was inhibited by treatment with BMP9 (Long et al., 2015). Meanwhile, BMP9 treatment also prevented TNF-α- mediated apoptosis in ECFCs with *BMPR2* mutations.

IPAH ECFCs replicate several features of the PAH endothelium, including changes in the expression of genes involved in the regulation of cell proliferation and angiogenesis such as *CLIC1*, *CLIC4* and *KLF2* (Alzaydi et al., 2023; Sindi et al., 2020; Wojciak-Stothard et al., 2014). A recent study using a microfluidic organ-on-a-chip model of PAH revealed that ECFCs

from PAH with disabling *BMPR2* mutations showed a significant increase in the expression of genes associated with inflammatory activation (*NFKB1*, *NFKB2*, *IL6*, *CXCL8* and *REL*) mitochondrial function (*STOML2* and *FIS1*), and glycolysis (*HK2*, *LDHA* and *PDK4*), as well as a downregulation in the expression of key marker genes of arterial identity such as *SOX17* and *ERG* (Ainscough et al., 2022a). In this model, ECFCs also displayed the upregulation of NO regulatory genes (*DDAH1*, *DDAH2* and *NOS3*) and EC repair and angiogenesis genes (*CLIC1*, *ARF6*, *VEGFA* and *VEGFB*).

1.7 The role of shear stress in the development of PAH

ECs lining the lumen of blood vessels are constantly exposed to blood flow, which regulates vascular tone, arterial structure and remodelling by acting on endothelial cells. The endothelium senses changes in shear stress through multiple mechanosensors including ion channels (e.g., K^+ and Cl^- channels), integrins, glycocalyx, caveolae, G proteins, VE-cadherin, PECAM1, tyrosine kinase receptors (e.g., VEGFR2) and the endothelial cytoskeleton (Li et al., 2022). These mechanosensors translate the mechanical forces into biochemical signalling events, inducing vasodilation as an early response to flow by activating ion channels and releasing nitric oxide. Later responses allow the endothelial cells to adapt to flow by mediating cytoskeletal alignment and modifying endothelial gene expression (Katoh, 2023; Fels & Kusche-Vihrog, 2020; Gerhold & Schwartz, 2016).

Endothelial cells can also be affected by changes in blood flow patterns (Nakajima & Mochizuki, 2017) (Figure 1.6). ECs, for example, are exposed to unidirectional laminar shear stress in the straight sections of pulmonary arteries and to a non-uniform, disturbed flow in the branching parts. These different flow patterns lead to the differential regulation of gene expression and endothelial function. Laminar shear stress induces EC homeostasis by activating flow-regulated transcription factors such as KLF2 and KLF4 (Davies et al., 2013). In contrast, disturbed and/or low flow induces EC activation and inflammatory gene expression, particularly the NF-κB, which in turn leads to the production of pro-inflammatory mediators such as TNF-α and CCL2 (Davies et al., 2013; Nagel et al., 1999).

Non-physiological (high or low) or non-laminar disturbed flow contributes to a variety of vascular diseases, including PAH (Kurakula et al., 2021; Baeyens et al., 2016; Dickinson et al., 2013; Chiu & Chien, 2011; Dai et al., 2004). KLF2 and KLF4 are the best characterised flow-responsive transcription factors, and act as master regulators of endothelial function by

mediating the expression of several anti-proliferative, anti-inflammatory, and anti-thrombotic genes in the ECs in response to laminar flow (Nayak, Lin & Jain, 2011). KLF2 and KLF4 are downregulated in ECs in response to disturbed flow (Sweet et al., 2018), but the mechanisms that responsible for this are not well understood.

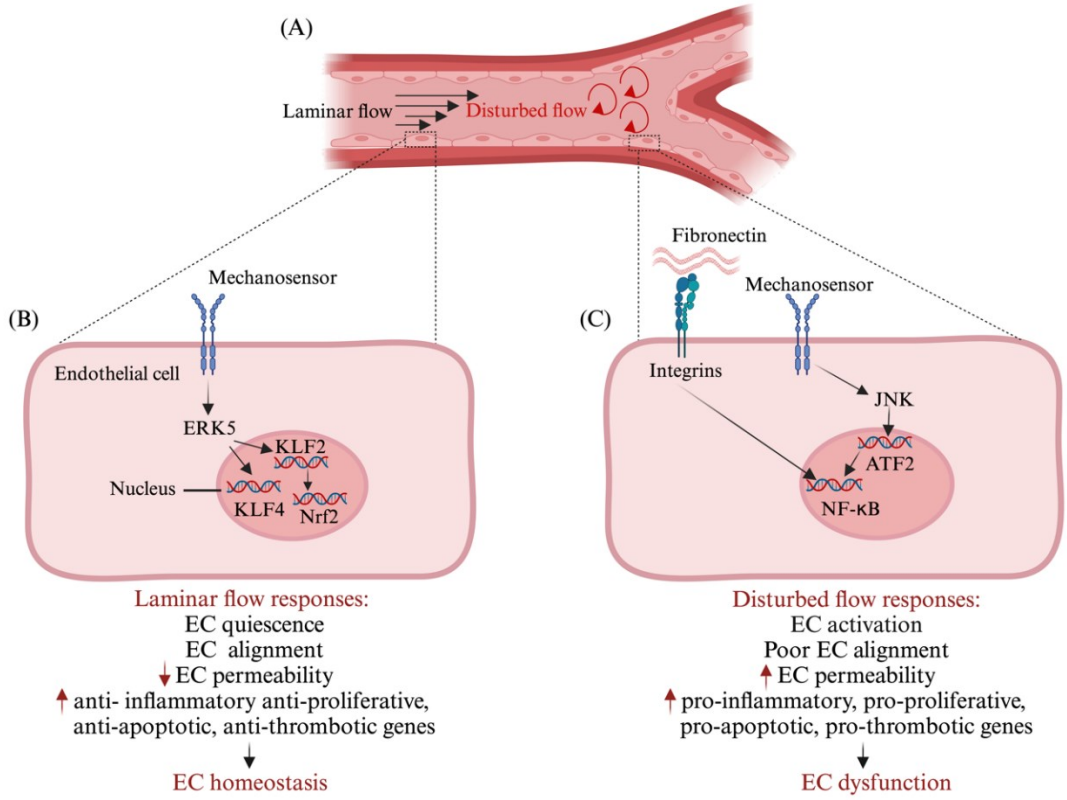

Figure 1.6: Endothelial responses to flow.
(**A**) Endothelial cells covering the intima of pulmonary arteries are exposed to either laminar flow in the straight sections of arteries and disturbed flow in the curved and branching sections of arteries. (**B**) Laminar flow induces endothelial homeostasis by promoting EC quiescent phenotypes, inducing EC alignment parallel to the flow direction, reducing EC permeability, and increasing the expression of anti-inflammatory, anti-proliferative, anti-thrombotic and anti-apoptotic genes. Laminar flow increases the transcriptional activity of KLF2 and KLF4 through the MEK5/ERK5/MEF2 signalling pathway. KLF2 stimulates Nrf2 activation, and both KLF2 and Nrf2 induce endothelial quiescence. (**C**) Disturbed flow causes endothelial dysfunction by preventing EC alignment, enhancing EC permeability and increasing the expression of pro-inflammatory, pro-proliferative, pro-thrombotic and pro-apoptotic genes. For example, disturbed flow increases NF-κB expression via JNK and its downstream ATF2. Flow-induced NF-κB activation is mediated by fibronectin binding to integrins. Adapted from (Nakajima & Mochizuki, 2017).

1.8 Krüppel-Like Factors (KLFs)

KLFs belong to a family of zinc finger transcription factors which contain three highly conserved C2H2 zinc finger domains located at the C-terminal of the protein. They are responsible for DNA- binding to GC-rich sequences, including GC boxes and GT boxes in promoters and enhancers of target genes (Figure 1.7) (Suske, Bruford & Philipsen, 2005). Although the C-terminal domains of KLF proteins have similar functions, their regulatory N-terminal domains are highly variable and can act as transcriptional activators or repressors, accounting for their functional diversity.

So far, more than seventeen KLFs have been identified in mammals (Zhang et al., 2023; Fan et al., 2017; McConnell & Yang, 2010). This chapter focuses predominantly on KLF2, KLF4 and KLF6, which are the main subject of this study. Detailed information regarding the structure and function of other KLFs can be found in recent comprehensive reviews (Jha et al., 2024; Yuce & Ozkan, 2024; Santoyo-Suarez et al., 2023; Zhang et al., 2023; Orzechowska-Licari et al., 2022).

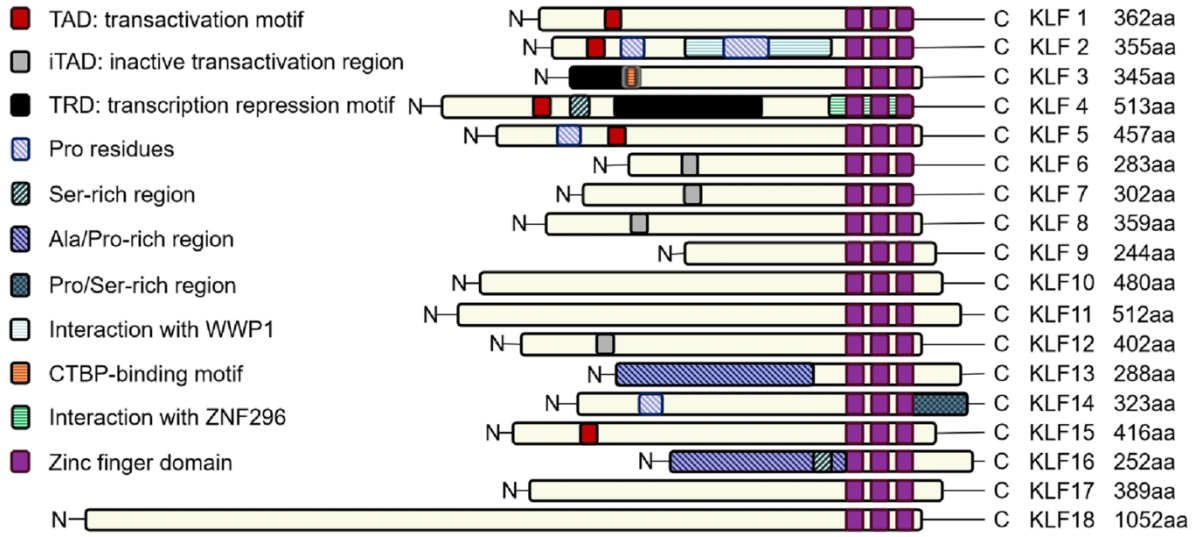

Figure 1.7: Protein structure of human KLFs.
All KLFs share similar motifs, with three C2H2 zinc fingers in their C-terminal DNA-binding domains. However, their N-terminal domains are extremely diverse, and consist of various activating, repressing and protein interaction domains. Image taken from (He, He & Xie, 2023).

KLFs have distinct functions and show different tissue distribution patterns (Fan et al., 2017). In the vasculature, for example, KLF2 is exclusively expressed in ECs and is essential for the normal lung development and function (McConnell & Yang, 2010; Wani, Wert & Lingrel, 1999). Like KLF2, KLF6 and KLF11 are also expressed in the endothelial cells (McConnell & Yang, 2010). KLF4 and KLF5 are two closely related KLF members that are expressed in ECs and SMCs (McConnell & Yang, 2010). KLF4 and KLF5 both induce a phenotypic switch in VSMCs, but they have opposite effects on cell proliferation: KLF4 promotes cell cycle arrest, whereas KLF5 promotes cell proliferation (Sweet et al., 2018; GHALEB et al., 2005).

Previous studies have shown that KLF2, KLF4, and KLF5 are involved in the regulation of vascular homeostasis and that their dysregulation may contribute to pulmonary vascular remodelling in PAH (Figure 1.8) (Sindi et al., 2020; Shatat et al., 2014; Courboulin et al., 2011). KLF2 and KLF4 are downregulated in PAH lungs, while KLF5 is upregulated in HPASMCs from PAH patients (Sindi et al., 2020; Shatat et al., 2014; Courboulin et al., 2011). However, the role of these KLFs in the pathogenesis of PAH has not yet been fully established.

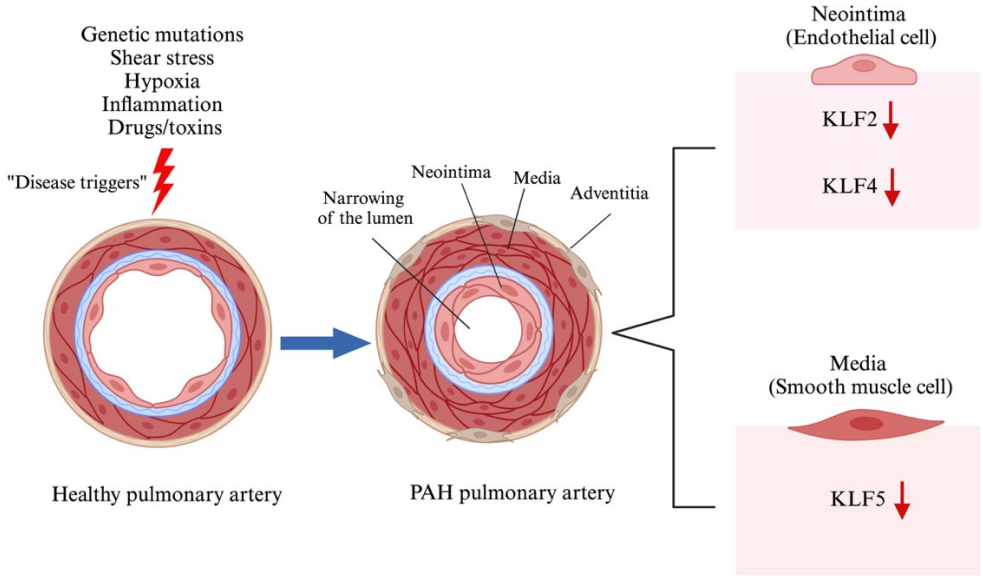

Figure 1.8: Schematic illustration of KLFs function in pulmonary arterial hypertension.
PAH is a severe lung disease that causes the pulmonary arteries to narrow due to extensive vascular remodelling and vasoconstriction. Genetic mutations, drugs/toxins, inflammation, shear stress and hypoxia act as disease triggers that contribute to the onset of PAH. KLFs are flow-responsive transcription factors that play a key role in maintaining vascular homeostasis. However, the dysregulation of KLF functions leads to vascular dysfunction which is manifested by excessive cell proliferation and apoptotic resistance, vasoconstriction, angiogenesis and extracellular matrix remodelling, leading to the development of PAH. Illustration created by the author using BioRender.com.

1.8.1 KLF2

KLF2 is a key flow-induced transcription factor that regulates roughly 46% of the flow-responsive genes in ECs (Atkins & Jain, 2007; Parmar et al., 2006). It plays an important role in the maintaining vascular homeostasis because of its anti-angiogenic, anti-inflammatory and anti-thrombotic effects on the endothelium (Alaiti et al., 2012). KLF2 is essential for blood vessel formation, as KLF2-null mice display abnormal angiogenesis and die embryonically from haemorrhage due to vascular damage (Wani, Means & Lingrel, 1998; Kuo et al., 1997). As well as the important role it plays in the blood vessel formation, chimeric mice with homozygous KLF2-null embryonic stem cells show impaired lung development, indicating that KLF2 also plays a crucial role in the normal development and function of the lung (Wani, Wert & Lingrel, 1999). Endothelial-specific loss of *KLF2* is embryonically lethal due to vascular complications resulting in heart failure (Lee et al., 2006).

A heterozygous, germline mutation in the *KLF2* gene was detected in HPAH, highlighting the potential role of KLF2 in PAH pathogenesis (Eichstaedt et al., 2017). This mutation in the C-terminal domain of KLF2 may affect the binding of KLF2 to target DNA sequences (Piva et al., 2015). The expression of KLF2 was also shown to be decreased in ECFCs and lung tissues of IPAH patients and animal models of PAH (Sindi et al., 2020). The molecular mechanisms that lead to compromised KLF2 signalling in PAH remain unknown, but impaired BMPR2 signalling, decreased activation of AMP-activated kinase (AMPK) and inflammation, may contribute to the downregulation of KLF2 (Eichstaedt et al., 2017; Chandra et al., 2011; Kumar et al., 2005). Low wall shear stress and turbulent blood flow patterns in the pulmonary arteries of PAH patients may also contribute to the downregulation of KLF2 (Barker et al., 2015; Reiter et al., 2008).

1.8.2 KLF4

Like KLF2, KLF4 is activated by laminar shear stress and is essential to vascular homeostasis due to its vaso-protective, anti-thrombotic and anti-inflammatory effects in ECs (Fan et al., 2017; Shen et al., 2009). KLF4 shares many functional similarities with KLF2; they both share gene targets, respond to similar stimuli and have a similar amino acid sequence in the DNA binding region (Sweet et al., 2018). Double *KLF2*/*KLF4* knockout mice die earlier than single KLF2 or KLF4 knockouts due to the severity of vascular damage, which suggests that KLF2 and KLF4 may have compensatory functions (Chiplunkar et al., 2013).

The expression of KLF4 is downregulated in PAH lungs in comparison with healthy controls (Shatat et al., 2014). Mechanisms leading to the downregulation of KLF4 in PAH may include the secretion of pro-inflammatory mediators, disturbed blood flow and post-transcriptional modifications such as the ubiquitination or phosphorylation of KLF4 (Nicoleau, Fellows & Wojciak-Stothard, 2021).

Because the functions of KLF2 and KLF4 overlap, identifying their specific contributions to PAH pathogenesis is problematic, and their potential compensatory effects in ECs will require further investigation.

1.8.3 KLF6 Location, Structure and Function

The KLF6 gene is located on the short arm of human chromosome 10 (10p15), and contains four exons, with a total length of 7 kb. It can be transcribed into seven transcripts, in which only KLF6-204, KLF6-206 and KLF6-207 are believed to be translated into proteins (Figure 1.9). KLF6-206, which is full-length KLF6, is the primary KLF6 transcript, and produces a protein of 283 amino acids, with a molecular weight of ~32 kDa. It was originally identified in the placenta as a core promoter-binding protein (CPBP) regulating the expression of pregnancy-related genes. In the KLF6 gene, a single nucleotide polymorphism (SNP) was identified at intervening sequence 1-27 (G > A) that creates *de novo* splicing sites resulting in three splice variants: KLF6-SV1, KLF6-SV2 and KLF6-SV3. These splice variants are different in length and structure because of the utilization of distinct splicing donor and/or splicing acceptor sites. The full-length KLF6 and KLF6-SV3 variants localise in the nucleus due to the presence of a nuclear localization signal (NLS), while KLF6-SV1 and KLF6-SV2 variants are localized in the cytoplasm as they lack the NLS domain due to alternative splicing. KLF6-SV1 and KLF6-SV2 are therefore unable to regulate the gene transcription process as they cannot transport to the nucleus. Of the three KLF6 splicing isoforms, KLF6-SV1 has been studied extensively, particularly in relation to cancer, but the functional roles of the other isoforms are not well understood (DiFeo et al., 2006b; Narla et al., 2005).

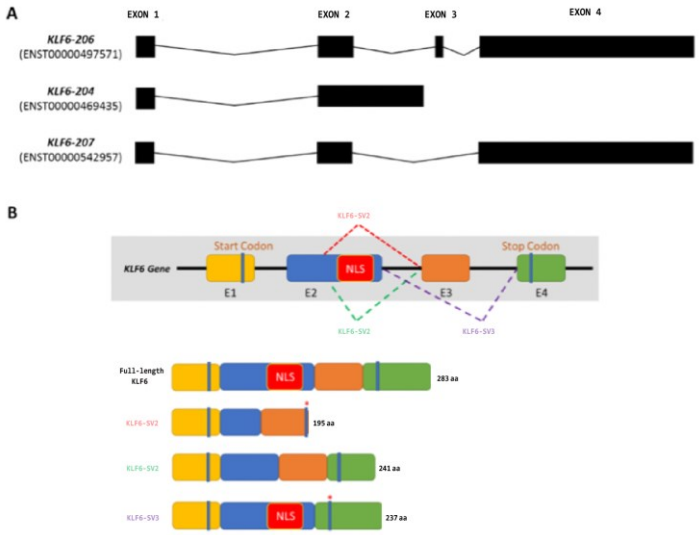

Figure 1.9: Gene structure of human KLF6 and its splice variants.
(**A**) The human KLF6 gene consists of 4 exons and can be transcribed into 7 distinct transcripts. Only three of these transcripts, KLF6-204, KLF6-206, and KLF6-207, are thought to be translated into proteins. (**B**) A germline mutation at the intervening sequence 1-27 G > A can promote alternative splicing, generating three KLF6 splice variants: KLF6-SV1, KLF6-SV2 and KLF6-SV3. Figures taken from (Syafruddin et al., 2020).

The structure of the KLF6 protein comprises three functional domains, including an acidic domain located in the N-terminal region, a serine/threonine-rich central domain and a C-terminal DNA-binding domain with three C2H2 zinc finger-type structures (Figure 1.10). These zinc fingers are responsible for specific DNA recognition and binding to guanine-rich sequences. The acidic N-terminal domain of KLF6 is involved in the recruitment and interaction with other transcription factors and co-factors to either activate or repress transcription, depending on the context. The central domain of KLF6 is rich in serine and threonine residues, which makes this domain sensitive to post-translational modifications (PTMs), particularly phosphorylation. KLF6 has been shown to be constitutively phosphorylated *in vivo* (Slavin et al., 2004).

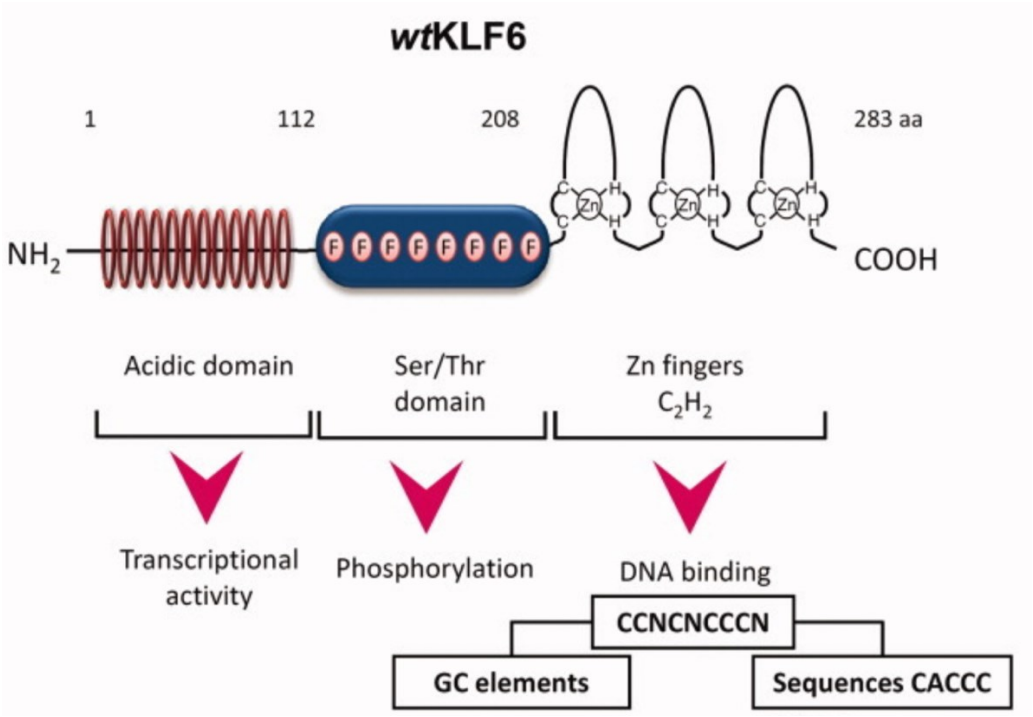

Figure 1.10: Structure of wild-type KLF6 protein.
The KLF6 protein comprises three domains: (1) The N-terminal acidic domain is responsible for the transcriptional activity of KLF6. (2) The serine/threonine-rich central domain is enriched in Ser and Thr residues which is responsible for post-translational modifications (PTMs) of KLF6, particularly phosphorylation. (3) The C-terminal DNA-binding domain, which contains three C2H2 zinc fingers that bind to GC elements and CACCC sequences in the promoters and enhancers of target genes. Illustration taken from (Andreoli, Gehrau & Bocco, 2010).

KLF6 plays a key role in cell development, proliferation, differentiation, and apoptosis. It is expressed in many tissues during embryonic development, particularly in the kidneys, lungs and heart. *KLF6*$^{-/-}$ mice are embryonically lethal due to defects in erythropoiesis and yolk sac vascularization, suggesting the importance of KLF6 in regulating developmental processes (Matsumoto et al., 2006). Meanwhile, the deletion of *KLF6*$^{-/-}$ in embryonic stem (ES) cells results in impaired cell differentiation and proliferation (Matsumoto et al., 2006).

The dysregulation of KLF6 expression has been implicated in the development of several diseases including cancer, cardiovascular disease, and inflammation-related diseases. KLF6 expression is either up- or down-regulated depending on the type of disease, mainly because of the alternative splicing events that generate isoforms with different functions (Syafruddin et al., 2020). For example, the full-length KLF6 acts as a tumour suppressor and can be inactivated by mutation, loss of heterozygosity (LOH) or reduced expression in various types of cancer (DiFeo, Martignetti & Narla, 2009). However, the exact mechanism by which KLF6 suppresses is still largely unknown. The suppression effect of KLF6 in cancer has been attributed to the inhibition of VEGF expression, the upregulation of E-cadherin, the activation of p21 through a p53-independent mode and the inhibition of c-Jun proto-oncoprotein activity (DiFeo et al., 2006b, 2006a; Narla et al., 2001). Among the KLF6 isoforms, KLF6-SV1 is pro-oncogenic, and its expression is increased in lung, breast, and prostate cancers. It is thought to act as an inhibitor of full-length KLF6 (DiFeo, Martignetti & Narla, 2009).

KLF6 is expressed in the endothelium as a key mediator of vascular repair in response to injury. It induces the expression of several endothelial target genes such as transforming growth factor beta (TGF-β), transforming growth factor beta receptor (TGFβR), plasminogen activator urokinase (PLAU), collagen type 1 alpha 1 (COL1A1) and endoglin (ENG) (Botella et al., 2002; Kojima et al., 2000; Kim et al., 1998; Ratziu et al., 1998)

The expression of KLF6 increases during vascular injury, leading to the activation of endoglin and activin receptor-like kinase 1 (ALK1), two important TGF-β receptors that are involved in the regulation of pulmonary vascular remodelling and angiogenesis in PAH (Garrido-Martín et al., 2013; Mahmoud, Upton & Arthur, 2011; Botella et al., 2002). KLF6 also regulates many of the genes involved in the regulation of EC motility and invasion during the angiogenesis process, such as VEGF, MMP9, E-cadherin, collagen α1, tissue factor pathway inhibitor 2 (TFPI2) and IL6 (Garrido-Martín et al., 2013; McConnell & Yang, 2010; Atkins & Jain, 2007; Kojima et al., 2000; Kim et al., 1998).

A recent study of a microfluidic model of PAH suggests that KLF6 expression and function may be dysregulated in the PAH endothelium (Ainscough et al., 2022a). In this study, human pulmonary artery endothelial cells (HPAECs) which were cultured under flow (6 dynes/cm^2 for 24h) and subjected to known triggers of PAH, BMPR2 knockdown and hypoxia, showed a significant decrease in KLF6 expression ($p=0.02$) (Ainscough et al., 2022b).

1.9 Summary

Pulmonary vascular remodelling in pulmonary arterial hypertension (PAH) is believed to commence with endothelial damage followed by exaggerated repair processes. This leads to the activation of proliferative, inflammatory and angiogenic responses in the vascular intima and media. The cause of endothelial dysfunction remains unknown, and may involve genetic and environmental factors. Krüppel-like factors (KLFs), which respond to blood flow, play a crucial role in maintaining endothelial quiescence and homeostasis. Accumulating evidence indicates that the expression and signalling of the flow-responsive transcription factors KLF2 and KLF4 are dysregulated in PAH. Recent data from microfluidic model of PAH suggest that KLF6 may also be implicated in the disease. While the roles of KLF2 and KLF4 have been extensively investigated, the function of KLF6 remains unknown. PAH shares many characteristics with cancer, such as increased cell proliferation and resistance to apoptosis, and accumulating evidence suggests that the dysregulation of KLF6 signalling may play a contributing role. KLF6 is expressed in the vascular endothelium and regulates the expression of many target genes involved in vascular repair, angiogenesis, and remodelling. It also regulates cell proliferation as well as modulates inflammation and immune responses, but its functional role in PAH has not been explored.

1.10 Hypothesis

Dysregulation of KLF6 signalling contributes to endothelial dysfunction in pulmonary arterial hypertension (Figure 1.11).

1.11 Study Aims

1. To investigate the effects of factors involved in the pathogenesis of PAH, including shear stress, hypoxia and inflammation, on KLF6 expression in human pulmonary arterial endothelial cells (HPAECs).
2. To evaluate the effects of changes in KLF6 expression on HPAEC function, including inflammatory activation, junctional integrity and barrier function, angiogenesis, proliferation, migration and apoptosis.
3. To investigate the expression of KLF6 in various experimental animal models of PAH including chronic hypoxia, Sugen/hypoxia (SuHx) and monocrotaline (MCT) at different stages of the disease, and in ECFCs from PAH patients with *BMPR2* mutations.
4. To characterise the effects of KLF6 overexpression on the endothelial transcriptome.
5. To investigate the relationship between KLF6 and hypoxia-induced changes in the endothelial transcriptome.
6. To investigate the relationship between KLF6 and TNF-α-induced changes in the endothelial transcriptome.
7. To compare the transcriptional responses of HPAECs overexpressing KLF6 versus transcriptional responses of HPAECs overexpressing KLF2 or KLF4.
8. To determine the role of KLF6 in PAH by investigating the differential gene expression of KLF6-regulated genes in the remodelled PAH blood vessels, including complex plexiform lesions.
9. To assess KLF6 expression in lung vessels from healthy controls and PAH patients.

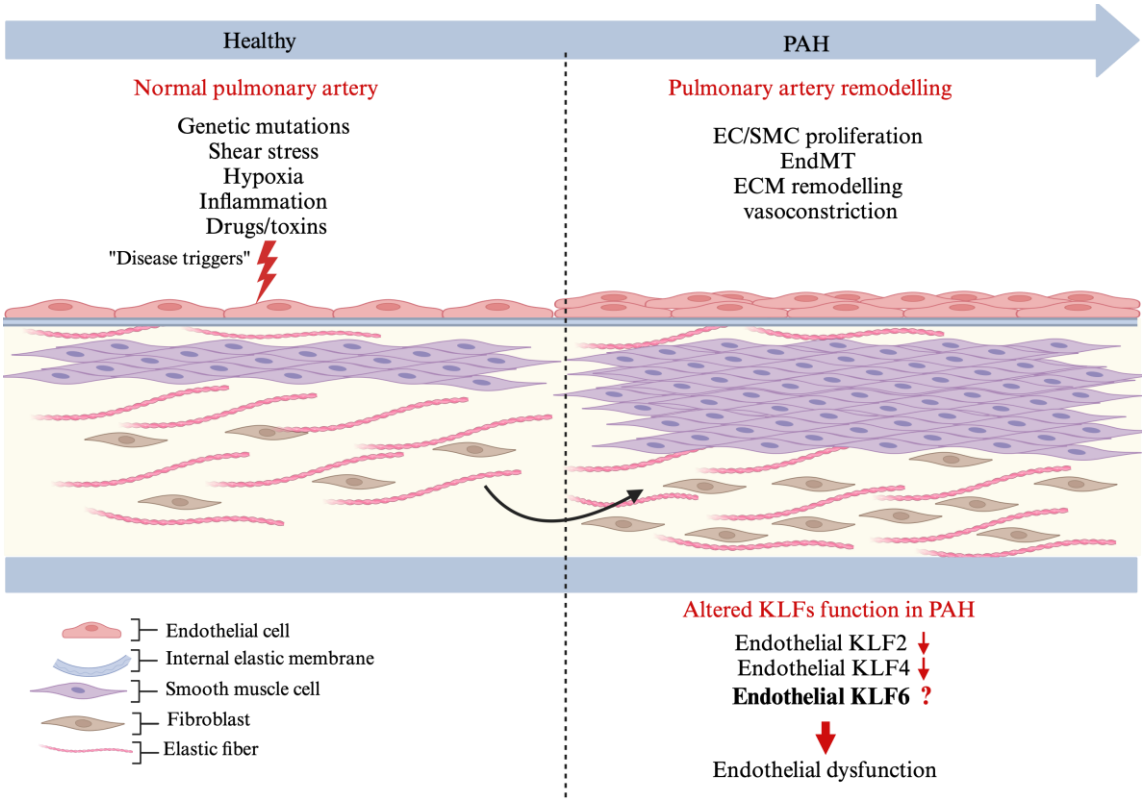

Figure 1.11: Hypothesized role of KLF6 in pulmonary arterial hypertension.
KLF2, KLF4 and KLF6 are expressed in the endothelium. The roles of KLF2 and KLF4 are well characterised and their expressions are known to be downregulated in PAH. However, the role of KLF6 in the pulmonary endothelium in PAH is unknown. I hypothesize that the dysregulation of KLF6 expression and signalling contributes to endothelial dysfunction in PAH. Illustration created by the author using BioRender.com.

Chapter 2 : Materials and methods

2.1 Declaration of Responsibilities

The work presented in this thesis is my own. Where information or contributions have been derived from other sources, this has been indicated in the thesis.

Specifically, the culture of ECFCs and the preparation of cDNA was carried out by Dr Mai Alzaydi and Dr Alexander Ainscough). I performed quantitative-PCR (qPCR) on cDNA samples from ECFCs experiments myself.

RNA samples from Monocrotaline and Sugen/hypoxia rats were kindly provided by Dr Chien-Nien Chen and Chongyang Xie from Professor Lan Zhao's group. I performed reverse transcription (RT) and qPCR on RNA samples from the Sugen/hypoxia rat model of PAH myself.

cDNA samples from hypoxic mice were kindly provided by member of my lab, Dr Adam Fellows. I performed qPCR on cDNA samples from the chronic hypoxia mouse model of PAH.

I also performed the RNA-sequencing experiments, while the bioinformatic analysis leading to the identification of differentially expressed genes (DEGs) was performed by Dr Nadia Fernandes (Imperial BRC Genomics Facility at Imperial College London). I performed the Gene ontology (GO) and disease ontology (GO) enrichment analyses.

Sample preparation for the spatial transcriptomics pf PAH lung sections was performed by Nathalie Lambie (Imperial BRC Genomics Facility at Imperial College London), and the Bioinformatics analysis was performed by Dr Felicia New (NanoString, USA). I performed the optimization of antibodies for the morphological markers and selected regions of interest (ROIs).

2.2 Cell Culture

2.2.1 Primary Human Pulmonary Artery Endothelial Cell Culture

Human Pulmonary Artery Endothelial Cells (HPAECs) that had been isolated from the left and right branches of the main human pulmonary artery were obtained from PromoCell (Germany, Cat. No. C-12241) at passage 3. Information on the HPAEC donors – including age and gender population doubling time – are provided in Table 2.1.

Lot #	Age	Gender	Doubling Time	Company
431Z031	23	Female	48.3h	PromoCell
433Z034.1	34	Female	55.4h	PromoCell
433Z034.2	34	Female	58.1h	PromoCell
458Z016.12	51	Female	28.5h	PromoCell
458Z016.13	51	Female	28.5h	PromoCell
483Z021.6	49	Male	43.3h	PromoCell
451Z031.14	68	Male	25.4h	PromoCell
18TL155113	42	Male	25.0h	Lonza

Table 2.1: Donor information for HPAECs used in cell culture experiments.

Cells were cultured in T75 culture flasks (Sarstedt, Germany, Cat. No. 83.3911.002) that had been pre-coated with bovine plasma fibronectin (10 µg/mL, EMD Millipore Corp, USA, Cat. No. 341631) in an endothelial cell basal medium 2 (EGM2, PromoCell, Germany, Cat. No. C-22211). This medium was supplemented with endothelial cell growth medium 2 (ECGM2 SupplementPack; PromoCell, Germany, Cat. No. C-39211) (for a list of components, see Table 2.2), 1% penicillin (100 U/mL)-streptomycin (100µg/mL, Invitrogen, UK, Cat. No. 15140-122) and 1% MycoZap™ Prophylactic (Lonza, Cat. No. VZA-2032). The cells were then incubated in a humidified incubator at 37 °C with 21% O_2, 5% CO_2, and the endothelial cell growth medium was replaced with a fresh medium every 2-3 days. All HPAECs were used between passages 5 and 8, and exhibited a cobblestone morphology at the point of confluence which was typical for endothelial cells.

Supplement	Final Concentration	Catalog Number
Foetal Calf Serum	0.02 ml / ml	C-37320
Epidermal Growth Factor	5 ng / ml	C-30224
Basic Fibroblast Growth Factor	10 ng / ml	C-30321
Insulin-like Growth Factor	20 ng / ml	C-31700
Vascular Endothelial Growth Factor 165	0.5 ng / ml	C-30260
Ascorbic Acid	1 µg / ml	C-31750
Heparin	22.5 µg / ml	C-31650
Hydrocortisone	0.2 µg / ml	C-31063

Table 2.2: Supplementary components of endothelial cell growth medium 2.

2.2.2 Isolation of Peripheral Blood Mononuclear Cells (PBMCs)

The isolation of PBMCs and ECFC cell cultures was carried out by Dr Mai Alzaydi and Dr Alexander Ainscough.

Peripheral blood mononuclear cells (PBMCs) were isolated using a method described by (Ormiston et al., 2015), and peripheral blood samples were collected into EDTA coated tubes to avoid coagulation. 50 mL of blood was diluted 1:1 with PBS (Mg^{2+}/Ca^{2+} free), and 22 mL of the diluted blood was carefully applied over 15 mL of Ficoll-Paque Plus gradient solution (GE Healthcare, Amersham, UK, Cat. No. 17-1440-03) in a 50mL falcon tube and then centrifuged at 400 g for 30 minutes at room temperature with the brake off. After centrifugation, the buffy coat layer containing the PBMCs was carefully collected into a new 50 mL falcon tube and then diluted 1:1 with PBS and centrifuged at 300 g for 20 minutes with the brake on. Pelleted PBMCs were then either immediately seeded in a 24-wells plate pre-coated with 1% gelatin or resuspended and cryopreserved in a freezing medium containing 10% dimethyl sulfoxide (DMSO; Sigma-Aldrich, UK, Cat. No. D2650) and 90% foetal bovine serum (FBS).

The cells were seeded (3-5 × 10^7 cells in 4 mL of EGM2 medium per well) in 6 well-plates which had been pre-coated with type 1 rat tail collagen (BD Biosciences, Bedford, MA, USA). The culture medium was changed every 24 hours for the first week to remove non-adherent cells and every 48 hours thereafter. Colonies typically appeared between days 7 and 28, and were isolated using an 8 mm or 10 mm in diameter attaching cloning cylinder (Millipore, Watford, UK) with vacuum grease. All the cells from the inside of the cylinder were trypsinised and resuspended in an EGM2 medium and then plated onto 24-well plates which had been precoated with fresh 1% gelatin.

After reaching 70-80% confluence, the colonies were trypsinised and subcultured into 6 well plates and T75 flasks. Cells within these colonies showed stable population doubling times and a typical endothelial cobblestone morphology. The cells were then stained with endothelial-specific markers VE-cadherin (CDH5), PECAM1 (CD31) and von Willebrand Factor (vWF) to confirm endothelial cell lineage (see Table 2.11).

2.2.2.1 Endothelial Colony Forming Cells

Endothelial colony forming cells (ECFCs) were clonally isolated from peripheral blood samples, expanded and characterised as described above. Venous blood samples were obtained from healthy volunteers (n=5) and from heritable PAH (HPAH) patients with rare pathogenic BMPR2 variants (n=5) with the informed written consent and approval of the local ethics committee (REC Ref 17/LO/0563). Demographic and clinical characteristics of HPAH patients and healthy volunteers are shown in Table 2.3. The *BMPR2* genotype in PAH ECFC is also shown in Table 2.3.

The cells were cultured in endothelial cell growth medium-2 (EGM-2, Lonza, Cat. No. CC-3156) containing 20% FBS (HyClone; GE Healthcare, USA, Cat. No. SH30070.03), 1% penicillin (100 U/mL)-streptomycin (100µg/mL, Invitrogen, UK, Cat. No. 15140- 122) and growth factors (EGM-2 bullet kit, Lonza, Cat. No. CC- 4176) in T75 culture flasks pre-coated with 1% gelatin. They were then incubated at 37 °C, 21% O_2, 5% CO_2. ECFCs were used for experiments between passages 3 and 6.

		Control (n=5)	HPAH (n=5)
Females		4/5	3/5
Age (years)		29 (23- 56)	43 (30-58)
Time from diagnosis (months)		-	84 (29-171)
mPAP (mmHg)		-	58 (58-70)
Six-minute walk distance (m)		-	366 (261-441)
WHO Functional Class	**I**	-	3
	II	-	1
PDE5 Inhibitors		-	5
ET-1R Antagonists		-	5
Prostanoids		-	2
Anticoagulants		-	3
Statins		-	1

Table 2.3: Demographic and clinical characteristics of HPAH patients and healthy volunteers. Data represented as median (range). mPAP=mean Pulmonary Arterial Pressure; PDE5=Phosphodiesterase type 5; ET-1R=Endothelin-1 Receptor.

2.3 Manipulation of gene expression in HPAECs

2.3.1 Adenoviral gene transfer

The overexpression of KLF2, KLF4 and KLF6 was achieved by adenoviral gene transfer (AdKLF2-GFP, AdKLF4, AdKLF6). AdGFP was used as an adenoviral control (AdCTRL) for KLF2, while AdTet-off was used as an adenoviral control (AdCTRL) for KLF4 and KLF6.

The long (L) isoforms of KLF2 and KLF4 and KLF6 listed in Table 2.4 were purchased from Vector Biolabs (Pennsylvania, USA). AdTet-off was a kind gift from Professor Stuart Yuspa (National Cancer Institute, NIH, Bethesda, USA), and its construction procedure is described in (Suh et al., 2004).

All recombinant adenoviral (Ad) constructs used in this study were produced using a human adenovirus serotype 5 (hAd5) vector with deletions in the E1 and E3 gene regions (ΔE1/ΔE3). This included target protein expression either with or without reporter genes such as green fluorescent protein (GFP), haemagglutinin (HA), and FLAG *(*DYKDDDDK) co-expression, driven by a cytomegalovirus (CMV) promoter. The deletion of the E1 and E3 gene regions was undertaken because the E1 region is not essential for viral replication and its deletion is important to allow the virus to be safely used as a gene delivery tool. The E3 region was deleted because it too is uninvolved in the replication of the virus. The deletion of both regions results in a higher packaging capacity allowing larger recombinant genes (up to 8 Kb) to be incorporated into the backbone.

All adenoviruses used in this study were multiplied in human embryonic kidney cells (HEK293A, Invitrogen, Cat. No. R70507). These cells were cultured in T25 flasks in a 5 mL DMEM medium supplemented with 5% FBS, 4500 mg/L glucose, L-glutamine and sodium pyruvate, but without penicillin-streptomycin, and were transduced with 50 µL of adenovirus stock at 80% confluence. Cells were then incubated in a humidified incubator at 37°C, 21% O_2, 5% CO_2 for roughly 4 days. Once the complete lysis of infected cells was achieved the flask was then frozen at -80°C. After thawing the cell lysate, the lysate was then transferred to a T75 flask containing confluent HEK293A cells and was incubated for approximately 4 days. Once all infected cells had been lysed, the T75 flask was freeze-thawed 3 times before transferring the medium into nine T175 flasks containing confluent HEK293A cells. The cells were then incubated for roughly 2 days until the cells were detached but sill retained an intact

cell membrane. Cell pellets were then harvested and transferred into 50 ml falcon tubes which were snap-frozen in liquid nitrogen three times to enable cell lysis. Adenoviruses were then purified using a caesium chloride (CsCl) density gradient for two cycles of centrifugation at 60,000 g for 24 hours. The collected sample was then passed through PD10 desalting columns (GE Healthcare, USA, Cat. No. GE17-0851-01) to reduce salt concentrations. Following cytopathic effects (CPE) scoring in HEK293A cells plated in 96-well plates, the titre of all the adenoviruses was determined and is listed in Table 2.4.

Adenovirus name	Target overexpression	Reporter /Tag	Titre (PFU/ml)	Cat No.	Company
Ad-h-KLF2-GFP	KLF2	GFP	2.79×10^9	ADV-213187	Vector Biolabs
Ad-h-KLF4-FLAG	KLF4	FLAG	$2.51X10^{10}$	ADV-213191	
Ad-h-KLF6-HA	KLF6	HA	$1.58X10^{10}$	ADV-213194	
Ad-NFκB-luc	NFκB	Luc	2.786×10^8	1740	
Ad-GFP	GFP	GFP	5.48×10^{10}	1060	
AdTet-off	None	-	2×10^{11}	-	Gift from Professor Stuart Yuspa

Table 2.4: List of adenoviral constructs used in this study.

2.3.2 Adenoviral Infection of HPAECs

HPAECs were cultured in 6-well cell culture plates or 8-well ibidi µ-slides (Thistle Scientific, UK, Cat. No.IB-80829). At 80% confluency, the cells were infected with AdCTRL, AdGFP, AdKLF2, AdKLF4, AdKLF6 and Ad-NFκB-Luc at a multiplicity of infection (MOI) of 1:100. Adenoviral vector maps for AdCTRL-GFP, AdKLF2-GFP, AdKLF4, AdKLF6, and Ad-NFKb-Luc are shown in Supplementary Figures S1, S2, S3, S4 and S5. MOIs were optimised to achieve equal overexpression levels of KLF2, KLF4 and KLF6. 3 hours post infection, the EGM2 media were replaced with a fresh medium, and the cells were then incubated at 37°C, 21% O_2, 5% CO_2 for 24 hours to allow for target gene overexpression before further experimentation.

2.3.3 siRNA

2.3.3.1 siRNA of KLF6

The knockdown of KLF6 expression was performed using silencer select siRNA targeting KLF6 (siRNA-KLF6, Thermo Fisher Scientific, UK, Cat. No. s3376). Control siRNA was also used, including a scrambled siRNA control (siRNA-CTRL Cat. No. 4390846) and a positive siRNA control targeting GAPDH (siRNA-GAPDH, Cat. No. 4390849).

HPAECs were cultured in 6-well plates in EGM2 media until confluence reached 90%. After 24 hours of incubation, 6 µl of Lipofectamine RNAiMAX reagent (Thermo Fisher Scientific, UK, Cat. No. 13778075) was diluted in a 100 µl Opti-MEM medium (Thermo Fisher Scientific, UK, Cat. No. 31985070). 2 µl (20 pmol) of the appropriate siRNA (10 µM) was diluted in a 100 µl Opti-MEM medium. Following this, 100 µl of Lipofectamine RNAiMAX/OPTIMEM mix was combined with 100 µl of the siRNA/OPTIMEM mix and the mixture was incubated at room temperature for 5 minutes. During this time, the EGM2 medium was removed from the wells, and the cells were then washed with 1 ml of phosphate buffered saline (PBS; Sigma-Aldrich, UK, Cat. No. D8537).

1 ml of OPTIMEM medium and 100 µl of the siRNA /Lipofectamine RNAiMAX/OPTIMEM mix were added to each well. After 6 hours, the cells were washed with 1 ml of PBS, and the EGM2 media (containing 10% FBS) were added to each well. After 24 hours, the medium was removed, the cells were washed with 1 ml PBS, and 1ml of reduced serum EGM2 (containing 0.2% FBS) was added to each well to synchronise the cells for maximal response to stimuli in further experiments. At 48 hours after transfection, the transfected cells were used for flow experiments.

2.4 Flow experiments

HPAECs were cultured in Nunc Slide Flaskettes (Thermo Fisher Scientific, UK, Cat. No. 170920) until 95% confluent. The bottom slides with the cells were then detached from the flask and placed inside the flow chamber in a parallel flow apparatus (Figure.2.1) (Wojciak-Stothard, 2011). The cells were then subjected to a laminar flow at 4 dynes/cm^2, physiological for lung arteries (Salibe-Filho et al., 2020), for different periods (30 mins,1h, 4h, 6h and 24h). After the flow exposure, the cells were used for RNA extraction and RT-qPCR to measure mRNA expression levels of *KLF2*, *KLF4* and *KLF6*.

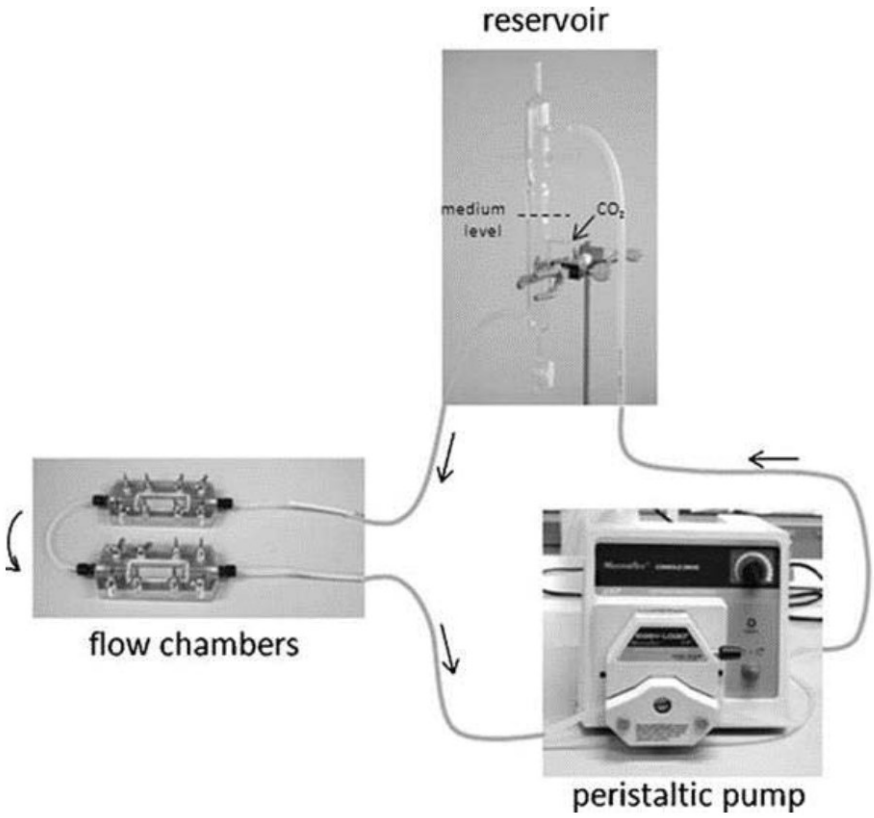

Figure 2.1:Schematic representation of a parallel-plate flow chamber system. Image taken from (Wojciak-Stothard, 2011).

For the knockdown of KLF6, HPAECs were cultured in an ibidi 6 channel µ-Slide VI 0.4 with optical bottom (Thistle Scientific, UK, Cat. No.IB-80806). All channels were then individually connected to media reservoirs (custom designed by Dr. Alex Ainscough) via 0.8 mm tubing (Thistle Scientific, UK, Cat. No. IB-10841) and an Elbow Luer Connector (Thistle Scientific, UK, Cat. No. IB-10802). The media reservoirs were connected to an Ismatec REGLO ICC 4 channel 12 Roller Pump (Cole-Parmer, UK, Cat. No. ISM4412) using 0.76 mm Ismatec Pump tubing (VWR, USA, Cat. No. MFLX95809-24) and 0.76 mm Ismatec Pump tubing (3-Stop) (VWR, USA, Cat. No. MFLX95714-24), connected by stainless steel 20 G tubes, as illustrated in Figure 2.2. The flow rate of all flow experiments was set up to generate a unidirectional flow of 4 dynes/cm^2 for 24h.

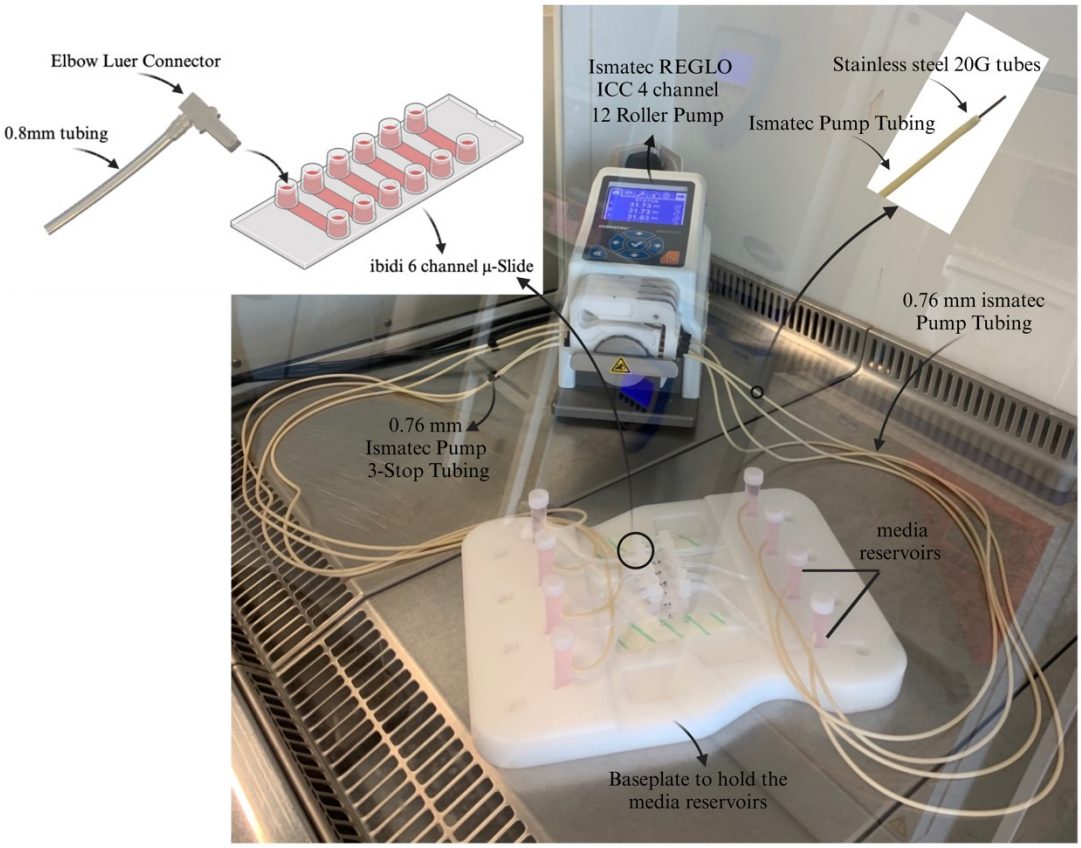

Figure 2.2: Flow system using a 6 channel µ-Slide from ibidi.

2.4.1 Calculation of shear stress

Shear stress in an ibidi 6 channel µ-Slide VI 0.4 (Thistle Scientific, UK, Cat. No.IB-80806) was calculated using the formula for µ-channel VI 0.4 previously adapted by ibidi (https://ibidi.com/img/cms/support/AN/AN11_Shear_stress.pdf), as shown below:

$$\tau = \eta \cdot 176.1 \cdot \Phi$$

Where:

- τ is shear stress (dyn/cm^2)
- η is dynamical viscosity (dyn·s/ cm^2)
-176.1 is a slide-dependent factor.
-Φ is flow rate (ml/min)

This formula was calculated based on the viscosity of the fluid. In this experiment, cell culture medium supplemented with 2% serum has a viscosity of ~ 0.0072 (dyn.s/cm^2) and the flow rate, which indicates the velocity of the perfused fluid in a channel, was set at 3.15 (ml/min) to create a unidirectional flow of 4 dynes/cm^2.

2.5 Real-time quantitative PCR (qPCR), RNA sequencing (RNA-seq) and spatial transcriptomics

2.5.1 RNA extraction

2.5.1.1 RNA extraction from tissues

For the monocrotaline (MCT) rat model of PAH, frozen lung tissue samples were cut into small pieces (approximately 10 mg) on dry ice and were placed in a BioMasher tube (Takara Bio Europe, France, Cat. No. 9791A) containing 100 µl of TRIzol Reagent (Life Technologies, UK, Cat. No. 15596026). The tissues were then manually crushed using a masher provided with the BioMasher tube. After grinding 10-15 times, 600 µl of TRIzol Reagent was added. When homogenization was complete, the homogenized solution was transferred into 1.5 mL Eppendorf tubes. After gentle vortexing for about 30 seconds, 140 µl RNase-free chloroform (Thermo Fisher Scientific, UK, Cat. No. 327155000) was added to the sample and incubated at room temperature for 2-3 minutes and then placed on ice. The mixture was centrifuged at 12,000 g for 15 minutes at 4°C. The upper aqueous phase was transferred into a new Eppendorf tube. 4 µl of Glycogen (5 mg/ml; Thermo Fisher Scientific, UK, Cat. No. AM9510) and 450 µl of Isopropanol (Thermo Fisher Scientific, UK, Cat. No. 327272500) were then added and inverted to mix for 10 seconds. The mixture was placed in a fridge at 4°C for 10 minutes to enhance RNA precipitation, and was then centrifuged at 12,000 g for 10 minutes at 4°C. The supernatant was aspirated, and the pellet was air dried for about 10 minutes. The RNA pellet was then resuspended in 20 µl RNase-free water. The total RNA was quantified using a NanoDrop™ ND-2000 spectrophotometer (Thermo Scientific, UK).

2.5.1.2 RNA extraction from cultured cells

Untreated and treated HPAECs were washed with pre-warmed PBS, then trypsin solution (Gibco, UK, Cat. No. 25200072) was added followed by incubation at 37°C, 21% O_2, 5% CO_2 for roughly 5 minutes. Dulbecco's Modified Eagle's Medium (DMEM; Sigma-Aldrich, UK, Cat. No. D6429), supplemented with 10% foetal bovine serum (FBS; Thermo Fisher Scientific, UK, Cat. No. 10270098), was then added to neutralize the enzymatic reaction of the trypsin. The cell suspension was transferred to a 1.5 ml RNase-free microcentrifuge tube and centrifuged at 500 g for 5 minutes at room temperature. The supernatant was discarded, and the cell pellet was washed once with PBS and pelleted again. The cell pellet was either stored at -80 °C to be used later, or was used immediately for RNA extraction. Before starting the

RNA extraction procedure, the bench surfaces, pipettes and all the equipment were sprayed with RNaseZap™ RNase Decontamination Solution (Invitrogen, USA, Cat. No. AM9780).

Total RNA was extracted using Monarch Total RNA Miniprep Kit (New England Biolabs UK, Cat. No. T2010S) according to the manufacturer's instructions. All centrifugation steps were performed at (8,000-16,000 x g). Briefly, 300 µL of RNA Lysis Buffer containing 1% beta-mercaptoethanol (β-ME) were added to the cell pellet and the sample was vortexed vigorously for 30 seconds to lyse the cells. The mixture was then transferred to a gDNA removal column and centrifuged for 30 seconds to remove the genomic DNA. After centrifuging, the gDNA removal column was discarded and the flow-through in the collection tube which contained the RNA was saved. 300 µL of ethanol (≥ 95%) was added to 300 µL of the flow-through and mixed thoroughly by pipetting up and down. The mixture was then transferred to an RNA Purification Column and centrifuged for 30 seconds. After discarding the flow-through, 500 µL of RNA Wash Buffer was added to the RNA Purification Column and centrifuged for 30 seconds. The flow-through was then discarded, and 500 µL of RNA Priming Buffer was added and centrifuged again for 30 seconds. For the second wash, another 500 µL of RNA Wash Buffer were added and centrifuged for 1 minute. After discarding the flow-through, the RNA Purification Column was placed in an RNase-free microcentrifuge tube, and the RNA was eluted in 50 µL nuclease-free water and centrifuged at a maximum speed of 16,000 x g for 1 minute. The elution step was repeated twice by pipetting the eluted RNA back into the same RNA purification column and centrifuging it for 1 minute to maximize total RNA yield per sample.

Finally, the RNA concentration and purity were determined using a NanoDrop™ ND-2000 spectrophotometer (Thermo Fisher Scientific, UK), and the extracted RNA was stored at -80°C for downstream analyses. RNA integrity and purity were determined by assessing the ratio of absorbance at 260 nm and 280 nm (A260/A280) with values greater than 1.8 considered good quality RNA. For the RNA sequencing experiment, RNA quality was assessed using a TapeStation 2200 system (Agilent Technologies, UK) in the Imperial BRC Genomics Facility at Imperial College London. All samples had RNA Integrity Numbers (RIN) of 8 or higher.

2.5.2 Reverse Transcription (RT)

100 ng of the total RNA was reverse-transcribed into complementary DNA (cDNA) using a LunaScript RT SuperMix Kit (New England Biolabs, UK, Cat. No. E3010L) according to the manufacturer's instructions. 20 µl reaction volume were prepared in 96-well PCR plates (Thermo Fisher scientific, UK, Cat. No. 4306737), as shown in Table 2.5. A negative No-RT control was added to each plate to verify the absence of DNA contamination in the RNA samples. Before the reverse transcription, the PCR plates were sealed, centrifuged and placed in a SimpliAmp™ Thermal Cycler (Applied Biosystems, USA). Thermal conditions are shown in Table 2.6. cDNA samples were then diluted to 1 ng/µL using nuclease-free water and stored at -20°C.

Component	20µL Reaction	Final Concentration
LunaScript RT SuperMix (5x)	4 µl	1X
RNA sample	variable	100ng
Nuclease-free Water	up to 20 µl	-

Table 2.5: Components of the reverse transcription reaction mix. Modified from New England Biolabs (https://uk.neb.com).

Cycle Step	Temperature	Time	Cycles
Primer Annealing	25°C	2 minutes	1
cDNA Synthesis	55°C	10 minutes	1
Heat Inactivation	95°C	1 minute	1
Hold	4°C	∞	1

Table 2.6: Thermal conditions for reverse transcription. Modified from New England Biolabs (https://uk.neb.com).

2.5.3 Real-time quantitative PCR (qPCR)

A qPCR master mix solution was prepared for each gene of interest as described in Table 2.7 below.

Component	10 µL Reaction	Final Concentration
Luna Universal qPCR Master Mix	5 µL	1X
10 µM forward primer	0.5 µL	0.25 µM
10 µM reverse primer	0.5 µL	0.25 µM
Nuclease-free water	3 µL	-
cDNA products	1 µL	1 ng

Table 2.7: Components of qPCR master mix. Modified from New England Biolabs (https://uk.neb.com).

9 µL of qPCR master mix solution were added in a 384-well PCR plate (StarLab, UK, Cat. No. E1042-3840). After preparing the qPCR master mix solution, 1ng/µL of the cDNA sample was first added in a 384-well PCR plate (StarLab, UK, Cat. No. E1042-3840), and 9 µL of qPCR master mix solution was then added to each well of the plate. A negative control was included for each gene of interest in which the cDNA was replaced by Nuclease-free water. The qPCR was carried out using a QuantStudio™ 6 Flex Real-Time PCR System (Applied Biosystems, USA). Amplification steps for qPCR reactions are described in Table 2.8. An example of a qPCR amplification plot is shown below in Figure 2.3.

Cycle Stage	Temperature	Time	Cycles
Hold Stage	50°C	2 minutes	1
	95°C	5 minutes	
PCR Stage	95°C	15 seconds	40
	62°C	30 seconds	
Melt Curve Stage	95°C	15 seconds	1
	60°C	1 minute	
	95°C	15 seconds	

Table 2.8: Cycling conditions for qPCR.

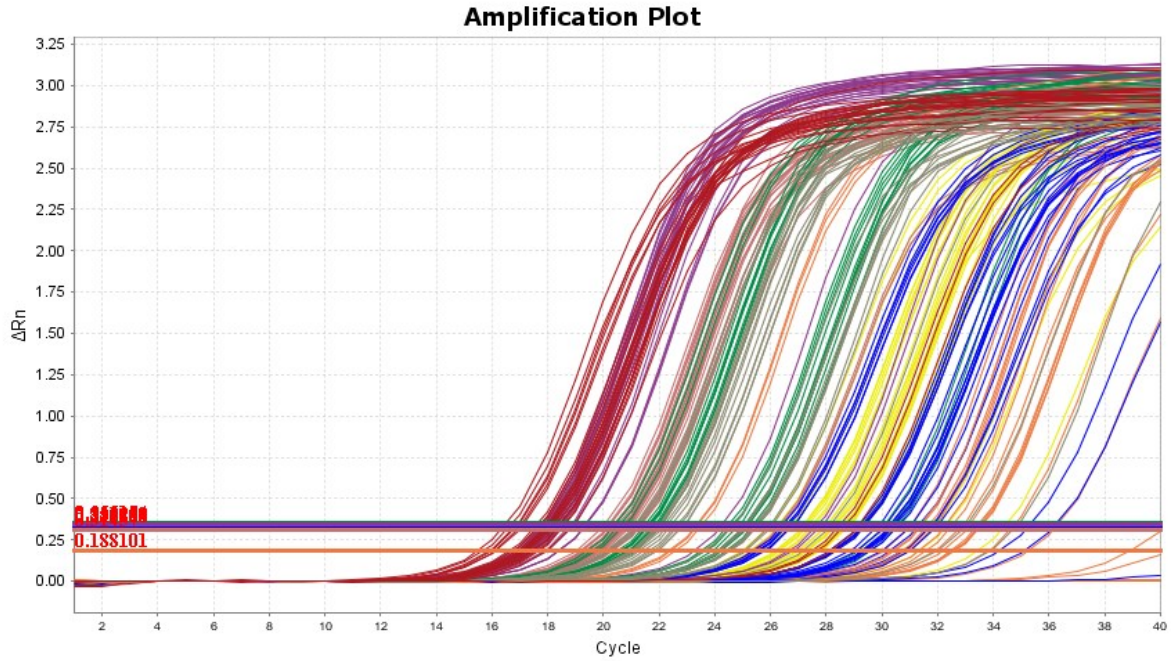

Figure 2.3: Example of a qPCR amplification plot.
In this plot, the x-axis represents cycle number, and the y-axis represents the log of change in fluorescence. Cycle threshold (C_T) indicates the cycle number at which the fluorescent signal within a reaction crosses the threshold line.

Gene-specific primers for qRT-PCR were designed using FASTA sequences (PubMed, NCBI) and PrimerBlast (NCBI, USA), using default parameters. At least one primer in each pair spanned the exon–exon junction. All primer sequences are listed in Table 2.9.

The relative expression level was calculated using the $2^{-\Delta\Delta CT}$ method with a target gene that had been normalized to the expression of appropriate housekeeping gene, which was actin beta (*ACTB*) for static experiments or beta-2 microglobulin (*B2M*) for flow experiments.

Gene	Forward Primer (5'-3')	Reverse Primer (5'-3')
Human		
KLF2	GCAAGACCTACACCAAGAGTTCG	CATGTGCCGTTTCATGTGC
KLF4	TGGACCCCCTCTCAGCAATG	CTCTTGGTAATGGAGCGGCG
KLF6	GGGTGTGGCTCTTTGCTTTA	AGCGTTAGTCACTGCTCATTTC
BMPR2	CTGCGGCTGCTTCGCAGAAT	TGGTGTTGTGTCAGGAGGTGG
SOX17	GGACCGCACGGAATTTGAAC	GGACACCACCGAGGAAATGG
ERG	GGAGTGGGCGGTGAAAGA	AAGGATGTCGGCGTTGTAGC
MKI67	TGCTCCCCACCTCAGAGAGTT	GACCTTCCTGACCTGTTTGCAG
PCNA	GTGAACCTCACCAGTATGTCCAA	ACTAGCGCCAAGGTATCCGC
BRD4	GATTGCCGGCTCCTCCAAGAT	ATGGTGCTTCTTCTGCTCCCTC
PECAM1	TGGAAGGAGTGCCCAGTCCCA	CGGAAGGATAAAACGCGGTCCTG
CDH5	CCTCCGATACATGAGCCCTCC	TCGGAAGAACTGGCCCTTGT
KDR	CACCAGAAATGTACCAGACCATGC	AGTCCAGAATCCTCTTCCATGCTC
HES1	AGAAAGATAGCTCGCGGCATT	CGGAGGTGCTTCACTGTCAT
FLT1	GTTTCCAGACCCGGCTCTCT	TGGTTACAGGGGTGCCAGAA
TIE2	CCCTGAATGCCCCAAACGTG	ACGGACCAGTTGCACACAGA
SLC2A1	GGGCCAAGAGTGTGCTAAAGA	GGTGACCTTCTTCTCCCGCA
ACTB1	GCACCACACCTTCTACAATGA	GTCATCTTCTCGCGGTTGGC
B2M	CCAGCGTACTCCAAAGATTCAGG	TCAATGTCGGATGGATGAAACCC
Rat		
ACTB	ACCCCAGCCATGTACGTAGC	TGCCTGGGTACATGGTGGTG
KLF2	ACTTGCAGCTACACCAACTG	CTGTGACCCGTGTGCTTG
KLF4	TGAACTGACCAGGCACTACC	GCCTCTTCATGTGTAAGGCA
KLF6	CGGACGCACACAGGAGAAAA	CGGTGTGCTTTCGGAAGTG
Mouse		
B2M	GCCTGTATGCTATCCAGAAAACC	TCAATGTGAGGCGGGTGGAA
KLF2	GAGCCTATCTTGCCGTCCTTT	CACGTTGTTTAGGTCCTCATCC
KLF4	CCAGAGGAGCCCAAGCCAAAG	CGGTAGTGCCTGGTCAGTTCAT
KLF6	ACTGTCTTTTCCAACCCGAC	AAGATAGCGTTCCAACTCCAG

Table 2.9: Primer sequences used for qPCR.

2.5.4 RNA Sequencing

RNA sequencing (RNA-seq) (75bp paired-end reads) was performed in an Illumina NextSeq 2000 sequencer (Illumina, USA) at the Imperial BRC Genomics Facility (Imperial College London) to assess the whole transcriptomic effects of KLF2, KLF4, and KLF6 overexpression by adenoviral gene transfer (AdKLF2, AdKLF4 and AdKLF6 conditions, respectively).

The quality of the paired end reads within the fastq files were assessed using FastQC (https://www.bioinformatics.babraham.ac.uk/projects/fastqc/) and MultiQC (Ewels et al., 2016). To determine transcript abundance values and obtain gene counts, Salmon (v1.5.2) (Patro et al., 2017) was used to map sequencing reads in the fastq files to the human genome (GENCODE v44) (https://www.gencodegenes.org/human/) (Frankish et al., 2020). To identify differentially expressed genes (DEGs), the gene expressions of the AdKLF2, AdKLF4 and AdKLF6 conditions (n=4 biological replicates/condition) were compared with the corresponding negative control conditions using the R package DESeq2 (v1.38.3) (Love, Huber & Anders, 2014), with default settings. Volcano plots of differential gene expression data were generated using the R package Enhanced volcano (v1.16.0) (Blighe, Rana & Lewis, 2019) and heatmaps were produced using the R package pheatmap (v1.0.12) (Kolde, 2019). Gene annotation was performed using biomaRt (2.46.3) (Durinck et al., 2009). The PAH genes for the heatmap were taken from (Haensel & Wojciak-Stothard, 2023; Welch et al., 2023). All the steps mentioned above were carried out by Dr Nadia Fernandes (Imperial BRC Genomics Facility).

2.5.4.1 Gene ontology (GO) and Kyoto Encyclopaedia of Genes and Genomes (KEGG) enrichment analysis

GO and KEGG pathway enrichment analyses were carried out separately on the sets of up- and down-regulated genes from each comparison using the Metascape (https://metascape.org) online tool (Zhou et al., 2019b), the WEB-based GEne SeT AnaLysis Toolkit (WebGestalt) (https://www.webgestalt.org) (Liao et al., 2019) and the clusterProfiler package (v3.14.3) in R. The DisGeNET enrichment analysis of up- and down-regulated genes was performed using Metascape (Zhou et al., 2019b). A network of enriched terms was generated separately for up and down-regulated genes using Metascape (Zhou et al., 2019b). Genes that passed the thresholds of FDR <0.01, $\log_2|FC|>2$ were used for GO and KEGG pathway enrichment analyses, unless indicated otherwise.

2.5.4.2 Comparative analysis with published RNA-seq datasets and disease-gene databases.

To investigate whether differentially expressed genes from KLF6-overexpressing HPAECs were enriched in PAH-related genes, a comparative analysis was carried out using RNA-seq datasets from HPAECs and ECFCs from the “double hit” microfluidic model of PAH

(Ainscough et al., 2022c), and from PAECs that had been isolated from IPAH patients (Rhodes et al., 2015) or with a previously curated list of PAH-associated genes (named herein as "known PAH genes") (Reyes-Palomares et al., 2020). Overlapping genes were visualized as UpSet plots using the ComplexUpset package (v1.3.3) in R (Krassowski et al., 2022). The significance of the overlaps between gene sets in comparison to the genomic background was calculated by Fisher's exact test using the GeneOverlap package (v.1.22.0) in R (Shen, 2016).

2.6. Spatial transcriptomics

To assess the transcriptomic changes in PAH lungs, spatial transcriptomics of lung tissues from healthy volunteers and PAH patients were carried out using NanoString GeoMx® to enable high-plex spatial profiling of RNA or protein within specific areas of interest in the tissue (Hernandez et al., 2022).

Formalin-fixed, paraffin-embedded (FFPE) lung tissue sections (3-4 μm) from PAH patients (n = 6) and age- and sex-matched healthy volunteers (n = 5) were obtained from the Royal Papworth Hospital NHS Foundation Trust Tissue Bank (Cambridge, UK) with informed written consent and ethical approval by (ICHTB HTA licence: 12275; REC Wales approval: 22/WA/0214). Donor information for FFPE lung tissue samples is shown in Table 2.10.

Pair	Category	Age	Sex
1	Control	49	Female
	PAH	32	Female
2	Control	53	Female
	PAH	51	Female
3	Control	60	Female
	PAH	57	Female
4	Control	21	Male
	PAH	27	Male
5	Control	58	Male
	PAH	37	Male
6	Control	64	Male
	PAH	61	Male

Table 2.10: List of human lung tissue donors used in this study. We excluded the first control (a 49-year-old female) due to the remodelled appearance of the lung tissue.

The antibodies that were used for morphological markers were validated using the immunohistochemistry protocol described in Section 2.7.2. Slide preparation for digital spatial profiling (DSP) in GeoMx was performed by Nathalie Lambie at the Imperial BRC Genomics

Facility (Imperial College London). The lung tissue slides were first hybridized overnight at 37°C with GeoMx Human Whole Transcriptome Atlas RNA probe mix (GeoMx Hu WTA, NanoString Technologies, USA). After incubation with the RNA probe mix, stringent washes were performed using a mixture of an equal volume of 100% (v/v) formamide and 4X saline-sodium citrate (SSC) to remove off-target probes and the slides were then blocked with 200 µL Buffer W (NanoString Technologies, USA) and incubated for 30 minutes at room temperature in a humidity chamber. The Slides were stained with SYTO 13 (nuclear marker), vWF (von Willebrand Factor; endothelial cell marker), and ACTA2 (Alpha-smooth muscle actin or α-SMA; smooth muscle cell marker) to allow the identification of blood vessels during the ROI selection. The Slides were then washed with 2x SSC for 5 minutes twice and immediately loaded into the GeoMx Digital Spatial Profiler (DSP) instrument for scanning (x20 magnification) and ROI selection. For each lung tissue section, a total of 30-45 regions of interest (ROIs) were selected with the "circle" or "freehand" selection tool available on the GeoMx DSP software to profile blood vessels within the lungs, specifically focusing on plexiform lesions observed in PAH patients. After ROI selection on the GeoMx DSP instrument, the DSP barcodes in ROIs were ultraviolet (UV)-cleaved and collected into a 96-well DSP collection plate before being sequenced on an Illumina sequencer (Illumina, USA) at the Imperial BRC Genomics Facility (Imperial College London).

2.6.1 Data analysis and visualization

The raw counts were processed using NanoString's GeoMx NGS pipeline software V2.2 (Nanostring Technologies, USA), where they were converted into digital count conversion (DCC) files. The GeomxTools package (V3.5.0) was used for quality control (QC), and the downstream analysis of the DCC files was performed using R (Ortogero et al., 2023). Differential gene expression analysis was performed using a linear mixed model (LMM) as recommended in the GeomxTools manual. The adjusted p values were calculated using the Benjamini-Hochberg multiple test correction, and differentially expressed genes in all analyses were defined as FDR <0.05, $\log_2|FC|>0.25$. For spatial deconvolution, the SpatialDecon R package (Danaher et al., 2022) was used to identify the cell type composition of each ROI using the idiopathic pulmonary fibrosis (IPF) Lung Cell Atlas (Adams et al., 2020) as the cell profile matrix, which is composed of 36 cell types. All the steps discussed above were carried out by Dr Felicia New (NanoString Technologies, USA).

Gene ontology and KEGG pathway analyses were performed using the WEB-based GEne SeT AnaLysis Toolkit (WebGestalt) (https://www.webgestalt.org) (Liao et al., 2019). The ComplexUpset R package (v1.3.3) was used to visualize the number of overlapping genes between different DE gene datasets (Krassowski et al., 2022). The GeneOverlap R package (v.1.22.0) was used to test the degree and significance of overlap between two gene lists in comparison with a genomic background using Fisher's exact test (Shen, 2016).

2.7 Immunostaining

2.7.1 Immunocytochemistry (ICC)

Cells were cultured in ibidi 8-well chamber slides (Thistle Scientific, UK, Cat. No. IB-80806) or on plastic coverslips (13mm diameter, Nunc Thermanox, USA, Cat. No. 174950). They were then washed once with pre-warmed PBS and fixed with 4% paraformaldehyde (w/v) (Sigma-Aldrich, UK, Cat. No. P6148) in PBS for 15 minutes at room temperature. After fixation, the cells were washed twice with PBS and permeabilized using 0.1% Triton X-100 (v/v) (Sigma-Aldrich, UK, Cat. No. 9002-93-1) in PBS for 3 minutes at room temperature. They were then gently washed twice with PBS.

For immunostaining of nuclear KLF6, the PBS was completely removed, and the cells were incubated in cold 100% methanol for 5 minutes at -20°C, then air dried for 1 minute. The non-specific binding sites were then blocked by incubating cells with 2% bovine serum albumin (w/v) (BSA; Sigma-Aldrich, UK, Cat. No. A2058) in PBS for 15 minutes at room temperature, followed by incubation with primary antibody overnight at 4 °C, then secondary antibody for 2 hours at room temperature. Primary and secondary antibodies were both diluted in 0.1% BSA (v/v) in PBS. After each incubation time with the antibody, the cells were washed three times for 5 minutes in PBS. All primary and secondary antibodies used are listed in Table 2.11. Samples were then mounted in Vectashield antifade mounting medium containing 4'6'-diamidino-2-phenylindole (DAPI) (Vector Laboratories, Cat. No. H-1200-10).

Immunofluorescence images were acquired using a STELLARIS 8 inverted confocal microscope (Leica Microsystems, Mannheim, Germany) at 10x or 20x objectives.

2.7.2 Immunohistochemistry (IHC)

Immunohistochemical staining was carried out as described in (Wojciak-Stothard et al., 2014) with some modifications. Briefly, formalin-fixed, paraffin-embedded (FFPE) lung tissue sections of healthy volunteers (n = 5) and PAH patients (n = 6) (for further details, see Table 2.10) were dewaxed in Histo-Clear (National Diagnostics, USA, Cat. No. HS-202) twice for 5 minutes, before being rehydrated in a graded series of ethanol solutions (100%, 70% and 50%) (v/v) in distilled water (VWR, UK, Cat. No. 20821.330) for 5 minutes each, and then washed twice in distilled water for 5 minutes per wash to rehydrate the tissues. The sections were then subjected to antigen retrieval by boiling them at 95°C for 10 minutes (2 x 5 minutes on a hot plate to avoid overboiling) in a solution containing 40 ml of low pH IHC Antigen Retrieval Solution (v/v) (Life Technologies, UK, Cat. No.00-4955-58) and 360 ml of distilled water. The sections were then washed in PBS three times for 5 minutes per wash. After air-drying, the tissue sections were encircled with a Hydrophobic Barrier PAP Pen (Thermo Scientific, UK, Cat. No. R3777). The tissue sections were then blocked with 5% bovine serum albumin (BSA) (v/v) in PBS with 4 drops of 2.5% normal horse serum (Vector Laboratories, USA, Cat. No. S-2012) added, and incubated for 1 hour at room temperature in a humidified chamber. After the removal of the blocking solution, sections were incubated overnight with primary antibodies diluted in 5% BSA in PBS in a humidified chamber at 4 °C before being washed with PBS three times for 5 minutes per wash. The sections were then incubated with secondary antibodies diluted in 5% BSA in PBS for 2 hours at room temperature in a humidified chamber before being washed with PBS three times for 5 minutes per wash. The primary and secondary antibodies used are listed in Table 2.11. The slides were then mounted in Vectashield antifade mounting medium containing 4'6'-diamidino-2-phenylindole (DAPI) (Vector Laboratories, Cat. No. H-1200-10). Immunofluorescence images of lung tissues were acquired using a STELLARIS 8 inverted confocal microscope (Leica Microsystems, Mannheim, Germany).

Antibody Name	Species	Type	Dilution	Cat No.	Company
KLF2 (Anti-Human)	Mouse	Monoclonal IgG	1:200	MAB5466	R&D Systems
KLF4/GKLF (Anti-Human)	Mouse	Monoclonal IgG	1:100	sc-393462	Santa Cruz Biotechnology
KLF6 (Anti-Human)	Mouse	Monoclonal IgG	1:100	sc-365633	Santa Cruz Biotechnology
KLF6 (Anti-Human)	Rabbit	Polyclonal IgG	1:100	PA5-84819	Invitrogen

ERG (Anti-Human)	Mouse	Monoclonal IgG	1:200	sc-376293	Santa Cruz Biotechnology
VE-Cadherin/CD144 (Alexa Fluor 488) (Anti-Human)	Mouse	Monoclonal IgG	1:200	53-1449-42	Invitrogen
α-SMA (Cy3-Conjugated) (Anti-Human)	Mouse	Monoclonal IgG	1:300	C6198	Sigma-Aldrich
CD31/PECAM1 (Anti-Human)	Mouse	Monoclonal IgG	1:500	M0823	Dako
HA-Tag (Anti-Human)	Rabbit	Monoclonal IgG	1:300	C29F4	Cell Signaling Technology
FLAG (Anti-Human)	Rabbit	Polyclonal IgG	1:300	F7425	Sigma-Aldrich
vWF (Anti-Human)	Rabbit	Polyclonal IgG	1:200	A0082	Dako
Cy5-Conjugated (anti-Mouse)	Goat	Polyclonal IgG	1:200	16855-AAT	AAT Bioquest
Alexa Fluor Plus 594 (Anti-Mouse)	Goat	Polyclonal IgG	1:200	A32742	Invitrogen

Table 2.11: List of primary and secondary antibodies used for immunofluorescence staining. vWF, von Willebrand factor; α-SMA and α-Smooth Muscle Actin. In addition to primary and secondary antibodies, phalloidin-TRITC (Bio-Techne, UK, Cat. No. 5783) was used as an affinity-stain for filamentous actin (F-actin) in endothelial cells.

2.8 Functional assays

2.8.1 NF-κB luciferase reporter assay

HPAECs that had been cultured in 96-well plates or in 6 channel µ-Slides (Thistle Scientific, UK, Cat. No. IB-80806) were left untreated or were infected with adenoviral NF-κB luciferase reporter (AdNFkB-luc, Vector Biolabs, Cat. No.1740), AdCTRL and AdKLF6 or were transfected with KLF6-siRNA and scrambled-siRNA control, as required. The NF-κB luciferase adenovirus (AdNFκB-luc) contains a firefly luciferase gene driven by four copies of the NF-κB consensus binding sequence fused to a TATA-like promoter from the herpes simplex virus thymidine kinase gene (Wojciak-Stothard et al., 2014).

24 hours after adenoviral infection or 48 hours after siRNA exposure, the culture media were replaced with a fresh EGM2 medium with or without 10 ng/ml of TNF-α (R&D Systems, USA, Cat. No. 210-TA-020). The cells were then incubated under either normoxic or hypoxic conditions for 24 hours. A luciferase reporter assay (Promega, USA, Cat. No. E1500) was then performed according to the manufacturer's instructions. Briefly, 20 µl of cell lysates were combined with 100 µl of luciferase assay reagent in 96-microwell white opaque polystyrene

plates (Thermo Scientific, UK, Cat. No. 136101). The intensity of luminescence, proportional to the level of NF-κB–driven luciferase activity, was measured in GloMax® luminometer (Promega, UK).

2.8.2 Transwell permeability assay

A cell permeability assay was carried out using a 6.5 mm transwell plates with sterile 0.4 μm pore size polycarbonate membrane inserts (Corning, USA, Cat. No. 3413). A schematic illustration of this assay is shown in Figure 2.4.

Cells were seeded at a density 2 x10^4 cells per insert with 200 μL of cell culture medium in the apical compartments of transwell inserts that had been pre-coated with bovine plasma fibronectin (10 μg/mL, EMD Millipore Corp, USA, Cat. No. 341631). 500 μL of the medium was then added to the basal compartments of the transwell. Once the cells formed a confluent monolayer, they were infected with either AdCTRL or AdKLF6. After 3 hours of adenoviral infection, the media were changed and the cells were either left untreated or were treated with 10 ng/mL of TNF-α (R&D Systems, USA, Cat. No. 210-TA-020). The cells were then placed in normoxia (21% O_2) or hypoxia (2% O_2) at 37°C and 5% CO_2 for 24 hours. After this period, the cells were incubated in fresh medium containing 1 mg/mL of 40 kDa FITC-Dextran (Sigma-Aldrich, Dorset, UK, Cat. No. FD40S) for 1 hour. After an hour of incubation, 500 μL of the medium was collected from the basal compartment, and the fluorescence intensity of FITC- dextran was measured at excitation/emission 490/525 nm using a GloMax® luminometer (Promega, UK).

To test thrombin-induced cell permeability, cells were infected with either AdCTRL or AdKLF6. 24 hours post-infection, they were left untreated or stimulated with 1 U/mL of thrombin (Sigma-Aldrich, Dorset, UK, Cat. No. T7513) in a serum-free medium containing 1 mg/mL FITC-Dextran for 1 hour, then the rest of experiment was carried out as described above.

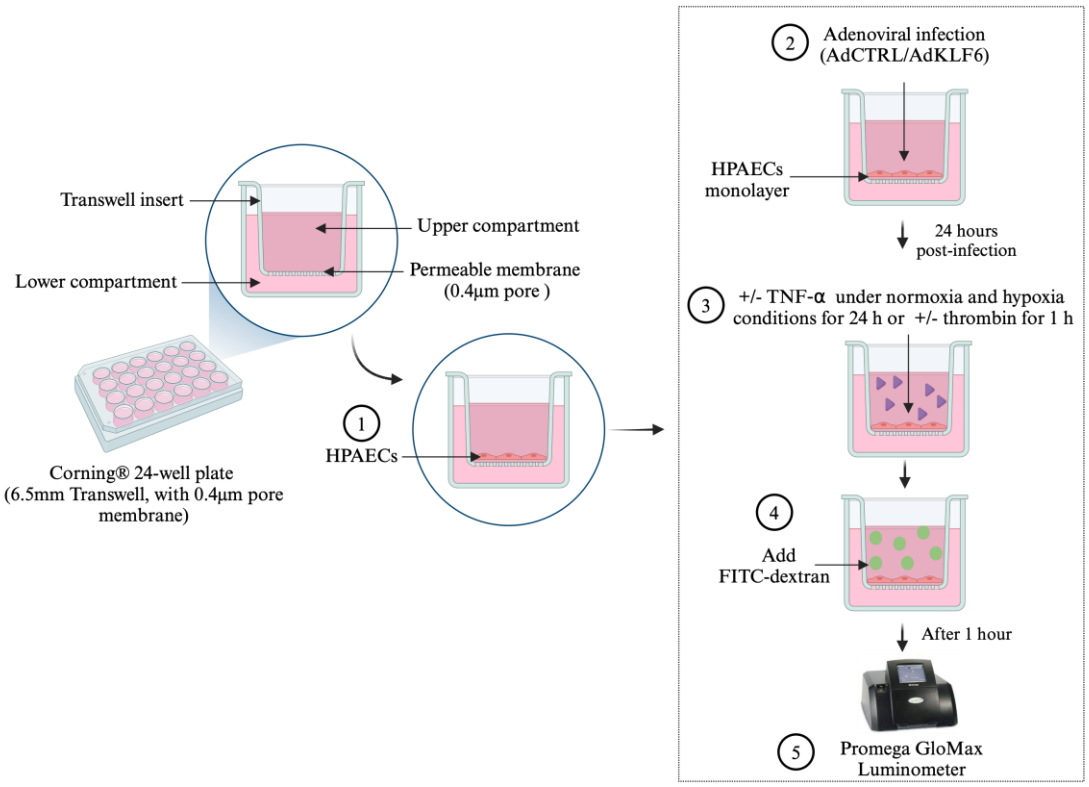

Figure 2.4: Schematic illustration of transwell permeability assay. Illustration created by the author using BioRender.com.

2.8.3 Angiogenesis assay

Angiogenesis was assessed in a tube formation assay *in vitro* and in an *ex vivo* pulmonary arterial explants sprouting assay.

2.8.3.1 Tube formation

For the tube formation assay, HPAECs were infected with either AdCTRL or AdKLF6. 24 hours post-infection, the cells were seeded into a 96-well plate pre-coated with growth factor-reduced Matrigel (Scientific Laboratory Supplies, UK, Cat. No. 354230). The cells were then incubated for 20 hours under normoxic conditions. After 20 hours of incubation, endothelial tube formation was imaged using a phase-contrast microscope (ECHO Rebel, USA) or an inverted fluorescent microscope (Olympus IX70) after fluorescent labelling of the cells with Vybrant™ CFDA SE Cell Tracer (Invitrogen, USA, Cat. No. V12883). Images were then analysed using ImageJ software (Fiji, version 2.14.0) with an Angiogenesis Analyzer plugin to quantify the number of nodes and meshes as well as the total tube length.

2.8.3.2 Arterial explants sprouting experiments *ex vivo.*

For the arterial explants sprouting assay, surgical samples of human pulmonary arteries were cleaned of blood and attached connective tissues in PBS. A schematic illustration of this assay is shown in Figure 2.5.

Donor characteristics – including age, gender, height, weight and diagnosis – are summarized in Table 2.12. The arteries were then cut longitudinally with a scalpel, opened up and pinned down on the dissection dish with the endothelium facing up. 100 µL of EGM2 containing AdCTRL or AdKLF6 was added on top of the endothelial cells, and the explants were then incubated for 3 hours in a humidified incubator. Afterwards, the arterial tissue was thoroughly washed with PBS and cut into roughly 1 mm^2 fragments which were then embedded in growth factor-reduced Matrigel (Scientific Laboratory Supplies, UK, Cat. No. 354230) and incubated for 3 weeks in a humidified incubator under normoxic conditions. AdCTRL or AdKLF6 was added to the explants again at 2 weeks to maintain the efficiency of gene transduction. Endothelial sprouts were fluorescently labelled with Vybrant™ CFDA SE Cell Tracer (Invitrogen, USA, Cat. No. V12883) before being imaged under an inverted fluorescent microscope (Olympus IX70). The total area of sprouting was measured using ImageJ software (Fiji, version 2.14.0).

To confirm the efficiency of adenoviral transduction in the endothelium of human pulmonary artery explants, surgically removed pulmonary arteries were opened, and the endothelial side was incubated with AdGFP for 24 hours. After 24 hours of incubation, the tissues were fixed and stained for endothelial adherens junction marker VE-cadherin. Images were acquired using a STELLARIS 8 inverted confocal microscope (Leica Microsystems, Mannheim, Germany).

ID	Age	Gender	Height (cm)	Weight (kg)	Diagnosis
CX22000050	56	M	170	79.8	Pulmonary AVM
CX22000077	33	F	160	88.9	Pulmonary AVM
CX22000115	70	F	158	53	Non-mucinous lung ADC
CX22000116	21	F	157	45.7	Pulmonary AVM
CX22000221	72	M	181	76	Non-mucinous lung ADC

Table 2.12: Pulmonary artery donor characteristics. ADC: adenocarcinoma, AVM: arteriovenous malformation.

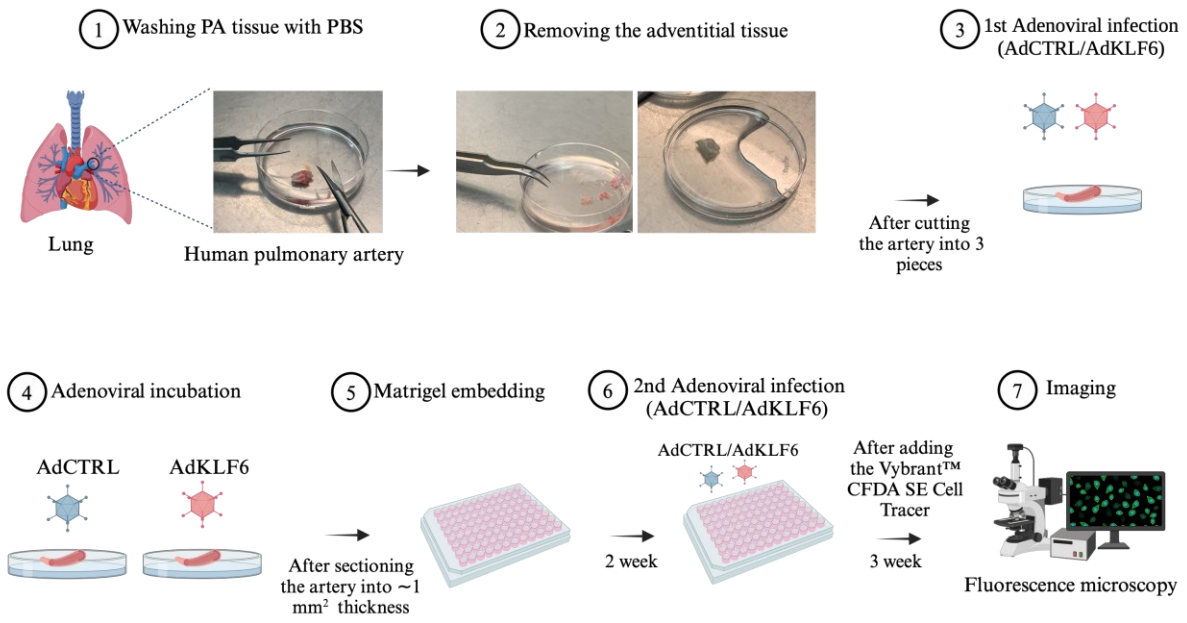

Figure 2.5: Schematic representation of arterial explants sprouting assay. Illustration created by the author using BioRender.com.

2.8.4 EdU Cell Proliferation Assay

Cell proliferation was measured by an EdU Cell Proliferation Assay Kit (EdU-594, EMD Millipore Corp, USA, Cat. No. 17-10527), according to the manufacturer's instructions. EdU nucleotides were added at a dilution of 1:1000 in a cell culture medium and incubated for 24 hours.

Cells were fixed with 3.7% formaldehyde (v/v) in PBS for 15 minutes and permeabilized using 0.5% Triton X-100 (Sigma-Aldrich, UK, Cat. No. 9002-93-1) (v/v) in PBS for 20 minutes at room temperature. The cells were washed twice with PBS containing 3% bovine serum albumin (w/v) (BSA; Sigma-Aldrich, UK, Cat. No. A2058) between each step. The cells were then treated with an EdU reaction cocktail which was prepared according to the manufacturer's instructions, and incubated for 30 minutes at room temperature.

The cells were then washed three times with 3% BSA (w/v) in PBS and mounted with Vectashield antifade mounting medium containing DAPI (Vector Laboratories, Cat. No. H-1200-10). Images of EdU positive cells were acquired under a fluorescent Zeiss Axio Observer

widefield microscope (Carl Zeiss AG, Germany) at a 10x magnification and analysed with ImageJ software (Fiji, version 2.14.0). The results were quantified as a ratio of the number of EdU-positive cells to the total number of cells.

2.8.5 Wound healing assay

Endothelial cell migration was assessed by a wound healing assay using ibidi Culture-Insert 2 Well in μ-Dish 35 mm (ibidi, Germany, Cat. No. 81176) or a scratch assay under flow.

For the experiments using the ibidi Culture-Insert 2 Well, cells were seeded at a density of $3x10^4$ cells per well. After overnight incubation, the cells were infected with either AdCTRL or AdKLF6. 24 hours post-infection, the cells were serum- and growth factor starved (0.2% FBS, with no growth factors) for 6 hours to suppress cell proliferation. Culture inserts were removed after starvation, and the cells were washed with PBS to remove non-adherent cells. They were then either left in a starvation medium (0.2% FBS, with no growth factors) or were stimulated by the addition of complete EGM2 medium containing serum and growth factors (EGM2, 2 mL) to the dish. Images of the cells were captured at 0 hour and 20 hours using a phase contrast microscope (ECHO Rebel, USA) with a 10x objective.

In the scratch assay, cells were seeded in Nunc Lab-Tek Flaskettes (Thermo Fisher Scientific, UK, Cat. No. 170920) at a density of 2 $x10^5$ cells per Flaskette. After overnight incubation, the cells were transfected with KLF6-siRNA or scrambled-siRNA control. After 48 hours, the confluent endothelial cell monolayers were serum- and growth factor starved (0.2% FBS, with no growth factors) for 6 hours. The bottom slides containing the cells were then detached and placed into petri dishes (150 x15 mm standard style, VWR International Ltd, UK, Cat. No. 391-2003). A straight "wound" was created by scratching endothelial monolayers with a sterile 200 μL pipette tip. The slide was then washed in PBS and placed inside the flow chamber of a parallel flow apparatus, where the cells were exposed to laminar flow (4 dynes/cm^2) for 20 hours. Images of the wound were taken at 0 hour and 20 hours using a phase contrast microscope (ECHO Rebel, USA) with a 10x objective.

The wound area was measured using a custom-made Wound Healing Tool ImageJ macro (written by Stephen Rothery, Facility for Imaging by Light Microscopy (FILM), Imperial College London).

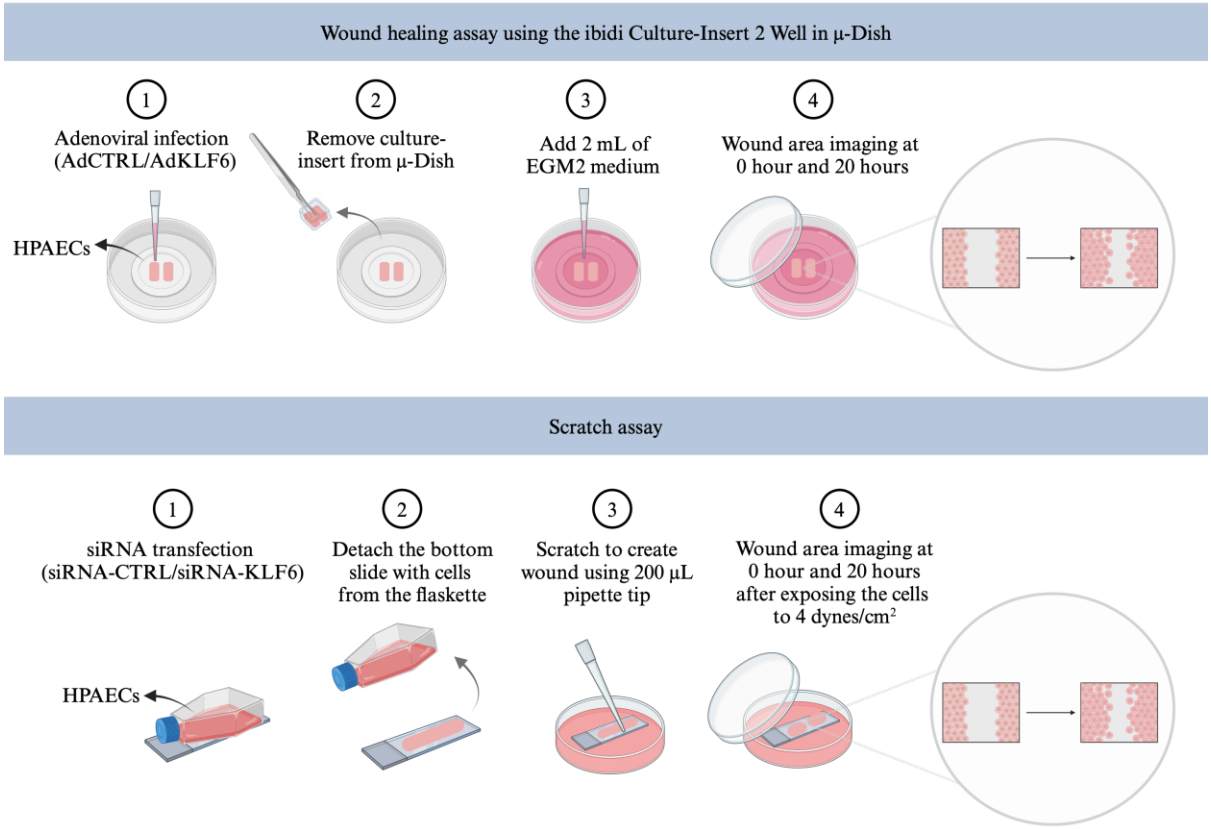

Figure 2.6: Schematic illustration of two cell migration assays. Endothelial cell migration was assessed by a wound healing assay using the ibidi Culture-Insert 2 Well in µ-Dish or a scratch assay. Illustration created by the author using BioRender.com.

2.8.6 Apoptosis Assay

2.8.6.1 Caspase-Glo 3/7 Assay

Apoptosis was assessed by measuring caspase 3/7 activity using a Caspase-Glo 3/7 Assay Kit (Promega, Southampton, UK, Cat. No. G8091), according to the manufacturer's instructions. Briefly, following the cell treatments, Caspase-Glo 3/7 reagent was prepared by adding a Caspase-Glo 3/7 substrate to buffer and allowing them to equilibrate to room temperature. An equal volume of reagent (100 µL) was added to each well of the 96-well plate containing 100µl of blank (medium only) and treated cells in a culture medium.

The plate was then placed on a plate shaker at 300-500 rpm for 30 seconds and incubated at room temperature for 1 hour. Caspase-3/7 activity was assessed by measuring the release of amino-luciferin as a result of active caspase-3/7 cleaving a luminogenic substrate which is consumed by luciferase and generates a luminescent signal that is proportional to caspase 3/7

activity. Luminescence was measured using a GloMax® luminometer (Promega, UK), according to the manufacturer's instructions.

2.8.6.2 TUNEL Apoptosis Assay

Apoptosis was quantified using a Click-iT Plus TUNEL Assay for In Situ Apoptosis Detection Kit with Alexa Fluor 647 dye (Invitrogen, Cat. No. C10619), according to the manufacturer's instructions. TUNEL positive cells were identified using a fluorescent Zeiss Axio Observer widefield microscope (Carl Zeiss AG, Germany) with a 10x objective, and analysed with ImageJ software (Fiji, version 2.14.0). Results were quantified as a ratio of TUNEL-positive cells to the total number of cells.

2.9 Study approval

Venous blood samples were obtained with the informed written consent and approval of the local ethics committee (REC Ref 17/LO/0563) from healthy volunteers and from HPAH patients with a rare pathogenic variant of *BMPR2* gene.

Human artery tissue samples were obtained following ethical approval from the Imperial College Healthcare Tissue Bank (ICHTB HTA licence: 12275; REC approval: 17/WA/0161).

Formalin fixed and paraffin embedded lung tissue sections from healthy volunteers and PAH patients were obtained from the Royal Papworth Hospital NHS Foundation Trust Tissue Bank (Cambridge, UK) with informed written consent and ethical approval by (ICHTB HTA licence: 12275; REC Wales approval: 22/WA/0214).

2.10 Statistical Analysis

All graphs and statistical analyses were performed using either GraphPad Prism software 9 (GraphPad Software, USA) or Rstudio (RStudio Inc, version 1.2.5042). All experiments were performed in at least four biological replicates, with 3 technical replicates performed per experiment, unless stated otherwise. All data were tested for normal distribution using the Shapiro-Wilk test. An unpaired student's t test was used to analyse the normally distributed data from two sample groups, while a one- or two-way ANOVA test was used to analyse three or more sample groups as appropriate.

Statistical significance was accepted when p-values were less than 0.05. All error bars are representative of mean (± SEM).

Chapter 3 Results: Effects of shear stress, hypoxia, and TNF-α on KLF6 expression in HPAECs

3.1 Introduction

Pulmonary arterial hypertension (PAH) is a rare and severe lung disease characterized by increased vascular resistance and excessive narrowing of the luminal arteries due to sustained vasoconstriction, persistent inflammation and the abnormal remodelling of the pulmonary artery. The molecular mechanisms that underlie the pathogenesis of PAH are still not fully understood, but PAH is believed to have a complex multifactorial aetiology involving genetic and environmental factors and possibly gene-environment interactions that influence the onset and progression of the disease (Section 1.3.2). Environmental factors such as fluid shear stress (FSS), hypoxia, inflammatory stimuli or genetic factors such as germline mutations in *BMPR2*, which encodes the bone morphogenetic protein receptor type 2 (BMPR2), are also thought to play a key contributory role. Persistent and continuous exposure to these environmental stresses induces a hyper-proliferative, apoptosis-resistant EC phenotype which leads to endothelial dysfunction.

3.1.1 Shear stress

ECs, which line the pulmonary arteries, are constantly exposed to flow. The level of physiological shear stress and the tangential force exerted by the blood flow on the vessel wall in the pulmonary arterial tree ranges from 4-15 dynes/cm^2 (Salibe-Filho et al., 2020). Significant reduction or elevation in shear stress levels leads to endothelial dysfunction, in which ECs experience either unidirectional laminar or disturbed flow depending on their position in the arterial tree. These distinct flow patterns have different effects on endothelial morphology, function and gene expression (Section 1.3.2.2.2) (Ando & Yamamoto, 2009; Sato & Ohashi, 2005; Dewey et al., 1981).

There is increasing evidence that PAH alters shear stress in the pulmonary arteries. Shear stress in the proximal pulmonary arteries is significantly decreased in PAH patients compared to healthy control subjects, and this may contribute to endothelial dysfunction leading to a remodelling of the proximal arteries and the development of PAH (Tang et al., 2012). ECs typically respond to flow by changing their morphology from a cobblestone-like appearance to elongation and orientation in the direction of flow (Section1.3.2.2.2), and the inability of the

endothelium to adapt morphologically to flow results in an increased propensity for pulmonary vascular remodelling (Humbert et al., 2019). Morphological flow adaptation of microvascular endothelial cells (MVECs) that have been isolated from PAH patients is delayed in response to a gradual increase in shear stress (2.5, 15, and 21 dynes/cm^2) for every 24 hours *in vitro* compared to MVECs from healthy controls (Szulcek et al., 2016a). Meanwhile, the exposure of BMPR2-silenced HPAECs to laminar flow (15 dynes/cm^2) for 72 hours results in endothelial maladaptation to shear stress, suggesting that this response may at least in part be responsible for endothelial dysfunction in PAH (Mahomed et al., 2019).

Previous studies have shown that a family of Krüppel-like transcription factors, including KLF2 and KLF4, act as key regulators of shear stress responses by regulating the expression of flow-responsive genes (Section 1.7) (Hamik et al., 2007; Dekker et al., 2002).

3.1.2 Hypoxia

Chronic hypoxia causes pulmonary arterial remodelling in human PAH and in pre-clinical rodent models of PAH (Humbert et al., 2019). However, the precise mechanisms underlying this effect remain unclear. Several *in vitro* studies have shown that hypoxia affects pulmonary vascular cell proliferation directly (Welsh, Scott & Peacock, 2006; Welsh et al., 2001, 1998). Hypoxia increases cell proliferation by increasing the production of growth factors (PDGF and VEGF), pro-inflammatory mediators (IL-6, IL-8, and MCP-1/CCL2) and mitogenic stimuli (serotonin and ET-1) and by inhibiting the production of anti-mitogenic factors (PGI2 and NO) from ECs, SMCs, fibroblasts and platelets (Eddahibi et al., 1999; Tamm et al., 1998; Mukhopadhyay et al., 1995; Kourembanas et al., 1991; Kourembanas, Hannan & Faller, 1990). Meanwhile, exposure to hypoxia also stimulates the deposition and cross-linking of extracellular matrix components by increasing the expression of lysyl oxidases (Loxs) and galectin-3 (Gal-3) (Luo et al., 2017; Nave et al., 2014).

Hypoxia also stimulates the expression of hypoxia-inducible transcription factors (HIFs: HIF-1 and HIF-2), which mediate the adaptive transcriptional response to oxygen deprivation (Section 1.3.2.2.2) (Pullamsetti et al., 2020). HIF-2α has been shown to increase in PAECs from patients with IPAH due to the reduced expression of prolyl hydroxylase domain protein 2 (PHD2), which regulates HIFs stability. HIF-2 activation is linked with EndMT in severe PAH (Tang et al., 2018). In addition, PHD2 gene (*egln1*)-deficient mice were shown to develop severe PAH spontaneously (Tang et al., 2018).

3.1.3 Inflammatory stimuli (TNF-α)

Inflammation plays a critical role in endothelial dysfunction as well as pulmonary vascular remodelling in PAH (Huertas et al., 2020; Humbert et al., 2019; Mushaben et al., 2012). Inflammatory cells, which are found around plexiform lesions, release cytokines and chemokines that promote the remodelling of pulmonary arteries in PAH (Section 1.3.2.2.3) (Ni et al., 2022; Pugliese et al., 2015; Rabinovitch et al., 2014; Sprague & Khalil, 2009). Elevated levels of pro-inflammatory cytokines have been shown to correlate with disease severity and mortality in PAH patients (Zhang et al., 2022). Specifically, the pro-inflammatory cytokine TNF-α was shown to play a major role in the pathogenesis of PAH (Schwiening et al., 2022; Groth et al., 2014).

3.2 Experimental aims

The experiments presented in this chapter investigated the effects of various factors involved in the pathogenesis of PAH – including shear stress, hypoxia and inflammation – on KLF6 expression in human pulmonary artery endothelial cells (HPAECs).

3.3 Experimental outline

This chapter summarises the key experimental methods and protocols involved; further details can be found in Chapter 2. The experimental outline is shown in Figure 3.1.

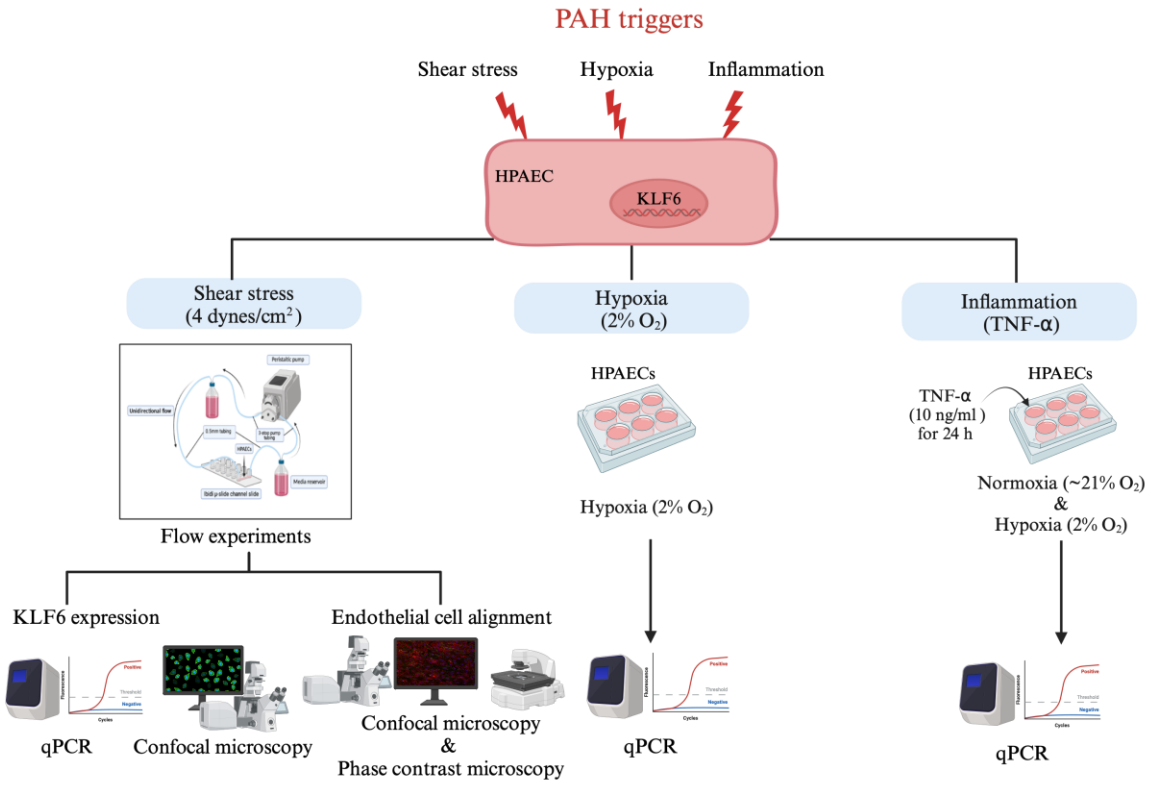

Figure 3.1: Outline of experiments presented in Chapter 3.
The effects of factors involved in PAH pathogenesis including shear stress (4 dynes/cm^2), hypoxia (2% O_2) and inflammatory stimuli (TNF-α;10 ng/mL) alone or combined with hypoxia (2% O_2) on KLF6 expression in HPAECs were assessed by qPCR and immunofluorescent imaging. The effect of shear stress on endothelial cell alignment was evaluated using phase-contrast microscopy and confocal microscopy. Illustration created by the author using BioRender.com.

3.3.1 Time course of cell exposure to laminar shear stress

HPAECs were grown in 10 cm^2 flaskettes with detachable bottom slides (Nunc Lab-Tek Flask on Slide) to an 80% confluence level. The cells were then cultured under static conditions or exposed to flow. To induce exposure to flow, the bottom slides with growing cells were detached from the flask and inserted into the flow chamber of a parallel flow apparatus to introduce a unidirectional flow. The cells were then exposed to physiological laminar shear stress of 4 dynes/cm^2 (Salibe-Filho et al., 2020) for 30 min, 1 h, 4 h, 6 h and 24 h, actuated by a peristaltic pump (Chapter 2, Section 2.4).

3.3.2 Immunofluorescent staining of KLF6 protein expression

HPAECs cultured in ibidi 6-channel μ-Slides with optical bottom or in 10 cm^2 flaskettes (Nunc Lab-Tek Flask on Slide) were cultured under static conditions or were exposed to a physiological laminar flow of 4 dynes/cm^2 (Salibe-Filho et al., 2020) for 24 h. Cells were immunostained for KLF6, VE-cadherin, TRITC-phalloidin labelled F-actin and DAPI, as described in Chapter 2, Section 2.7.1.

3.3.3 Time course exposure to hypoxia

Confluent HPAECs grown in 6-well plates were left in normoxia (21% O_2) or were exposed to hypoxia (2% O_2) for 1 h, 3 h, 6 h, and 12 h, 16 h and 24 h respectively.

3.3.4 Endothelial response to pro-inflammatory stimuli

Confluent HPAECs cultured in 6-well plates in an EGM2 medium were left untreated or were treated with 10 ng/mL of TNF-α. Cells were then left under normoxic (21% O_2) or hypoxic (2% O_2) conditions for 24 hours.

3.3.5 qPCR measurement of *KLF6* mRNA expression

HPAECs that had been stimulated with shear stress, hypoxia or TNF-α were collected and subjected to RNA extraction, reverse transcription and RT-qPCR analysis to measure the mRNA expression levels of *KLF2*, *KLF4*, and *KLF6*. For further details, see Chapter 2, Section 2.5.

3.4 Results

3.4.1 Effects of shear stress on KLF6 expression in HPAECs.

To investigate the effect of laminar shear stress on KLF6 expression in the pulmonary endothelium and compare it to KLF2/KLF4 expression, HPAECs were subjected to a physiological laminar flow of 4 dynes/cm^2 for 30 min, 1 h, 4 h, 6 h, and 24 h in a parallel-plate flow chamber apparatus.

KLF2 and *KLF4* mRNA expression levels were significantly increased in shear stress-stimulated HPAECs (a 9-fold increase at 6 h, p<0.0001 and a 10.4-fold increase at 4 h, p<0.0001 respectively) compared to static HPAECs (Figure 3.2A and B). Meanwhile, laminar shear stress significantly increased mRNA expression levels of *KLF6* HPAECs (a 9-fold increase at 24 h, p<0.0001) in HPAECs, compared to static controls (Figure 3.3A). The nuclear localization of KLF6 in flow-stimulated HPAECs was confirmed using immunofluorescence (Figure 3.3B)

Shear stress stimulated HPAECs developed an elongated morphology with cytoskeletal orientation and cell alignment parallel to the direction of flow (Figure 3.4).

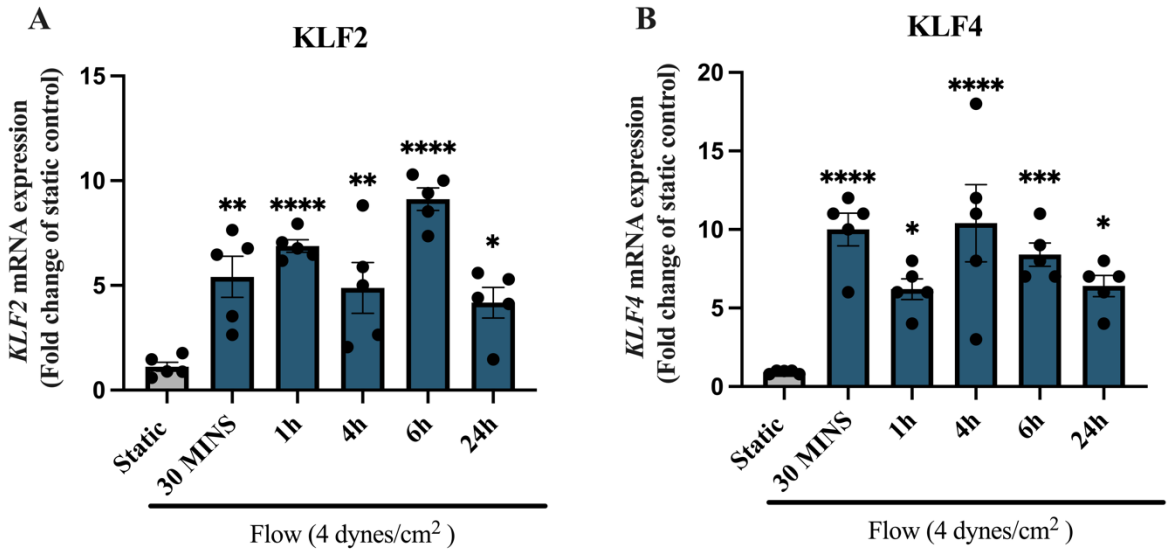

Figure 3.2: *KLF2*, and *KLF4* mRNA expression in laminar shear stress-stimulated HPAECs. mRNA expression levels of **(A)** *KLF2* and **(B)** *KLF4* in HPAECs were subjected to a laminar shear stress of 4 dynes/cm^2 for 30 min,1 h, 4 h, 6 h, and 24 h, or in HPAECs maintained at static condition. Data were normalized to the reference gene (*B2M*). *P<0.05, **P<0.01, ***P<0.001, ****P<0.0001, in comparison with the static control. One-way ANOVA with Tukey's post-hoc test; n=5. Error bars indicate mean ±SEM.

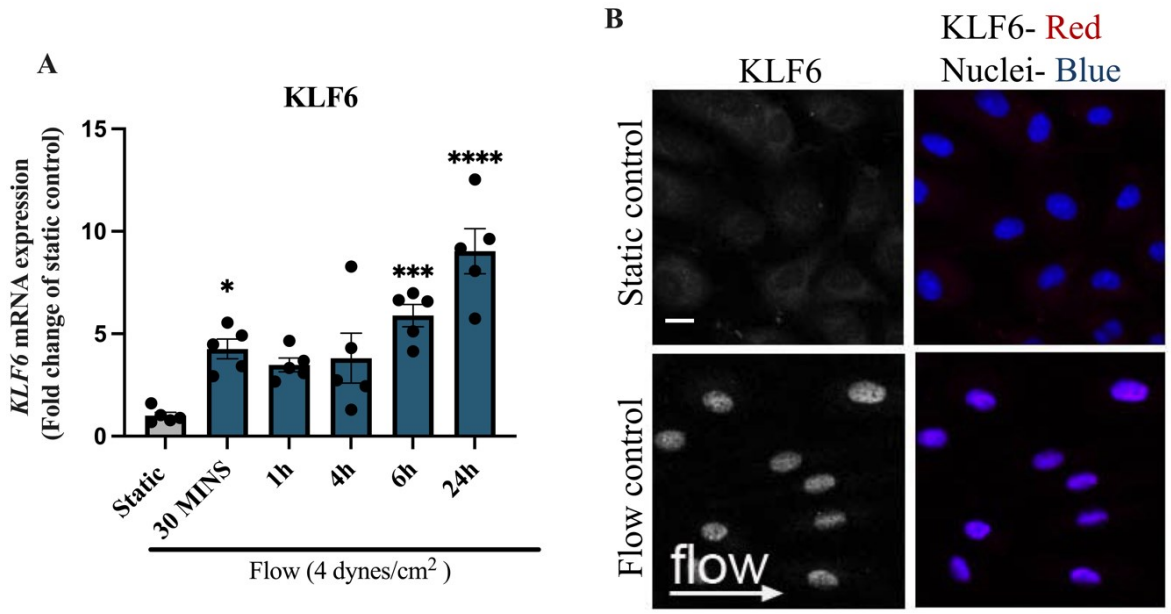

Figure 3.3: KLF6 expression in laminar shear stress-stimulated HPAECs.
(A) mRNA expression levels of *KLF6* in HPAECs subjected to laminar shear stress of 4 dynes/cm^2 for 30 min,1 h, 4 h, 6 h, and 24 h, or in HPAECs maintained at static condition. Data were normalized to the reference gene (*B2M*). *P<0.05, ***P<0.001, ****P<0.0001, in comparison with the static control. One-way ANOVA with Tukey's post-hoc test; n=5. Error bars indicate mean ±SEM. **(B)** Representative confocal immunofluorescence images showing the nuclear localization of KLF6 in HPAECs exposed to laminar flow at 4 dynes/cm^2 for 24 hours. Nuclei are blue, and KLF6 is red. Scale bar = 10 µm; n=3.

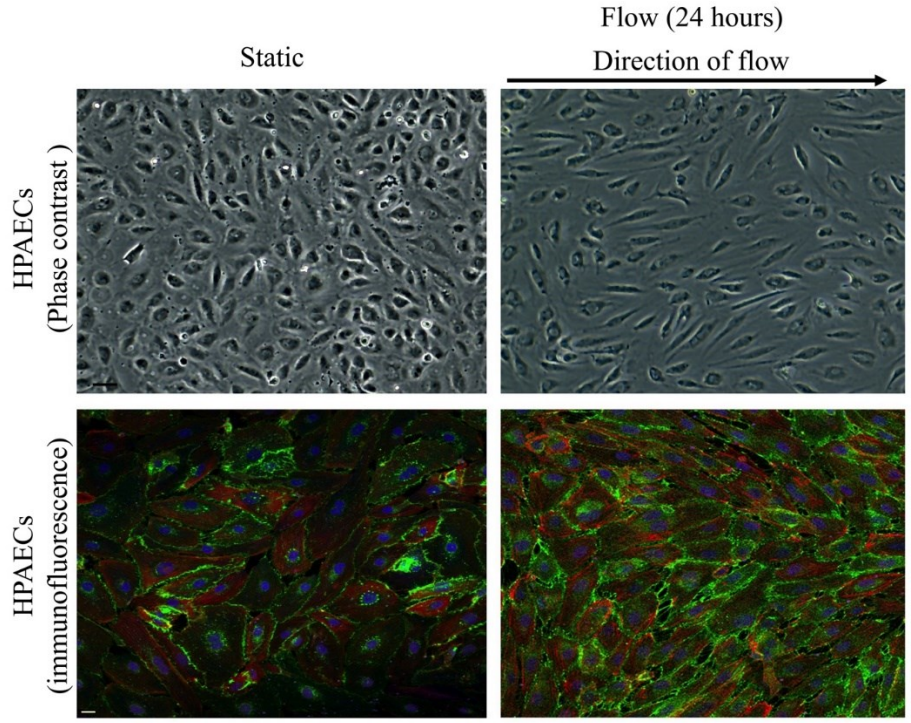

Figure 3.4: Morphology of HPAECs in response to flow.
Representative phase-contrast and immunofluorescence images of static HPAECs or HPAECs exposed to laminar shear stress of 4 dynes/cm^2 for 24 hours. The cells were immunostained for VE-cadherin (green) and F-actin (TRITC-phalloidin; red) and nuclei (DAPI; blue). Scale bars=20 µm (top images) and 10 µm (bottom images); n=3.

3.4.2 Effects of hypoxia on *KLF6* expression in HPAECs.

Hypoxia plays a well-established role in PAH pathogenesis by inducing vasoconstriction and pulmonary vascular remodelling (Young, Williams & Thompson, 2019).

HPAECs subjected to hypoxia (2% O_2) for 1 h, 3 h, 6 h, 12 h, 16 h and 24 h showed no significant changes in *KLF2* mRNA levels, although *KLF4* mRNA levels were significantly increased in comparison to normoxic controls (8-fold increase at 24 h, $p < 0.0001$) (Figure 3.5A, B). *KLF6* mRNA levels appeared to increase after 1h of hypoxic exposure, but the change was too small to reach a level of statistical significance (Figure 3.5C). The mRNA expression of *SLC2A1* (solute carrier family 2A1) – a known hypoxia-regulated gene acting here as a positive control – was also significantly elevated (Figure 3.6).

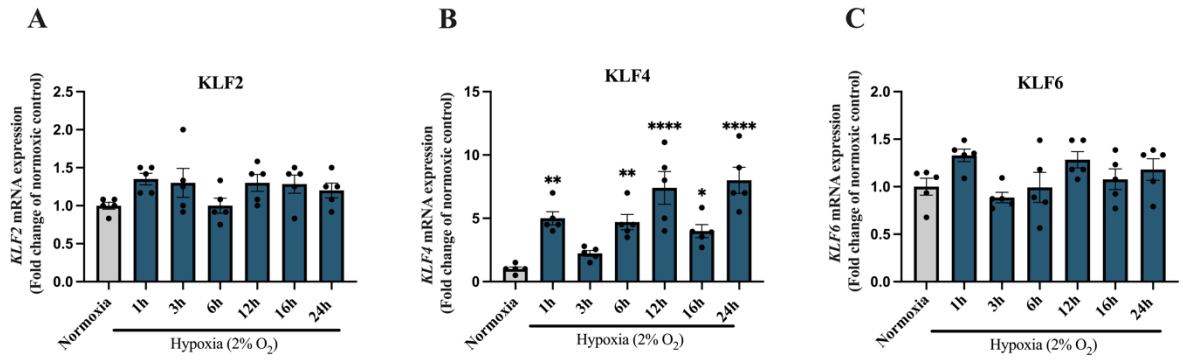

Figure 3.5: Expression of *KLF2*, *KLF4* and *KLF6* mRNA in hypoxia-treated HPAECs.
mRNA expression levels of **(A)** *KLF2*, **(B)** *KLF4* and **(C)** *KLF6* were measured in normoxic HPAECs or in HPAECs exposed to hypoxia (2% O_2) for 1 h, 3 h, 6 h, 12 h, 16 h and 24 h. Data were normalized to the reference gene (*β-actin*). *P<0.05, **P<0.01, ****P<0.0001 in comparison with static control. One-way ANOVA with Tukey's post-hoc test; n=5. Error bars indicate mean ±SEM.

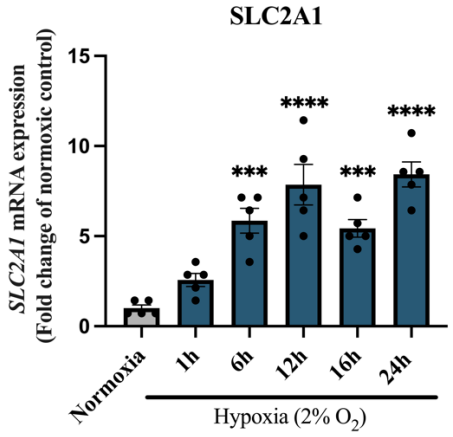

Figure 3.6: *SLC2A1* mRNA expression in hypoxia-treated HPAECs.
mRNA expression levels of *SLC2A1* were measured in normoxic HPAECs and in HPAECs exposed to hypoxia (2% O_2) for 1 h, 6 h, 12 h, 16 h and 24 h. Data were normalized to the reference gene (*β-actin*). ***P<0.001, ****P<0.0001 in comparison with static control. One-way ANOVA with Tukey's post-hoc test; n=5. Error bars indicate mean ±SEM.

3.4.3 Effects of TNF-α on *KLF6* expression in normoxic and hypoxic HPAECs.

To determine the role of inflammatory stimuli on KLF6 expression in ECs and compare it to KLF2/KLF4 expression, HPAECs were treated with TNF-α alone or in combination with hypoxia (2% O_2; 24 hours). The "double hit" conditions of combined hypoxic and inflammatory insults are thought to resemble the environment required for pulmonary vascular remodelling in PAH most closely (Yang & Yu, 2019).

KLF2 mRNA levels were significantly decreased (a 0.5-fold decrease, $p<0.0001$), whereas *KLF4* mRNA levels remained relatively unchanged in TNF-α-treated HPAECs compared with untreated controls (Figure 3.7A and B). However, *KLF6* expression levels were elevated by TNF-α (a 1.5-fold increase, $p<0.05$) compared with untreated controls (Figure 3.7C).

Under the "double hit" conditions of combining TNF-α and hypoxia, *KLF2* and *KLF4* mRNA levels were both significantly reduced (a 0.2-fold and 0.4-fold decrease, $p<0.0001$ and $p<0.01$ respectively) (Figure 3.7A and B), while *KLF6* mRNA expression was significantly elevated (~ 2-fold increase, $p<0.001$) compared with untreated controls (Figure 3.7C).

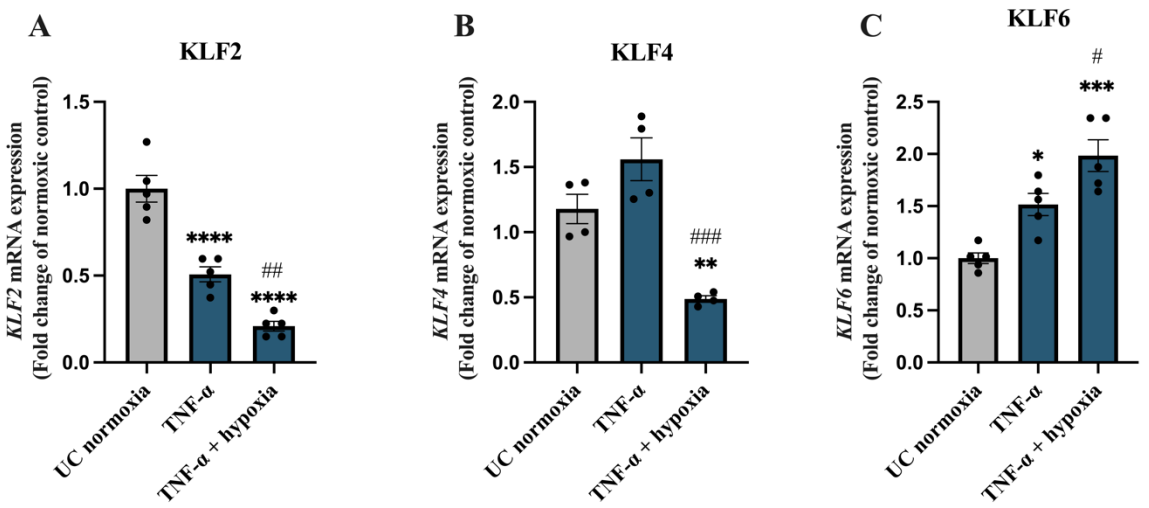

Figure 3.7: *KLF2*, *KLF4* and *KLF6* expression levels in HPAECs under "single hit" and "double hit" conditions.
mRNA expression levels of **(A)** *KLF2*, **(B)** *KLF4* and **(C)** *KLF6* were measured in the untreated or TNF-α-treated (10 ng/mL) HPAECs grown under normoxic (21% O_2) or hypoxic (2% O_2) conditions for 24 hours. Data were normalized to *β-actin*. *P<0.05, **P<0.01, ***P<0.001, ****P<0.0001, in comparison with untreated normoxic controls; $^{\#}$P<0.05, $^{\#\#}$P<0.01, $^{\#\#\#}$P<0.001, in comparison with TNF-α treated cells under normoxic conditions. One-way ANOVA with Tukey's post-hoc test; n=5. Error bars indicate mean ±SEM.

3.5 Discussion

The experiments presented in this chapter examined the effects of flow and the vascular insults that are involved in the pathogenesis of PAH, including hypoxia and inflammation, on KLF6 expression in pulmonary endothelial cells.

Physiological flow maintains EC homeostasis and quiescence by regulating the expression of endothelial identity markers such as KLF2 and KLF4, and enhancing endothelial barrier function through anti-inflammatory, anti-proliferative and anti-apoptotic effects (Sindi et al., 2020; Fan et al., 2017; Alaiti et al., 2012; Dekker et al., 2006). In this study, HPAECs that were exposed to laminar flow became elongated and aligned in the direction of flow, and this process was accompanied by the reorganization and alignment of F-actin cytoskeleton, consistent with previous reports (Steward et al., 2015; Wechezak, Viggers & Sauvage, 1985; Dewey et al., 1981).

Endothelial adaptation to flow is largely orchestrated by KLF2 and KLF4 (Nayak, Lin & Jain, 2011), but the role of KLF6 has not yet been clearly identified. The experiments described in this chapter demonstrated the stimulatory effect of flow on KLF2, KLF4 and KLF6 expression,

and the result was consistent with published RNA-seq data from flow-exposed HPAECs (Hirata et al., 2021).

Interestingly, the expression of *KLF2* and *KLF4* peaked at earlier time points of shear stress stimulation (6 h and 4 h, respectively) in comparison with *KLF6*, which increased more slowly, reaching peak stimulation at 24 h. This observation suggests that KLF2 and KLF4 may be involved in earlier adaptive responses to flow, while KLF6 may be more critical in the regulation of endothelial homeostasis during later times of flow exposure. Immunostaining confirmed a flow-induced increase in the expression and nuclear localization of KLF6 protein in HPAECs. Unfortunately, despite numerous efforts, we could not source the necessary anti-KLF6 antibodies that would be suitable for determining protein expression changes by western blotting. This will be a subject for future investigation.

Chronic hypoxia induces pulmonary vascular remodelling (Humbert et al., 2019). *KLF2* and *KLF6* mRNA levels were not affected by hypoxia, but *KLF4* expression was significantly increased. Previous reports have shown an increase in KLF2 expression in human umbilical vein endothelial cells (HUVECs) under hypoxic conditions (1% O_2) (Kawanami et al., 2009) which differs from our result. However, hypoxia-induced increase in the expression of *KLF4* was consistent with results from another study in which HUVECs were exposed to 3% O_2 hypoxia (Hale et al., 2014). Potential discrepancies are likely to result from differences in experimental setup such as cell types used and the level and duration of hypoxia.

Inflammation is a key pathological driver of PAH (Huertas et al., 2020). Preclinical experimentation shows that inflammation and hypoxia are not capable of inducing severe PAH alone, but a combination of these two insults under "double hit" conditions is far more effective in inducing vascular phenotypes that are characteristic of PAH (Pugliese et al., 2015; Ciuclan et al., 2011; Yuan & Rubin, 2005). I therefore investigated changes in *KLF2*, *KLF4* and *KLF6* mRNA expression levels in HPAECs that were exposed to single or combined insults of hypoxia (2% O_2) and TNF-α.

KLF6 expression was significantly increased by TNF-α, while *KLF2* expression was reduced. The upregulation of *KLF6* expression in response to pro-inflammatory stimuli was also observed in human macrophages, suggesting that this regulatory response is shared among different cell types (Date et al., 2014).

The reduction of *KLF2* expression is consistent with a previous report (Kumar et al., 2005). *KLF4* expression in HPAECs was relatively unaffected, which contrasts with another report showing the stimulatory effect of TNF-α on *KLF4* expression in HUVECs that were treated with TNF-α for 2 hours (Hamik et al., 2007). This discrepancy could be attributed to differences in cell type and/or the duration of TNF-α exposure.

Under the "double hit" conditions, *KLF6* expression in endothelial cells was significantly increased, while expressions of *KLF2* and *KLF4* were reduced. The reduction of KLF2 and KLF4 in PAH endothelium has been reported previously (Shatat et al., 2014; Chandra et al., 2011), and correlates with the severity of vascular remodelling. In this respect, the significant downregulation of KLF2 and KLF4 under disease conditions that were observed here may represent changes occurring in PAH vasculature. The novel observation of KLF6 activation under the same conditions suggests that this closely related transcription factor may also play a role in vascular repair, which is consistent with its effects in other types of cells and tissues (Li et al., 2023b; Garrido-Martín et al., 2013; Kim et al., 1998).

Interestingly, BMPR2 knockdown in HPAECs cultured in an organ-on-a-chip model of PAH under flow reduced the expression of *KLF6* (an 0.8-fold decrease, p=0.02, in comparison with untreated controls), and this reduction was further maintained under hypoxic conditions (a 1-fold decrease, p=0.03, in comparison with untreated controls) (Ainscough et al., 2022a). In the same study, *KLF6* expression was increased under both normoxia and hypoxia (p=0.01 and p=0.002 respectively) in PAH ECFCs with a *BMPR2* mutation that were cultured in an organ-on-a-chip model of PAH under flow conditions (Ainscough et al., 2022a). This suggests that regulatory mechanisms that affect *KLF6* expression are likely to be dependent upon cell type.

3.6 Conclusion

The key findings presented in this chapter show that KLF6, like KLF2 and KLF4, is induced during the process of endothelial adaptation to flow (Figure 3.8). However, its expression is upregulated under conditions of severe stress, while the expressions of *KLF2* and *KLF4* are reduced. This suggests a potential divergent role of KLF6 in comparison to the most closely related KLF2 and KLF4.

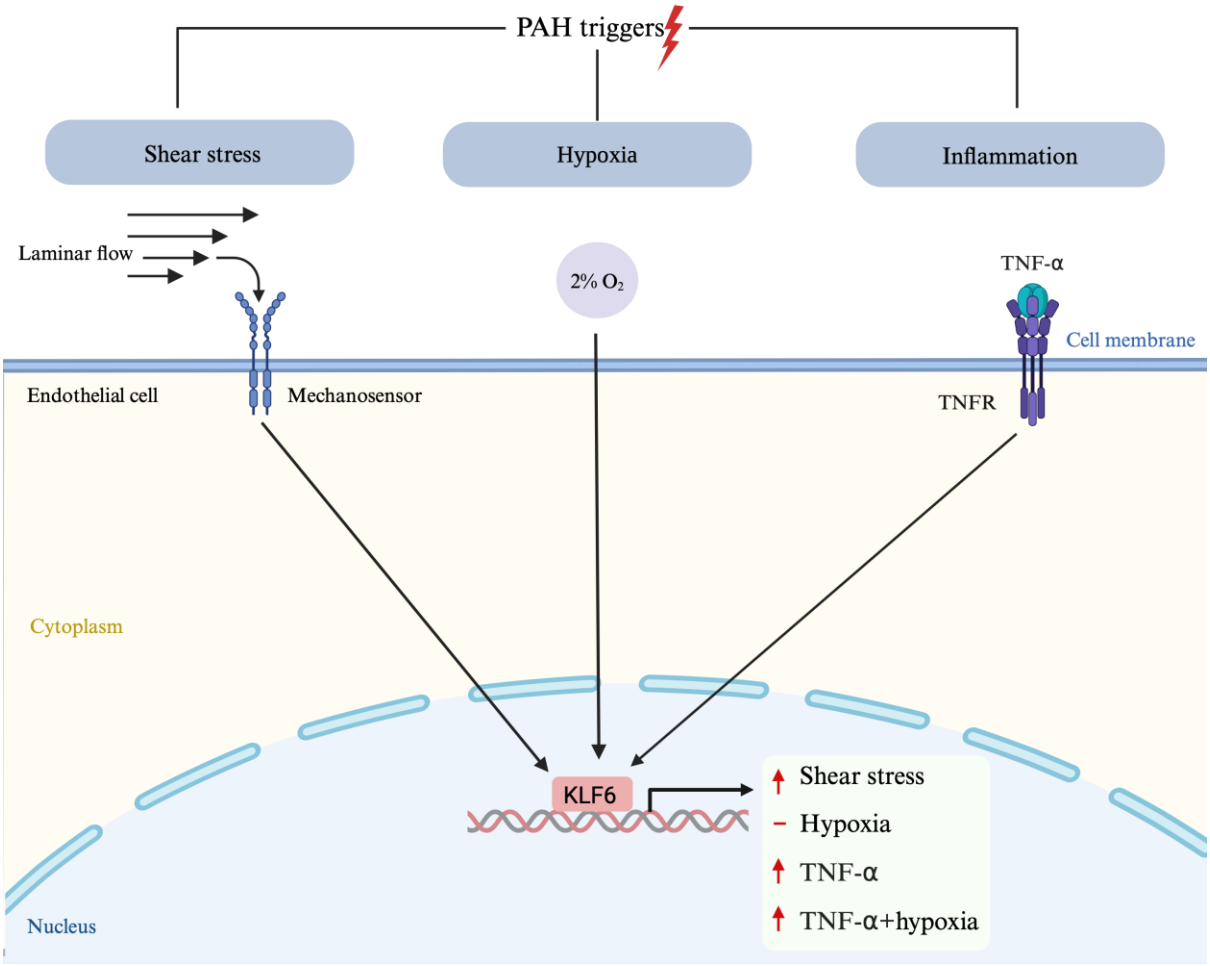

Figure 3.8: A brief summary of the main findings of Chapter 3.
Illustration created by the author using BioRender.com.

Chapter 4 Results: Effects of KLF6 on endothelial function

4.1 Introduction

Vascular remodelling in PAH is triggered by the loss of pulmonary endothelial homeostasis, which is characterised by the activation of inflammatory, proliferative and angiogenic pathways. PAH shares several characteristics with cancer, including excessive cell proliferation and resistance to apoptosis, as well as chronic inflammation and impaired angiogenesis. Growing evidence suggests that KLF6, which acts as a tumour suppressor in various types of human cancer, may also play a role. Recent transcriptomic data from a microfluidic model of PAH suggests that KLF6 is downregulated in the PAH endothelium (Ainscough et al., 2022a). However, while the roles of KLF2 and KLF4 have been studied in the context of PAH, the role of KLF6 is still largely unknown.

KLF6 is expressed in the vascular endothelium, and promotes vascular repair (Atkins & Jain, 2007). KLF6 is considered to be an immediate-early injury-response factor, as it regulates the expression of various genes related to vascular repair, including *TGFB1*, *COL1A1*, *ACVRL1* and *ENG* (Garrido-Martín et al., 2013; Botella et al., 2002; Kim et al., 1998; Ratziu et al., 1998). KLF6 translocates to cell nuclei during vascular injury to activate the expression of its target genes. After the repair process is complete, the expression of *KLF6* and its target genes gradually returns to normal levels, which suggests that the repair process is highly dependent on physiological conditions (Yang et al., 2019). However, the precise role of KLF6 in pathological repair mechanisms remains unknown. A recent study showed that KLF6 plays a role in the pathological form of vascular repair and angiogenesis in hepatopulmonary syndrome (HPS), and that its expression is increased by bone morphogenetic protein 9 (BMP9), leading to the activation of the pro-angiogenic genes *ENG* and *ACVRL1* (Yang et al., 2019).

4.2 Experimental aims

To evaluate the effects of changes in KLF6 expression on pulmonary endothelial (HPAEC) function, including inflammatory activation, junctional integrity and barrier function, angiogenesis, proliferation, migration and apoptosis.

4.3 Experimental outline

The outline of the experiments described in this chapter is shown in Figure 4.1. A more detailed description of the methods and protocols used in this chapter can be found in Chapter 2.

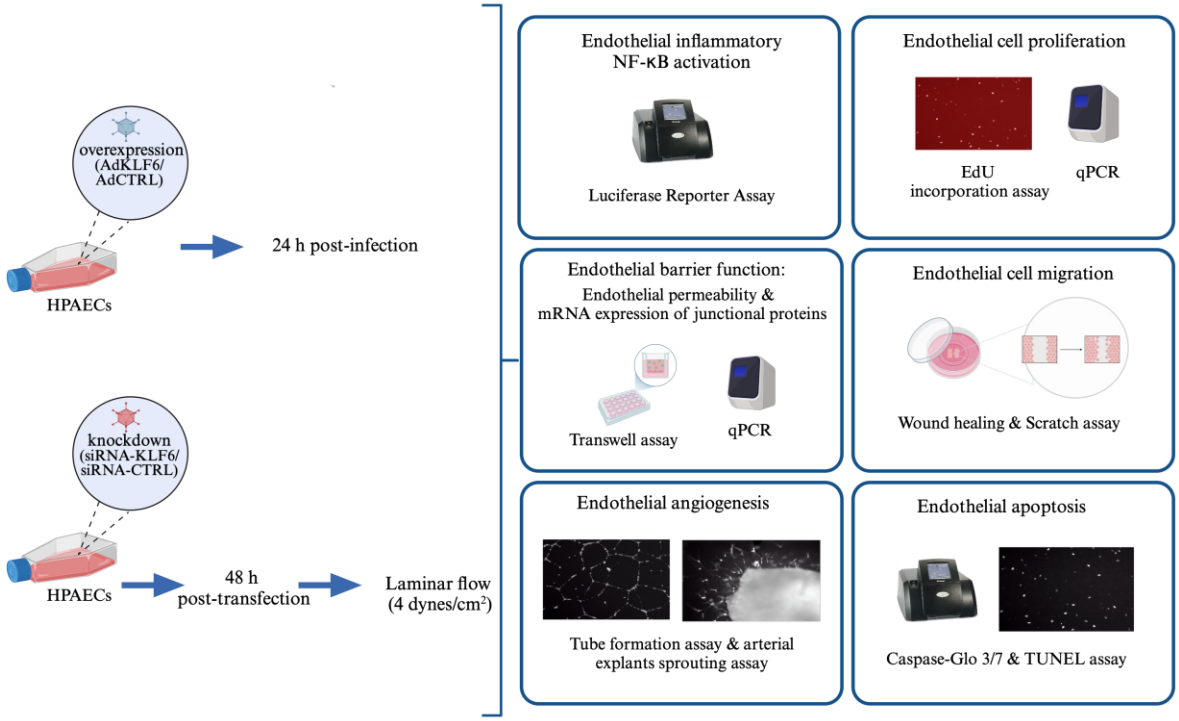

Figure 4.1: Outline of experiments presented in chapter 4.
In order to determine the role of KLF6 on endothelial cell function, KLF6 was overexpressed through adenoviral gene transfer in HPAECs. The effects of siRNA-induced KLF6 knockdown were studied in flow-stimulated HPAECs, as basal expression levels of KLF6 in a static, quiescent endothelium were below the level of detection. HPAEC function was studied using various functional assays and qPCR analysis as indicated. Illustration created by the author using BioRender.com.

4.4 Results

4.4.1 Manipulation of KLF6 expression in HPAECs

KLF6 was overexpressed through adenovirus-mediated gene transfer to replicate the effects of KLF6 activation in HPAECs. Full-length KLF6 was tagged with a C-terminal hemagglutinin (HA) to detect the precise intracellular localization of the recombinant protein. The nuclear localization of the KLF6 protein, which was required for its activation, was determined by immunofluorescence staining with anti-KLF6 and anti-HA antibodies using confocal microscopy as previously described in Chapter 2, Section 2.7.1.

A marked increase in the nuclear localization of KLF6 (Figure 4.2A and B) and a significant increase in KLF6 protein levels (~5-fold increase, $P<0.01$, in comparison with adenoviral control) and *KLF6* mRNA levels (~170-fold-increase, $P<0.0001$, in comparison with adenoviral control) were observed in AdKLF6- overexpressing HPAECs 24 hours post-infection (Figure 4.2C).

KLF6 knockdown was induced by transfection with KLF6 siRNA. As the expression levels of KLF6 in quiescent HPAECs cultured under static conditions were too low to determine the effect of gene knockdown, KLF6 knockdown was induced in HPAECs cultured under a physiological flow of 4 dynes/cm^2. *KLF6* mRNA levels in flow-exposed HPAECs were effectively reduced to basal control levels by KLF6 siRNA 48 hours after transfection (Figure 4.2D).

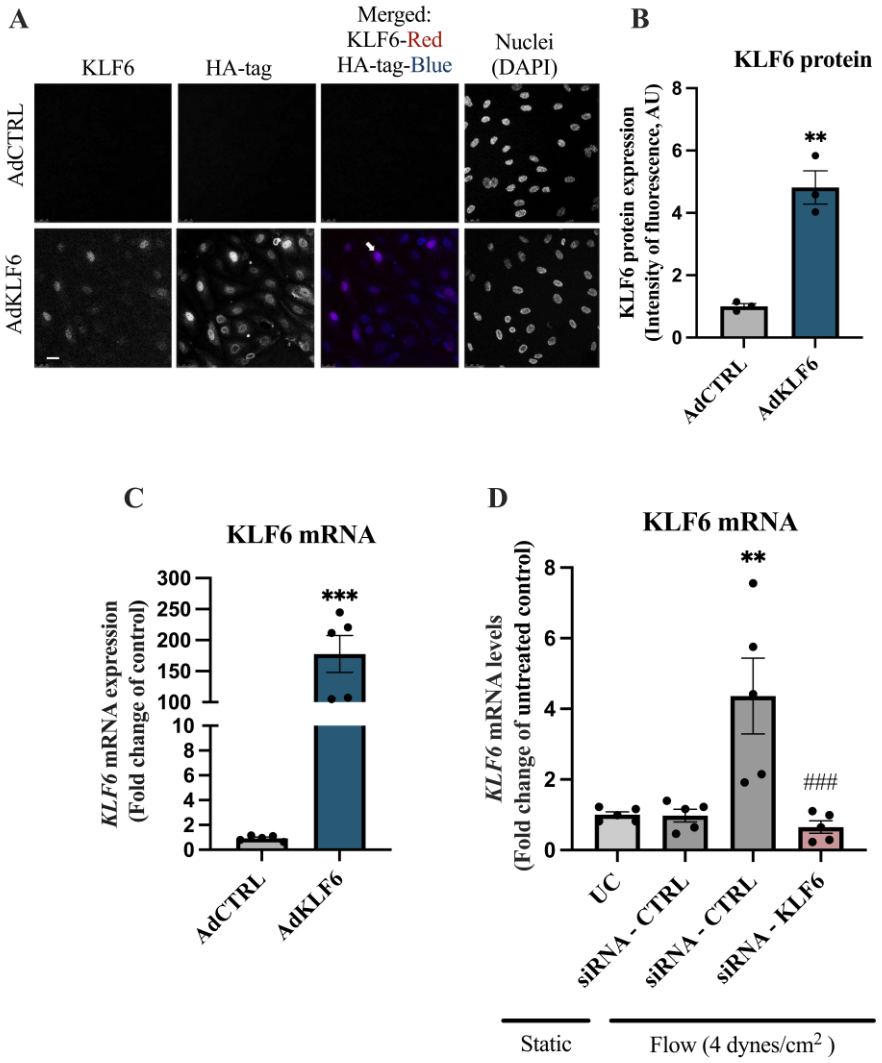

Figure 4.2: KLF6 overexpression and knockdown in HPAECs.
(A) Representative confocal microscopy images showing nuclear localization of recombinant HA-tagged KLF6 (AdKLF6) in HPAECs 24 hours post-infection. Cells were infected with adenoviral control (AdCTRL) or AdKLF6 (MOI 1:100). In the merged image, the KLF6 is red, and the HA-tag marking localization of KLF6-HA is blue. All nuclei were marked with DAPI, shown here in the black and white image on the right. Scale bar=10μm; n=3. **(B)** Bar graph showing KLF6 protein levels assessed by measuring the intensity of fluorescence in HPAECs infected with AdCTRL or AdKLF6. **P<0.01, in comparison with AdCTRL. Unpaired t-test; n=3. Error bars indicate mean ±SEM. (**C)** *KLF6* mRNA expression in HPAECs transfected with AdCTRL or AdKLF6. Data were normalized to the reference gene (*ACTB*). ****P<0.0001, in comparison with AdCTRL. Unpaired t-test; n=5. Error bars indicate mean ±SEM. **(D)** siRNA mediated knockdown of KLF6 in HPAECs exposed to laminar shear stress of 4 dynes/cm^2 for 24 h. HPAECs were either left untreated (untreated static control=UC) or were transfected with non-targeting siRNA and cultured under static conditions (siRNA-CTRL) or were exposed to flow and transfected either with siRNA-CTRL or with siRNA-KLF6 as indicated. The KLF6 mRNA level was measured by qPCR 48 hours post-transfection. Data were normalized to the reference gene (*B2M*). **P<0.01, in comparison with UC; $^{\#\#}$P<0.001, in comparison with siRNA-CTRL under flow conditions. One-way ANOVA with Tukey's post-hoc test; n=5. Error bars indicate mean ±SEM.

4.4.2 KLF6 attenuates NF-κB inflammatory activation in HPAECs.

To assess the effect of KLF6 on inflammatory responses, HPAECs were stimulated using two factors implicated in the endothelial inflammatory activation in PAH, namely TNF-α and hypoxia. These factors were applied alone and in combination, to replicate the "double hit" conditions. The activation of NF-κB, a master-regulator of inflammatory gene expression, was measured using a luciferase reporter assay.

TNF-α and hypoxia induced a 29-fold and a 3-fold increase in NF-κB activity respectively (Figure 4.3A and B). TNF-α combined with hypoxia induced a 6-fold increase in NF-κB activity in HPAECs, compared with untreated normoxic adenoviral controls (Figure 4.3B). KLF6 overexpression effectively reduced NF-κB activity under all experimental conditions (Figure 4.3A and B).

KLF6 knockdown in flow-stimulated HPAECs did not affect NF-κB activity under basal conditions but markedly increased NF-κB activation in TNF-α-stimulated cells (a 2-fold increase, $p<0.05$) compared with siRNA controls (Figure 4.3C).

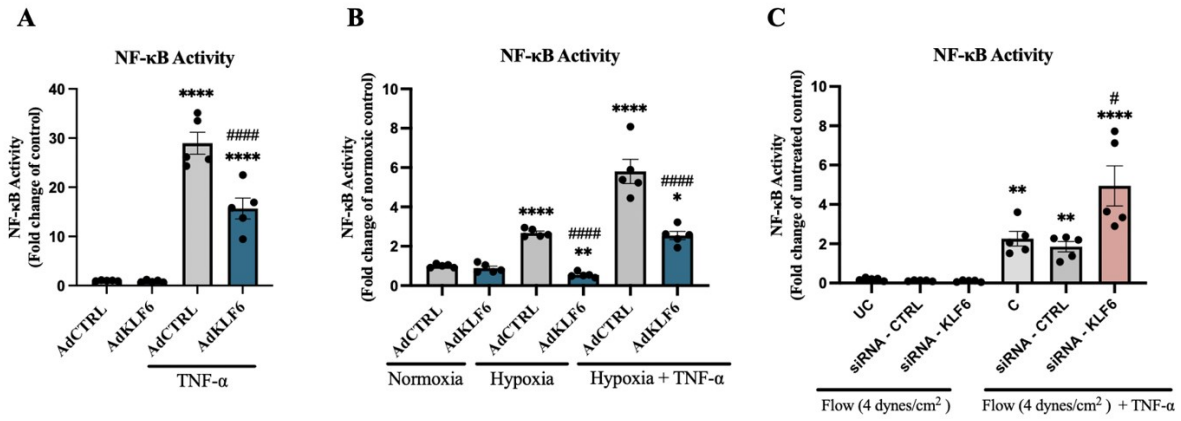

Figure 4.3: Effect of KLF6 overexpression and knockdown on NF-κB activity in HPAECs.
(A) and **(B)** Bar graphs represent the levels of NF-κB activity in HPAECs infected with AdCTRL or AdKLF6 which were left untreated or treated with TNF-α (10 ng/mL) under normoxic or hypoxic (2% O_2) conditions for 24 hours. NF-κB activity was assessed using the luciferase reporter assay. **P<0.01, ****P<0.0001, in comparison with normoxic controls; ####P<0.0001, in comparison with corresponding treated controls using one-way ANOVA with Tukey's post-hoc test; n=5. Error bars indicate mean ±SEM. **(C)** Bar graph showing the levels of NF-κB activity in HPAECs transfected with siRNA-KLF6 or siRNA-negative controls (siRNA-CTRL). The NF-κB activity in untreated HPAECs subjected to laminar shear stress of 4 dynes/cm^2 and/or in HPAECs simulated with TNF-α (10 ng/mL) for 24 hours was assessed using the luciferase reporter assay. *P<0.05, **P<0.01, ****P<0.0001, in comparison with untreated controls; #P<0.05, in comparison with corresponding treated controls (siRNA-CTRL). One-way ANOVA with Tukey's post-hoc test; n=5. Error bars indicate mean ±SEM.

4.4.3 KLF6 enhances endothelial barrier function in HPAECs.

To investigate the effect of the overexpression of KLF6 on endothelial barrier function, AdCTRL and AdKLF6-infected HPAECs were stimulated with known endothelial permeability inducers thrombin, hypoxia and TNF-α (Wojciak-Stothard, Tsang & Haworth, 2005; Rabiet et al., 1996; Goldblum, Ding & Campbell-Washington, 1993). Endothelial permeability was assessed spectrophotometrically by measuring the passage of fluorescein isothiocyanate-dextran (FITC-Dextran, MW= 40 kDa) across the pulmonary endothelial cell monolayer.

Endothelial permeability was significantly elevated by thrombin and TNF-α (Figure 4.4A, B). Hypoxia had no significant impact on endothelial barrier function, but a "double hit" condition using a combination of hypoxia and TNF-α resulted in markedly enhanced endothelial leakage (a roughly 20-fold increase compared with normoxic AdCTRL, and a 4-fold increase compared with TNF-α alone) (Figure 4.4A and B). The overexpression of KLF6 had a protective effect on endothelial barrier function in all treatment groups.

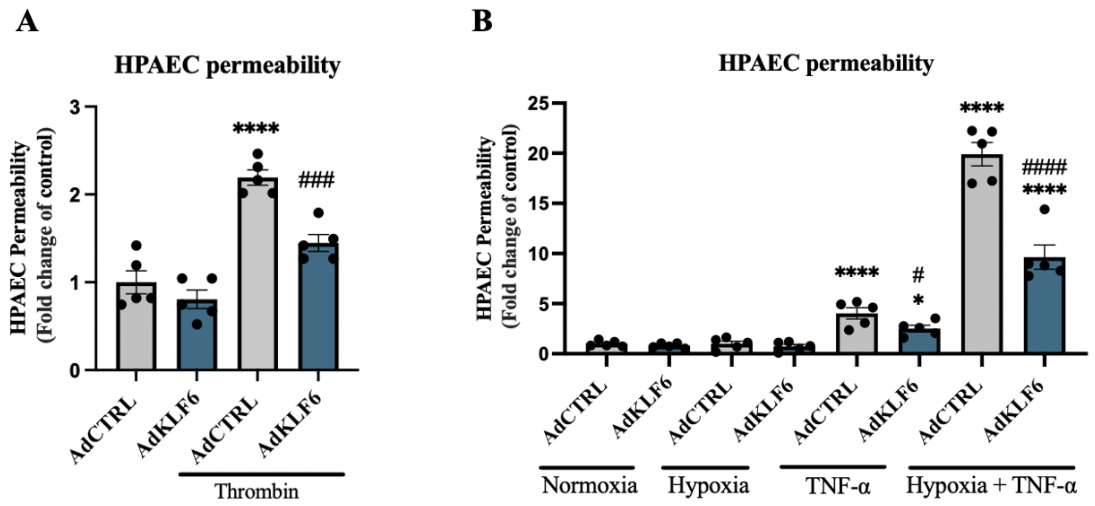

Figure 4.4: Effect of KLF6 overexpression on HPAEC permeability.
HPAECs were infected with either AdCTRL or AdKLF6. Cells were then left untreated or were stimulated with **(A)** thrombin (1 U/mL) for 1 hour or **(B)** TNF-α (10 ng/mL) alone or in combination with hypoxia (2% O_2) for 24 hours. The effect of KLF6 overexpression on HPAEC permeability was assessed by measuring the passage of FITC-dextran (40 kDa, 1 mg/mL) from the upper chamber to the lower chamber. *P<0.05, ***P<0.001, ****P<0.0001, in comparison with untreated adenoviral controls (normoxia); $^{\#}$P<0.05, $^{\#\#\#\#}$P<0.0001, in comparison with corresponding treatment controls. One-way ANOVA with Tukey's post-hoc test; n=5. Error bars indicate mean ±SEM.

4.4.4 KLF6 increases the expression of endothelial junctional proteins in HPAECs.

To explore the potential mechanisms of KLF6-induced effects, changes in the mRNA expression of key regulators of endothelial junctional integrity, CDH5/VE-cadherin and PECAM1 induced by KLF6 overexpression or knockdown were measured by qPCR. The overexpression of KLF6 increased *CDH5*/VE-cadherin and *PECAM1* mRNA expression levels in HPAECs under static conditions (~2-fold-increase, $p<0.001$ and 2.3-fold-increase, $p<0.001$ and $p<0.0001$ respectively compared with adenoviral control) (Figure 4.5A and B), while KLF6 knockdown in HPAECs cultured under flow conditions had no significant effect (Figure 4.5C and D).

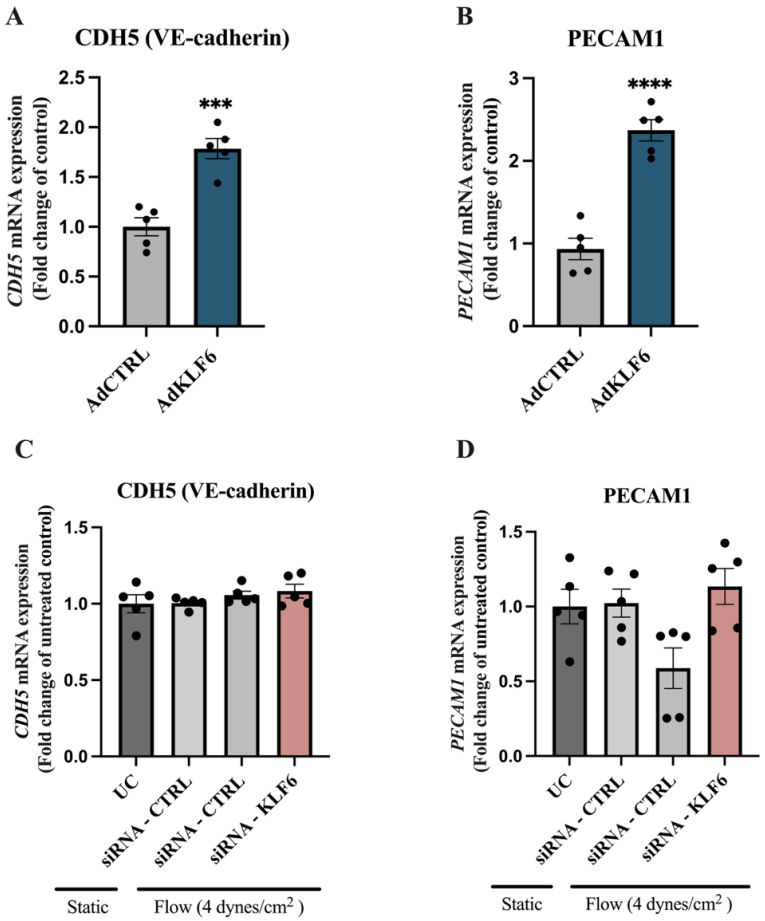

Figure 4.5: Effect of KLF6 overexpression and knockdown on the expression of *CDH5* and *PECAM1* in HPAECs.
(A) *CDH5* (VE-cadherin) and **(B)** *PECAM1* mRNA expression in HPAECs infected with AdCTRL or AdKLF6 for 24 hours. Data were normalized to the reference gene (*ACTB*). ***P<0.001, ****P<0.0001, in comparison with adenoviral controls. Unpaired t-test; n=5. Error bars indicate mean ±SEM. **(C)** *CDH5* (VE-cadherin) and **(D)** *PECAM1* mRNA expression in HPAECs transfected with siRNA-CTRL and siRNA-KLF6 for 48 hours. Data were normalized to the reference gene (*B2M*). Error bars indicate mean ±SEM; n=5.

4.4.5 KLF6 promotes endothelial angiogenesis.

The effect of KLF6 overexpression on angiogenesis was studied using a Matrigel tube formation assay *in vitro* and an arterial explant sprouting assay *ex vivo*, as described in chapter 2, section 2.8.3.

KLF6 overexpression markedly increased the endothelial tube formation (Figure 4.6A). KLF6-overexpressing cells showed a significant increase in the total tube length and the number of nodes and meshes, reflecting the network maturity compared with control cells (Figure 4.6B).

The next set of experiments used an *ex vivo* arterial sprouting angiogenesis model using tissue fragments of human pulmonary artery. To confirm the efficiency of adenoviral transduction in the endothelium of the pulmonary artery tissue, tissue fragments were infected with adenoviruses expressing green fluorescent protein (GFP). After a 24-hour incubation period, the tissues were fixed and stained to identify the endothelial adherens junction marker, VE-cadherin. Endothelial transduction efficiency was >80%, which was similar to that seen in cultured endothelial cells (Figure 4.6C) (Supplementary Figure S6).

Fragments of pulmonary artery were subsequently infected with AdKLF6 before being embedded in Matrigel. After a 2-week incubation period, KLF6-overexpressing explants showed a significant increase in endothelial sprouting (Figure 4.6D), compared with corresponding adenoviral controls (Figure 4.6E).

Consistent with the observed functional effects, KLF6 overexpression significantly increased mRNA expression levels of the key angiogenic markers *FLT1*, *KDR*, *TEK* (TIE2), *HES1*, *SOX17* and *ERG* in HPAECs (Figure 4.7).

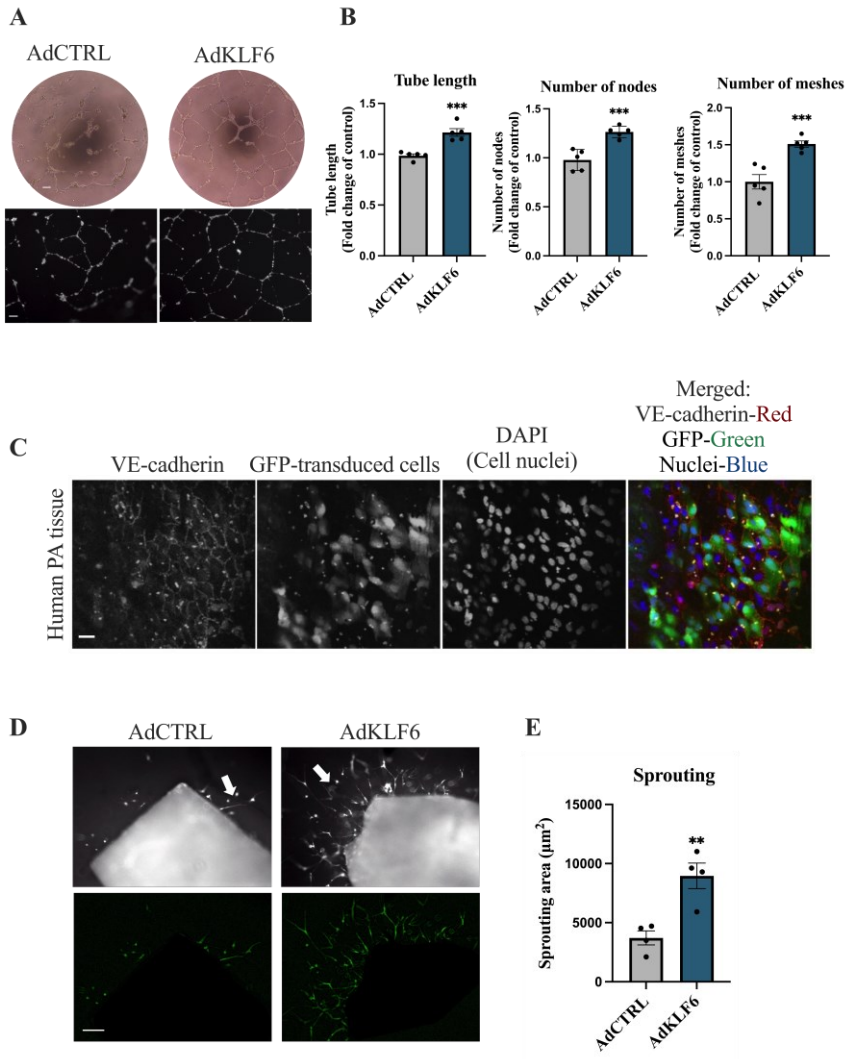

Figure 4.6: Effect of KLF6 overexpression on endothelial tube formation *in vitro* and arterial explants sprouting *ex vivo*.

HPAECs were infected with either AdCTRL or AdKLF6. 24h post-infection, the cells were seeded into a 96-well plate pre-coated with growth factor-reduced Matrigel. The cells were then incubated for 20 hours under normoxic conditions. **(A)** Representative phase contrast and fluorescent images showing HPAEC tube formation and **(B)** quantification of total tube length, number of nodes and meshes in cells treated, as indicated. Total tube length, number of nodes and meshes were quantified using ImageJ software with the Angiogenesis Analyzer plugin. Scale bar = 50µm **(C)** Adenoviral transduction efficiency in the endothelium of human pulmonary artery explants. Surgically removed pulmonary arteries were opened, and the endothelial side was incubated with AdGFP for 24 hours. After 24 hours of incubation, the tissues were fixed and stained for endothelial adherens junction marker VE-cadherin. In the merged image, VE-cadherin is red, nuclei are blue (DAPI) and AdGFP-overexpressing cells are green; n=2. Scale bar = 20µm. **(D)** Representative fluorescence microscopy images of sprouting angiogenesis of human pulmonary artery explants and **(E)** quantification of the total sprouting area using ImageJ. After the removal of the adventitia, the tissue was transfected with AdCTRL or AdKLF6. 4 hours post-transfection, the tissue was cut into approximately 1 mm thick fragments which were embedded in growth factor-reduced Matrigel and incubated under normoxic conditions for 3 weeks. AdKLF6 was added again to the culture at 2 weeks. Endothelial sprouts were fluorescently labelled with Vybrant CFDA SE cell tracer-green (white arrows). Scale bar = 50µm. **P <0.01, in comparison with adenoviral control using unpaired t-test; Error bars indicate mean ±SEM; n=5 for tube formation and n=4 donors for human arteries (with 8 separate explants/groups analysed for each donor).

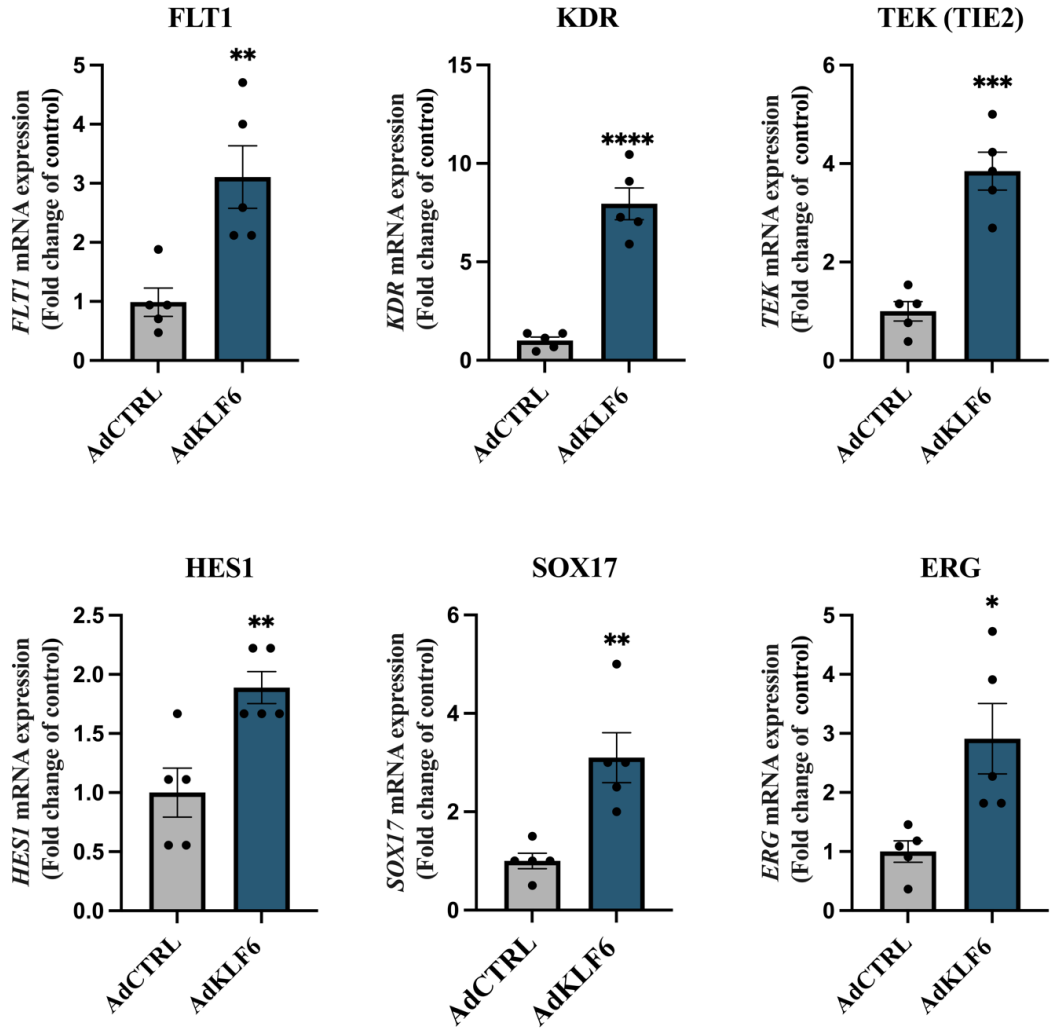

Figure 4.7: KLF6 increases expression of pro-angiogenic markers in HPAECs.
FLT1, *KDR*, *TEK* (TIE2), *HES1*, *SOX17* and *ERG* mRNA expression in HPAECs infected with AdCTRL or AdKLF6 for 24 h. Data were normalized to the reference gene (*ACTB*). *P<0.05, **P<0.01, ***P<0.001, ****P<0.0001, comparison with adenoviral controls. Unpaired t-test; n=5. Error bars indicate mean ±SEM.

4.4.6 KLF6 inhibits endothelial cell proliferation.

To investigate the cellular processes involved in endothelial angiogenesis, the effect of KLF6 overexpression on the proliferative activity of HPAECs was evaluated using an EdU incorporation assay and a qPCR analysis of endothelial proliferation markers.

The overexpression of KLF6 significantly inhibited EC proliferation (a 0.5-fold-decrease, p<0.001) (Figure 4.8A). In contrast, KLF6 knockdown significantly increased endothelial cell proliferation under flow with ~2 -fold-increase, p<0.01 compared to siRNA controls (Figure

4.8B). Notably, the inhibitory effects of KLF6 on HPAEC proliferation were also observed under starvation conditions (Supplementary Figure S7).

Consistent with the observed inhibitory effect, the expression of endothelial proliferative markers *MKI67*, *PCNA* and *BRD4* was significantly decreased by KLF6 overexpression compared with adenoviral controls (Figure 4.9A).

Interestingly, no obvious effect of KLF6 knockdown on the studied proliferation markers was observed under flow (Fig. 4.9B). It may be that cell proliferation under flow involves other pathways that compensate for the absence of KLF6. To validate these results, a more direct method of evaluating cell proliferation, such as a cell counting assay, should be conducted.

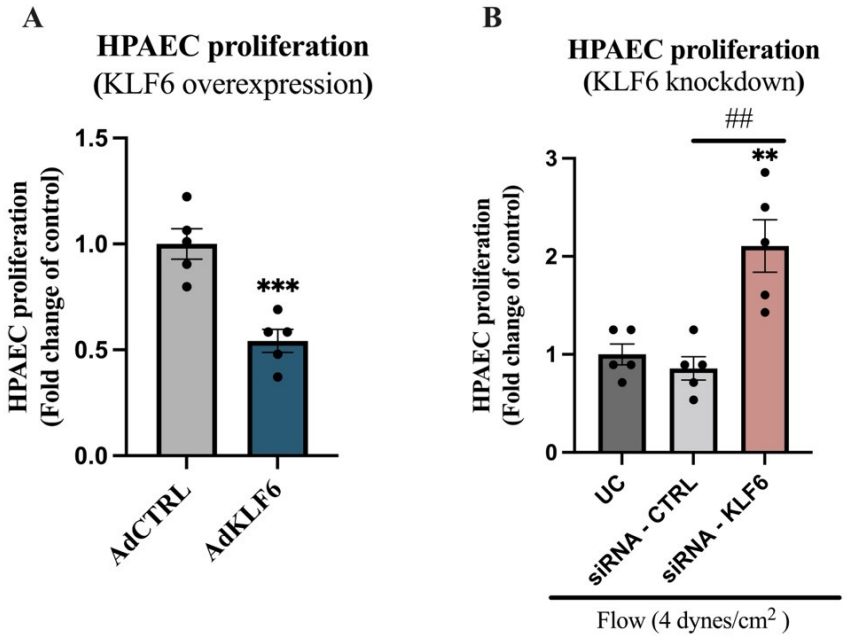

Figure 4.8: Effect of KLF6 overexpression and knockdown on HPAEC proliferation.
HPAEC proliferation was assessed using an EdU incorporation assay in **(A)** HPAECs infected with AdCTRL or AdKLF6 for 24 h. **(B)** HPAECs transfected with KLF6 siRNA or siRNA-CTRL for 48 h. EdU nucleotides were directly added to cell culture medium at a final concentration of 10 µM. CTRL-siRNA and KLF6-siRNA-transfected cells were then subjected to laminar flow of 4 dynes/cm^2 for 24h. Afterwards, EdU-positive cells were observed using a fluorescent Zeiss Axio Observer widefield microscope (Carl Zeiss AG, Germany) with a 10x objective. From the total number of cells, EdU-positive cells were quantified using ImageJ software. ***P<0.001, in comparison with adenoviral controls. Unpaired t-test; n=5. **P<0.01, in comparison with untreated control; $^{\#\#}$P<0.01, in comparison with siRNA negative controls. One-way ANOVA with Tukey's post-hoc test; n=5. Error bars indicate mean ±SEM.

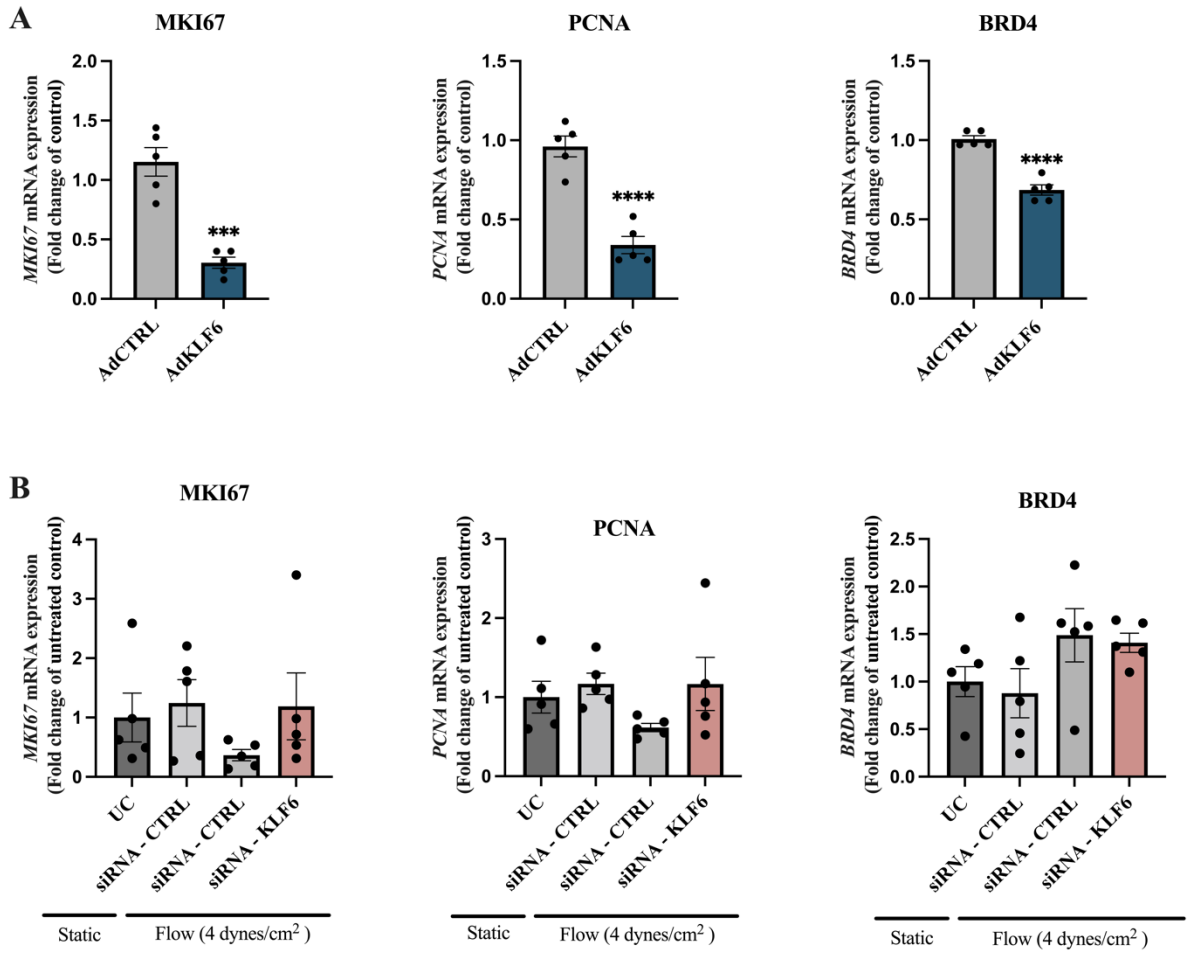

Figure 4.9: Effect of KLF6 on expression of proliferation markers in HPAECs.
MKI67, *PCNA* and *BRD4* mRNA expression in **(A)** HPAECs infected with AdCTRL or AdKLF6 for 24 h. Data were normalized to the reference gene (*ACTB*). ***P<0.001, ****P<0.0001, in comparison with adenoviral controls. Unpaired t-test; n=5. Error bars indicate mean ±SEM. **(B)** HPAECs transfected with siRNA-KLF6 or siRNA-CTRL and stimulated with flow for 24 h. Data were normalized to the reference gene (*B2M*). Error bars indicate mean ±SEM; n=5.

4.4.7 KLF6 increases endothelial cell migration.

The effects of KLF6 overexpression and knockdown on endothelial cell migration were assessed in a wound healing assay, as described in chapter 2, Section 2.8.5.

Cells that overexpressed KLF6 were cultured in a complete medium and a serum- and growth factor-reduced medium (starvation medium), and results showed a significant reduction in the wound area, indicating an increase in the number of cells migrating towards the wounded area (Figure 4.10). In contrast, KLF6-knockdown significantly reduced endothelial cell migration and wound healing under flow (Figure 4.11).

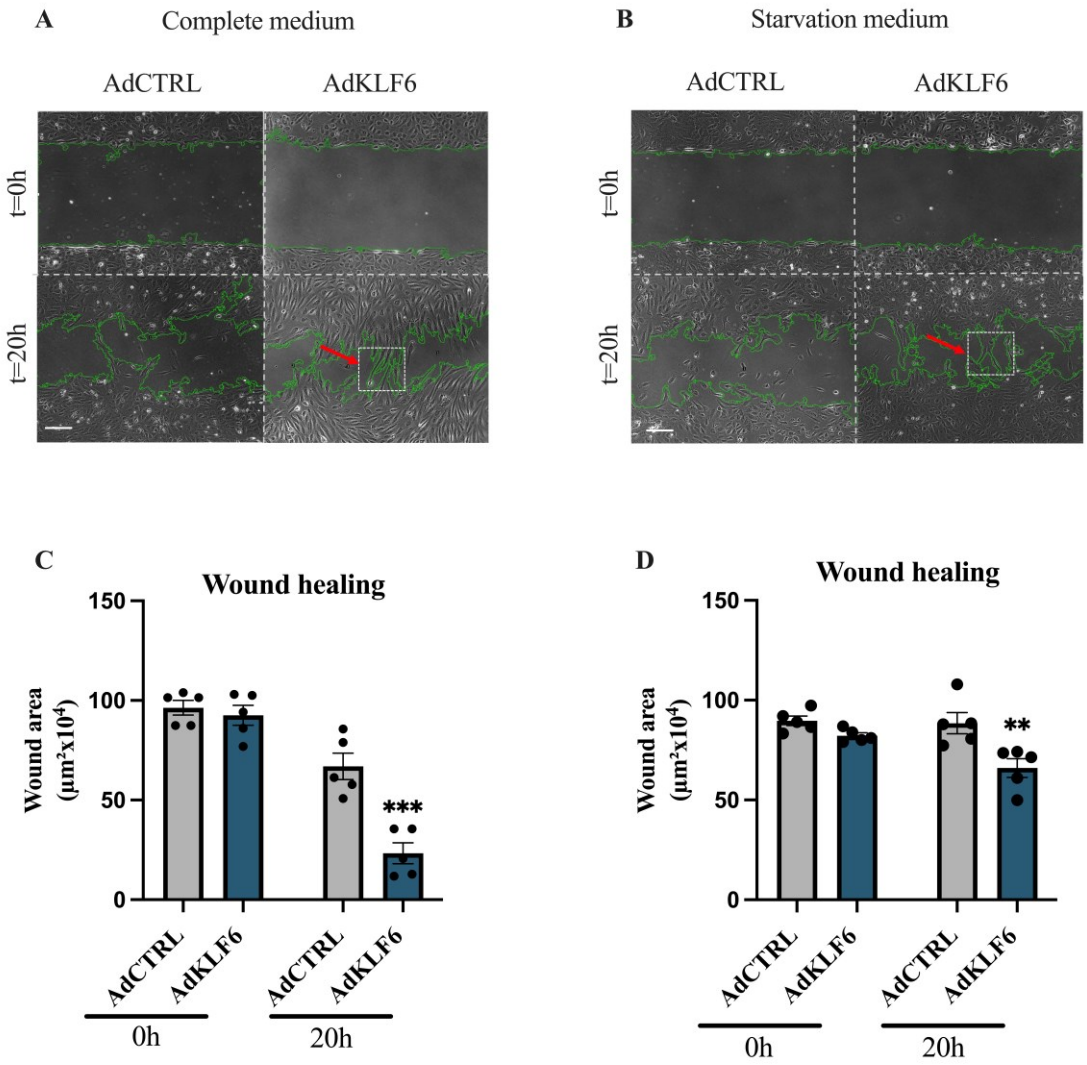

Figure 4.10: Effect of KLF6 overexpression on HPAEC Migration.
The effect of KLF6 overexpression on endothelial cell migration was assessed by wound healing assay using an ibidi Culture-Insert 2 Well. HPAECs were infected with AdCTRL or AdKLF6, and were starved in 0.2% FBS with no growth factors. After 6 hours of starvation, the culture insert was removed. Representative phase-contrast microscopy images show a monolayer of HPAECs cultured in **(A)** a complete medium or **(B)** a starvation medium at 0 h and 20 h post-wounding. The green lines highlight the edges of the wound. The red arrows pointing to the boxed areas indicate cells migrating into the wound. Scale bar = 50µm. Quantitation of wound area in **(C)** the complete medium and **(D)** the starvation medium was undertaken using ImageJ. **P<0.01, ****P<0.0001, in comparison with adenoviral controls. Two-way ANOVA with Tukey's post-hoc test; n=5. Error bars indicate mean ±SEM.

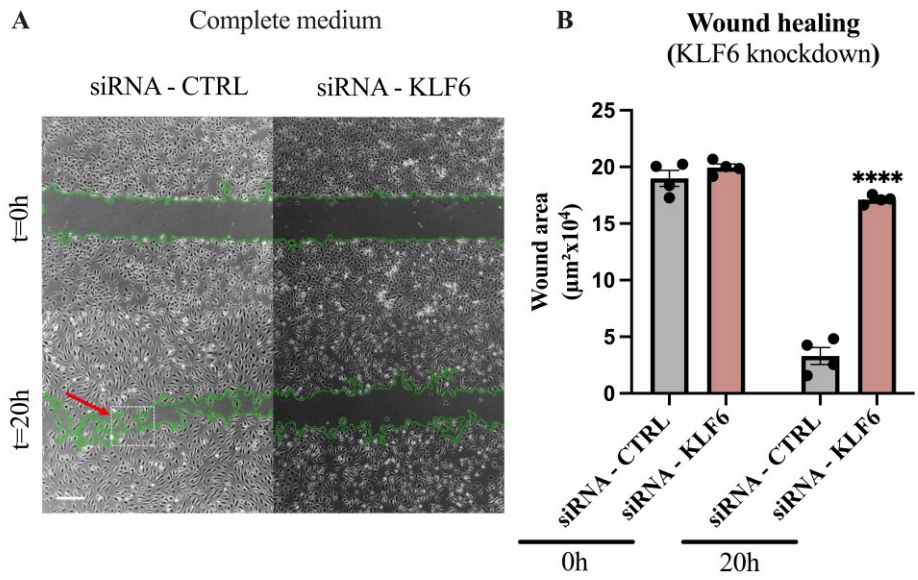

Figure 4.11: Effect of KLF6 knockdown on HPAEC Migration.
The effect of KLF6 knockdown on endothelial cell migration was examined in a scratch assay using a sterile 200 µl pipette tip. HPAECs were transfected with siRNA-KLF6 or siRNA-CTRL. After 48 h of siRNA exposure, cells were starved (0.2% FBS with no growth factors) for 6 h. The cells were then vertically scratched using a sterile 200 µl pipette tip and subjected to laminar flow at 4 dynes/cm^2 for 20 h. **(A)** Representative phase-contrast microscopy images showing HPAECs monolayer cultured in complete medium at 0 h and 20 h post-wounding. The green lines highlight the edges of the wound. The red arrow pointing to a boxed area shows cells that migrated into the wound. Scale bar = 50µm. **(B)** Quantitation of wound area using ImageJ. ****P<0.0001, in comparison with siRNA control. Two-way ANOVA with Tukey's post-hoc test; n=5. Error bars indicate mean ±SEM.

4.4.8 The effect of KLF6 on apoptosis in HPAECs.

To induce apoptosis, KLF6-overexpressing HPAECs were cultured in a reduced serum (0.2% FBS), and a serum- and growth factor-free medium for 24 h. Serum starvation is a known inducer of apoptosis (Hogg et al., 1999), which mimics the conditions of suboptimal nutrient supply to cells that can occur at sites of vascular obstruction. Serum starvation induced cell detachment in flow-stimulated cells, which is likely to result from deficiency in adhesion molecules (fibronectin and vitronectin) present in the serum. A second apoptosis inducer, staurosporine (STS) (Kabir, Lobo & Zachary, 2002) was therefore chosen to study apoptotic cell responses under flow, while cells grown under optimal conditions in the complete medium were treated as a negative control. Apoptosis was measured using a Caspase-Glo 3/7 assay and a Click-iT Plus TUNEL assay. The Caspase-Glo 3/7 assay was used to measure caspase-3 and -7 activities in cells that overexpressed KLF6 which had been cultured under static conditions, while the Click-iT Plus TUNEL assay was used to detect apoptotic cells in KLF6 knockdown

cells cultured in a microfluidic 6-channel µ-slide from ibidi and subjected to laminar flow (4 dynes/cm^2). Both assays were used to measure the late stage of apoptosis.

KLF6 overexpression significantly reduced caspase-3 and -7 activity under all experimental conditions, in comparison with treated controls (Figure 4.12A). KLF6 siRNA- mediated KLF6 knockdown significantly increased the number of apoptotic, TUNEL-positive cells (a 21-fold-increase, p<0.01) in HPAECs that had been treated with STS, compared with non-targeting siRNA controls (Figure 4.12B).

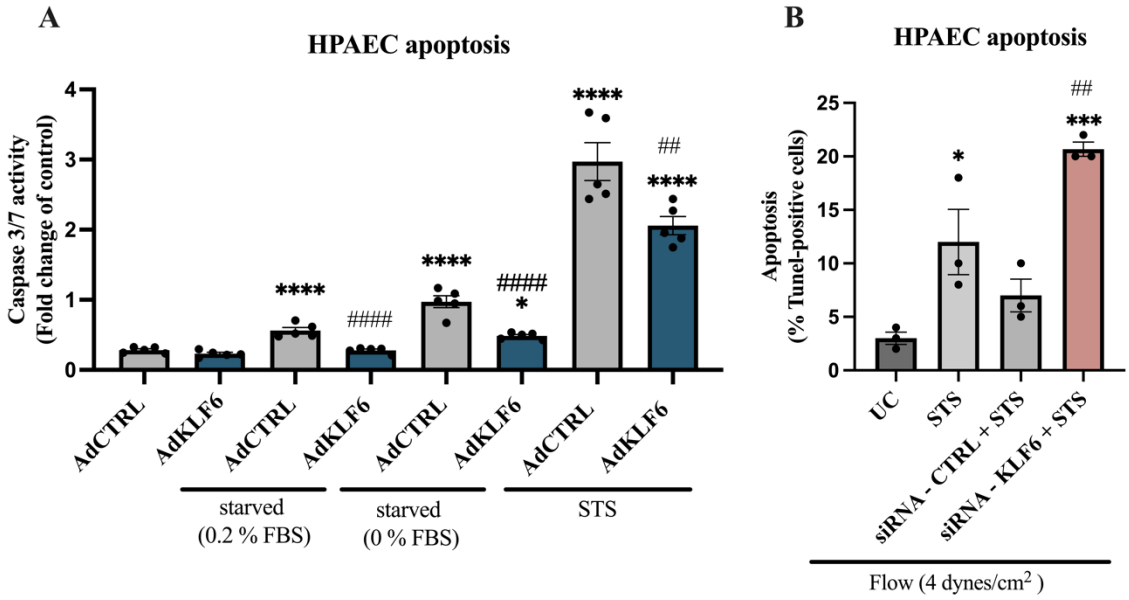

Figure 4.12: Effect of changes in KLF6 expression on HPAEC apoptosis.
(A) Bar graph showing the effects of KLF6 overexpression on caspase-3 and -7 activity in HPAECs cultured in a complete growth medium or in a starvation medium, with either 0.2% FBS or serum- and growth factor-free medium, or in HPAECs stimulated with STS for 24 h. *P<0.05, ****P<0.0001, in comparison with untreated control; $^{\#\#}$P<0.01, $^{\#\#\#\#}$P<0.0001, in comparison with corresponding treated controls. One-way ANOVA with Tukey's post-hoc test; n=5. Error bars indicate mean ±SEM. **(B)** Bar graph showing effects of KLF6 knockdown on HPAEC apoptosis under flow, assessed in a TUNEL assay 48 h after siRNA transfection. KLF6-siRNA-transfected cells were subjected to a laminar flow of 4 dynes/cm^2 with or without STS (1µM) for 24 h. *P<0.05, ***P<0.001, in comparison with untreated control; $^{\#\#}$P<0.01, in comparison with siRNA negative controls. One-way ANOVA with Tukey's post-hoc test; n=5. Error bars indicate mean ±SEM.

4.5 Discussion

The experiments described in this chapter examined the role of KLF6 in the regulation of pulmonary endothelial function *in vitro*.

Endothelial damage resulting from various vascular stresses including hypoxia and inflammation is thought to be a critical initiating factor in the development of PAH (Hu et al., 2020b). I therefore investigated the effects of KLF6 overexpression and knockdown on the activation of pro-inflammatory transcription factor NF-κB in pulmonary endothelial cells that had been stimulated with TNF-α, hypoxia and a combination of the two. The overexpression of KLF6 had an anti-inflammatory effect, while KLF6 knockdown enhanced inflammatory response that was similar to the effects of closely related flow-induced transcription factors KLF2 and KLF4 (Hamik et al., 2007; SenBanerjee et al., 2004). In contrast to KLF2 and KLF4 – which were either suppressed or unaffected by TNF-α – KLF6 activity was upregulated in response to this cytokine (the results are described in Chapter 3, Section 3.4.3). These results suggest that KLF6 is induced as a response to vascular injury, and acts as a negative regulator of NF-κB. Recent reports confirm our observations, showing that KLF6 mediates the anti-inflammatory effects of the drugs naproxen and apremilast in HUVECs and human aortic endothelial cells (HAECs) (Wu et al., 2021; Wang et al., 2020a). These anti-inflammatory drugs increased the expression of KLF6, which then inhibited monocyte adhesion to ECs by reducing the expression of MCP-1/*CCL2* and *VCAM1* in HAECs or by reducing the expression of *ICAM1* and *SELE*/E-selectin in HUVECs. This complements our findings, and suggests that KLF6 may potentially have a protective effect on the inflammatory responses seen in the intimal and medial layers of the pulmonary artery in PAH.

The loss of endothelial barrier integrity is thought to be an early event in PAH pathogenesis (Budhiraja, Tuder & Hassoun, 2004). Endothelial cell permeability is enabled by various inflammatory mediators, including thrombin, TNF-α and hypoxia, which stimulate endothelial cell leakage and permeability by affecting the expression and stability of endothelial junctional proteins (Aghajanian et al., 2008). The integrity of the endothelial monolayer is maintained, in part by the endothelial junctional proteins VE-cadherin and PECAM1 (Privratsky & Newman, 2014; Giannotta, Trani & Dejana, 2013). The overexpression of KLF6 significantly improves endothelial barrier function in response to thrombin, TNF-α and hypoxia. My results suggest

that the mechanism is likely to involve a KLF6-induced increase in the mRNA expression of junctional proteins *CDH5*/VE-cadherin and *PECAM1* in the pulmonary endothelium. Previous studies have shown that KLF6 plays a role in the regulation of blood-tumour barrier (BTB) integrity and permeability in glioma endothelial cells, and can directly target tight junction proteins such as occludin, claudin-5 and zonula occludens-1 (ZO-1) by binding to their promoters (Ma et al., 2014).

We did not observe any effect of KLF6 knockdown on junctional protein expression under flow, and this is probably due to the homeostatic and barrier-enhancing effect of flow on the endothelium. Laminar shear stress plays a role in maintaining endothelial junctional integrity through the upregulation of the expression of tight junction proteins ZO-1 and occludin in HUVECs (Yang et al., 2020). Interestingly, HUVECs that were stimulated with laminar shear stress showed an increase in the expression of endothelial junctional proteins VE-cadherin and PECAM1 (Xie et al., 2020; Mahmoud et al., 2017). In future studies, it would be useful to investigate the effect of KLF6 knockdown on endothelial barrier function using an organ-on-a-chip containing 0.4 μm polyethylene terephthalate (PET) membrane to directly test the effect of KLF6 on endothelial permeability under flow conditions.

Disorganized angiogenesis is a key factor in the development of plexiform lesions in severe PAH, as shown by increased expression of angiogenesis markers such as VEGF and VEGFR2/KDR (Tuder et al., 2001a). The overexpression of KLF6 significantly increased endothelial angiogenesis according to the tube formation assay *in vitro* and in the human pulmonary artery explants sprouting assay *ex vivo*. This was accompanied by a significant increase in the mRNA expression levels of endothelial pro-angiogenic markers *FLT1*, *KDR*, *TEK*/TIE2, *HES1*, *SOX17* and *ERG*. VEGF, along with its main receptors VEGF receptor 1 (VEGFR1/FLT1) and VEGF receptor 2 (VEGFR2/KDR), are important regulators of physiological and pathological angiogenesis (Shibuya, 2013), while TIE2 is an endothelial-specific receptor tyrosine kinase (RTK) that is crucially involved in vascular development (Sato et al., 1993, 1995). HES1 stimulates Notch signalling and regulates endothelial cell proliferation, differentiation and death, which are important processes required for angiogenesis (Kageyama, Ohtsuka & Kobayashi, 2007; Miele, 2006). SOX17 acts as a proangiogenic regulator by enhancing VEGF signalling, promoting EC migration and angiogenesis in both mice and human endothelial cells (Lee et al., 2014b; Yang et al., 2013) and ERG is a key regulator of EC homeostasis and angiogenesis (Shah, Birdsey & Randi,

2016). All of these pro-angiogenic markers have been implicated in PAH (Zhong & Yu, 2023; Wang et al., 2021a; Eyries et al., 2020; Looney et al., 2017; Song et al., 2015; Dewachter et al., 2006). Increased KLF6 expression has previously been linked with the angiogenic activation of pulmonary microvascular endothelial cells (PMVECs) in a rat model of hepatopulmonary syndrome (HPS) (Yang et al., 2019). KLF6 expression induced by BMP9 also increased in PMVECs cultured *in vitro* using a common bile duct ligation (CBDL) rat serum (Yang et al., 2019). In the same study, KLF6 siRNA inhibited PMVEC-induced endothelial tube formation *in vitro*, and the mechanism underlying this response was associated with suppression of ALK1 and ENG expression (Yang et al., 2019).

Angiogenesis involves three important cellular processes: the remodelling of endothelial junctions, endothelial cell proliferation and migration (Wang et al., 2020c). My results show that KLF6 increases the expression of *CDH5*/VE-cadherin and *PECAM1*, which are important components of the intercellular junctions that are required for the formation of new blood vessels. KLF6 has an inhibitory effect on endothelial cell proliferation, similar to the effects of the other two flow-induced KLF factors, KLF2 and KLF4. KLF6 has been shown to act as a tumour suppressor because of its ability to inhibit cell proliferation in a cell type- and context-specific manner through a variety of cancer-related pathways, including the regulation of p21, the disruption of interactions between cyclin D1 and CDK4 and the inhibition of c-Jun proto-oncoprotein (Benzeno et al., 2004; Slavin et al., 2004; Narla et al., 2001). In contrast, the loss of *KLF6* has been shown to promote cell growth in several types of cancer, including non-small-cell lung cancer and prostate cancer (Zeng et al., 2022; Narla et al., 2001). In this study, KLF6 knockdown significantly increased endothelial cell proliferation as assessed by EdU incorporation assay, although the expression of proliferation markers was relatively unaffected. This potential discrepancy may be due to the different regulatory mechanisms that operate during different phases of the cell cycle. Other methods of evaluating cell proliferation should be used to further verify the effect of KLF6 knockdown under flow.

The results presented in this chapter show that the overexpression of KLF6 enhanced endothelial cell migration and accelerated endothelial wound healing, whereas KLF6 knockdown reduced EC migration and prolonged wound healing time. This suggests that the mechanism of KLF6-induced endothelial angiogenesis mainly involves EC migration. Consistent with this, KLF6 and SP2 have been shown to regulate cell motility in ECFCs in a MMP-9-dependent way (Das et al., 2006). After the activation of farnesoid X receptor (FXR),

the small heterodimeric partner (SHP) interacts with KLF6 and SP2, leading to the disruption of the KLF6/SP2 repressor complex. This results in upregulation of MMP-9 as well as increased cell motility (Das et al., 2006). In contrast, KLF6 siRNA inhibited PMVEC migration in response to CBDL rat serum (Yang et al., 2019). In future studies it would be interesting to use an organ-on-a-chip model of the pulmonary artery with a PET membrane containing 8.0 μm pores to mimic the arterial basement membrane, in order to observe the effect of KLF6 knockdown on endothelial cell migration in response to pro-angiogenic stimuli relevant to PAH, such as VEGF.

Increased endothelial apoptosis occurs early in the development of PAH, and is thought to be followed by a clonal selection of highly proliferative, apoptosis-resistant cells that contribute to vascular remodelling in PAH (Sakao, Tatsumi & Voelkel, 2009; Lévy et al., 2007; Sakao et al., 2006). In this study, endothelial cell apoptosis was induced using two different stimuli: serum and growth factor deprivation or staurosporine, a protein kinase inhibitor known to trigger apoptosis in various cell types (Bertrand et al., 1994). The overexpression of KLF6 significantly inhibited endothelial cell apoptosis in response to pro-apoptotic stimuli, while the knockdown of KLF6 significantly increased EC apoptosis. Our findings are consistent with reports on other cell types, where KLF6 knockdown by siRNA in MCF-7 and HepG2 cells treated with cisplatin increased the number of sub-G1 apoptotic cell populations, suggesting the antiapoptotic activity of KLF6 (D'Astolfo et al., 2008).

4.6 Conclusion

The functional studies described in this chapter show that KLF6 has anti-proliferative, anti-inflammatory, anti-apoptotic and barrier-protective effects in the pulmonary vascular endothelium which are similar to the actions of closely related flow-dependent transcription factors KLF2 and KLF4 (Figure 4.13) (Sindi et al., 2020; Sweet et al., 2018; Shen et al., 2009). Unlike the effects of KLF2 and KLF4, KLF6 promotes endothelial angiogenesis, most probably through enhanced endothelial cell migration and the increased expression of junctional proteins.

These results, along with the results described in the previous chapter, suggest that KLF6 is induced in response to endothelial injury to orchestrate the process of repair. Considering its regulatory role in endothelial survival and angiogenesis, any dysregulation in KLF6 signalling could potentially contribute to pulmonary endothelial dysfunction in PAH.

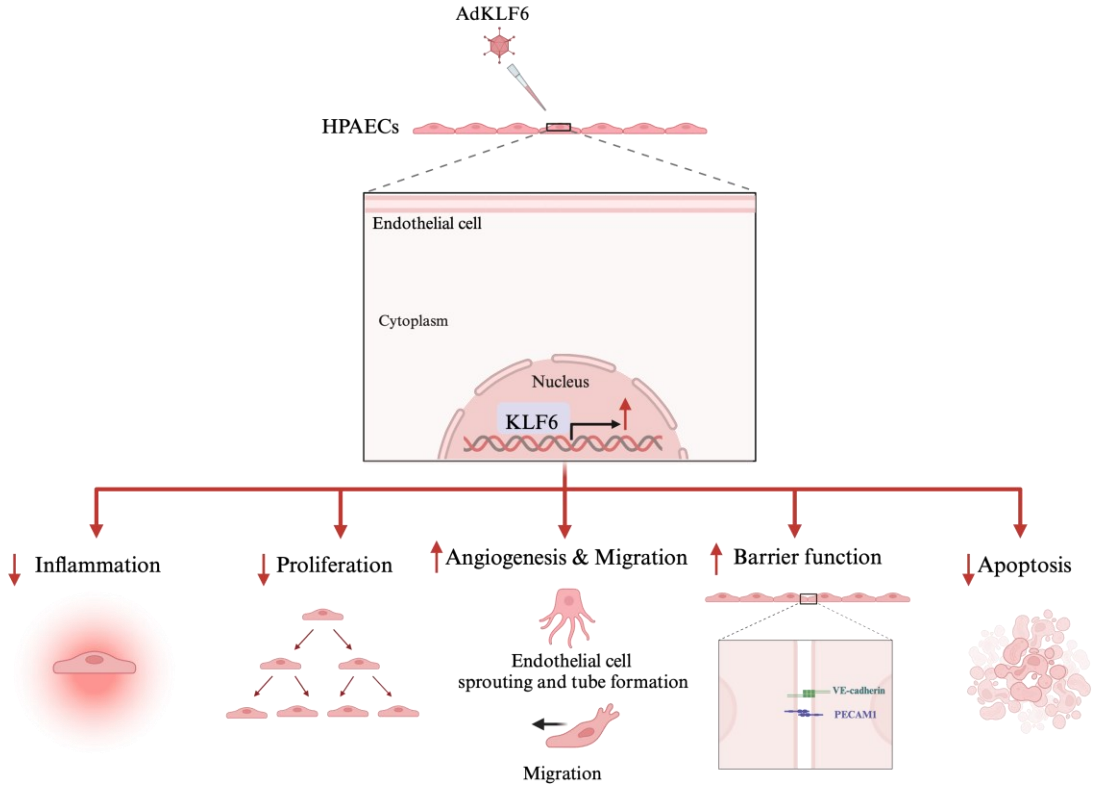

Figure 4.13: Summary of the key findings of Chapter 4.
Illustration created by the author using BioRender.com.

Chapter 5 Results: KLF6 expression in preclinical models of PAH and in endothelial cells from PAH patients

5.1 Introduction

Preclinical animal models of PAH were used to investigate pathological changes that take place in the early and late stages of the disease in order to identify potential molecular targets for therapeutic intervention. Animal models of PAH share many pathological features with human PAH, including hemodynamic changes and histopathological alterations. However, none of the preclinical animal models can accurately replicate the pathophysiological aspects of severe human PAH (Stenmark et al., 2009). In particular, the formation of the plexiform lesions observed in severe human PAH cannot be fully reproduced in preclinical animal models (Coste et al., 2017).

Monocrotaline (MCT) rats, chronic hypoxia or Sugen/hypoxia (SuHx) rats and mice are the most commonly used preclinical animal models of PAH (Stenmark et al., 2009). These models are described in more detail in Chapter 1, Section 1.4, and a brief summary of key histopathological features of preclinical rodent models of PAH is provided in Figure 1.5.

The chronic hypoxia mouse model is achieved by keeping the animals under hypoxic conditions for at least 2 weeks. Exposure to hypoxia induces muscularisation in the small pulmonary arteries due to increased PASMC proliferation and the trans-differentiation of endothelial cells into mesenchymal-like cells (Stenmark et al., 2009). The chronic hypoxia mouse model is characterized by increased mPAP and pulmonary vascular remodelling, and these vascular alterations are fully reversible upon re-exposure to normoxia, in contrast to the changes observed in human PAH (Chen et al., 2017b).

The MCT rat model is the most commonly used *in vivo* model of PAH, as the necessary procedure to establishing PAH is inexpensive and can be induced by a single subcutaneous injection of monocrotaline (MCT), a toxic pyrrolizidine alkaloid that causes injury to the pulmonary endothelial cells, followed by excessive inflammatory responses and progressive pulmonary vascular remodelling (Gomez-Arroyo et al., 2012).

The SuHx rat model is based on the "double hit" exposure to chronic hypoxia combined with Sugen 5416, the VEGFR2 antagonist. This model develops severe and irreversible PAH as the disease persists and progresses – even after animal is re-exposed to normoxia (Ciuclan et al., 2011). The SuHx rat model is characterized by the hyperproliferation of the intimal layer, causing luminal obliteration and the formation of plexiform-like lesions which to some degree recapitulate the pulmonary plexogenic arteriopathy of human PAH (Abe et al., 2010; Taraseviciene-Stewart et al., 2001).

As well as using preclinical animal models, blood-derived endothelial colony forming cells (ECFCs) can also facilitate the modelling of many cardiovascular diseases by maintaining the disease phenotype in culture (Besnier et al., 2021). PAH ECFCs show several disease-related cellular abnormalities, including highly proliferative pro-angiogenic phenotypes that show exaggerated or uncontrolled repair processes in the remodelled vessels, suggesting that these cells may contribute to the formation of pulmonary vascular obstructions (Paschalaki & Randi, 2018; Duong et al., 2011; Toshner et al., 2009). However, their precise role in health and disease conditions is still unknown.

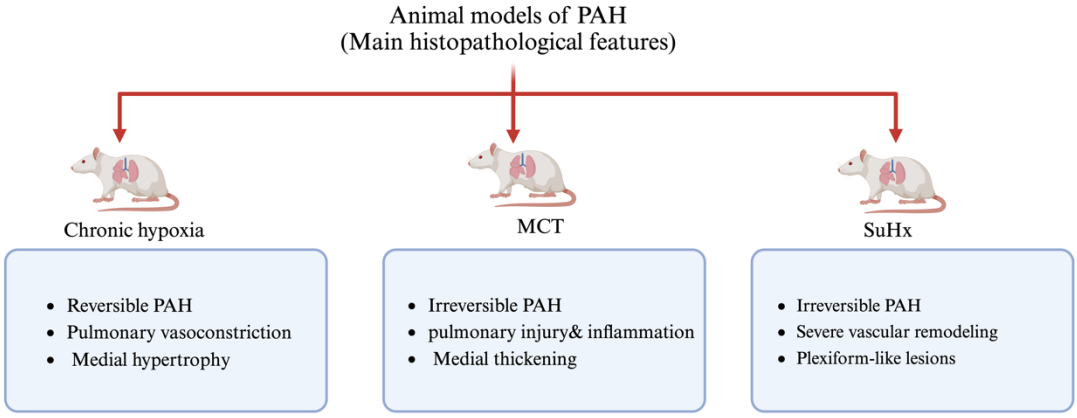

Figure 5.1: Summary of the main histopathological features found in preclinical animal models. Illustration created by the author using BioRender.com.

5.2 Experimental aims

To investigate the expression of KLF6 in various experimental animal models of PAH including chronic hypoxia, Sugen/hypoxia (SuHx) and monocrotaline (MCT) at different stages of the disease and in ECFCs from PAH patients with *BMPR2* mutations.

5.3 Experimental outline

The outline of the experiments described in this chapter is shown in Figure 5.2. A brief description of the experimental design and methodology is provided below.

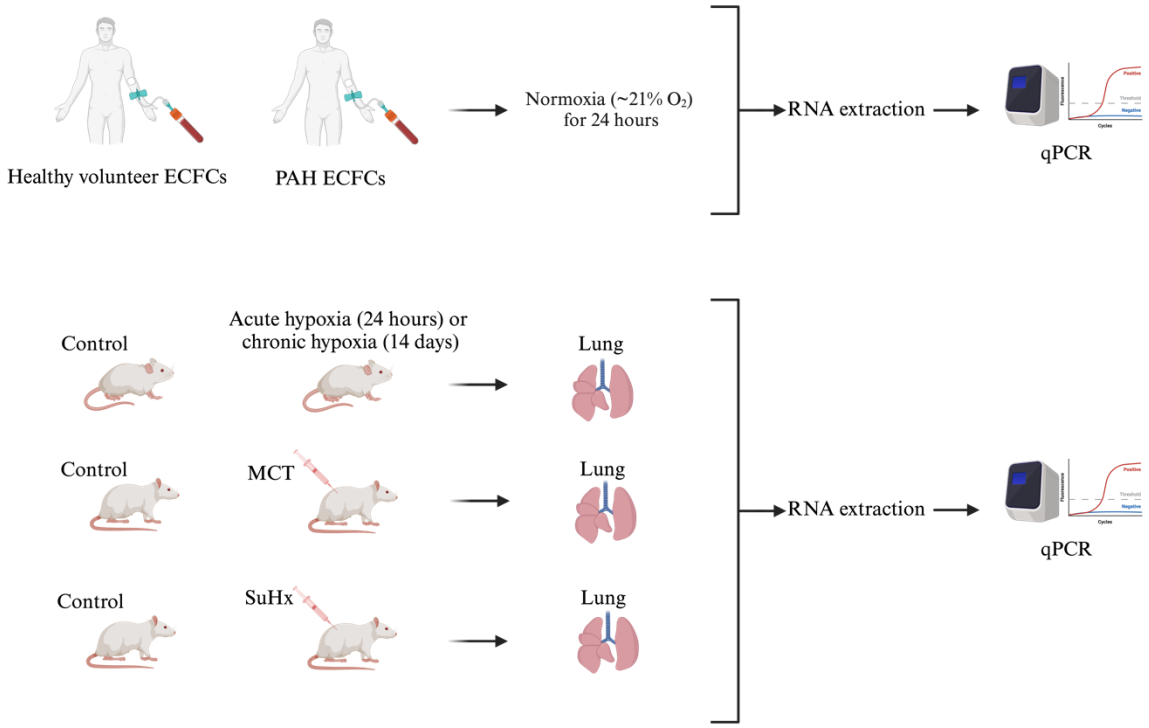

Figure 5.2: Outline of experiments presented in chapter 5.
KLF6 expression was measured in blood derived late outgrowth endothelial colony forming cells (ECFCs) from healthy volunteers and PAH patients with *BMPR2* mutations exposed to normoxic conditions (21% O_2; 24 hours) using qPCR. KLF6 expression was also measured in the lungs of preclinical animal models of PAH, including chronic hypoxia mouse models and Sugen/hypoxia (SuHx) and MCT rat models. Illustration created by the author using BioRender.com.

5.3.1 Animal experiments

All animal studies were carried out in accordance with the UK Home Office Animals (Scientific Procedures) Act 1986. All animals were assigned randomly to groups, and all personnel involved in data collection and analysis were blinded to the treatment status of each animal, including haemodynamic and histopathologic measurements. Only males that were weight- and age-matched were used in the experiment because in contrast to clinical studies on humans, most animal studies have demonstrated that female sex and oestrogen supplementation have a protective effect against hypoxia-induced PH in rodents (Umar, Rabinovitch & Eghbali, 2012; Umar et al., 2011).

5.3.1.1 Experimental design

5.3.1.1.1 Acute and chronic hypoxia mouse model

In the acute hypoxia study, C57/BL male mice (n=10; 10-12 weeks old, 20 g; Charles River, UK) were allowed to acclimatise in the facility for 7 days before experimentation began. The mice were randomly divided into two groups: normoxia (n=5) and hypoxia (n=5). Hypoxic mice were exposed to normobaric hypoxic (FiO_2=10%) conditions for 24 hours.

In the chronic hypoxia-induced pulmonary hypertension study, C57/BL male mice (n=12; 10-12 weeks old, 20 g; Charles River, UK) were allowed to acclimatise themselves to the facility for 2 days before experimentation. The mice were then randomly divided into two groups: normoxia (n=4) and hypoxia (n=8) and were exposed to either normoxic or normobaric hypoxic (10% O_2) conditions for 14 days.

At 2 weeks, the mice were anaesthetised intraperitoneally with a Ketamine/Dormitor (75 mg/kg + 1mg/kg). The development of PH was verified as previously reported (Zhao et al., 1999). Briefly, right ventricular systolic pressure (RVSP) was assessed in the spontaneously breathing anesthetized animal by measuring direct cardiac puncture using a closed-chest technique. The mice were then euthanized, and the hearts were removed. The left and right ventricles were weighed, and right ventricular hypertrophy was evaluated by calculating the ratio of the weight of the right ventricle to the left ventricle plus septum (RV/LV+S). The right lungs were either placed in RNAlater^{TM} RNA Stabilization Solution for RNA isolation or snap-frozen in liquid nitrogen and stored at -80°C for future experiments.

5.3.1.1.2 MCT rat model of PAH

Sprague-Dawley rats (250-360 g; Charles River, Margate, UK) were either untreated (control, n=5) or injected subcutaneously with MCT solution (60 mg/kg, Sigma-Aldrich) to induce PAH (n=5) (Wojciak-Stothard et al., 2014).

At 3, 7 and 14 days after MCT injection, the rats were anaesthetised intraperitoneally with a Ketamine/Dormitor (75 mg/kg + 1 mg/kg). The development of PH was verified by right ventricular systolic pressure (RVSP). RVSP was assessed in the spontaneously breathing, anesthetized animals by measuring direct cardiac puncture using a closed-chest technique. The rats were then euthanized, and the hearts were removed. The left and right ventricles were weighed, and right ventricular hypertrophy was evaluated by calculating the ratio of the weight of the right ventricle to the left ventricle plus septum (RV/LV+S). The right lungs were either placed in RNAlater^{TM} RNA Stabilization Solution for RNA isolation or snap-frozen in liquid nitrogen and stored at -80°C for future experiments.

5.3.1.1.3 Sugen/hypoxia rat model of PAH

C57/BL male rats (n=8; 8 weeks old, 20 g; Charles River, UK) were given a single subcutaneous injection of Sugen (SU5416; 20 mg/kg; Tocris Bioscience, UK), suspended in 0.5% [w/v] carboxymethylcellulose sodium, 0.9% [w/v] sodium chloride, 0.4% [v/v] polysorbate 80, 0.9% [v/v] benzyl alcohol in deionized water once per week. The rats were then exposed to normobaric hypoxic (FiO_2=10%) conditions for 4 weeks followed by a return to normoxia for 4 weeks (n=5 SuHx group) as described previously (Sindi et al., 2020). The rats in the control groups were kept under normoxic conditions (n=3 for control group).

At 8 weeks the rats were anaesthetised intraperitoneally with a Ketamine/Dormitor (75 mg/kg + 1 mg/kg). The development of PH was verified as previously reported (Zhao et al., 1999). Briefly, right ventricular systolic pressure (RVSP) was assessed in the spontaneously breathing anesthetized animal by measuring direct cardiac puncture using a closed-chest technique. The rats were then euthanized, and the hearts were removed. The left and right ventricles were weighed, and right ventricular hypertrophy was evaluated by calculating the ratio of the weight of the right ventricle to the left ventricle plus septum (RV/LV+S). The right lungs were either placed in an RNAlater^{TM} RNA Stabilization Solution for RNA isolation or snap-frozen in liquid nitrogen and stored at -80°C for future experiments.

5.3.2 Measurement of *KLF6* mRNA expression levels in ECFCs using qPCR.

Human endothelial colony forming cells (ECFC) from heritable PAH patients with *BMPR2* mutations and healthy controls were clonally isolated from peripheral blood samples and expanded and characterised as previously described in Section 2.2.2. ECFCs from HPAH patients with rare pathogenic *BMPR2* variants (n=5) and healthy volunteers (n=4) were cultured, harvested and subjected to RNA extraction, reverse transcription and RT-qPCR analysis to measure the mRNA expression levels of *KLF6*. Further details regarding the demographic and clinical characteristics of HPAH patients, including *BMPR2* mutation type and treatment regimen, is provided in Section 2.2.2.

5.4 Results

5.4.1 *KLF6* expression in chronic hypoxia mouse model

The expression of *KLF6* mRNA in the lung was measured in three experimental groups: normoxia (n=4/group), acute hypoxia (10% O_2 for 24 hours, n=5) and chronic hypoxia (10% O_2 for 14 days, n=8) (Figure 5.3A). *KLF6* mRNA expression levels were significantly increased in the lung tissues of mice that had been exposed to acute (24 hours) hypoxia (~ 4-fold increase, p<0.0001) compared to normoxic control mice (Figure 5.3B). *KLF6* mRNA expression levels in mice were unaffected by chronic hypoxic exposure (14 days).

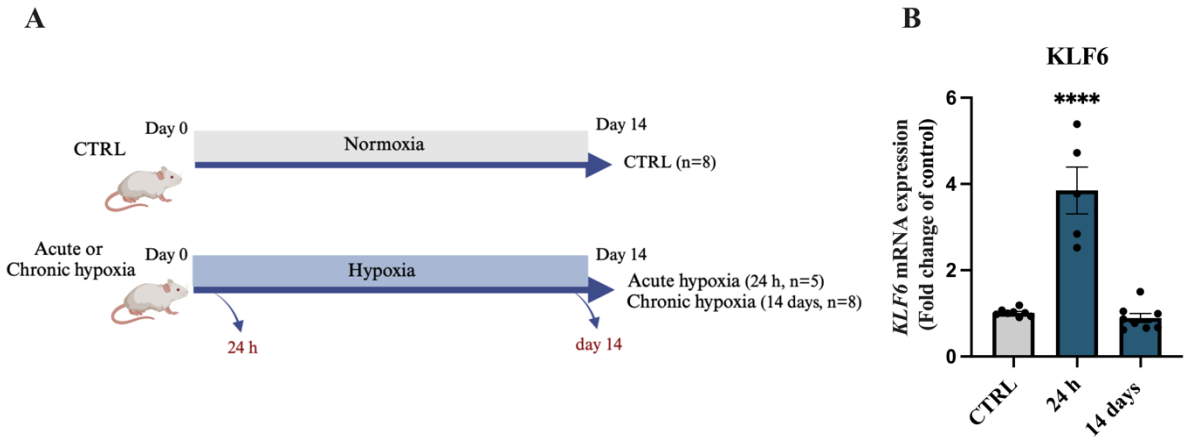

Figure 5.3: *KLF6* mRNA expression levels in the lungs of chronic hypoxia mouse model of PAH. **(A)** Schematic diagram of experimental timeline. **(B)** *KLF6* mRNA expression levels in the lung tissues of a chronic hypoxia mouse at 14 hours and 14 days after hypoxia exposure. Data were normalized to the reference gene (*B2M*). ****P<0.0001, in comparison with normoxic control rats using one-way ANOVA with Tukey's post-hoc test; n=4-8. Error bars indicate mean ±SEM.

5.4.2 *KLF6* expression in MCT rat model

KLF6 expression was measured in the lung tissue of rats 3, 7 and 14 days after the MCT injection (Figure 5.4A). *KLF6* mRNA expression levels in the lung were significantly increased (a 1.3-fold increase, p<0.5) at day 3 but subsequently fell, returning to base levels at 7 days and showing a significant ~ 2-fold decrease 14 days post-MCT injection (Figure 5.4B).

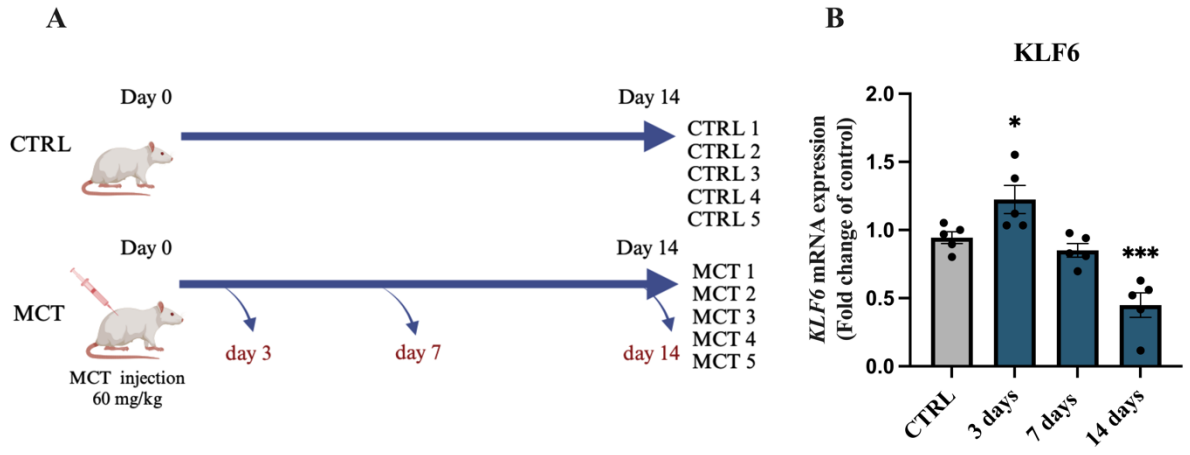

Figure 5.4: *KLF6* mRNA expression levels in the lungs of an MCT rat model of PAH.
(A) Schematic diagram of experimental timeline. **(B)** *KLF6* mRNA expression levels in lung tissues of MCT rats at days 3, 7 and 14 after MCT injection. Data were normalized to the reference gene (*ACTB*). CTRL: healthy control; MCT: MCT PAH model. *P<0.05, ***P<0.001, in comparison with control rats using one-way ANOVA with Tukey's post-hoc test; n=5. Error bars indicate mean ±SEM.

5.4.3 *KLF6* expression in Sugen/hypoxia rat model

KLF6 expression was measured in the lung tissue of Sugen/hypoxia rats at day 56 (Figure 5.5A).

In the Sugen/hypoxia rat model, *KLF6* mRNA expression levels were significantly decreased (a 2.5 decrease, p<0.0001) in the lung tissues of the Sugen/hypoxia rat model of PAH compared with controls (Figure 5.5B).

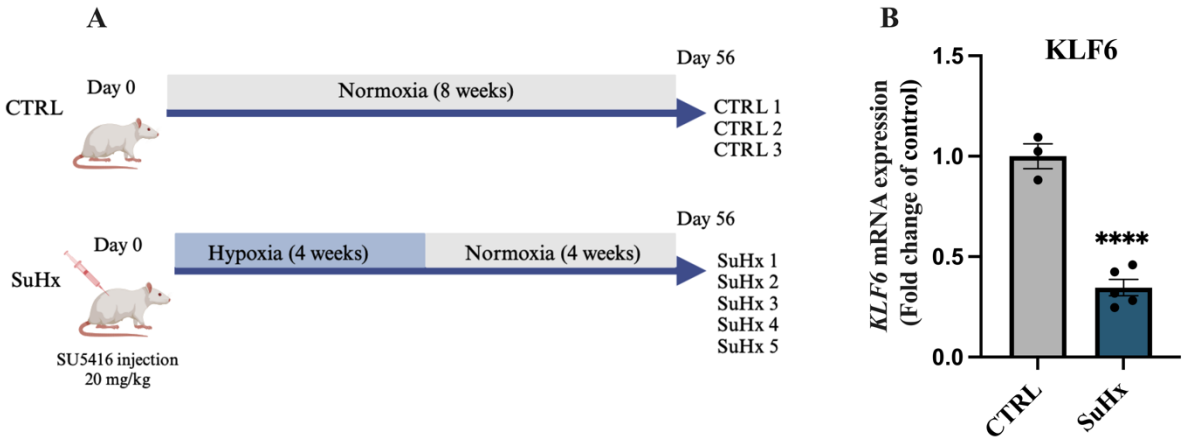

Figure 5.5: *KLF6* mRNA expression levels in the lungs of a Sugen/hypoxia rat model of PAH. **(A)** Schematic diagram of experimental design. **(B)** *KLF6* mRNA expression levels in the lung tissues of Sugen/hypoxia rats at day 56. Data were normalized to the reference gene (*ACTB*). CTRL: healthy control; SuHx: SuHx PAH model. ****P<0.0001, in comparison with normoxic control rats using unpaired t-test; n=3-5. Error bars indicate mean ±SEM.

5.4.4 *KLF6* expression in healthy and PAH ECFCs

ECFCs are an important tool that allows us to investigate the molecular mechanisms of vascular diseases, including PAH (Medina et al., 2012). PAH ECFCs display disease phenotypes, which are characterised by high proliferative and angiogenic capacities (Smits et al., 2018). To investigate the role of KLF6 in PAH, *KLF6* mRNA expression was measured in ECFCs from healthy controls and PAH patients with *BMPR2* mutations cultured under normoxic conditions for 24 hours controls (Figure 5.6A). *KLF6* expression was significantly increased in PAH ECFCs (~ 2-fold increase, p<0.001), compared with healthy controls (Figure 5.6B).

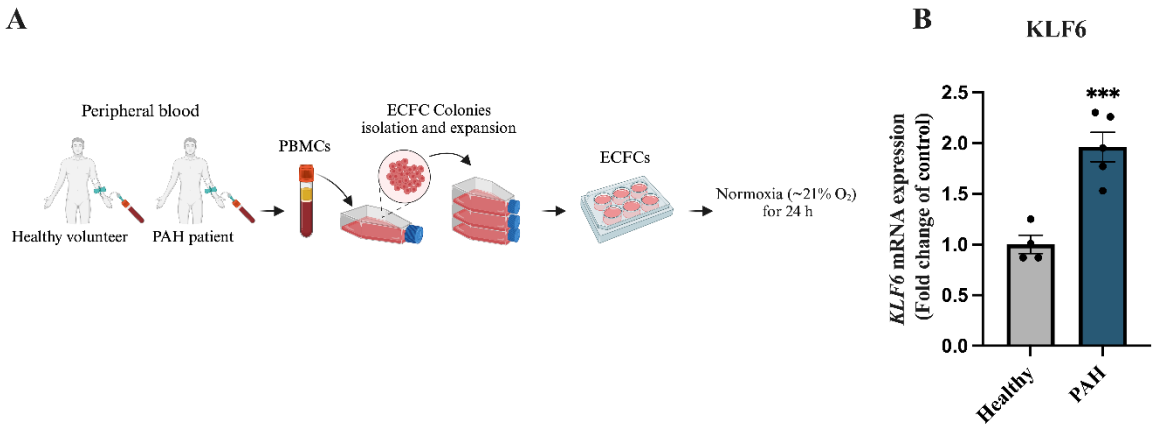

Figure 5.6: *KLF6* mRNA expression levels in healthy and PAH ECFCs.
(A) Schematic diagram of the experimental setup. Fresh peripheral blood samples were collected from healthy volunteers and PAH patients. Peripheral blood mononuclear cells (PBMCs) were then isolated from peripheral blood using a Ficoll density gradient. PBMCs were cultured in an endothelial medium until ECFC colonies were formed. ECFC colonies were isolated and expanded in T75 flasks. After expansion, ECFCs were frozen in liquid nitrogen or used for experiments. In this experiment, ECFCs were cultured under normoxic conditions. **(B)** *KLF6* mRNA expression levels in normoxic healthy ECFCs and PAH ECFCs with *BMPR2* mutations. Data were normalized to the reference gene (*ACTB*). ***P<0.001, in comparison with heathy normoxic controls using one-way ANOVA with Tukey's post-hoc test; n=4-5. Error bars indicate mean ±SEM.

5.5 Discussion

The experiments described in this chapter investigated disease-related expression changes in *KLF6* in ECFCs from PAH patients with *BMPR2* mutations as well as lung tissue from chronic hypoxia, Monocrotaline (MCT) and Sugen/hypoxia (SuHx) models of PAH.

The results show that *KLF6* expression was significantly elevated during the early stages of the response to hypoxia and MCT. This agrees with the known function of KLF6 as an early injury response factor (Garrido-Martín et al., 2013), and with our previous observations showing that *KLF6* expression is increased in HPAECs stimulated with hypoxia and pro-inflammatory cytokine TNF-α (Chapter 3, Section 3.4.3).

Following this early increase, the *KLF6* mRNA levels returned to control levels in the lungs of mice that had been exposed to hypoxia for 2 weeks, when the disease was well established. In contrast, in the MCT and Sugen/hypoxia tests on rats, the expression of *KLF6* fell significantly below the healthy control levels. This response is probably associated with different degrees of endothelial damage and vascular remodelling observed in these models.

Chronic hypoxia induces a relatively mild vascular phenotype which is fully reversed upon return to normoxia. Consistent with this, the changes in *KLF6* expression that were seen in the end stage of the disease in this model were far less pronounced than those observed in the more severe and irreversible Sugen/hypoxia and MCT models of PAH. In the Sugen/hypoxia PAH model, a combination of hypoxia and VEGFR inhibitor was shown to increase EC apoptosis, eventually leading to the obliteration of pulmonary arterioles and formation of angio-obliterative lesions (Nicolls et al., 2012; Taraseviciene-Stewart et al., 2001). In the MCT model, the administration of MCT to rats caused severe injury to the pulmonary endothelium, leading to irreversible vascular remodelling and death within 14-21 days after MCT injection (Rosenberg & Rabinovitch, 1988). The course of the disease induced by MCT administration is progressive, with persistent inflammation that includes two distinct phases: an acute phase and a chronic inflammatory phase (Tang et al., 2021). During both phases, the disease progresses gradually and is accompanied by pulmonary artery remodelling in a time-dependent manner (Tang et al., 2021).

Taken together, these findings suggest that KLF6 is likely to be involved in healing and repair processes in the early stages of PAH, but the disruption of its signalling during the later stages of the disease may potentially contribute to irreversible endothelial damage, resulting in progressive vascular remodelling.

Interestingly, *KLF6* expression was markedly elevated in PAH ECFCs compared with age- and sex-matched healthy controls. PAH ECFCs have been shown to replicate many of the characteristics of PAH, and have therefore been used as endothelial surrogates in PAH (Boucherat et al., 2022; Zhang, Cannavicci & Kutryk, 2022; Weisel et al., 2014; Hoshikawa et al., 2003a). Growing evidence suggests that the number of ECFCs increases in end-stage PAH, suggesting that these cells may be related to disease severity (Smits et al., 2018; Schiavon et al., 2012; Asosingh et al., 2008). However, the exact role of ECFCs in the pathogenesis of PAH is unclear, and remains controversial. On one hand, ECFCs can promote endothelial repair and help prevent endothelial dysfunction in PAH. On the other hand, the abnormal behaviour of ECFCs may possibly contribute to the development of angio-obliterative vascular lesions (Smits et al., 2018). PAH ECFCs have elevated angiogenic potential and can influence the process of arterial remodelling (Banno & Yoder, 2018), so high levels of *KLF6* expression in PAH ECFCs may reflect the pro-angiogenic properties of these cells. Our experiments clearly demonstrated the stimulatory effect of KLF6 on pulmonary endothelial angiogenesis in the tube formation assay *in vitro* as well as the arterial explants sprouting assay *ex vivo* (Chapter 4, Section 4.4.5). Our findings are consistent with a recent study that showed increased *KLF6* expression ($p=0.01$) in PAH ECFCs with *BMPR2* mutation in an organ-on-a-chip model of PAH (Ainscough et al., 2022a).

KLF2, KLF4 and KLF6 showed differential regulation properties in the early and late stages of the disease. In acute hypoxic mice (after 24 hours), *KLF2* expression was relatively unaffected by acute hypoxia, while *KLF4* expression was increased compared with normoxic controls (Supplementary Figure S.8B and C). In chronic hypoxic mice (after 14 days), *KLF2* and *KLF4* expression remained relatively unchanged (Supplementary Figure S.8B and C). Previous studies showed that *KLF2* expression decreased in apelin/*APLN* knockout mice that had been exposed to chronic hypoxia (FiO_2=10% for 3 weeks), which correlated with the increased severity of PH in this mouse model (Chandra et al., 2011). Nuclear localization of KLF4 was reduced in the lung tissues of hypoxic rats because of the increased S-nitrosation of KLF4 (Ban et al., 2019). The potential discrepancy could be attributed to variations in strains.

Previous studies have shown that the effects of chronic hypoxia may be strain-dependent, as the degree of pulmonary vascular remodelling is less prominent in mice than in rats (Stenmark et al., 2009; Tada et al., 2008; Hoshikawa et al., 2003b). Meanwhile, in the MCT rat model of PAH, *KLF2* and *KLF4* expression was significantly reduced at 3 days as well as at 14 days in rat MCT-exposed lungs (Supplementary Figure S9B and C), which is consistent with previous reports that showed downregulation of *KLF2* and *KLF4* in the MCT rat model of PAH (Hong et al., 2021; Chen et al., 2017a; Rhodes et al., 2013). In the Sugen/hypoxia rat model of PAH, the expression of *KLF2* and *KLF4* were relatively unchanged compared with normoxic controls (Supplementary Figure S10B and C). To support our findings further, single-cell RNA sequencing analysis in Sugen/hypoxia (SuHx) rat lungs showed no significant change in *KLF2* and *KLF4* expression compared with controls (Hong et al., 2021).

5.6 Conclusion

The information presented in this chapter shows that *KLF6* expression was elevated in the blood-derived late outgrowth endothelial colony-forming cells (ECFCs) from PAH patients with *BMPR2* mutations. Meanwhile, *KLF6* expression was elevated in the early stages of PAH in chronic hypoxia mice and MCT rats (Figure 5.7). However, *KLF6* expression was significantly reduced in the later stages of the disease in MCT and Sugen/hypoxia rats.

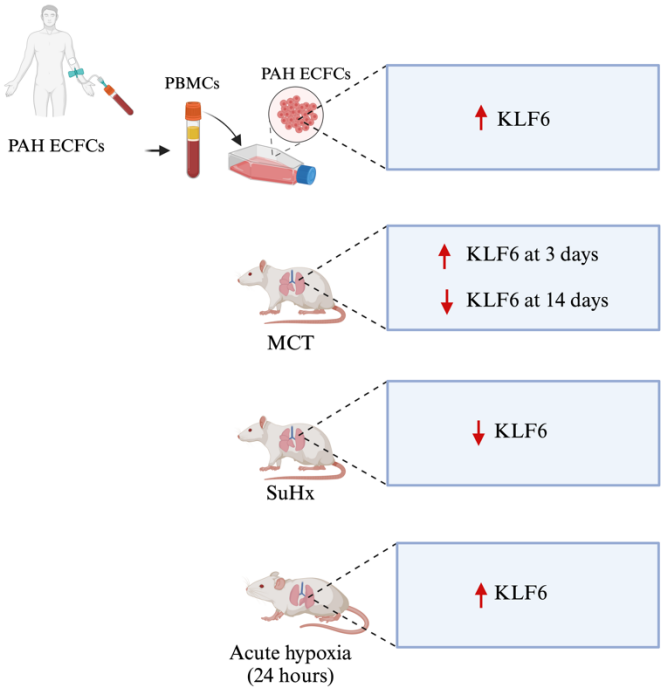

Figure 5.7:Summary of the key findings of Chapter 5.
Illustration created by the author using BioRender.com.

Chapter 6 Results: Transcriptomic profiling of KLF6-overexpressing HPAECs

6.1 Introduction

KLF6 is a zinc finger transcription factor that has a well-documented role as a tumour suppressor. The overexpression of KLF6 inhibits tumour growth and progression, while KLF6 silencing accelerates tumorigenesis in non-small cell lung cancer (NSCLC), gastric cancer and oral cancer (Syafruddin et al., 2020; Hsu et al., 2017; Sangodkar et al., 2009; Ito et al., 2004). KLF6 also regulates the expression of key cancer-associated genes, including *TGFB1* and *CDKN1A* (p21) (Narla et al., 2007; Tarabishi et al., 2005).

PAH shares many characteristics with cancer, including increased cell proliferation and apoptosis resistance (Cool et al., 2020). It is well known that EC injury is a distinctive feature of PAH, and it is thought to be an early contributor in the onset and progression of the disease (Cober et al., 2022; Evans et al., 2021; Kurakula et al., 2021). In addition to its well-documented functions in cancer biology, KLF6 also plays an important role as an early response factor induced in ECs after vascular injury, leading to the induction of a large number of endothelial marker genes through direct binding to their promoters, including *TGFB1* and its receptors (*TGFBR1* and *TGFBR2*), *ENG*, *MMP14* and *ACVRL1* (Yang et al., 2019). However, the role of KLF6 signalling has not been studied in the context of PAH.

Previous studies show that the expression and activity of two members of the Krüppel-like transcription factor family, KLF2 and KLF4, are compromised in PAH (Sindi et al., 2020; Shatat et al., 2014). KLF2 and KLF4 promote endothelial quiescence and homeostasis, and are involved in the transcriptional regulation of several endothelial genes that are associated with anti-inflammatory, antithrombotic, anti-apoptotic and anti-proliferative effects in ECs (Sindi et al., 2020; Sangwung et al., 2017; Shatat et al., 2014; Ohnesorge et al., 2010a). KLF2 and KLF4 have a similar amino acid sequence in the DNA binding region and share key endothelial gene targets, which accounts for their overlapping roles (Sweet et al., 2018). The presence of either KLF2 or KLF4 is necessary for endothelial cell survival, but the simultaneous endothelial-specific deletion of both genes is embryonically lethal, highlighting the redundant nature and the compensatory mechanisms of these two transcription factors (Sangwung et al., 2017; Chiplunkar et al., 2013). While KLF2 and KLF4 can regulate the expression of

endothelial genes independently, they also regulate the expression of specific endothelial genes in a non-redundant manner, with approximately 40% of endothelial gene targets co-ordinately regulated by both transcription factors (Mastej et al., 2022; Sangwung et al., 2017). A recent study has shown that the promoter and enhancer regions of the human KLF2 locus possess six potential binding sites for KLF4 and KLF2 based on transcription factor motif analysis (Mastej et al., 2022). The same study reported that KLF2 and KLF4 worked together in quiescent ECs to control a combinatorial mechanism, while the disruption of this mechanism by loss of *KLF4* led to an increase in the expression of KLF2 as an adaptive response which resulted in an EndMT phenotype. This suggests that KLF2 and KLF4 may regulate endothelial gene expression in a collaborative and cooperative manner (Mastej et al., 2022).

In addition to KLF2 and KLF4, KLF6 is also expressed in vascular endothelial cells (Zhang et al., 2019b). The KLF6 protein consists of 283-amino acids, which include an 82-amino acid C-terminal DNA-binding domain that is identical to the DNA-binding domains of KLF2 and KLF4. It also shares a 201-amino acid N-terminal activation domain with only 41 amino acids in common with KLF7, but it does not share any amino acid with KLF2 and KLF4 in its N-terminal domain (Li et al., 2005b). The protein structure of all members of the human KLF family of transcription factors including KLF2, KLF4 and KLF6 is illustrated in Section 1.8, Figure 1.6. Despite the similar DNA-binding domains of KLF2, KLF4 and KLF6, the effects of KLF6 and its potential functional redundancy with KLF2 and KLF4 in ECs have not yet been well described.

The previous chapter showed that KLF6 is induced in the pulmonary endothelium in response to shear stress and vascular insults involved in PAH pathogenesis such as hypoxia and inflammatory stimuli (TNF-α). Functional studies also revealed that KLF6 has anti-proliferative, anti-inflammatory, anti-apoptotic, pro-angiogenic and barrier-protective effects in the pulmonary endothelium. This chapter focuses on the investigation of transcriptomic changes induced by KLF6 overexpression in the human pulmonary endothelium and on comparing them with those changes that are dependent on KLF2 and KLF4, the two closely related transcription factors implicated in PAH.

6.2 Experimental aims

1. To characterise the effects of KLF6 overexpression on the endothelial transcriptome.
2. To investigate the relationship between KLF6 and hypoxia-induced changes in the endothelial transcriptome.
3. To investigate the relationship between KLF6 and TNF-α-induced changes in the endothelial transcriptome.
4. To compare the transcriptional responses of overexpressing KLF6 versus overexpressing KLF2 or KLF4.

6.3 Experimental outline

The experimental outline is shown in Figure 6.1. For further experimental details, see Chapter 2 section 2.5.4.

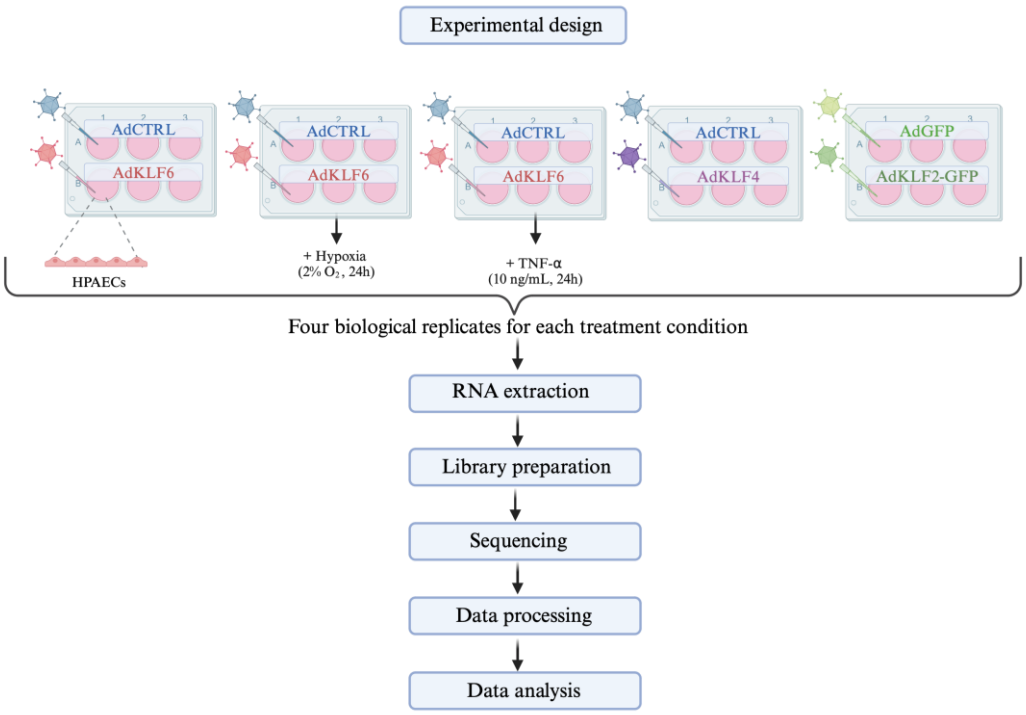

Figure 6.1: Experimental outline for Chapter 6.
The overexpression of KLF2, KLF4, KLF6 was achieved by adenoviral gene transfer (AdKLF2-GFP, AdKLF4, AdKLF6). Adenoviral overexpressing GFP (AdGFP) was used as an adenoviral control for KLF2 as the adenoviral-mediated overexpression of KLF2 is co-expressed with green fluorescent protein (GFP), while adenoviral containing a tetracycline (Tet)-off system was used as adenoviral control (AdCTRL). RNA-seq of HPAECs overexpressing KLF2, KLF4 or KLF6 – either kept in basal conditions, exposed to hypoxia (2% O_2), or treated with TNF-α (10 ng/mL) – was performed in four biological replicates for each condition. Library preparation, sequencing, data processing and analysis were carried out at the Imperial BRC Genomics Facility (Imperial College of London, UK). Illustration created by the author using BioRender.com.

6.4 Results

6.4.1 RNA-seq analysis of HPAECs overexpressing KLF6

To assess the transcriptomic changes that follow KLF6 overexpression, RNA-seq was conducted on HPAECs infected with AdCTRL and AdKLF6 (n=4 biological replicates/conditions), followed by differential gene expression analysis.

KLF6 overexpressing HPAECs showed a significant increase in KLF6 protein levels (roughly a 5-fold increase, P<0.01, compared to the adenoviral negative control) and *KLF6* mRNA levels (an approximately ~170-fold increase, P<0.0001 compared to the adenoviral control) at 24 hours post-infection (Chapter 4, Section 4.4.1, Figure 4.2B and C).

A total of 6621 genes were identified as differentially expressed (FDR < 0.05, $\log_2|FC|>0.25$), comprising 3225 downregulated and 3396 upregulated genes, as a result of the overexpression of KLF6 in HPAECs (Figure 6.2). The 50 most differentially up- or down-regulated genes are shown in Supplementary Table S1.

Interestingly, this list includes *KDR*, a gene previously implicated in PAH (Eyries et al., 2020), which was increased (p=3.27E-20) in HPAEC overexpressing KLF6. In addition to *KDR*, KLF6 markedly increased the expression of other arterial identity regulators and PAH genes including *ERG*, *SOX17*, and *BMPR2*. Changes in the expression of *ERG, SOX17* and *KDR* were confirmed by qPCR in an independent set of HPAECs (see Chapter 4, Section 4.4.5). KLF6 increased *BMPR2* mRNA expression levels in HPAECs under basal conditions by roughly 4-fold, p<0.001 compared with adenoviral control, whereas KLF6 knockdown had no significant effect (Figure 6.3A and 6.3B).

To investigate the transcriptomic signature of KLF6 overexpressing HPAECs in more detail, I applied more stringent criteria (FDR <0.01, $\log_2|FC|>2$), which reduced the list to 856 DEGs, comprising 624 downregulated and 232 upregulated genes.

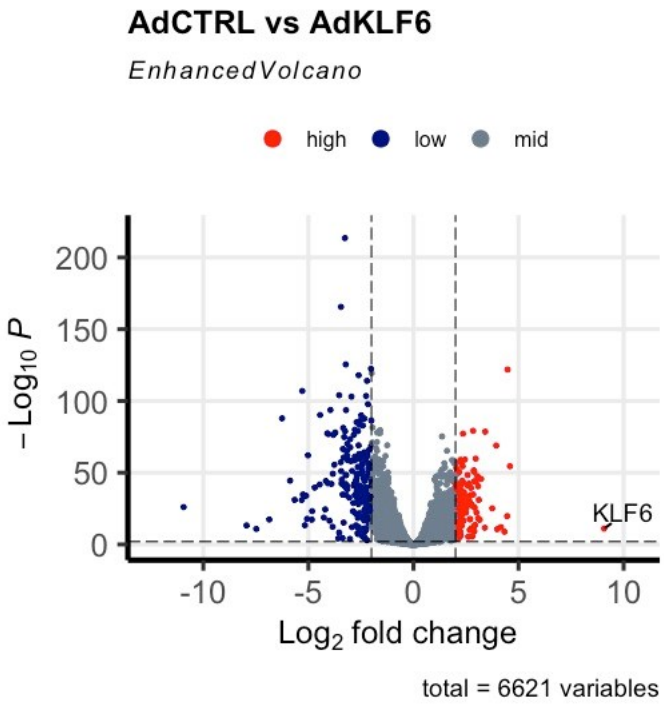

Figure 6.2: Differentially expressed genes following KLF6 overexpression in HPAECs.
Volcano plot showing differentially expressed genes (DEGs) in AdKLF6- vs AdCTRL-infected cells. Downregulated genes ($p<0.05$ and $\log_2$ fold change <-0.25) are represented in blue and upregulated genes ($p<0.05$ and $\log_2$ fold change >0.25) are represented in red, n=4 donors/condition, n= 6621 DEGs (3225 downregulated and 3396 upregulated genes).

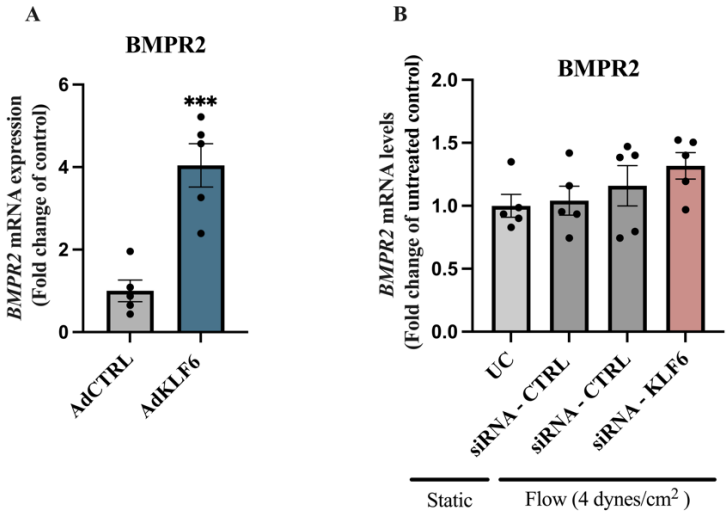

Figure 6.3: Effect of KLF6 overexpression and knockdown on *BMPR2* expression.
BMPR2 mRNA expression was measured in **(A)** HPAECs infected with AdCTRL or AdKLF6 for 24 h and **(B)** HPAECs transfected with KLF6 siRNA or siRNA-CTRL for 48 h and stimulated with flow (4 dynes/cm^2) for 24 h. Data were normalized to the reference gene (*ACTB*) or (*B2M*) for the flow experiments. ***P<0.001, in comparison with adenoviral controls using unpaired t-test. Error bars indicate mean ±SEM; n=5.

6.4.2 KLF6 modulates pathways involved in endothelial repair

The gene enrichment analysis of up- and down-regulated genes, that met a more stringent criteria (FDR <0.01, $\log_2|FC|>2$), in HPAECs overexpressing KLF6 was performed using Metascape (Zhou et al., 2019b). A functional network of enriched terms showed that the upregulated genes were significantly enriched in various biological processes such as angiogenesis, cell migration, wound repair and tissue homeostasis, whereas the downregulated genes were mainly enriched in cell cycle progression, DNA replication and DNA metabolic process (Figures 6.4A and 6.5A). A DisGeNET database disease enrichment analysis of up- and down-regulated genes in KLF6-overexpressing HPAECs revealed that the up-regulated genes were enriched in vascular diseases including PAH, IPAH and pulmonary emphysema, while the down-regulated genes were enriched in abnormal aortic and carotid artery morphology (Figures 6.4B and 6.5B). Meanwhile, KEGG pathway enrichment analysis showed that genes which were upregulated by KLF6 overexpression were enriched in various pathways implicated in PAH pathogenesis, including FOXO (Savai et al., 2014), p53 (Wang et al., 2019b; Mizuno et al., 2011), TNF (Hurst et al., 2017), NF-κB (Price et al., 2013), PI3K-Akt (Berghausen et al., 2021; Garat et al., 2013) and Ras signalling pathways (de Man et al., 2012), whereas downregulated genes were enriched in DNA replication, cell cycle and small cell lung cancer (Figure 6.6). Taken together, these results show that KLF6 regulates endothelial repair and angiogenesis and is involved in the regulation of multiple signalling pathways that have previously been implicated in the onset and progression of PAH.

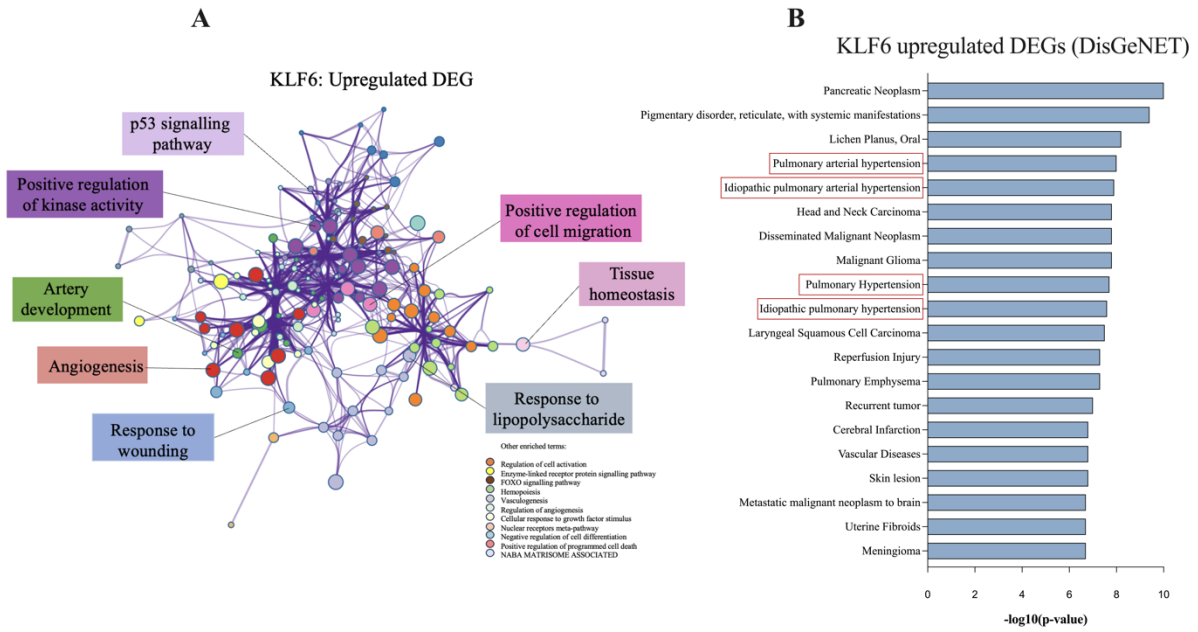

Figure 6.4: Metascape enrichment analysis of upregulated genes in HPAECs overexpressing KLF6.
(A) Network of enriched terms of upregulated genes in HPAECs overexpressing KLF6 coloured according to cluster ID, where nodes with the same cluster ID are close to each other. **(B)** Bar graph showing the DisGeNET database disease enrichment analysis of upregulated genes in HPAECs overexpressing KLF6. n= 856 DEGs (624 downregulated and 232 upregulated genes). Pulmonary hypertension terms are highlighted in red boxes.

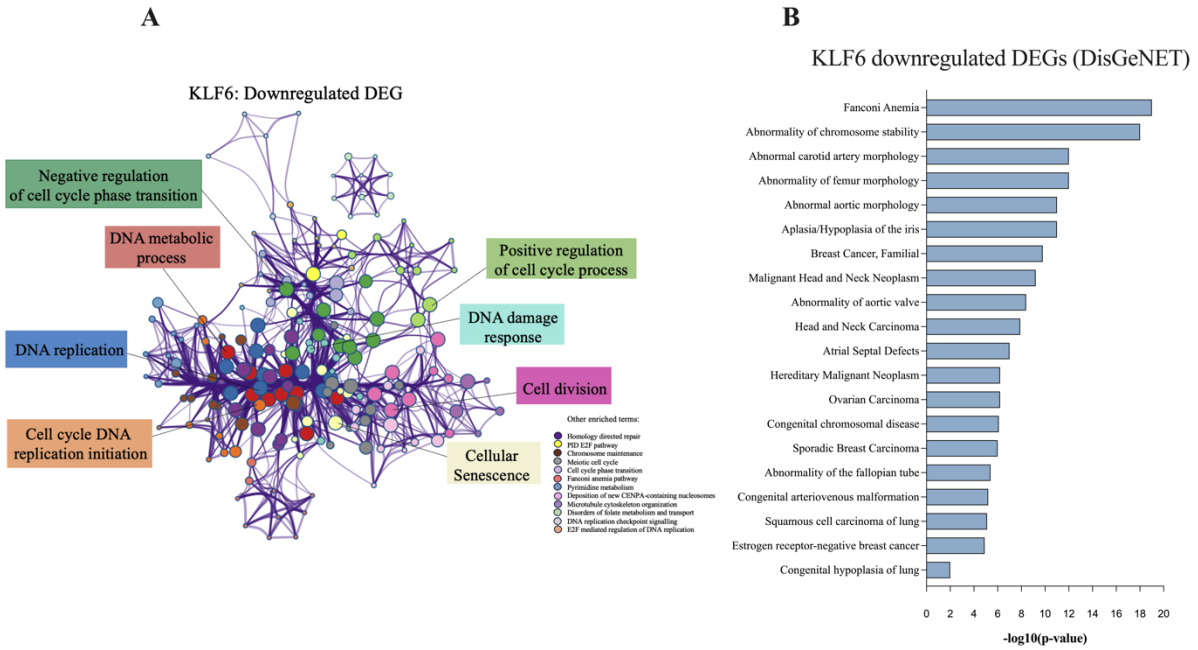

Figure 6.5: Metascape enrichment analysis of downregulated genes in HPAECs overexpressing KLF6.
(A) Network of enriched terms of downregulated genes in HPAECs overexpressing KLF6 coloured according to cluster ID, where nodes with the same cluster ID are close to each other. **(B)** Bar graph showing the DisGeNET database disease enrichment analysis of downregulated genes in HPAECs overexpressing KLF6. n= 856 DEGs (624 downregulated and 232 upregulated genes).

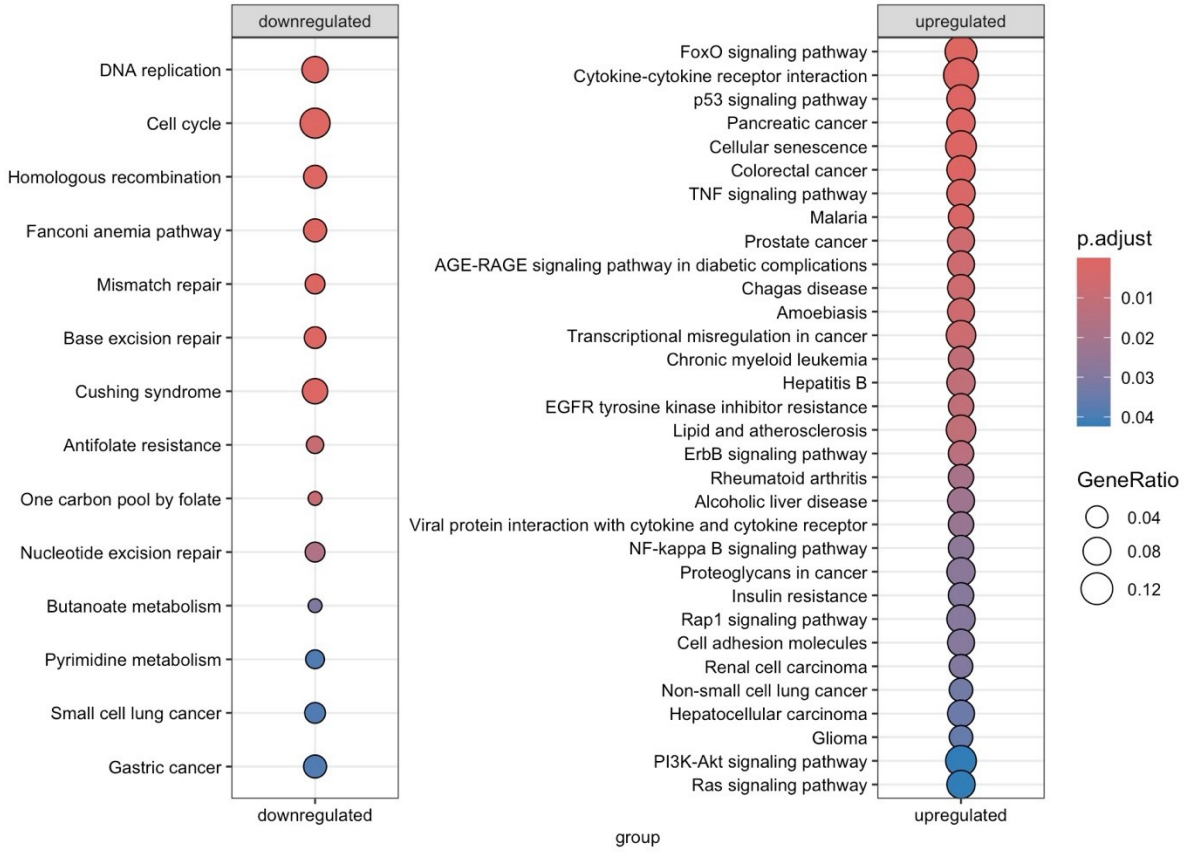

Figure 6.6: KEGG pathway analysis for up- and down-regulated genes in HPAECs overexpressing KLF6.

Dot plot showing the enriched KEGG pathways of DEGs (left, down-regulated genes; right, up-regulated genes) in KLF6 overexpressing HPAECs. The colour of the dots represents the adjusted P-value, and the size of the dots represents the number of DEGs in the pathway. n= 856 DEGs (624 downregulated and 232 upregulated genes).

6.4.3 KLF6-dependent genes in PAH

In addition to the DisGeNET database disease enrichment analysis, I decided to explore this further by analysing a series of publicly available datasets. Differentially expressed genes from KLF6-overexpressing HPAECs (FDR <0.01, $\log_2|FC|>2$) were compared with publicly available sets of differentially expressed genes in PAH and IPAH, including PAH HPAECs and ECFCs from microfluidic models of PAH (Ainscough et al., 2022a), IPAH lung transplants (IPAH PAECs) (Rhodes et al., 2015), and a previously curated list of PAH-associated genes (named herein as "known PAH genes") (Reyes-Palomares et al., 2020) (Figure 6.7). The list of differentially expressed genes common to KLF6 HPAECs, PAH HPAECs, PAH ECFCs, IPAH PAECs and known PAH genes are shown in Supplementary Table S2. DEGs from KLF6-overexpressing HPAECs (KLF6 HPAECs) and PAH ECFCs had the most genes in common (100 genes, p-value = 0.015) (Figure 6.7C) while PAH HPAECs were found to have the second largest number of genes in common with KLF6 HPAECs, but were most significant in terms of their overlap (74 genes, p-value = 1.7E-08) (Figure 6.7B). KLF6 HPAECs and PAH PAECs had 33 genes in common (Figure 6.7D), whereas KLF6 HPAECs and known PAH genes had 18 genes (Figure 6.7E).

To explore the association of KLF6 DEGs with genes related to the pathogenesis of PAH further, we generated a heatmap using a curated list of PAH-related genes from (Haensel & Wojciak-Stothard, 2023; Welch et al., 2023). A heatmap of selected genes associated with PAH pathogenesis is shown in Figure 6.8. Among these genes, *KLK1*, *NOTCH3*, *BMPR1B*, *ENG*, *TOPBP1*, *THBS1*, *SOX17*, *KDR*, *CAV1*, *ACVRL1*, *SMAD1*, *SMAD4*, *BMPR2*, *EDN1* and *AQP1* were differentially expressed in KLF6-overexpressing HPAECs. Most of these genes, including *ENG*, *TOPBP1*, *THBS1*, *SOX17*, *KDR*, *CAV1*, *ACVRL1*, *SMAD1* and *BMPR2*, were downregulated in PAH (Wang et al., 2021a; Eyries et al., 2020; de Jesus Perez et al., 2014; Han et al., 2013; Austin et al., 2012; Maloney et al., 2012; Chaouat et al., 2004; Harrison et al., 2003; Trembath et al., 2001; Lane et al., 2000). These genes were significantly upregulated following KLF6 overexpression in HPAEC, and they have been shown to play a key role in endothelial repair and angiogenesis such as *SOX17*, *ENG* and *KDR* (Saygin et al., 2020; Lee et al., 2014b). This suggests that KLF6 upregulates PAH genes that are essential for endothelial identity, repair and angiogenesis.

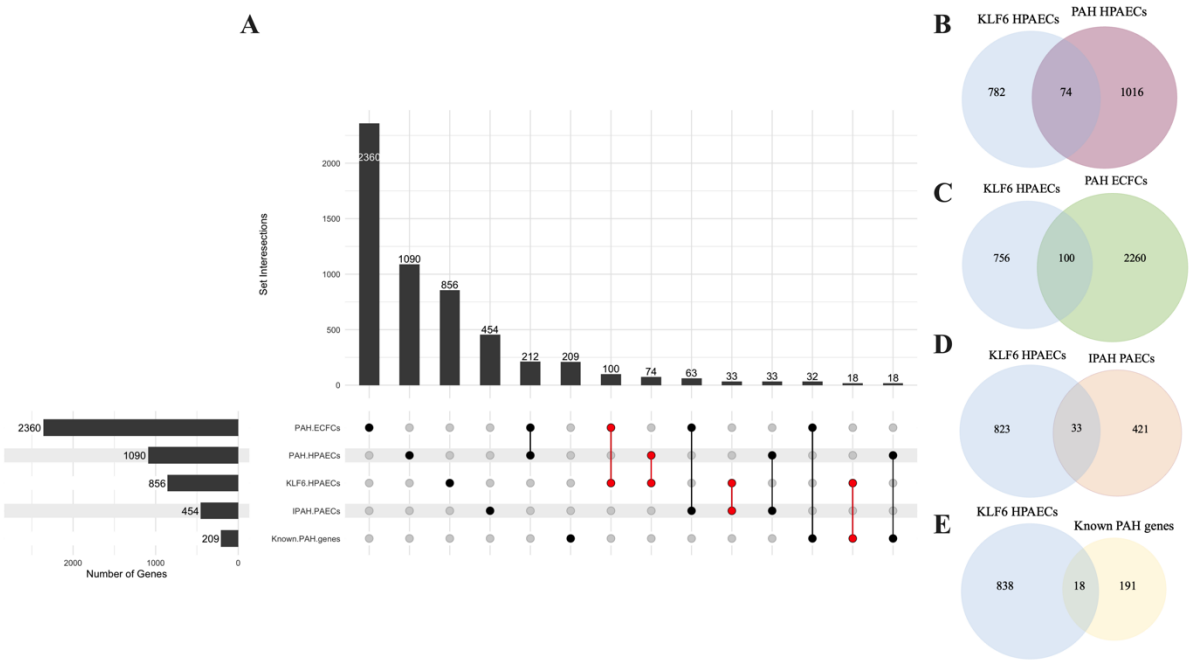

Figure 6.7: Overlap analysis of differentially expressed genes in KLF6 overexpressing HPAECs and PAH-associated genes.

(A) Upset plot showing the intersections between differentially expressed gene lists of KLF6 HPAECs, PAH HPAECs, PAH ECFCs (Ainscough et al., 2022a) and IPAH PAECs (Rhodes et al., 2015) and a previously curated list of PAH-associated genes (named herein as "known PAH genes") (Reyes-Palomares et al., 2020), where connected black dots represent overlapping DEG lists and vertical bars in intersection sets show the number of overlapping genes. **(B)** Venn diagram showing the number and percentage of common DEGs in KLF6 HPAECs and PAH HPAECs. The overlap of 74 genes is significant at p= 1.7E-08. **(C)** Venn diagram showing the number and percentage of common DEGs in KLF6 HPAECs and PAH ECFCs. The overlap of 100 genes is significant at p=0.015. **(D)** Venn diagram showing the number and percentage of common DEGs in KLF6 HPAECs and IPAH PAECs. The overlap of 33 genes is significant at p=4.6E-05. **(E)** Venn diagram showing the number and percentage of common DEGs in KLF6 HPAECs and known PAH genes. The overlap of 18 genes is significant at p=3.3E-04. The statistical significance of overlaps between gene sets in comparison to the genomic background was calculated by one-tailed Fisher's exact test using the GeneOverlap package in R (Shen, 2016).

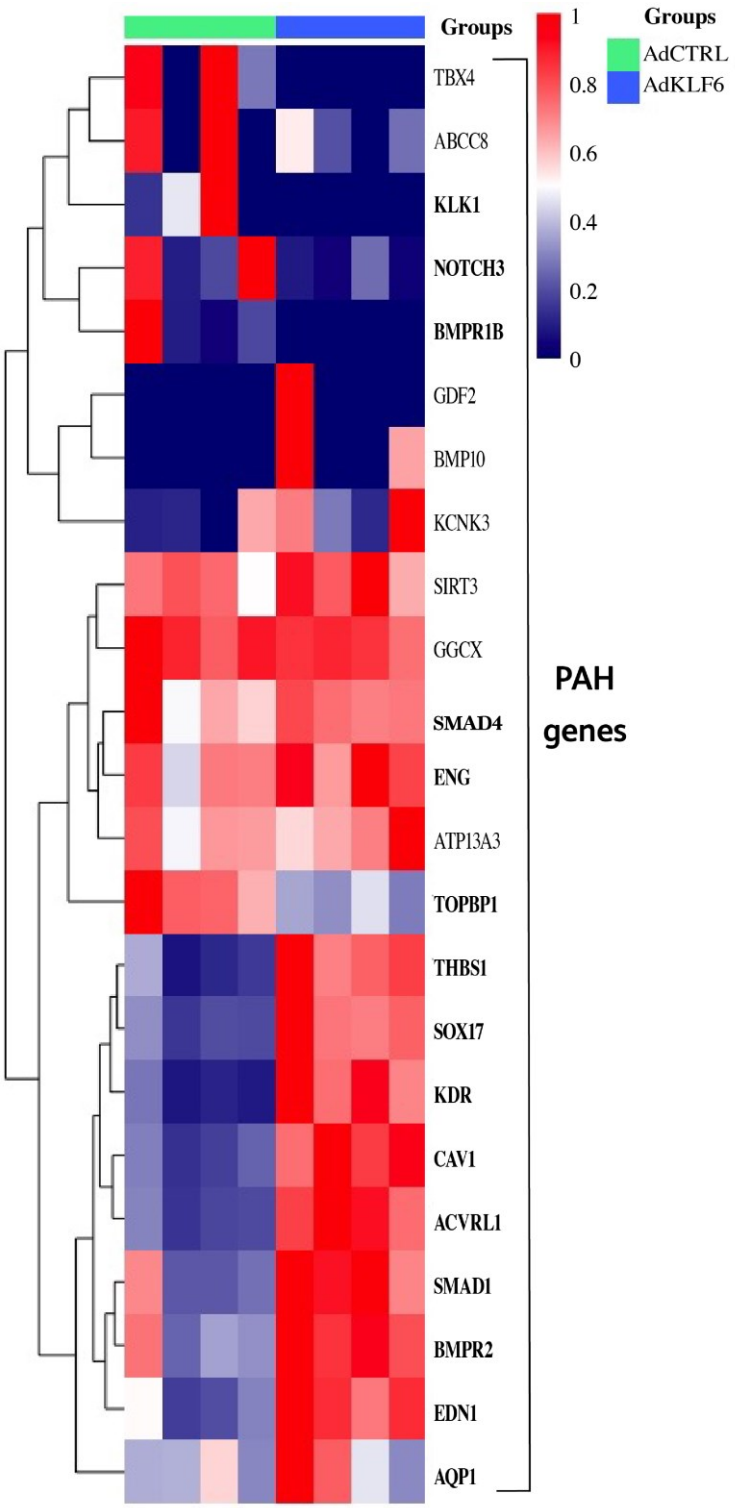

Figure 6.8: Heatmap of key PAH-associated genes following KLF6 overexpression in HPAECs. The hierarchical clustering of PAH-associated genes shows a subset of genes that are differentially upregulated upon KLF6 overexpression in HPAECs (marked in bold).

6.4.4 KLF6 modifies endothelial transcriptional response to hypoxia

To assess the transcriptomic changes that occurred after the exposure of HPAECs to hypoxia, RNA-seq was conducted on HPAECs infected with AdCTRL and exposed to either normoxic (21% O_2) or hypoxic (2% O_2) conditions for 24 hours.

200 genes were identified as differentially expressed (FDR <0.05, $\log_2|FC|>0.25$), including 124 downregulated and 76 upregulated genes, as result of exposure of HPAECs to hypoxia (comparison AdCTRL vs AdCTRL+hypoxia). The Metascape pathway and functional enrichment analysis of differentially expressed genes in HPAECs exposed to hypoxia showed that DEGs were mainly enriched in response to hypoxia, glycolysis, gluconeogenesis and hypoxia-related pathways such as hypoxia-inducible factor 1 (HIF-1) and TGF-β signalling pathways (Figure 6.9).

KLF6 overexpression under hypoxic conditions (in a comparison between hypoxic AdCTRL and hypoxic AdKLF6) revealed 3405 DEGs (FDR <0.05, $\log_2|FC|>0.25$), including 862 downregulated and 2543 upregulated genes. The 50 most differentially up- or down-regulated genes are shown in Supplementary Table S3.

KEGG pathway enrichment analysis showed that the upregulated genes were enriched in various pathways, including p53, TNF, TGF-β, FOXO, RAS, PI3K-AKT and NF-κB signalling pathway, while the downregulated genes were mainly enriched in cell cycle, DNA replication and pyrimidine metabolism (Figure 6.10). These findings suggest that KLF6 modulates the endothelial transcriptional responses to hypoxia by regulating these pathways.

Interestingly, RNA-seq analysis showed that KLF6 overexpression under hypoxic conditions reduced the expression of HIF-1 target genes and glycolysis-related genes including *PDK1*, *PGK1*, *LDHA*, *ENO1*, *BNIP3*, and *ICAM1*.

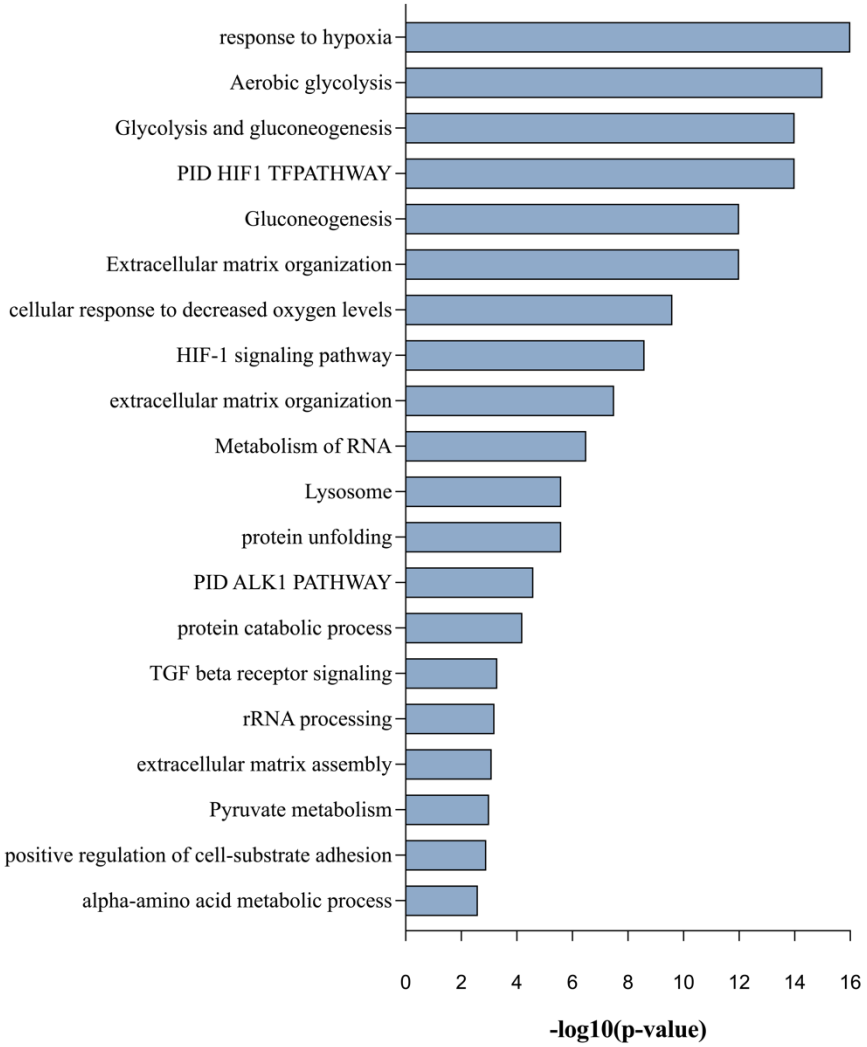

Figure 6.9: Metascape pathway and functional enrichment analysis of differentially expressed genes in HPAECs exposed to hypoxia.
Bar graph showing the Metascape pathway and process enrichment analysis of differentially expressed genes following exposure of HPAECs to hypoxia (2% O_2) for 24 hours. Bars are coloured by -log10 (p-value) and the darker colour indicates more significant enrichment. n= 200 DEGs (124 downregulated and 76 upregulated genes).

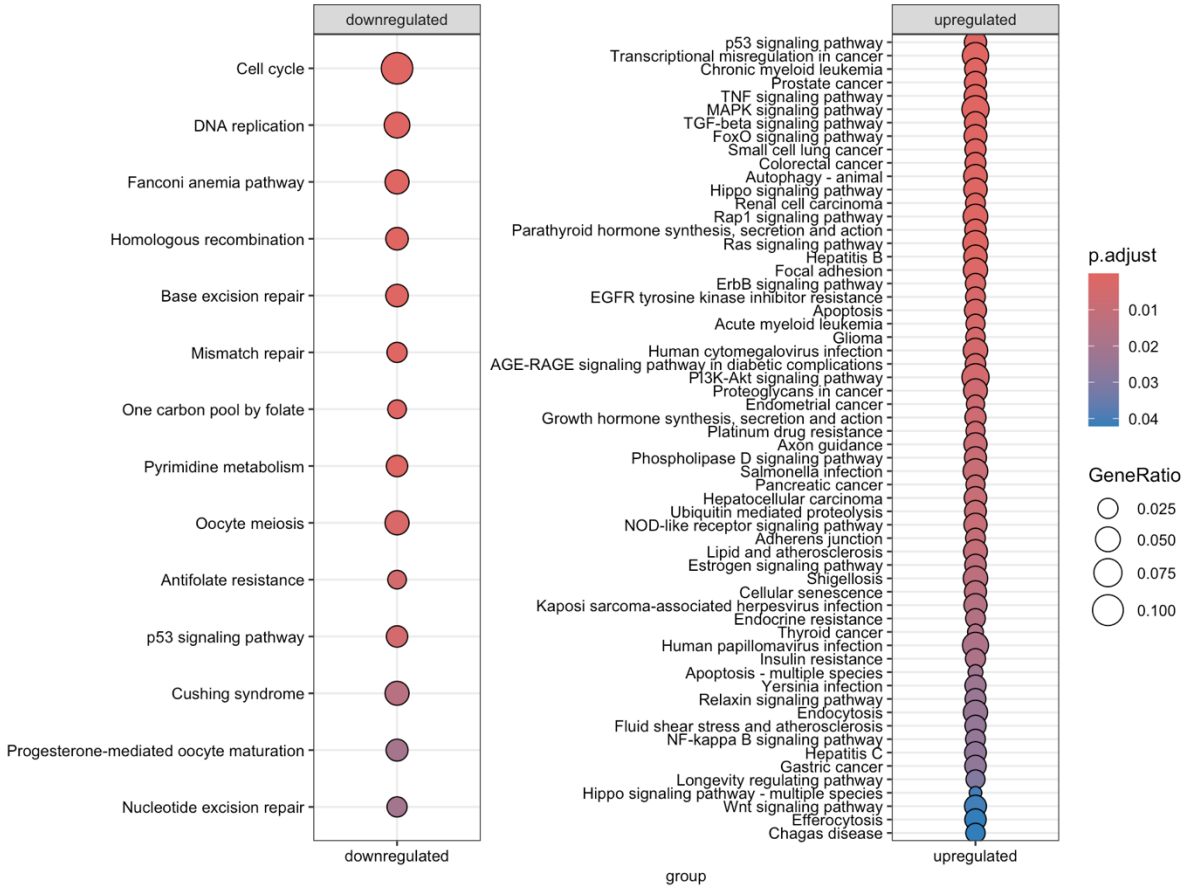

Figure 6.10: Effect of KLF6 on hypoxia-induced changes in gene expression profile in HPAECs. Dot plot showing the enriched KEGG pathways of DEGs (left, down-regulated genes; right, up-regulated genes) in KLF6 overexpressing HPAECs under hypoxic conditions (2% O_2) for 24 hours. The colour of the dots represents the adjusted p-value, and the size of the dots represents the number of DEGs in the pathway. n= 3405 DEGs (862 downregulated and 2543 upregulated genes).

6.4.5 RNA-seq analysis of HPAECs overexpressing KLF6 following TNF-α treatment

The TNF-signalling pathway has been implicated in the pathogenesis of PAH (Bell et al., 2020; Fujita et al., 2002). To assess transcriptomic changes following treatment of HPAECs with TNF-α, RNA-seq was conducted on the untreated or TNF-α-treated (10 ng/mL, 24h) HPAECs infected with AdCTRL.

753 DEGs were identified (FDR <0.05, $\log_2|FC|>0.25$), including 525 downregulated and 228 upregulated genes, as result of TNF-α exposure. Consistent with the known pro-inflammatory effects of TNF-α, DEGs were significantly enriched for TNF and NF-κB signalling pathways (Figure 6.11).

The transcriptomic analysis of AdKLF6- and AdCTRL-treated HPAECs exposed to TNF-α for 24h identified 4361 DEGs (FDR <0.05, $\log_2|FC|>0.25$), including 2316 downregulated and 2045 upregulated genes. The 50 most differentially up- or down-regulated genes are shown in Supplementary Table S4.

The enrichment analysis of the KEGG pathway showed that upregulated genes were enriched in several pathways, including the FOXO and p53, PI3K-AKT, JAK-STAT, TNF and NF-κB signalling pathways, whereas downregulated genes were mainly enriched in cell cycle and DNA replication (Figure 6.12).

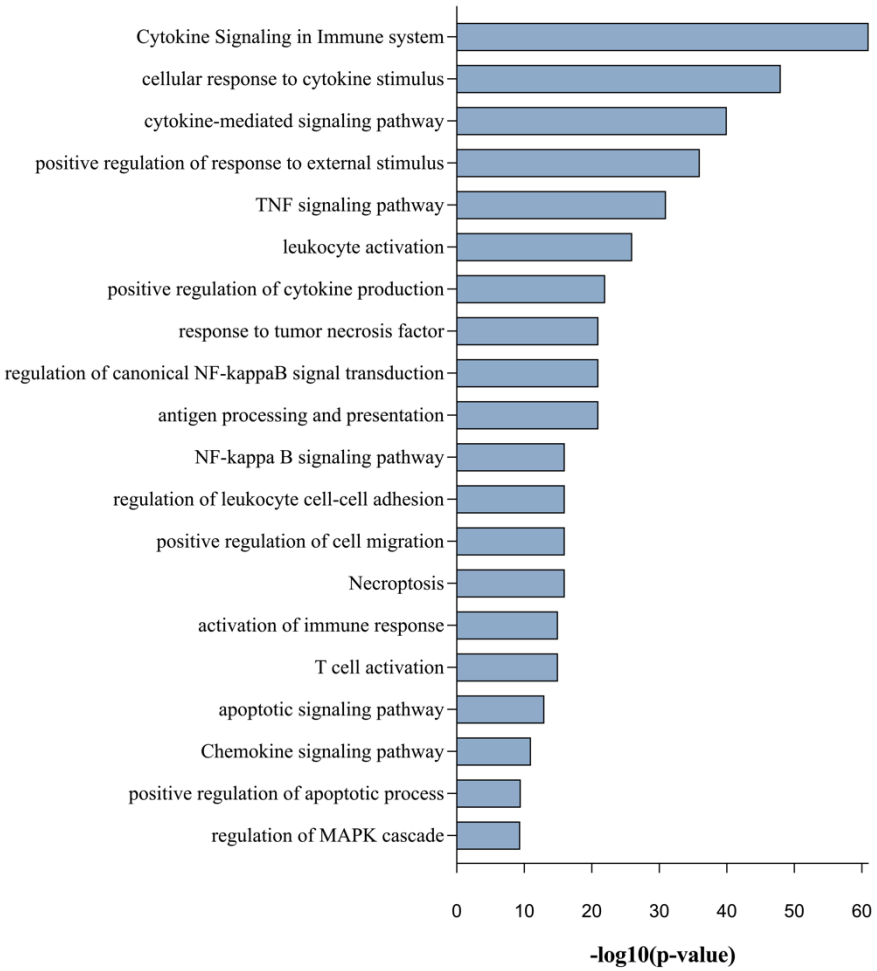

Figure 6.11: Metascape pathway and functional enrichment analysis of differentially expressed genes in HPAECs treated with TNF-α.
Bar graph showing the Metascape pathway and process enrichment analysis of differentially expressed genes following treatment of HPAECs with TNF-α (10 ng/mL) for 24 hours. Bars are coloured by -log10 (p-value) and darker colours indicate more significant enrichment. n= 753 DEGs (525 downregulated and 228 upregulated genes).

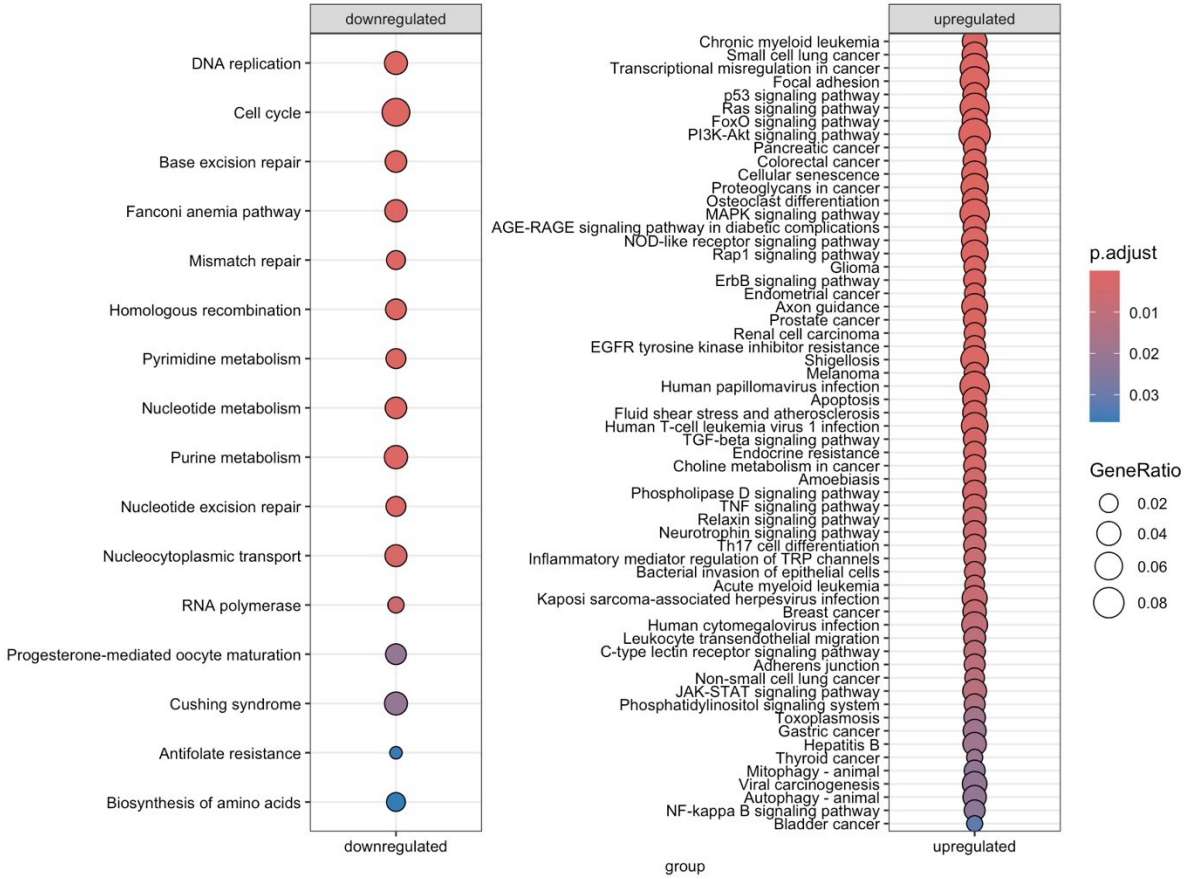

Figure 6.12: Effect of KLF6 on TNF-α -induced changes in gene expression profile in HPAECs. Dot plot showing the enriched KEGG pathways of DEGs (left, down-regulated genes; right, up-regulated genes) in KLF6 overexpressing HPAECs treated with TNF-α (10 ng/mL) for 24 hours.The colour of the dots represents the adjusted P-value, and the size of the dots represents the number of DEGs in the pathway. n= 4361 DEGs (2316 downregulated and 2045 upregulated genes).

6.4.6 Comparative analysis of differentially expressed genes in HPAECs overexpressing KLF2, KLF4 and KLF6

To identify common and KLF2-, KLF4-, and KLF6-dependent genes in HPAECs, RNA-seq was conducted on HPAECs that had been infected with AdCTRL, AdCTRL-GFP, AdKLF2-GFP, AdKLF4 and AdKLF6 as shown in Figure 6.1.

A marked increase in nuclear localization of KLF2 and KLF4 was observed in KLF2- and 4-overexpressing HPAECs (Figure 6.13A and B) and a significant increase in mRNA levels was also observed in AdKLF2/4- overexpressing HPAECs at 24 hours post-infection (shown in Supplementary Figure S11).

6655 genes were identified as differentially expressed (FDR <0.05, $\log_2|FC|>0.25$) as result of KLF2-overexpression in HPAECs (Figure 6.13C), while 6703 genes were identified as differentially expressed (FDR <0.05, $\log_2|FC|>025$) following KLF4 overexpression in HPAECs (Figure 6.13D). The 50 most differentially up- or down-regulated genes for KLF2/4-overexpressing HPAECs are shown in Supplementary Tables S5 and S6.

I compared the transcriptomic signature of KLF2/4-overexpressing HPAECs with the transcriptomic signature of KLF6-overexpressing HPAECs, focussing on the set of genes showing the strongest differential expression (FDR<0.01, $\log_2|FC|>2$), which reduced the list to 893 DEGs (205 downregulated and 688 upregulated genes) for KLF2-overexpressing HPAECs and 1603 DEGs (523 downregulated and 1080 upregulated genes) for KLF4-overexpressing HPAECs.

A comparison of KLF2, KLF4 and KLF6 transcriptomic databases, including up-regulated and down-regulated genes that met more stringent criteria (FDR <0.01, $\log_2|FC|>2$) for each KLF identified 248 shared genes (Figures 6.14A and 6.15A; Supplementary Table S7).

A Metascape pathway and process enrichment analysis of common DEGs between KLF2-, KLF4- and KLF6-overexpressing HPAECs revealed enrichment in processes that are associated with DNA metabolism, DNA replication and cell cycle regulation (Figure 6.15B), and these genes were predominantly downregulated in KLF2-, KLF4- and KLF6-overexpressing HPAECs (Supplementary Figures S12 and S13)

Interestingly, 308 genes were unique to KLF2, and were primarily involved in the regulation of vasculature development, cell proliferation and migration (Figure 6.16A and B; Supplementary Table S8), while 1203 genes were specific to KLF4 and were enriched in blood vessel development, actin cytoskeleton and extracellular matrix organization (Figure 6.17A and B; Supplementary Table S8). However, 214 genes were unique to KLF6 and were mainly enriched in vasculature development, wound healing, angiogenesis, actin filament bundle assembly, extracellular matrix organization and regulation of glycolytic process (Figure 6.18A and B; Supplementary Table S8).

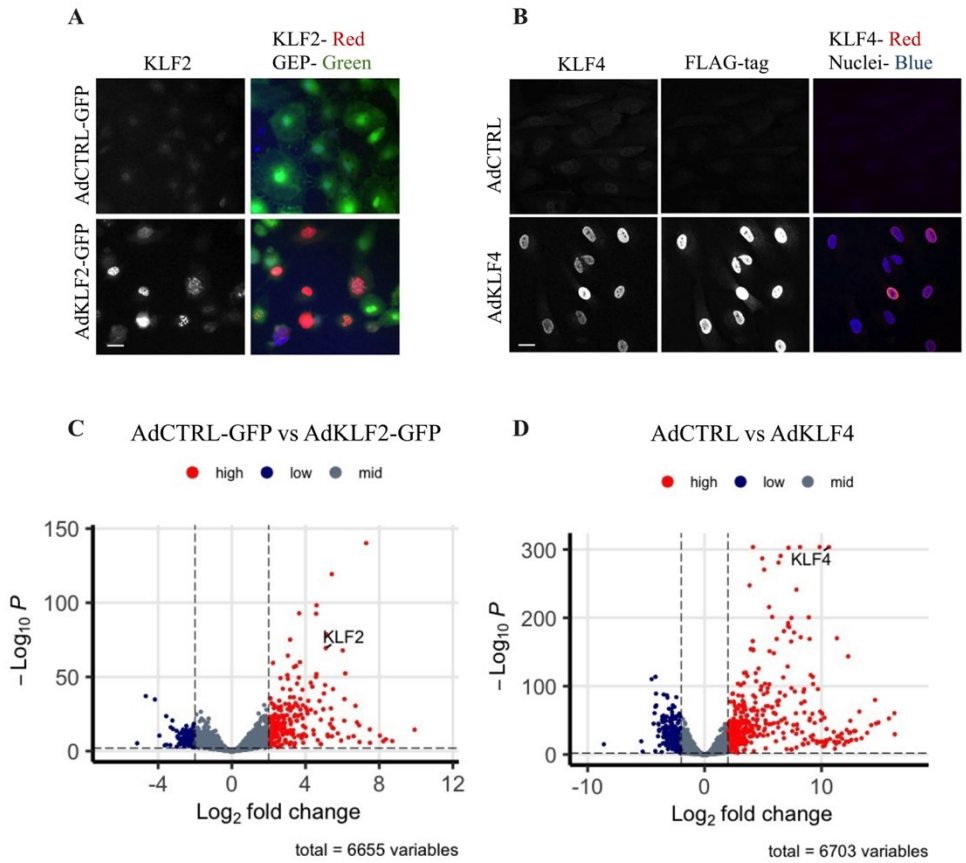

Figure 6.13: KLF2 and KLF4 overexpression in HPAECs.
(A) Representative confocal microscopy images showing nuclear localization of KLF2 (AdKLF2-GFP) in HPAECs 24 hours post-infection. Cells were infected with adenoviral control (AdCTRL-GFP) or AdKLF2-GFP (MOI 1:100). In the merged image, KLF2 is red, and cells infected with AdGFP or AdKLF2-GFP are green. Scale bar=10 μm; n=3. **(B)** Representative confocal microscopy images showing nuclear localization of KLF4 (AdKLF4) in HPAECs 24 hours post-infection. Cells were infected with adenoviral control (AdCTRL) or AdKLF4 (MOI 1:100). FLAG-tag marking the localization of KLF4-FLAG is shown in the central black-and-white image. In the merged image, KLF4 is red, Nuclei are blue (DAPI). Scale bar =10μm; n=3. **(C)** Volcano plot showing differentially expressed genes (DEGs) in AdKLF2-GFP- vs AdCTRL-GFP-infected cells. Downregulated genes ($p<0.05$ and $\log_2$ fold change <-0.25) are represented in blue and upregulated genes ($p<0.05$ and $\log_2$ fold change >0.25) are represented in red, n=4 donors/condition, 6655 DEGs (3381 downregulated and 3274 upregulated genes). **(D)** Volcano plot showing differentially expressed genes (DEGs) in AdKLF4- vs AdCTRL-infected cells. Downregulated genes ($p<0.05$ and $\log_2$ fold change <-0.25) are represented in blue and upregulated genes ($p<0.05$ and $\log_2$ fold change >0.25) are represented in red, n=4 donors/condition, 6703 DEGs (3308 downregulated and 3395 upregulated genes).

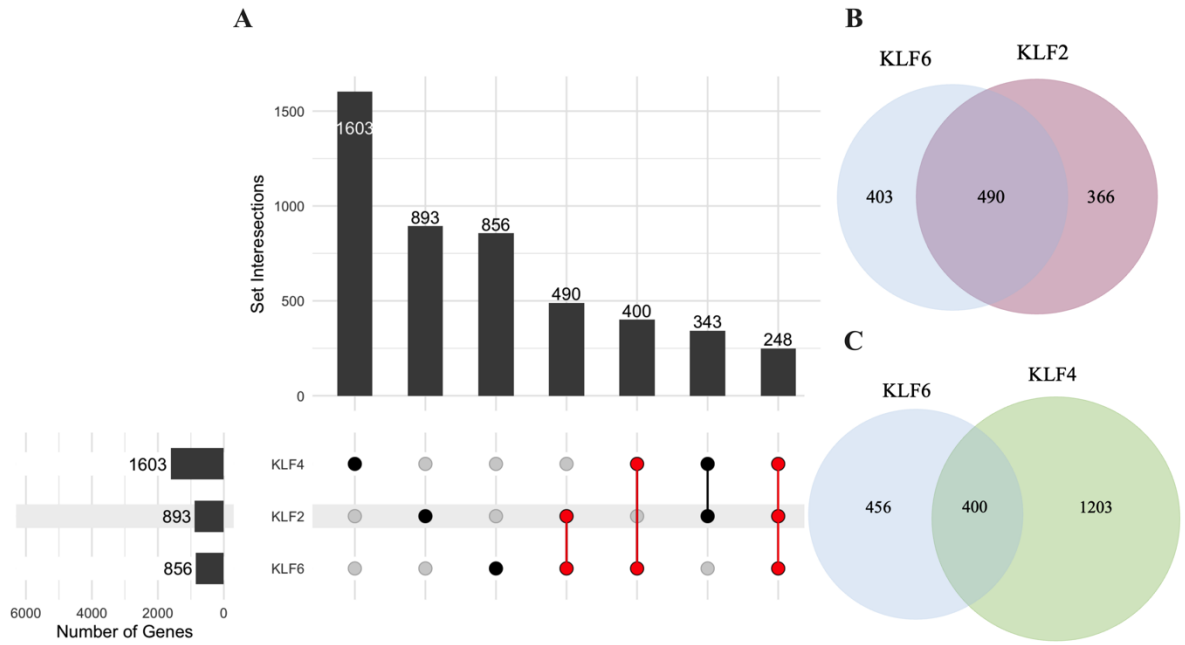

Figure 6.14: Overlap analysis of differentially expressed genes following KLF2, KLF4 and KLF6 overexpressing in HPAECs.
(A) Upset plot showing the overlap between KLF2-, KLF4- and KLF6-regulated DEGs in HPAECs. Connected black dots represent overlapping DEG lists and vertical bars in the intersection set show the number of overlapping genes. **(B)** Venn diagram showing the number and percentage of shared DEGs in HPAECs overexpressing KLF6 and KLF2. The overlap of 490 genes is significant at p= 0.00E+00 (This means that the overlapping p-value is highly significant as the p-value is a very small number that was rounded to zero). **(C)** Venn diagram showing the number and percentage of common DEGs in HPAECs overexpressing KLF6 and KLF4. The overlap of 400 genes is significant at p= 6.80E-255. The statistical significance of the overlaps between gene sets, in comparison to the genomic background, was calculated by the one-tailed Fisher's exact test using the GeneOverlap package in R (Shen, 2016).

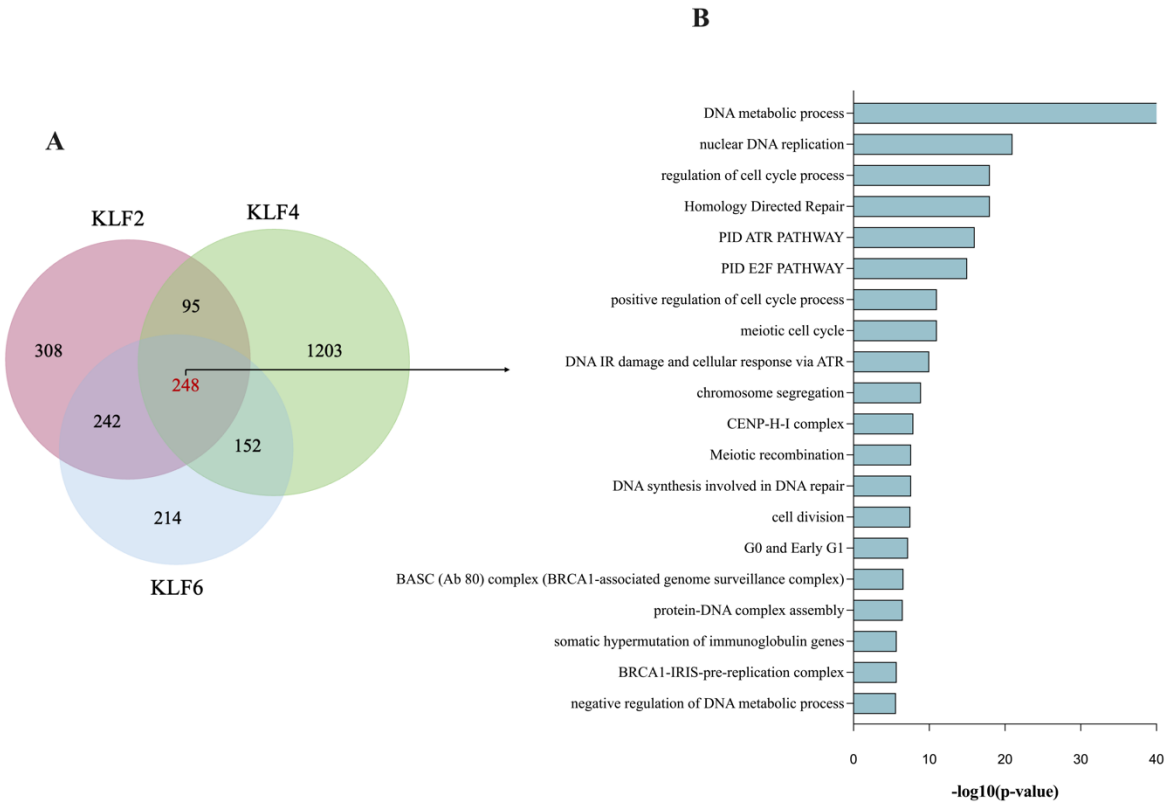

Figure 6.15: Metascape pathway and functional enrichment analysis of shared genes between KLF2, KLF4 and KLF6.
(A) Venn diagram showing the number and percentage of common differentially expressed genes in HPAECs overexpressing KLF2, KLF4 and KLF6. **(B)** Bar graph showing the Metascape pathway and process enrichment analysis of common differentially expressed genes between KLF2, KLF4 and KLF6. These enriched processes and pathways are predominantly associated with downregulated genes.

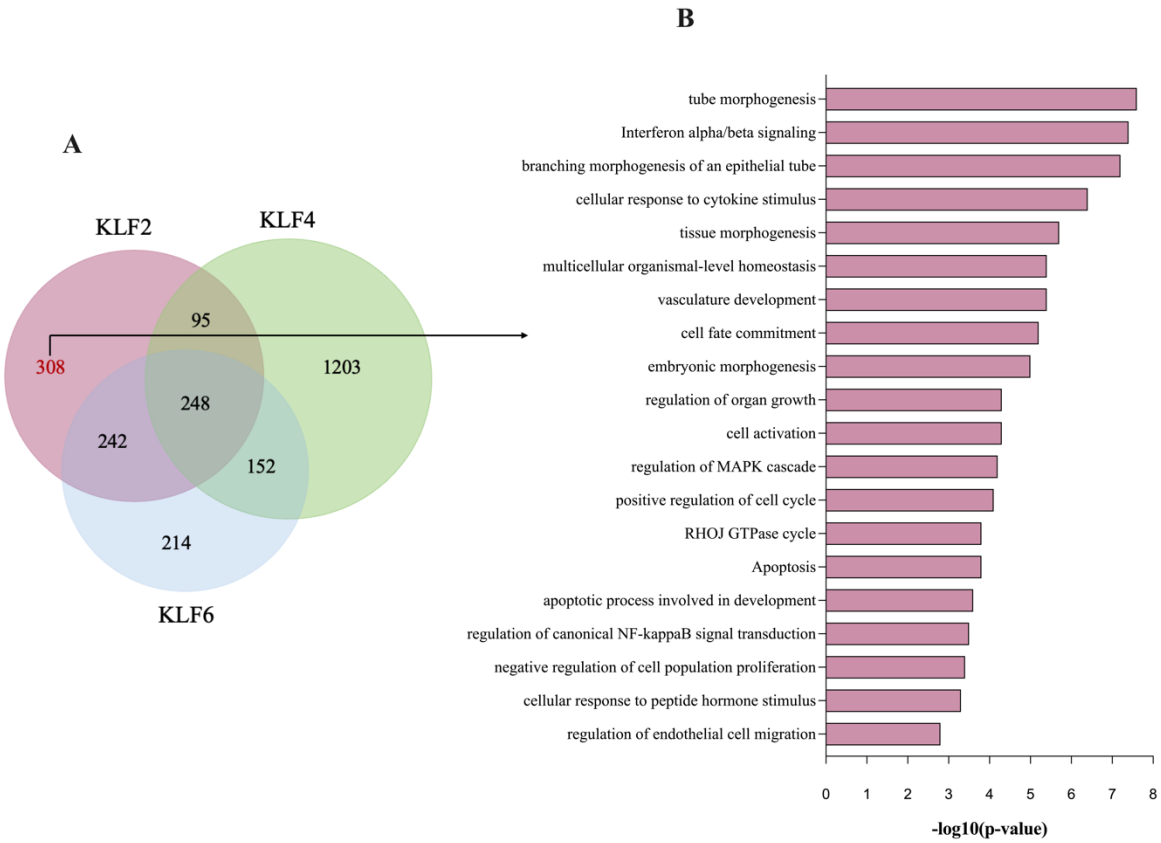

Figure 6.16: Metascape pathway and functional enrichment analysis of unique differentially expressed genes for KLF2.
(A) Venn diagram showing the number and percentage of unique differentially expressed genes in HPAECs overexpressing KLF2. **(B)** Bar graph showing the Metascape pathway and process enrichment analysis of unique differentially expressed genes for KLF2.

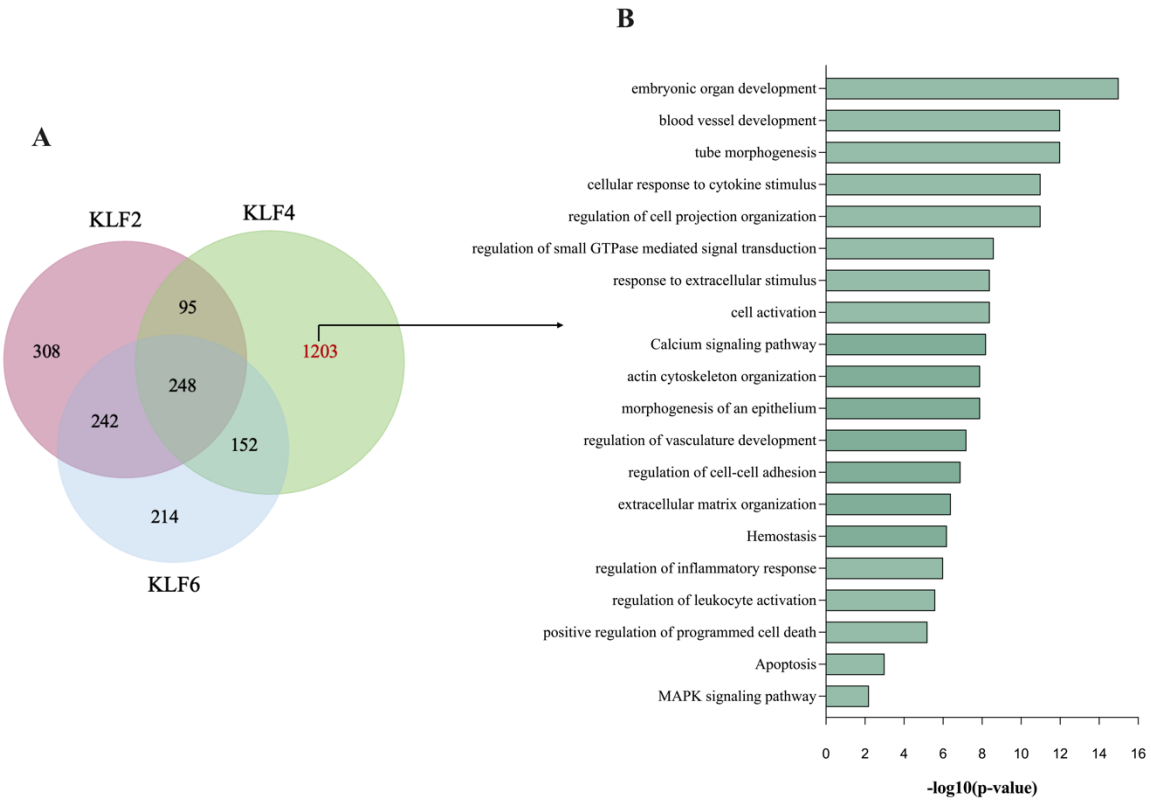

Figure 6.17: Metascape pathway and functional enrichment analysis of unique differentially expressed genes for KLF4.
(A) Venn diagram showing the number and percentage of unique differentially expressed genes in HPAECs overexpressing KLF4. **(B)** Bar graph showing the Metascape pathway and process enrichment analysis of unique differentially expressed genes for KLF4.

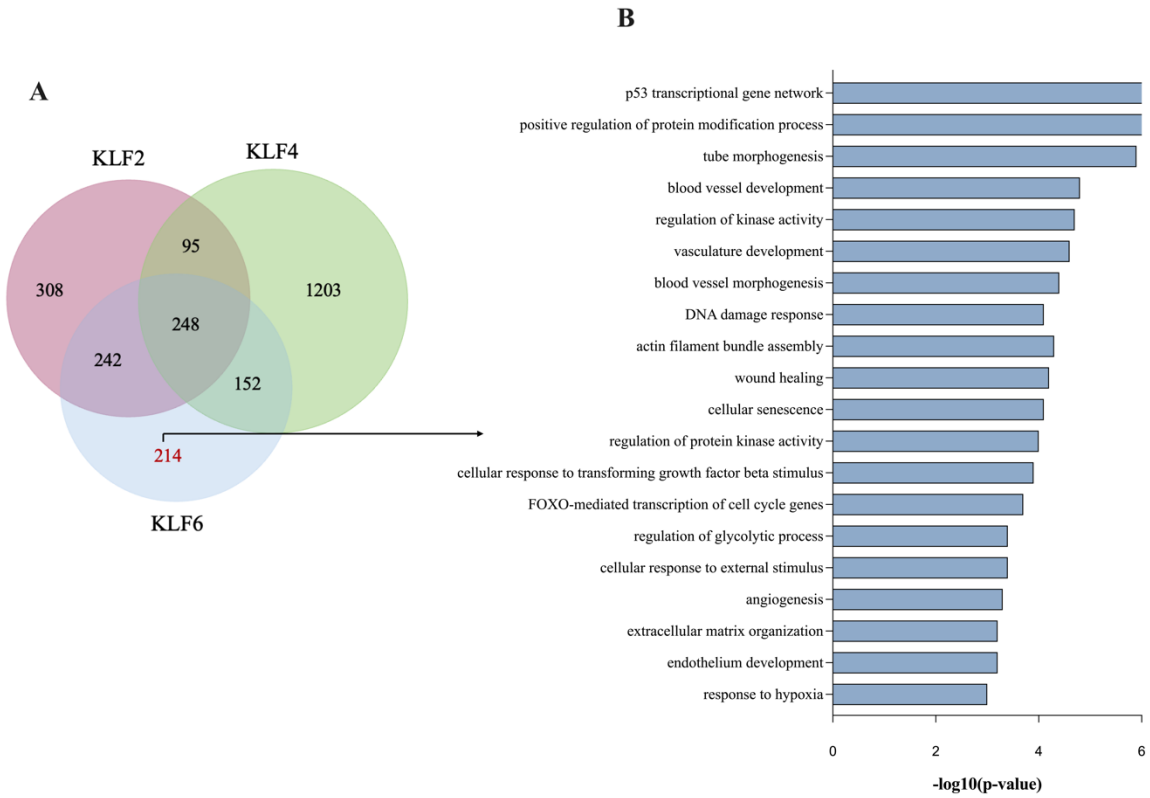

Figure 6.18: Metascape pathway and functional enrichment analysis of unique differentially expressed genes for KLF6.
(A) Venn diagram showing the number and percentage of unique differentially expressed genes in HPAECs overexpressing KLF6. **(B)** Bar graph showing the Metascape pathway and process enrichment analysis of unique differentially expressed genes for KLF6.

6.4.7 Regulatory feedback regulation of KLF2, KLF4 and KLF6 expression

Considering the known structural similarities between KLF2, KLF4 and KLF6, we aimed to establish whether the manipulation of KLF6 expression would affect the expression of KLF2 and/or KLF4 and *vice versa* using qPCR and the RNA-seq data from Section 6.4.6.

The overexpression of KLF6 significantly increased the expression of KLF2, whereas KLF4 was unaffected (Figure 6.19A, B). In line with these results, the RNA-seq analysis of HPAECs overexpressing KLF6 showed a significant increase in *KLF2* expression (p=0.002), whereas *KLF4* expression remained unchanged. Meanwhile, KLF2 significantly reduced *KLF6* expression (Figure 6.19C), suggesting that this transcription factor, which is known to promote endothelial quiescence and homeostasis, may act to restrict the effects of KLF6 activation. Consistent with this observation, the RNA-seq analysis of HPAECs overexpressing KLF2 showed a significant decrease in *KLF6* expression (p=0.03). *KLF4* overexpression did not change *KLF6* expression in HPAECs. There appeared to be a trend, but it was not statistically significant (p=0.056) (Figure 6.19D). Interestingly, the RNA-seq analysis of HPAECs overexpressing KLF4 showed a significant increase in KLF6 expression (p=2.74E-08).

However, KLF6 knockdown under flow (see Chapter 4, Section 4.4.1) did not significantly affect *KLF2* or *KLF4* expression (Figure 6.19E, F), which suggests that the flow-induced activation of KLF2 and KLF4 is regulated independently of KLF6.

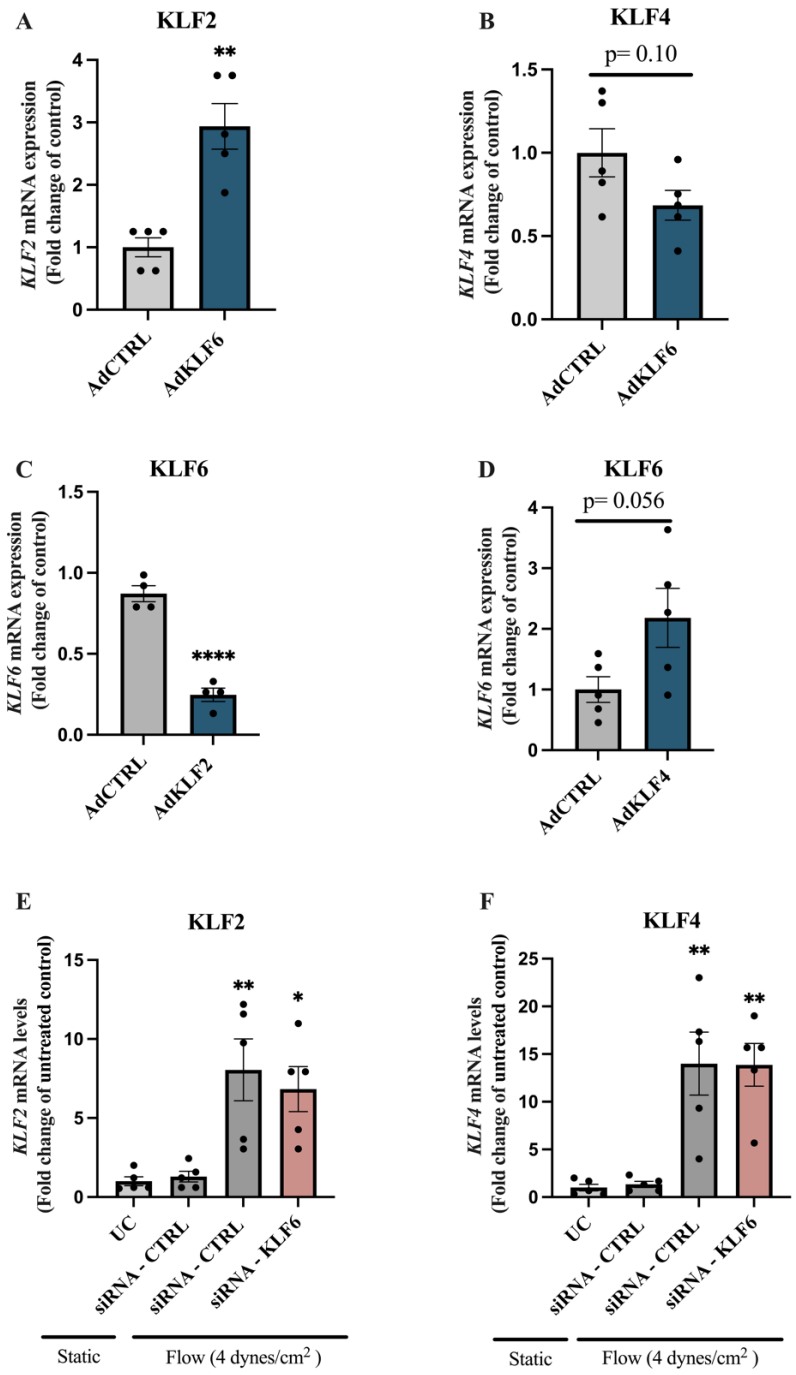

Figure 6.19: Regulatory feedback regulation of KLF2, KLF4 and KLF6 expression.
(A) *KLF2* and **(B)** *KLF4* mRNA expression in HPAECs infected with AdCTRL or AdKLF6 for 24 h. Data were normalized to the reference gene (*ACTB*). **P<0.01, in comparison with adenoviral controls using the unpaired t-test. Error bars indicate mean ±SEM; n=5. **(C)** *KLF6* mRNA expression in HPAECs infected with AdCTRL or AdKLF2 for 24 h. Data were normalized to the reference gene (*ACTB*). ****P<0.0001, in comparison with adenoviral controls using the unpaired t-test. Error bars indicate mean ±SEM; n=5. **(D)** *KLF4* mRNA expression in HPAECs infected with AdCTRL or AdKLF4 for 24 h. Data were normalized to the reference gene (*ACTB*). Error bars indicate mean ±SEM; n=5. **(E)** *KLF2* and **(F)** *KLF4* mRNA expression in HPAECs transfected with KLF6 siRNA or siRNA-CTRL for 48 h. Data were normalized to the reference gene (*B2M*). *P<0.05, **P<0.01, in comparison with untreated control using one-way ANOVA with Tukey's post-hoc test; n=5. Error bars indicate mean ±SEM.

6.5 Discussion

The aim of this chapter was to characterize KLF6-induced changes in the pulmonary endothelial transcriptome and to identify genes that are uniquely affected by KLF6, as well as those shared with the structurally and functionally related endothelial transcription factors KLF2 and KLF4.

The results showed that KLF6 overexpression increased the expression of endothelial identity and survival genes, including *BMPR2*, *ERG*, *SOX17*, *CDH5*, *PECAM1*, *KDR*, *ACVRL1*, *CAV1* and *SMAD1*. Interestingly, the expression of these genes is dysregulated in PAH (Eyries et al., 2020; Villar et al., 2020; Zhu et al., 2018b; Looney et al., 2017; Nikitopoulou et al., 2016; Szulcek et al., 2016a; Han et al., 2013; Austin et al., 2012; Maloney et al., 2012; Fujiwara et al., 2008; Harrison et al., 2003; Lane et al., 2000). Changes in the mRNA expression of a subset of these genes including *KDR*, *ERG*, *SOX17*, *CDH5* and *PECAM1* were confirmed using qPCR in an independent validation (Chapter 4, section 4.4.4 and 4.4.5). More work will be required to validate the expression of these targets at protein level.

A KLF6-induced increase in *BMPR2* expression may also be beneficial, as BMPR2 function and expression are compromised in PAH (Lane et al., 2000). Loss of *BMPR2* function increases endothelial apoptosis and migration, and increases the secretion of proinflammatory cytokines and vasoconstrictors (Andruska & Spiekerkoetter, 2018). KLF6 also increases the expression of endothelial pro-angiogenic markers *SOX17* and *ERG*, both of which are known to be downregulated in PAH (Yi et al., 2023; Looney et al., 2017). Deficiencies in *SOX17* were shown to increase endothelial cell proliferation and apoptosis resistance, and disrupt EC junctional integrity (Yi et al., 2023), which is consistent with the endothelial phenotype observed in PAH. Furthermore, the loss of *SOX17* was shown to enhance glycolysis, which is a key mechanism that drives PAEC and PASMC dysfunction and vascular remodelling in PAH (Yi et al., 2023; Chan & Rubin, 2017). Meanwhile, the loss of *ERG* in ECs leads to heightened permeability of the EC monolayer, increased release of pro-inflammatory cytokines and infiltration of inflammatory cells, suggesting that the loss of *ERG* in pulmonary ECs may contribute to the pathogenesis of PAH through the induction of inflammation (Yang et al., 2023; Looney et al., 2017).

The effect of endothelial KLF6 on PAH-related genes has not so far been investigated. Interestingly, we identified a substantial overlap between KLF6 DEGs in HPAECs and publicly

available sets of differentially expressed genes in PAH (Ainscough et al., 2022a; Reyes-Palomares et al., 2020; Rhodes et al., 2015). Additionally, using a previously curated PAH gene list from (Haensel & Wojciak-Stothard, 2023; Welch et al., 2023), we found that KLF6 upregulates most PAH genes that are related to endothelial identity, repair and angiogenesis. This finding suggests that KLF6 promotes the upregulation of PAH-related genes that control endothelial identity, repair and angiogenesis.

Functional enrichment analysis showed that the overexpression of KLF6 upregulates the genes that are involved in angiogenesis, cell migration, endothelial repair and tissue homeostasis, but downregulates genes related to DNA replication, DNA metabolic process and cell cycle progression. These results agree with the observed functional effects of KLF6 overexpression in HPAECs, including the stimulation of cell migration (Section 4.4.7), junctional assembly (Section 4.4.4), angiogenesis (Section 4.4.5), the inhibition of cell proliferation (Section 4.4.6) and apoptosis (Section 4.4.8).

The upregulated genes in KLF6 overexpressing HPAECs are involved in several signalling pathways that have been previously implicated in the development and progression of PAH, including forkhead box transcription factor O (FOXO), p53, TNF, NF-κB, PI3K-Akt and Ras signalling pathways (Berghausen et al., 2021; Wang et al., 2019b; Hurst et al., 2017; Savai et al., 2014; Garat et al., 2013; Price et al., 2013; de Man et al., 2012). I will discuss these pathways and their implications to endothelial function and PAH in more detail in the following paragraphs.

FOXO1 is a member of the winged-helix family of transcription factors. It is a crucial regulator of cell cycle progression, apoptosis, autophagy, metabolism, DNA damage repair and oxidative stress resistance (Li et al., 2023a). FOXO1 is expressed in the embryonic vasculature, and its loss of function results in embryonic lethality, showing that FOXO1 is essential for the maintenance and function of the embryonic vasculature (Deng et al., 2017). FOXO1-deficient endothelial cells show distinct morphological changes in response to VEGF in comparison to normal ECs, indicating that FOXO1 is essential for the normal physiological function of the endothelium (Furuyama et al., 2004). *FOXO1* expression is reduced in PAH PASMCs, promoting hyperproliferation and apoptotic response in those cells (Savai et al., 2014). Restoring FOXO1 activity *in vivo* reverses vascular remodelling and right ventricular hypertrophy in preclinical PAH (Savai et al., 2014).

Impaired p53 signalling in PAECs and PASMCs has been observed in human PAH and in a hypoxic mouse model of PAH, which shows that the genetic deletion of p53 can aggravate the disease (Wang et al., 2019b; Mizuno et al., 2011). In addition to p53 signalling pathway, TNF-α signalling via NF-kB is involved in the pathogenesis of PAH, and its inhibition attenuates the development of monocrotaline-induced PAH in rats (Hurst et al., 2017; Price et al., 2013; Wang et al., 2013).

The PI3K/Akt signalling pathway is involved in the regulation of cell growth, survival, migration, angiogenesis and vascular tone (Lee et al., 2014a; Morello, Perino & Hirsch, 2009). This pathway has also been implicated in the pathogenesis of PAH, as evidenced by enhanced PI3K/AKT signalling in PAH patients and hypoxic PH mice (Berghausen et al., 2021). The activation of the PI3K/AKT pathway promotes PASMC proliferation and vascular remodelling, which worsens PAH, although the *in vivo* administration of PI3K and Akt inhibitors can attenuate hypoxia-induced pulmonary vascular remodelling (Garat et al., 2013). On the other hand, PI3K/AKT activation has an anti-apoptotic and pro-survival effect in endothelial cells (Shiojima & Walsh, 2002), which may help to counteract the effects of endothelial damage.

Meanwhile, the dysregulation of the renin-angiotensin system (RAS) signalling pathway is also associated with the pathogenesis of PAH (de Man et al., 2012). Elevated levels of angiotensin II (Ang II), a key effector molecule of the RAS, are correlated with disease progression in IPAH patients, indicating that the increased activation of the RAS pathway is associated with pulmonary vascular remodelling (de Man et al., 2012).

Hypoxia is a key contributory factor in the development of PAH (Pak et al., 2007). HIF-1 and HIF-2 regulate transcriptional responses to hypoxia by binding to hypoxia-response elements (HREs) in the DNA, resulting in the expression of genes associated with angiogenesis, survival, proliferation and metabolism (Carmeliet et al., 1998; Semenza et al., 1994). A pathway enrichment analysis of differentially expressed genes in hypoxic HPAECs showed enrichment in HIF-1 and TGF-β signalling pathways, while RNA-seq analysis showed that overexpression of KLF6 in these cells reduced expression of key HIF-1 targets, including *PDK1*, *PGK1*, *LDHA*, *ENO1*, *BNIP3*, and *ICAM1*. These findings suggest that KLF6 regulates the hypoxic response in HPAECs by reducing the expression of genes related to glycolysis in endothelial cells.

Increased aerobic glycolysis in the pulmonary vasculature promotes vascular remodelling (Xu, Janocha & Erzurum, 2021), and numerous studies have reported elevated levels of key glycolytic enzymes in PAH, including PDK1, PGK1, LDHA and ENO1 as a result of HIF-1α activation (Ryan & Archer, 2015). The downregulation of these key glycolytic enzymes by KLF6 is therefore likely to have a beneficial effect on vascular remodelling in PAH. I will discuss the involvement of these HIF-1 target genes in the pathogenesis of PAH in detail in the following paragraphs.

The activation of pyruvate dehydrogenase kinase (PDK) subsequently inhibits pyruvate dehydrogenase (PDH), which re-directs pyruvate towards glycolysis and induces the conversion of glucose to lactate through anaerobic respiration (Chan & Rubin, 2017; Papandreou et al., 2006). It has been reported that PDK1 levels in human PAH lungs were higher than in healthy lungs, and that the PDK1 inhibitor dichloroacetate (DCA) improved haemodynamics in PAH patients (Michelakis et al., 2017). Phosphoglycerate kinase 1 (PGK1) is a key enzyme that is responsible for facilitating the production of ATP in the aerobic glycolysis pathway (Zhang, Sun & Kang, 2023). It has been reported that *PGK1* levels were significantly increased in peripheral blood mononuclear cells obtained from PAH patients (Benincasa et al., 2023).

Lactate dehydrogenase A (LDHA) is an enzyme that plays an important role in glycolysis by facilitating the conversion of pyruvate into lactate. LDHA is highly expressed in several types of tumours (Zhou et al., 2019a), and *LDHA* levels have been shown to be elevated in endothelial cells obtained from PAH patients (Smolders et al., 2022).

Enolase 1 (ENO1), also known as Alpha-enolase, is a crucial glycolytic enzyme that has been associated with various cancer types by promoting cell glycolysis, growth, migration and invasion (Huang et al., 2022). *ENO1* levels have been found to be increased in IPAH patients and in animal models of chronic hypoxic pulmonary hypertension (Shi et al., 2023; Dai et al., 2018).

Increasing evidence suggests that reduced mitochondrial biogenesis and increased mitophagy as a result of HIF activation also contribute to PAH (Haslip et al., 2015; Ryan et al., 2015). Bcl 2/adenovirus E1B 19 kDa interacting protein 3 (BNIP3), a mitochondrial outer membrane protein, regulates mitophagy during hypoxia and is activated by HIF-1α (He et al., 2022). It

has been reported that levels of BNIP3 increase following exposure to hypoxia in primary mouse lung endothelial cells (MLECs) isolated from male and female C57Bl6 wild-type (WT) mice, which suggests that BNIP3 may be involved in the pathogenesis of PAH (Bazan et al., 2022).

Intercellular adhesion molecule 1 (ICAM1), a transmembrane glycoprotein, is expressed on the surface of many cell types, including endothelial cells and leukocytes at a low basal level, and is expressed in ECs following chronic exposure to hypoxia (Liang et al., 2019; Hubbard & Rothlein, 2000) or TNF-α stimulation (Zhu et al., 2016). ICAM-1 protein levels are increased in response to hypoxia via an increase in arginase type II (Arg-II) protein levels mediated by HIF-1α (Liang et al., 2019). Elevated ICAM-1 levels have been detected in the pulmonary endothelium of IPAH patients (Le Hiress et al., 2015). In contrast to our findings, a recent study has shown that KLF6 increases the expression of inflammatory and glycolytic genes in macrophages by upregulating HIF-1α expression (Kim et al., 2020a). This suggests that the effects of KLF6 may be cell type-specific.

TNF-α is a major contributor to the pathogenesis of PAH (Bell et al., 2020; Fujita et al., 2002). TNF-α is thought to enhance PAH by inhibiting BMPR2 and modulating the Notch signalling pathway (Hurst et al., 2017). DEGs in TNF-α-treated cells showed enrichment in TNF and NF-κB signalling pathways, although this is expected as TNF-α is widely recognized for its ability to stimulate NF-κB signalling (Hayden & Ghosh, 2014). The upregulated genes in KLF6-overexpressing HPAECs treated with TNF-α also showed enrichment in NF-κB signalling pathways. DEGs in KLF6-overexpressing HPAECs treated with TNF-α showed an increase in *NFKBIA* expression, but the expression of *NFKBIB*, *NFKB1*, *NFKB2*, *EGR2*, *ATF3* and *NR4A2* was significantly decreased, so the enrichment of KLF6 DEGs in NF-κB signalling is likely to account for the anti-inflammatory effects of KLF6 seen in cultured HPAECs (Chapter 4, Section 4.4.2). I will discuss the roles of NFKBIA and NFKBIB in NF-κB signalling pathway and how KLF6 is involved in regulating this signalling pathway in the following paragraph.

NFκB inhibitor alpha (NFKBIA) and NFκB inhibitor beta (NFKBIB) are proteins located in the cytoplasm that bind to NF-KB in order to suppress its activity. Following the stimulation of NF-κB, NFKBIA and NFKBIB are phosphorylated by IKK, and these proteins are subsequently ubiquitinated and degrade, leading to the activation and nuclear translocation of NF-κB and the induction of transcription of target genes (Napetschnig & Wu, 2013; Chen &

Ghosh, 1999). Previous studies have shown that KLF6 acts as a transcriptional activator of the NF-κB-negative regulator NFKBIA in glioblastoma cells (LN229) and in two brain tumour-derived stem-like cells (BTSCs) (BTSC23, BTSC233) transduced with a lentivirus expressing KLF6-wt. This suggests that KLF6 exerts a negative regulatory effect on the NF-κB pathway by reducing the nuclear localization of NF-κB and suppressing the expression of its target genes (Masilamani et al., 2017). In our study, the expression of *KLF6* was induced in response to TNFα and inhibited the activation of TNF-α-induced NF-κB (Chapter 3, Section 3.4.3; Chapter 4, Section 4.4.2). In accordance with our results, KLF6 has been shown to decrease pro-inflammatory mediators such as TNF-α, IL-6 and CXCL2, and to suppress neutrophil and macrophage infiltration in liver tissues induced by ischemia-reperfusion (I/R) injury (Li et al., 2023b). KLF6 knockdown in keratinocytes has been shown to promote inflammatory responses during aging by increasing the expression and secretion of pro-inflammatory cytokine *IL6* (Zou et al., 2021). KLF6 appears to act as a stress-response protective gene. Azilsartan, an angiotensin II receptor antagonist, was shown to attenuate oscillatory shear stress (OSS)-induced endothelial dysfunction and inflammation by upregulating KLF6 (Wei et al., 2021).

Previous studies have shown a functional redundancy between KLF2 and KLF4. For example, *KLF2* hemizygous ($KLF2^{+/-}$) mice showed increased expression of *KLF4* in lung tissues, whereas endothelial *KLF4* deficient mice showed an increased expression of *KLF2*, suggesting the existence of compensatory mechanisms. KLF2 and KLF4 also cooperate in the regulation of endothelial quiescence, as demonstrated in a recent report showing that KLF4 and KL2 share roughly 30% of their binding sites in mouse ECs (Sweet et al., 2023). The loss of *KLF4* induces auto-regulation of *KLF2* by binding to its own promotor in an adaptive response (Mastej et al., 2022). However, increased *KLF2* expression in *KLF4* deficient mice increased endothelial-mesenchymal transition (EndMT), indicating that the presence of both factors is required for the maintenance of endothelial cell quiescence and homeostasis (Mastej et al., 2022).

Interestingly, it was shown in this chapter that KLF6 increased the expression of *KLF2*, while KLF2 reduced *KLF6* expression, suggesting the existence of a regulatory feedback mechanism between KLF2 and KLF6 in ECs. *KLF4* expression was unaffected by KLF6 overexpression in HPAECs, but *KLF6* expression was significantly increased in HPAECs overexpressing KLF4, indicating that KLF6 may be a downstream target of KLF4. However, KLF6 knockdown did not affect *KLF2* or *KLF4* expression in HPAECs cultured under flow

conditions for 24 hours. It is possible that the regulation of *KLF2* and *KLF4* expression under flow is KLF6-independent. KLF expression is highly dependent on the cellular context and the type of environmental stimuli, and is subject to mutual regulatory effects (Oishi & Manabe, 2018). To obtain a more complete scenario, future studies should investigate the effects of KLF6 knockdown on KLF2 and KLF4 expression at different time points of flow stimulation as well as the effects of KLF2 and KLF4 knockdown on KLF6 expression under flow.

This study is the first to demonstrate differences and similarities between the endothelial transcriptional responses of KLF2, KLF4 and KLF6. There is a statistically significant overlap between the DEGs of KLF6-overexpressing HPAECs and KLF2 and KLF4-overexpressing HPAECs. KLF2, KLF4 and KLF6 have common gene targets in HPAECs, which were predominantly downregulated and mainly associated with the regulation of cell cycles, DNA replication and DNA metabolic processes. Interestingly, the unique genes for KLF2, KLF4 and KLF6 were associated with vascular development and tube morphogenesis, although the functional effects of these unique genes on vascular development and angiogenesis may vary. For example, KLF2 has been shown to have a potent anti-angiogenic effect, as demonstrated by previous studies showing that KLF2 overexpression inhibits endothelial angiogenesis and tube formation by suppressing the expression of VEGF receptor 2 (VEGFR2/*KDR*) and hypoxia-inducible factor 1alpha (HIF1A) (Kawanami et al., 2009; Bhattacharya et al., 2005), whereas KLF2 knockdown has the opposite effect (Zeng et al., 2015). Interestingly, the expression of *KDR* and *HIF1A* was significantly decreased (p=8.99E-23, p=1.47E-08 respectively) in KLF2 overexpressing HPAECs. Like KLF2, KLF4 overexpression inhibits endothelial angiogenesis, as assessed by measuring tube formation in human umbilical vein endothelial cells (HUVECs) through upregulating miR-15a (Zheng et al., 2013). However, KLF4 enhances endothelial angiogenesis in retinal microvascular ECs by activating the VEGF signalling pathway (Wang et al., 2015), suggesting that the role of KLF4 appears to be cell type-specific and context-dependent. The expression of *VEGFA* was also significantly increased (p=1.00E-37) in KLF4 overexpressing HPAECs. These results suggest that KLF2 is crucial for maintaining endothelial quiescence, while KLF4 and KLF6 induce endothelial repair to restore vascular homeostasis.

Overall, the work discussed in this chapter begins to define the transcriptomic and functional pathway effects of activating KLF6 in HPAECs, highlighting the important role of KLF6 in enhancing EC repair and angiogenesis. In future, the connectivity map (CMap) – an online

genetic signature database that uses cellular responses to perturbation to identify connections between compounds, diseases, and genes (Lamb et al., 2006), – should be queried using transcriptomic data from KLF6 overexpression in HPAECs to identify compounds that might cause similar transcriptomic signatures to KLF6 activation. Interestingly, it has been shown that KLF6 reactivation can be accomplished by targeting the KLF6 regulators FOXO1 and EGFR by combining two FDA-approved drugs: trifluoperazine hydrochloride, a FOXO1 nuclear export inhibitor, and erlotinib, a small molecule inhibitor of EGFR signalling (Sangodkar et al., 2012).

6.6 Conclusion

Transcriptional analyses have shown that KLF6 increases the expression of arterial endothelial identity markers and promotes endothelial survival by increasing the expression of genes related to endothelial repair and angiogenesis. The transcriptomic data also suggest some redundancy between KLF6 and the other two KLF family members, KLF2 and KLF4, which were previously implicated in PAH. Meanwhile, a substantial number of KLF6-upregulated genes are known to be downregulated in PAH, which suggests the potentially beneficial role of KLF6 activation in this disease.

Chapter 7 Results: Spatial transcriptomics of PAH lung sections

7.1 Introduction

PAH is a severe lung disease that is characterised by extensive pulmonary vascular remodelling, leading to the narrowing of the pulmonary arteries. This narrowing occurs due to the thickening of the arterial walls and subsequent occlusion caused by the formation of plexiform lesions. These changes depend on a complex network of interactions between different cell types within the pulmonary arterial wall (Chan & Loscalzo, 2008; Humbert et al., 2004). While current preclinical models improve our understanding of the molecular mechanisms involved in PAH (Stenmark et al., 2009), they do not accurately reproduce the pathophysiological characteristics of the human condition.

Recently, spatial transcriptomics has emerged as a powerful tool for characterising cellular heterogeneity and investigating potential cell-to-cell interactions. This allows for the exploration of the structural organisation of tissues and its influence on cellular behaviour (Dong & Yuan, 2021). Spatial transcriptomics is a new technique that enables the capture of gene expression patterns within intact tissue sections (such as fresh or frozen FFPEs) and provides comprehensive transcriptome data accompanied by spatial information (Chen et al., 2023; Li & Wang, 2021). Spatial transcriptomic methodologies vary in terms of the number of detected genes, the level of resolution, the size of tissue assayed and the whole transcriptome analysis (Chen et al., 2023; Pour & Yanai, 2022). The methodologies used in spatial transcriptomics can be classified into four main groups according to detection strategies involved, and include probe-based, sequencing-based, imaging-based and image-guided spatially resolved single cell RNA sequencing (scRNA-seq) methods (Chen et al., 2023). In this chapter, we used probe-based methods such as the NanoString GeoMx digital spatial profiler (DSP) system to capture transcripts in manually selected regions of interest (ROIs) of human lung tissue sections from healthy control individuals and PAH patients, thus offering the possibility to explore region-specific gene expression profiles in PAH lungs, such as plexiform lesions.

7.2 Experimental aims

1. To determine the role of KLF6 in PAH by investigating the differential expression of KLF6-regulated genes in remodelled PAH blood vessels, including complex plexiform lesions.
2. To assess KLF6 expression in lung vessels from healthy controls and PAH patients.

7.3 Experimental outline

The experimental outline is shown in Figure 7.1. A brief description of the experimental design and methodology is provided below. For further experimental details, see Chapter 2, Section 2.6.

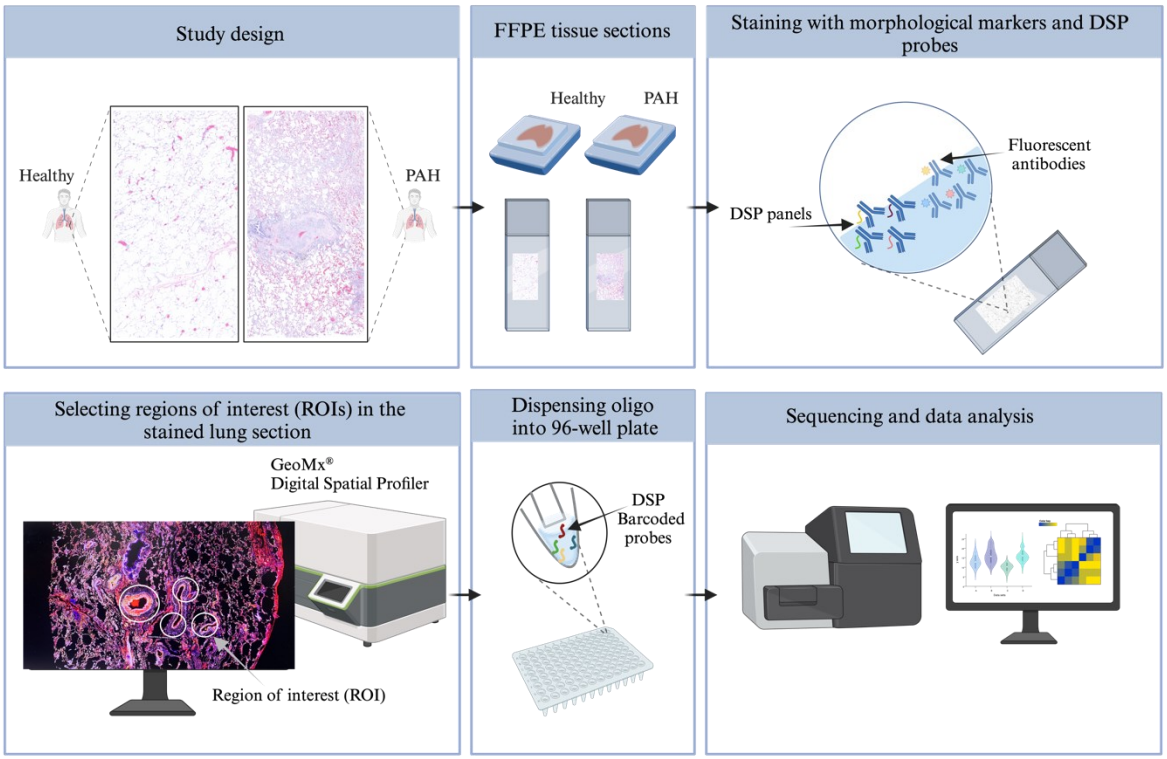

Figure 7.1: Schematic illustration of the experimental workflow for spatial transcriptomics. Spatial transcriptomics was conducted on human lung tissues sections from age- and sex-matched healthy control individuals (n=5) and PAH patients (n=6) using the Nanostring GeoMx DSP platform. Lung tissue sections were stained for endothelium and smooth muscle markers to define vessels and plexiform lesions, and a total of 30-45 regions of interest (ROIs) were selected in each lung section. Each ROI was illuminated with UV light to release the indexing oligonucleotides, which were then collected in microtiter plates before being sequenced on an Illumina sequencer (Illumina, USA) at the Imperial BRC Genomics Facility (Imperial College London). Illustration created by the author using BioRender.com.

7.4 Results

7.4.1 Spatial transcriptomics analysis of lung vessels of PAH patients and healthy control individuals

To investigate alterations in PAH transcriptome, spatial transcriptomics was performed using the Nanostring GeoMx platform on human lung tissue sections obtained from age- and sex-matched healthy control individuals (n=5) and PAH patients (n=6). Donor information for FFPE lung tissue samples is provided in Chapter 2, Section 2.6.

The haematoxylin and eosin (H&E) staining of human lung tissue sections from healthy control individuals and PAH patients for histopathological analysis of lung tissues is shown in Figure 7.2. The lung sections were prepared in accordance with the Nanostring GeoMX Digital Spatial Profiler (DSP) slide preparation user manual (MAN-10151-01).

Before conducting spatial transcriptomics analysis, we first optimised the immunostaining method to allow the identification of endothelial and smooth muscle cells using von Willebrand Factor (vWF) as the endothelial cell marker and α-smooth muscle actin (α-SMA) as the smooth muscle cell marker, as shown in Supplementary Figure S14.

The lung sections were then stained with SYTO 13 (nuclear marker), vWF (von Willebrand Factor; endothelial cell marker), and ACTA2 (alpha-smooth muscle actin or α-SMA; smooth muscle cell marker) (Figure 7.3). In each lung section, 30-45 regions of interest (ROIs) were selected using the “circle” or “freehand” selection tool available on the GeoMx DSP software to profile blood vessels within the lungs, specifically focusing on plexiform lesions observed in PAH patients. The study design of spatial transcriptomics analysis is summarised in Figure 7.4.

A spatial transcriptomics analysis of PAH lung vessels showed a total of 677 differentially expressed genes ($p < 0.05$, $\log_2|FC| > 0.25$), compared with heathy controls. The 100 most significantly differentially expressed genes are shown in Supplementary Table S9.

To investigate changes in gene expression patterns in plexiform lesions, we also conducted a spatial transcriptomics analysis on remodelled non-plexiform vessels and plexiform lesions in PAH lungs.

A total of 541 genes were found to be differently expressed ($p < 0.05$, $\log_2|FC| > 0.5$) between remodelled non-plexiform vessels and plexiform lesions in PAH lungs (Supplementary Table S10).

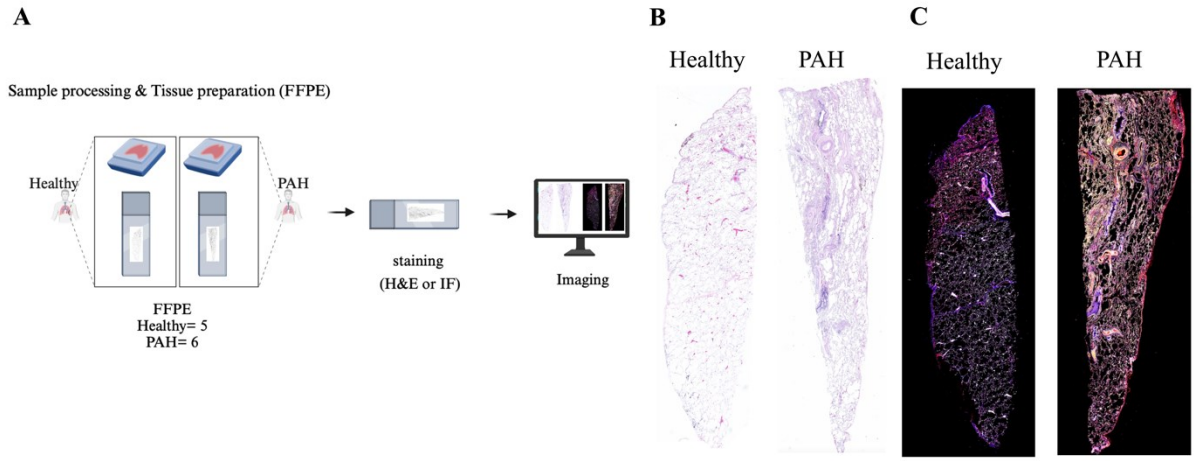

Figure 7.2: Preparation of human lung tissue sections for spatial transcriptomic analysis.
(A) Schematic diagram of patient sample processing and tissue preparation for spatial transcriptomics analysis. Human lung tissue sections were obtained from healthy controls and PAH patients (n= 5 for healthy controls and n= 6 for PAH patients). **(B)** Haematoxylin and eosin (H&E) staining of human lung tissue sections for histopathological analysis. **(C)** Immunofluorescence (IF) staining of human lung tissue sections for ROIs selection.

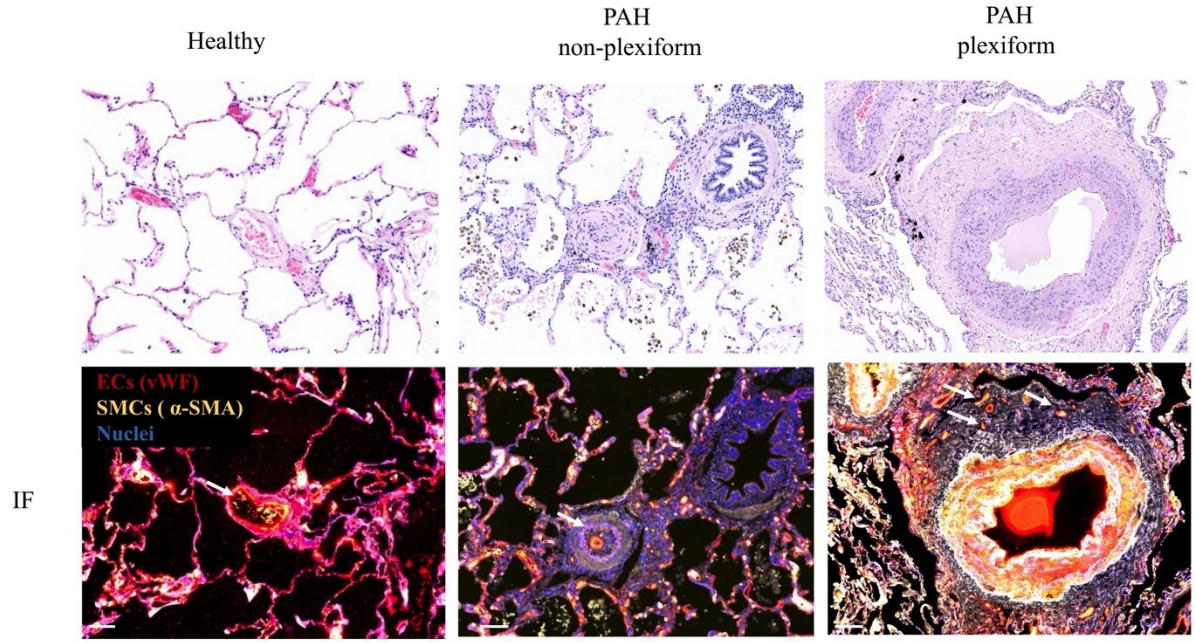

Figure 7.3: ROI selection and annotation for spatial transcriptomic analysis.
Representative examples of haematoxylin and eosin (H&E) and immunofluorescence (IF) staining of lung tissue sections were obtained from healthy controls and PAH patients. H&E and IF staining was used to guide the selection of ROIs in GeoMx Digital Spatial Profiler. The lung sections were stained for endothelial cell markers (vWF; red), smooth muscle cell markers (α-SMA; yellow) and with a counterstain for nuclei (SYTO 13; blue). 30-45 ROIs were selected in lung sections from healthy (n=5) and PAH (n=6) individuals, with separate annotations for non-plexiform and plexiform lesions. The ROIs are indicated by a white arrow. Scale bar= 50 µm.

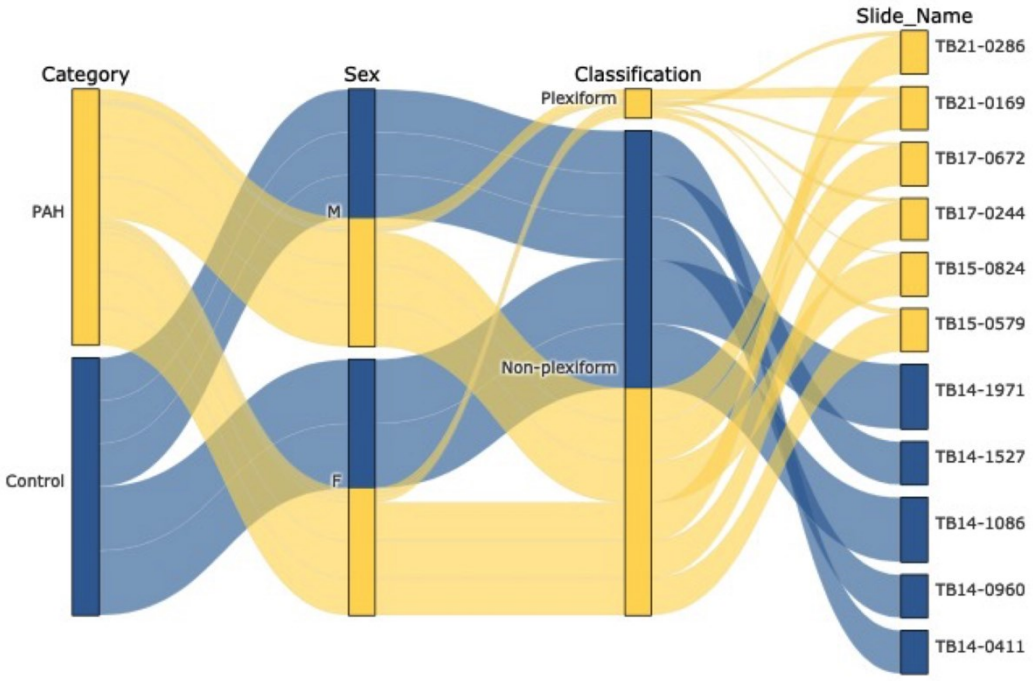

Figure 7.4:Sankey diagram illustrating the study design of spatial transcriptomics analysis. Individual ROI segments are annotated according to slide name, category (control and PAH), sex (female and male), and classification (non-plexiform and plexiform). Of a total of 11 slides analysed, 5 were from healthy controls (n=2 for female and 3 for male) and 6 were from PAH patients (n=3 for female and 3 for male), and 6 had plexiform lesions. Out of 359 regions of interest (ROIs) that were selected, 169 successfully met the quality control criteria.

7.4.2 Identification of KLF6-dependent genes within PAH DEGs

Spatial transcriptomics did not detect KLF6 as it is lowly expressed in ECs, so we looked at KLF6-dependent genes (identified in RNA-seq analysis of KLF6-overexpressing HPAECs, see Chapter 6, Section 6.4.1) in spatial transcriptomics datasets.

To assess the enrichment of KLF6 dependent genes within PAH DEGs, KLF6-dependent DEGs (FDR <0.05, $\log_2|FC|>0.25$) were overlapped with “all PAH” (named herein as “control vs PAH”) and plexiform lesion-specific DEGs (named herein as “non-plexiform vs plexiform”). 193 genes were shared between the KLF6 and “all PAH” DEGs, while 180 genes were shared between KLF6 and plexiform lesions DEGs (Figure 7.5; Supplementary Table S11).

GO ontology and KEGG pathway enrichment analysis of the shared KLF6/PAH DEGs showed significant enrichment in biological processes. These processes included actin cytoskeleton reorganization, cell proliferation, migration, motility, growth and ROS metabolic processes;

molecular functions, including collagen binding, receptor tyrosine kinase binding, cell adhesion molecule binding, ECM structural constituent and GTPase activity, cellular components including focal adhesion, adherens junction, cell junction and ECM and pathways including the HIF-1, PI3K/AKT and JAK/STAT signalling pathway (Figure 7.6).

The overlapping of KLF6/plexiform PAH DEGs showed significant enrichment in biological processes including cell junction assembly and organization, ECM organization, vascular development, and angiogenesis; molecular functions including myosin binding, actin binding and cytoskeletal protein binding; cellular components including actin cytoskeleton, cell-cell junction and ECM and pathways including the P53, cAMP, Hippo, and oestrogen signalling pathway (Figure 7.7).

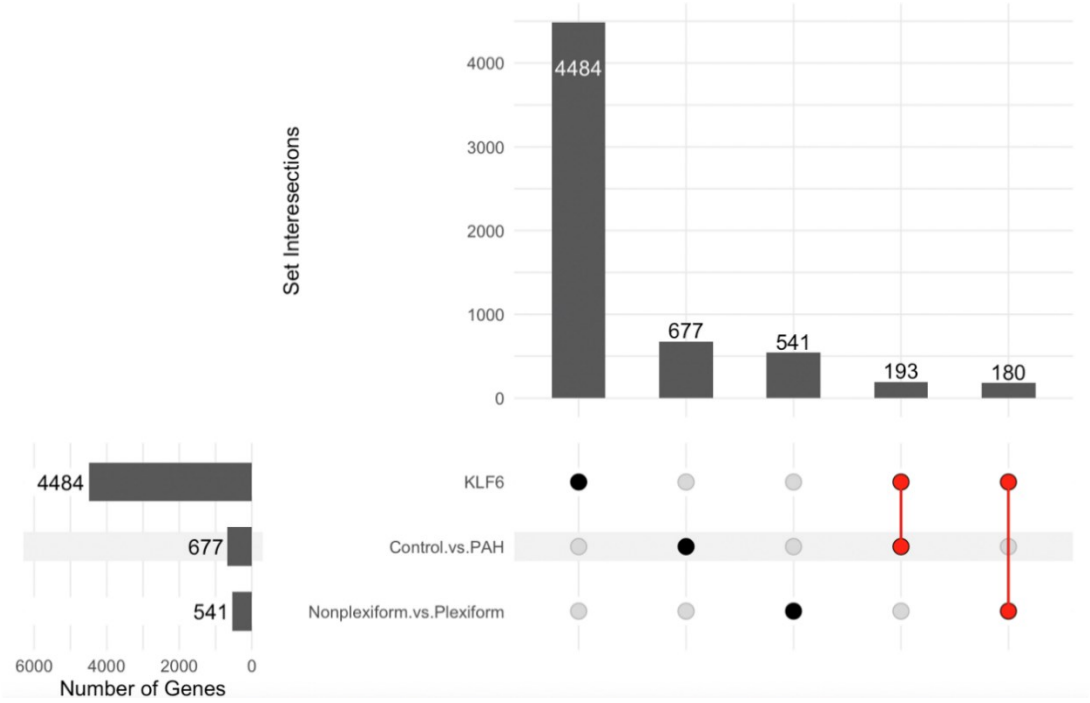

Figure 7.5: Overlap analysis of differentially expressed gene lists of KLF6-overexpressing HPAECs, control vessels vs PAH vessels and non-plexiform vs plexiform lesions.
Upset plot showing the interactions between differentially expressed gene lists of KLF6 overexpression in HPAECs, control vessels vs PAH vessels and non-plexiform vs plexiform lesions, where the connected red dots represent overlapping DEG lists and vertical bars in intersection set show the number of overlapping genes.

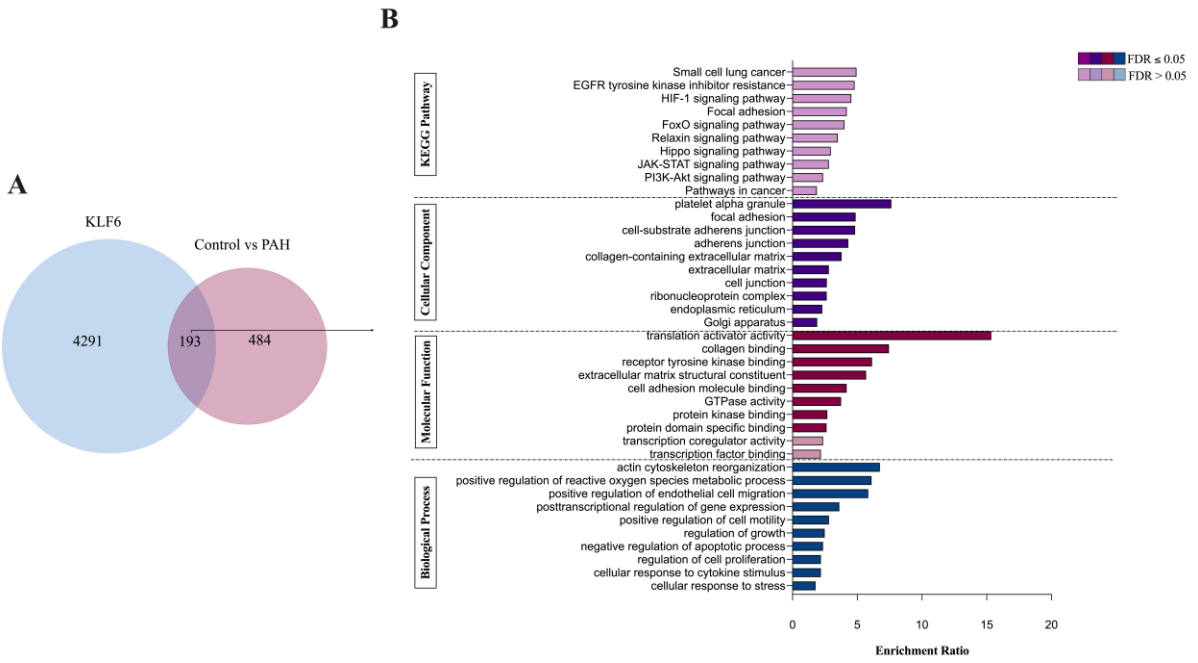

Figure 7.6:Enrichment analysis of shared KLF6/PAH DEGs.
(A) Venn diagram showing the number and percentage of common KLF6-regulated and PAH DEGs. The overlap of 193 genes is significant at p= 5.1E-12, as calculated by Fisher's exact test using the GeneOverlap package in R (Shen, 2016). **(B)** Gene ontology and KEGG pathway enrichment analysis of overlapping DEGs between KLF6 and PAH. The x-axis represents enrichment ratios (obtained from WebGestalt), while the y-axis represents enriched KEGG pathways/GO terms. (Darker colours = FDR ≤ 0.05; Lighter colours = FDR > 0.05).

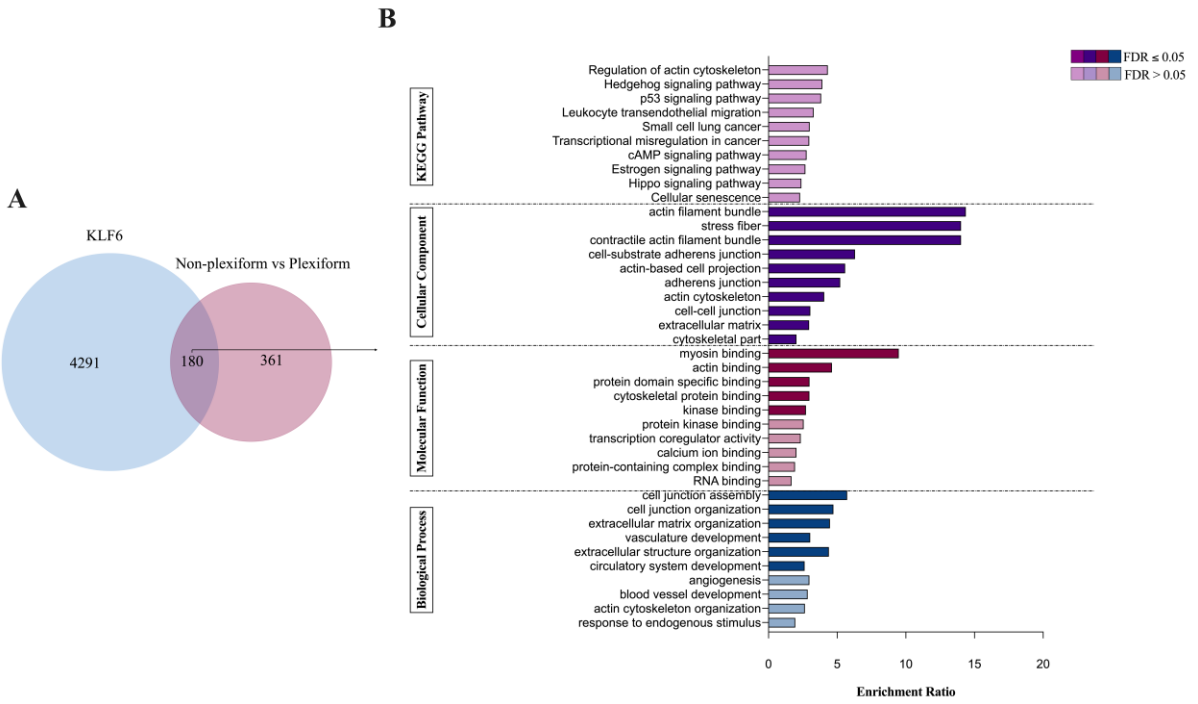

Figure 7.7:Enrichment analysis of shared KLF6-regulated genes and plexiform lesion-specific DEGs.
(A) Venn diagram showing the number and percentage of common DEGs in HPAECs overexpressing KLF6 and plexiform lesions. The overlap of 180 genes is significant at p= 3.3E-18. The significance of the overlap was calculated using Fisher's exact test using the GeneOverlap package in R (Shen, 2016). **(B)** Gene ontology and KEGG pathway enrichment analysis of the overlapping of differentially expressed genes between KLF6 and plexiform lesions. The x-axis represents enrichment ratios (obtained from WebGestalt), while the y-axis represents enriched KEGG pathways/GO terms. (Darker colours = FDR ≤ 0.05; Lighter colours = FDR > 0.05).

7.4.3 KLF6 expression in PAH endothelium of remodelled non-plexiform and plexiform lesions

To investigate changes in the expression of KLF6 in human lung tissues from PAH patients, we performed immunofluorescent staining of KLF6 in human lung tissues from healthy controls and PAH patients.

Endothelial cells within the PAH plexiform lesions showed a marked increase in the nuclear localization of KLF6 compared with healthy controls and other areas of the PAH lung (Figure 7.8C). The endothelial origin of $KLF6^+$ cells was confirmed by immunofluorescent staining using endothelial cell markers vWF and ERG (Figure 7.9A and B).

$KLF6^+$ cells were only detected occasionally in and around the pulmonary arteries of healthy control lungs (Figure 7.10C). In the PAH lungs, accumulations of $KLF6^+$ ECs were noted around the remodelled pulmonary arteries, but to a much lesser extent than those in plexiform lesions (Figure 7.10 D).

KLF6 is also highly expressed in the human placenta (Miranda et al., 2022), hence placental tissues were used as a positive control in the immunofluorescent staining of KLF6 (Figure 7.10E). A negative, secondary antibody only control was also included (Figure 7.10E).

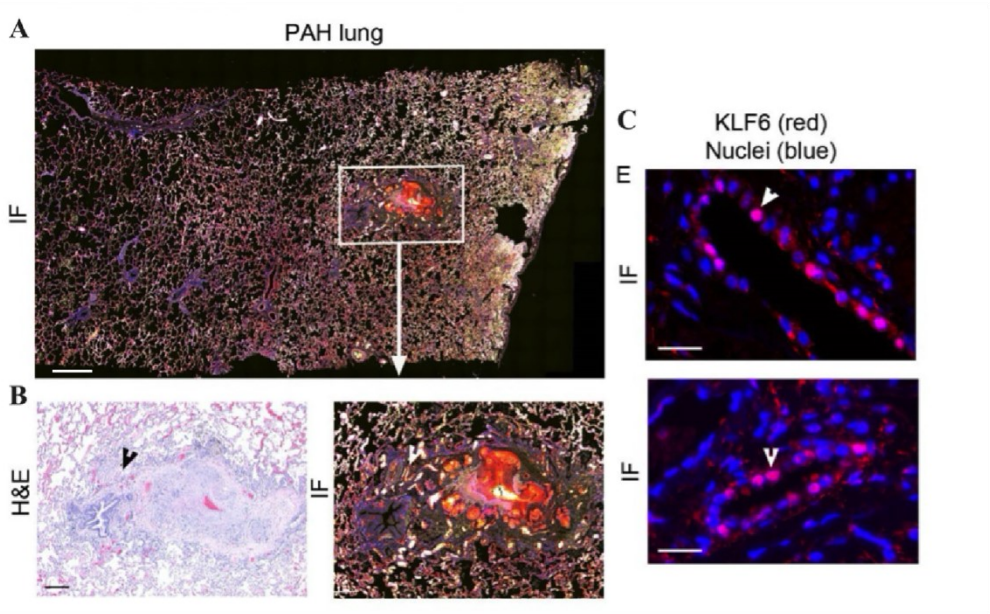

Figure 7.8: KLF6 in PAH endothelium.
(A, B) Representative images of haematoxylin and eosin (H&E) and immunofluorescent (IF) staining of a PAH lung tissue section using von Willebrand Factor (vWF; red), α-smooth muscle actin (α-SMA; yellow) and nuclei (SYTO 13, blue). Scale bars= 400 μm in (A) and 200 μm in (B). **(B)** Higher magnification of the area indicated by the white box on (A) shows the plexiform lesion. **(C)** Nuclear localization of KLF6 in endothelial channels within the plexiform lesion. Arrows point to $KLF6^{+}$ nuclei. In (C) KLF6 is red, and nuclei are blue. Scale bars= 50 μm.

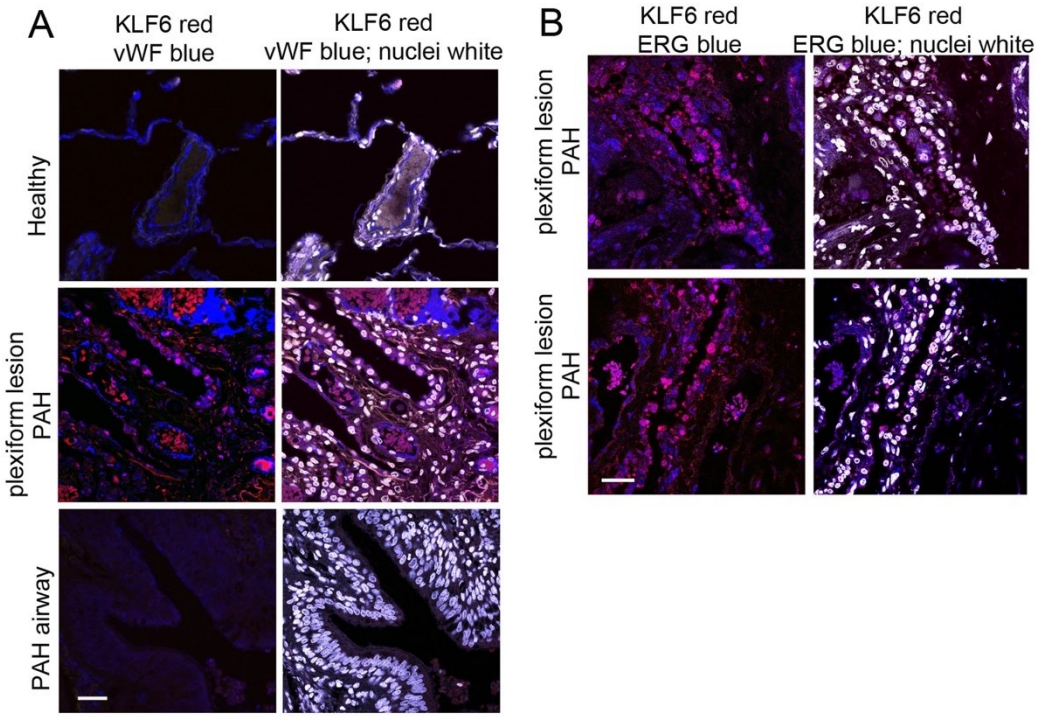

Figure 7.9: KLF6 colocalization with endothelial markers ERG and vWF.
(A) vWF and **(B)** ERG immunostaining in healthy and PAH lung tissues, as indicated. KLF6 is red, vWF and Erg are blue, and in the merged images, nuclei are white. Immunofluorescence, pseudocolours. Scale bar = 50 μm.

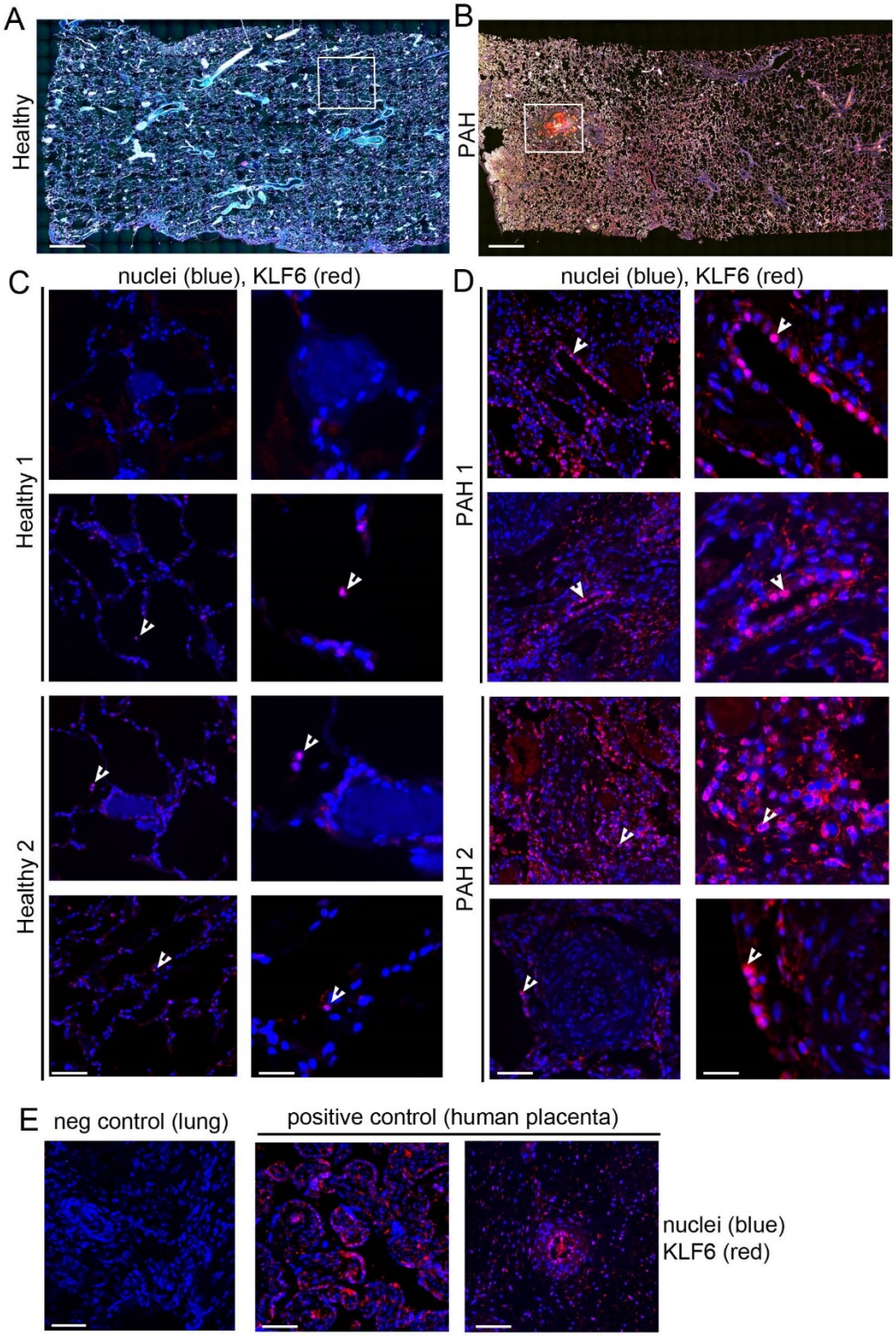

Figure 7.10: Representative images of tissue sections used for spatial transcriptomic and KLF6 localization.

(A) Human healthy and **(B)** PAH lung immunofluorescence: vWF (red), α-SMA (yellow), nuclei (blue). Scale bar =500 µm. Boxed areas show regions illustrated in (Healthy 1) and (PAH 1) images below. KLF6 localization **(C)** in healthy and **(D)** PAH lung tissues from 2 donors (PAH1 and PAH2); immunofluorescence: KLF (red) and nuclei (blue). Scale bar =50 µm. Enlarged corresponding images are shown in the right panel. Arrows point to nuclear localization of KLF6 (pink). Scale bar =20 µm. **(E)** negative control (secondary antibody only) and positive control showing the localization of KLF6 in the human placenta as indicated. Scale bar =50 µm.

7.5 Discussion

This chapter described the potential contribution of KLF6 to pulmonary vascular remodelling in PAH. Spatial transcriptomic analysis identified differentially expressed genes in human PAH vessels of varying sizes found both in non-plexiform and plexiform lesions, termed here as "all PAH DEGs," as well as differentially expressed genes unique to plexiform lesions, termed here as "plexiform DEGs". The lists of all PAH DEGs and Plexiform DEGs were then overlapped with KLF6-regulated DEGs that had been previously identified by RNA-seq analysis in HPAECs to identify KLF6-regulated subsets of genes (Chapter 6, Section 6.4.1)

The analysis of KLF6/PAH DEGs identified several known PAH targets, including *VWF*, *FOSL2*, *VIM*, *ENO1*, and *EGFR* (Nayakanti et al., 2023; Shi et al., 2023; Hołda et al., 2020; Merklinger et al., 2005; Veyradier et al., 2000). GO enrichment analysis of KLF6/ PAH DEGs further showed that KLF6 stimulates angiogenesis by affecting endothelial cell migration, actin cytoskeleton reorganization, motility, proliferation, growth and apoptosis. This is consistent with the observed stimulatory effects of KLF6 on endothelial angiogenesis and endothelial cell migration in cultured HPAECs and human pulmonary arterial explants *ex vivo* (Chapter 4, Section, 4.4.5, 4.4.6 and 4.4.7). In addition to this, KLF6-regulated PAH DEGs showed a significant enrichment in metabolic processes involving reactive oxygen species (ROS) and in cellular responses to cytokine stimulation. ROS have been implicated in vasoconstriction and vascular remodelling in PAH (Shen, 2023, 2016; Guo et al., 2016; Fike et al., 2011; Crosswhite & Sun, 2010). KLF6 was shown to regulate ROS levels in trophoblast cells (HTR-8/SVneo) (Kourdova et al., 2022) and hepatocytes (Li et al., 2023b), but its effect on ROS generation in endothelial cells has not been investigated.

Our transcriptomic and functional analyses showed that KLF6 is likely to play a protective role in endothelial responses to pro-inflammatory cytokine TNF-α, which is involved in PAH pathogenesis (Chapter 3, Section 3.4.3). In contrast to its effects on endothelial cells, KLF6 was shown to increase the release of pro-inflammatory cytokines in human hepatocytes (Sweet et al., 2018). The effects of KLF6 are likely to vary depending on the cell type, the duration and type of stimulus, and cell culture conditions.

The KLF6/PAH overlapping genes also revealed significant links with critical PAH pathways including HIF-1, PI3K/AKT and JAK/STAT signalling (Berghausen et al., 2021; Roger et al.,

2021; Lei et al., 2016; Garat et al., 2013). These pathways and their contributions to the pathogenesis of PAH will be discussed in detail later in this thesis.

Hypoxia-inducible factor 1 (HIF-1) is essential for cellular adaptation to hypoxia, and its expression is elevated in PAH lung tissues (Lei et al., 2016). Interestingly, a recent study found that KLF6 also induces HIF-1 activity in hypoxic macrophages (Kim et al., 2020c).

The PI3K/Akt signalling pathway has been implicated in several cardiovascular pathologies, including PAH (Garat et al., 2013), and the inhibition of PI3K/AKT signalling was shown to attenuate hypoxia-induced pulmonary vascular remodelling (Garat et al., 2013). Interestingly, the inhibition of PI3K/AKT signalling in proliferating T98G cells upregulates KLF6 expression, which suggests that the PI3K-AKT signalling may act upstream of KLF6 (Terragni et al., 2008).

Accumulating evidence shows that the JAK2/STAT3 signalling pathway plays a critical role in the pathogenesis of PAH (Fu et al., 2021). JAK2 phosphorylation (p-JAK) was increased in PASMCs from PAH patients (Leopold, 2021), and the level of STAT3 phosphorylation (P-STAT3) was shown to be elevated in the pulmonary endothelium, particularly in the plexiform lesions of PAH patients (Paulin, Meloche & Bonnet, 2012). The phosphorylation of JAK and STAT3 activates several transcription factors and proteins that regulate cell proliferation and apoptosis resistance and contribute to the development of PAH (Roger et al., 2021). KLF6 has also been linked to the Jak-Stat signalling pathway in the central nervous system (CNS) (Laitman et al., 2016), where functional interaction between STAT3 and KLF6 is required for axon development (Wang et al., 2018). KLF6-dependent DEGs found in plexiform lesions – such as *CLIC4*, *ACVRL1* and *MMP14* – show significant associations with angiogenesis and vascular development. Chloride intracellular channel 4 (CLIC4) is highly expressed in the endothelium of the remodelled pulmonary arteries of PAH patients, particularly in the plexiform lesions, which are histopathological hallmarks of PAH characterised by abnormal angiogenesis (Wojciak-Stothard et al., 2014). In addition to CLIC4, mutations in activin A receptor type II-like kinase-1 (*ACVRL1*), a member of the transforming growth factor-β receptor family, led to pulmonary arteriole obstruction and occlusion in PAH patients (Zhang et al., 2021). Matrix metalloproteinases (MMPs), including MMP-2, MMP-9, and MMP-14, are important in the formation of plexiform lesions (Tuder, Ponticos & Holmes, 2017; Matsui et al., 2002). Interestingly, previous studies have shown that KLF6 regulates the expression of

ACVRL1 and *MMP14* (Gallardo-Vara et al., 2016; Garrido-Martín et al., 2013). Endothelial KLF6 expression increases upon vascular injury and KLF6 subsequently translocates to the nucleus to enhance the transcriptional activity of ACVRL1 and MMP14 (Gallardo-Vara et al., 2016; Garrido-Martín et al., 2013).

Enrichment analysis of the shared KLF6 and plexiform lesions gene datasets also confirmed that KLF6 regulates cell junction assembly and actin cytoskeleton, the two key biological processes involved in angiogenesis. The overlapping genes were also enriched in the structural organization of the extracellular matrix (ECM), which is essential for regulating the basement membrane in blood vessels. The basement membrane thickness is greater in IPAH l compared with controls (Jandl et al., 2020).

The shared KLF6/plexiform lesion DEGs were also enriched in other PAH pathways, including the P53, cAMP, Hippo and oestrogen signalling pathway. These pathways and their associations with the development of PAH are discussed in more detail below.

The activation of p53 signalling suppresses cellular proliferation and may potentially ameliorate PAH, but the reduction of p53 expression and activity may exacerbate the disease (Wakasugi et al., 2019). *TP53* knockout mice developed more severe PH when exposed to chronic hypoxia compared to wild-type mice (Mizuno et al., 2011). Functional interaction between KLF6 and p53 (Rubinstein et al., 2004) has been demonstrated in human breast cancer tissues, where KLF6 expression was reduced by *TP53* mutation and negatively correlated with EGFR expression (Sun et al., 2020).

Intracellular levels of cyclic adenosine monophosphate (cAMP) play an important role in regulating endothelial barrier integrity through protein kinase A (PKA)- dependent and PKA-independent mechanisms (Birukova et al., 2010). The activation of cAMP signalling in PAECs and PASMCs inhibits their proliferation *in vitro* and reverses pulmonary vascular remodelling *in vivo* in MCT rat and SuHx mouse models of PAH (Jones et al., 2020). It has also been reported that the activation of cAMP/PKA suppresses the transcriptional activity of myocyte enhancer factor 2 (MEF2) and its downstream target KLF6 in cardiomyocytes, which suggests that cAMP/PKA signalling negatively regulates KLF6 function (Hashemi et al., 2015).

Increasing evidence also suggests that YAP, a hippo signalling pathway effector protein, is involved in the pathogenesis of PAH (Zuo et al., 2021; Kudryashova et al., 2016). The activation of YAP induces the proliferation of PASMCs, resulting in pulmonary vascular remodelling and the exacerbation of PAH (Tang et al., 2022). The activation of YAP in response to intestinal epithelial cell injury induces KLF6 expression, which inhibits metastatic colorectal cancer (Cheung et al., 2020). This suggests that the Hippo signalling pathway may positively regulate KLF6 expression and function.

Oestrogen receptor-mediated signalling has been implicated in the development of PAH (Lahm & Kawut, 2017), and oestrogen receptor alpha (Erα), which is highly expressed in female PAH PASMCs, is thought to promote the proliferation of PASMCs (Wright et al., 2015). KLF6 suppresses oestrogen receptor-mediated cell proliferation in ER-positive (ER^+) breast cancer cells by interrupting ERα-c-Src interaction, resulting in the inactivation of the c-Src-MAPK signalling cascade (Liu et al., 2010; Sarfstein, Belfiore & Werner, 2010). Future studies should explore the potential role of KLF6 in sex-dependent regulation of pulmonary vascular remodelling in PAH.

Previous studies have shown that the expression of pro-angiogenic agents such as VEGF, KDR (VEGFR2), ENG and ANGPT2 (angiopoietin-2) is upregulated in endothelial cells in plexiform lesions (Malhotra et al., 2013; Kümpers et al., 2010; Tuder et al., 2001a). In this study we observed an accumulation of $KLF6^+$ Erg^+ vWF^+ cells in plexiform lesions and around the remodelled pulmonary arteries in human PAH lung, and these cells may originate from the circulating endothelial progenitor cells. Interestingly, KLF6 expression was significantly increased in blood-derived PAH-ECFCs in comparison with healthy ECFCs and HPAECs (Chapter 5, Section 5.4.4), suggesting that KLF6 activation may contribute to their heightened angiogenic potential. Taken together, these findings suggest that KLF6 may drive pulmonary angiogenic responses in severe forms of human PAH.

7.6 Conclusion

The findings presented in this chapter highlight the potential involvement of KLF6 in key processes regulating vascular remodelling in PAH. The analysis of shared genes between KLF6 and all PAH and plexiform DEGs showed strong associations with pathways related to endothelial cell migration and angiogenesis, and this was confirmed independently by functional assays described in Chapter 4, Sections 4.4.5 and 4.4.7. Overall, the data show that KLF6 has a significant impact on the expression and function of several PAH-related genes, and that its sustained activation in some subsets of endothelial cells which are likely to be endothelial progenitors may contribute to the exaggerated repair and exuberant angiogenesis seen in advanced human PAH.

Chapter 8 : General discussion, conclusions and future work

8.1 General Discussion

8.1.1 Summary of the study rationale

PAH is a rare, chronic and progressive lung disease that is believed to be initiated by endothelial damage. This damage triggers multiple cellular signalling pathways within the endothelium, leading to exaggerated repair characterised by uncontrolled proliferation and resistance to apoptosis of the endothelial cells (ECs).

Flow-responsive Krüppel-like transcription factors expressed in vascular endothelium, are crucial for the maintenance of vascular homeostasis (Mastej et al., 2022; Kuo et al., 1997). The expression and function of KLF2 and KLF4 are dysregulated in PAH, resulting in maladaptive endothelial responses to increased shear stress and heightened vulnerability of the endothelium to proinflammatory and prothrombotic stimuli (Nicoleau, Fellows & Wojciak-Stothard, 2021; Sindi et al., 2020; Ban et al., 2019; Eichstaedt et al., 2017; Shatat et al., 2014). Recent study suggests that KLF6, another transcription factor from the KLF family, may contribute to endothelial dysfunction in PAH. A downregulation of *KLF6* expression was noted in HPAECs from the microfluidic model of PAH (Ainscough et al., 2022a), as well as PH secondary to congenital shunt and pulmonary venous hypertension in valvular heart disease (Park et al., 2008). Meanwhile, *KLF6* expression was also reduced in pulmonary arterioles obtained from patients with idiopathic pulmonary fibrosis (IPF) (Patel et al., 2013). However, the specific role of KLF6 in PAH remains unknown.

KLF6 is expressed in the vascular endothelium and regulates the expression of genes involved in vascular repair, angiogenesis and remodelling (Yang et al., 2019; Gallardo-Vara et al., 2016; Atkins & Jain, 2007; Botella et al., 2002). The downregulation of KLF6 may therefore augment endothelial damage. KLF6 acts as a tumour suppressor in several cancers – including gastric (Cho et al., 2005), prostate (Narla et al., 2001), colon (Reeves et al., 2004) and nasopharyngeal cancers (Chen et al., 2002) – so its downregulation in PAH, which bears many similarities to cancer, could potentially enhance cell proliferation and apoptosis resistance (Frump, Lai & Lahm, 2020; Boucherat et al., 2017).

In this study, I hypothesized that the dysregulation of KLF6 signalling contributes to endothelial dysfunction in pulmonary arterial hypertension.

8.1.2 Key Findings

8.1.2.1 KLF6 regulates pulmonary endothelial function

The work in this thesis investigated the function of KLF6 in HPAECs, a crucial cell type in PAH aetiology. Alterations in KLF6 expression were found to affect pulmonary endothelial angiogenesis, barrier function, migration, proliferation, apoptosis and inflammatory responses. KLF6 had a protective effect on the pulmonary endothelium, as shown by the reduced activation of pro-inflammatory transcription factor NF-κB, reduced endothelial proliferation and apoptosis and enhanced endothelial barrier function. KLF6 stimulated endothelial cell migration and angiogenesis.

The pro-angiogenic effect of KLF6 is most likely mediated by enhanced endothelial cell migration associated with increased expression of matrix metalloproteinases *MMP2* and *MMP14*, *ENG* and *ACVRL1*, the increased expression of endothelial junctional proteins *CDH5*/VE-cadherin and *PECAM1* and the elevated expression of endothelial pro-angiogenic markers *FLT1*, *KDR*, *TEK* (TIE2), *HES1*, *SOX17* and *ERG*. To support our data, elevated KLF6 expression has been linked to the angiogenic activation of pulmonary microvascular endothelial cells (PMVECs) in a rat model of hepatopulmonary syndrome (HPS) (Yang et al., 2019). In this study, the expression of KLF6 was elevated in PMVECs cultured *in vitro* with a common bile duct ligation (CBDL) rat serum (Yang et al., 2019). In the same study, KLF6 siRNA prevented PMVEC-induced endothelial tube formation *in vitro* under the stimulation of CBDL rat serum by suppressing the expression of *ACVRL1* and *ENG* (Yang et al., 2019). Interestingly, previous studies have shown that KLF6 regulates the expression of *ACVRL1* and *MMP14* (Gallardo-Vara et al., 2016; Garrido-Martín et al., 2013). Endothelial KLF6 expression increases upon vascular injury, and KLF6 translocates to the nucleus to enhance the transcriptional activity of ACVRL1 and MMP14 (Gallardo-Vara et al., 2016; Garrido-Martín et al., 2013). It has also been reported that KLF6, in conjunction with Sp2, modulates endothelial cell motility by influencing *MMP9* gene transcription in ECFCs (Das et al., 2006). Mechanistically, the disruption of the SP2/ KLF6 expression complex increases *MMP9* levels and encourages endothelial cell migration (Das et al., 2006).

Uncontrolled EC proliferation is a defining characteristic of endothelial dysfunction in PAH (Kurakula et al., 2021). KLF6 functions as a suppressor of cancer cell proliferation, acting in a cell type- and context-specific manner via the regulation of p21, the disruption of the interaction of cyclin D1 and CDK4 and the inhibition of c-Jun proto-oncoprotein (Narla et al., 2007; Benzeno et al., 2004; Slavin et al., 2004). A loss of *KLF6* promotes cell proliferation in prostate cancer and non-small cell lung cancer (Zeng et al., 2022; Narla et al., 2001). Interestingly, the overexpression of KLF6 inhibited endothelial cell proliferation in HPAECs, which is consistent with its anti-proliferative effect in cancer cells. Reductions in endothelial cells were associated with the decreased expression of proliferation markers, including *MKI67*, *PCNA* and *BRD4*.

Endothelial apoptosis in the early stages of PAH is thought to be followed by a clonal selection of apoptosis-resistant, highly proliferative cells which contribute to vascular remodelling in PAH (Sakao, Tatsumi & Voelkel, 2009; Lévy et al., 2007; Sakao et al., 2006). In this study, endothelial cell apoptosis was triggered by two distinct stimuli: by serum and growth factor deprivation or by staurosporine, a protein kinase inhibitor and a known inducer of apoptosis (Bertrand et al., 1994). The overexpression of KLF6 significantly suppressed endothelial cell apoptosis under all experimental conditions, while KLF6 knockdown had the opposite effect. Our results are consistent with previous research, and show that KLF6 knockdown in MCF-7 and HepG2 cancer cell lines treated with cisplatin increases the apoptotic cell populations (D'Astolfo et al., 2008). In the context of PAH, KLF6 activation may be beneficial during the early stages of the disease, as this period is characterised by EC injury and apoptosis. However, as PAH advances, the prolonged activation of KLF6 may result in apoptosis resistance and an increase in vascular remodelling (Evans et al., 2021).

Endothelial damage in PAH can be induced by a variety of vascular stresses, including hypoxia and inflammation (Hu et al., 2020b). Hypoxia and pro-inflammatory cytokine TNF-α are major contributing factors in the pathogenesis of PAH (Pugliese et al., 2015; Groth et al., 2014; Price et al., 2013; Pak et al., 2007). We found that *KLF6* expression was significantly increased under "double hit" conditions of combined TNF-α and hypoxia (2% O_2), while hypoxia alone had no effect, possibly because of the different degrees of endothelial stress.

Functional and transcriptomic analyses clearly demonstrated the anti-inflammatory effects of KLF6 in HPAECs. KLF6 overexpression inhibited NF-κB activation in HPAECs treated with

TNF-a, which is consistent with previously reported anti-inflammatory effects of KLF6 in liver tissues following ischemia-reperfusion (I/R) injury (Li et al., 2023b). The mechanism of these anti-inflammatory effects may involve several mediators.

HPAECs overexpressing KLF6 that were treated with TNF-α showed a significant increase in *BMPR2* and *NOTCH4* (p=5.16E-12, p=1.29E-06, respectively), which is likely to have a beneficial anti-inflammatory effect (Quillard et al., 2010) and reduce vascular remodelling in PAH (Hurst et al., 2017). In our study, the overexpression of KLF6 in TNF-α-treated HPAECs also increased the expression of the NF-κB-negative regulator *NFKBIA* (p= 4.63E-07), which is consistent with observations on glioblastoma and brain tumour-derived cells (Masilamani et al., 2017). In accord with the observed role of protecting the endothelium, KLF6 also mediated the anti-inflammatory actions of Azilsartan, an angiotensin II receptor antagonist (Wei et al., 2021), as well as Naproxen and Apremilast in HUVECs and HAECs (Wu et al., 2021; Wang et al., 2020a).

In addition to inflammation, hypoxia is a major contributor to the development of PAH (Pak et al., 2007). and the activation of PAH-relevant HIF-1 and TGF-β signalling pathways was confirmed by RNA-seq analysis in hypoxic HPAECs. In response to hypoxic stress, HIF-1α regulates glycolysis by controlling the transcription of genes that encode glycolytic enzymes (Kierans & Taylor, 2021). Increased aerobic glycolysis in the pulmonary vasculature is known to promote vascular remodelling in PAH (Xu, Janocha & Erzurum, 2021) and numerous studies have reported elevated levels of key glycolytic enzymes – including PDK1, PGK1, LDHA, and ENO1 – as a result of HIF-1α activation in PAH (Ryan & Archer, 2015). The overexpression of KLF6 in hypoxic HPAECs reduced the expression of key HIF-1 targets, including glycolytic enzymes *PDK1*, *PGK1*, *LDHA*, *ENO1*, and *BNIP3*. The inhibition of glycolysis, which provides intermediate metabolites for the pentose phosphate pathway (PPP) essential for nucleotide biosynthesis (Lunt et al., 2015), could also account for the anti-proliferative effects of KLF6. The downregulation of these key glycolytic enzymes by KLF6 is therefore likely to have a beneficial effect on vascular remodelling in PAH. Interestingly, a hypoxia-induced increase in KLF6 protein expression in trophoblast cells (Racca et al., 2016) was dependent on HIF-1α, as shown by the reduction in KLF6 levels following HIF-1α silencing (Racca et al., 2016). This suggests the existence of a regulatory feedback loop between HIF and KLF6 signalling, while KLF6 has also been shown to play an important role in controlling

inflammatory and hypoxic responses in macrophages through the regulation of HIF-1α expression (Kim et al., 2020b).

8.1.2.2 Differences and similarities between KLF6 and other members of the KLF family (KLF2 and KLF4) in the regulation of pulmonary endothelial function

KLF2, *KLF4* and *KLF6* mRNA expression was induced in HPAECs at different time points of the flow stimulation. *KLF2* and *KLF4* expression peaked at earlier time points (6 h and 4 h, respectively), while *KLF6* expression increased more slowly, reaching a maximum at 24 h. This suggests that these three transcription factors may have distinct functions during the endothelial adaptation to flow. KLF2 and KLF4 may play a role in the early stages of adaptive response to flow, while KLF6 may be more important in the later stages of flow exposure. In accordance with these results, the transcriptomic signature of human umbilical vein endothelial cells (HUVECs) subjected to flow (11.5 dynes/cm^2) for between 30 min and 48h varied, depending on the duration of flow exposure (Afshar et al., 2023).

KLF2, KLF4 and KLF6 were also differentially regulated in response to TNF-α and hypoxia. *KLF2* and *KLF6* expression was unaffected by hypoxia (2% O_2) but KLF4 expression was significantly increased. Previous studies have reported a transient increase in *KLF2* and *KLF6* expression in HUVECs and trophoblast cells respectively when exposed to hypoxia (1% O_2) for 1 hour (Racca et al., 2016; Kawanami et al., 2009). Hypoxia-induced increase in the expression of KLF4 was consistent with results from another study in which HUVECs were exposed to 3% O_2 hypoxia (Hale et al., 2014). Potential discrepancies between their data and our findings are likely to be associated with differences in the setup of the experiment, such as cell types and levels of hypoxia.

In addition to the effects of hypoxia, *KLF2* expression was reduced in response to TNF-α treatment, which is consistent with previous reports (Kumar et al., 2005). However, *KLF4* expression was relatively unaffected by TNF-α in HPAECs, which contrasts with a report showing a stimulatory effect of TNF-α on *KLF4* expression in HUVECs (Hamik et al., 2007). The discrepancy between these results could be attributed to the differences in the cell type. EC phenotypes differ between organs, suggesting heterogeneity in EC function (Becker et al., 2023; Marcu et al., 2018).

Preclinical studies show that inflammation and hypoxia alone are insufficient to induce severe PAH, and that a "double hit" condition involving both insults is much more effective in inducing vascular remodelling than either insult on its own (Pugliese et al., 2015; Ciuclan et al., 2011; Yuan & Rubin, 2005). Under "double hit" conditions that combine TNF-α and hypoxia, the expression of *KLF2* and *KLF4* was decreased, while *KLF6* expression was significantly increased in the pulmonary endothelium.

Reduction in *KLF2* and *KLF4* expression in the pulmonary endothelium was linked to the severity of PAH (Shatat et al., 2014; Chandra et al., 2011), so the downregulation of KLF2 and KLF4 under the disease conditions observed here may reflect alterations in the PAH vasculature. The activation of KLF6 under the "double hit" conditions suggests that this transcription factor might be involved in vascular repair, which is consistent with its effects in other types of cells and tissues (Li et al., 2023b; Garrido-Martín et al., 2013; Kim et al., 1998). For example, KLF6 overexpression alleviates liver damage and inflammation caused by hepatic ischemia-reperfusion (I/R) injury (Li et al., 2023b).

Recent studies show a functional redundancy between KLF2 and KLF4 in the regulation of endothelial function (Sweet et al., 2023; Mastej et al., 2022), although the effects of KLF6 on the expression of *KLF2* and *KLF4*, as well as potential functional overlap between KLF2, KLF4 and KLF6, have not yet been investigated. This study shows that KLF6 increases *KLF2* expression, while KLF2 decreases *KLF6* expression in HPAECs, suggesting the existence of mutual regulatory mechanisms between KLF2 and KLF6 in the pulmonary endothelium. Surprisingly, KLF6 knockdown had no effect on the expression of *KLF2* or *KLF4* in HPAECs that were cultured under flow conditions, possibly as a result of the extracellular signal-regulated kinase 5 (ERK5)-mediated stimulation of KLF2/4 expression (Paudel, Fusi & Schmidt, 2021; Kim et al., 2012; Clark et al., 2011; Young et al., 2009). KLF2 and KLF4 may also be regulated independently of KLF6 under flow. To obtain a more complete picture, future research should investigate the effects of KLF6 knockdown on KLF2 and KLF4 expression at different time points of flow stimulation as well as the effects of KLF2 and KLF4 knockdown on KLF6 expression under flow conditions.

This study is first to identify differences and similarities between KLF2-, KLF4- and KLF6-regulated transcriptional responses in the vascular endothelium. Consistent with the known and observed anti-proliferative effects of KLF2, KLF4 and KLF6, DEGs shared between these

transcription factors were mostly associated with the inhibition of the cell cycle, DNA replication and DNA metabolic processes.

DEGs that are specific to KLF2 and KLF4 were predominantly involved in the regulation of vascular development and homeostasis, while DEGs that are unique to KLF6 were mainly associated with the regulation of endothelial repair and angiogenesis. KLF2 has been shown to inhibit angiogenesis in HUVECs by reducing the expression of *VEGF2* and *HIF1A* (Kawanami et al., 2009; Bhattacharya et al., 2005). Consistent with this finding, our results revealed a significant reduction in the expression of *KDR* (VEGFR2) and *HIF1A* in KLF2 overexpressing HPAECs.

KLF4 was shown to suppress endothelial angiogenesis in HUVECs (Zheng et al., 2013) and promote angiogenesis in human retinal microvascular endothelial cells (HRMECs) (Wang et al., 2015), which suggests that the role of KLF4 may vary according to cell type. Meanwhile, the pro-angiogenic effects of KLF4 have been linked to the activation of the Notch and VEGF signalling pathways (Wang et al., 2015; Hale et al., 2014). Interestingly, KLF4 overexpression in HPAECs increased the expression of *NOTCH3* in this study, but reduced expression of *NOTCH4*, indicating that KLF4 modulates the expression of Notch receptors in the pulmonary endothelium differently, which is consistent with the observations in HUVECs (Hale et al., 2014).

KLF6 overexpressing HPAECs increased the expression of genes that regulate endothelial repair and angiogenesis, including *KDR* (VEGFR2), *SOX17* and *ERG*, which is consistent with the observed functional effects of KLF6 overexpression in HPAECs (Chapter 4, Section 4.4.5). Taken together, these findings suggest that KLF2 and KLF4 are crucial for maintaining endothelial homeostasis, while KLF6, which is induced in response to the loss of endothelial homeostasis, orchestrates endothelial repair.

8.1.2.3 The role of KLF6 in pulmonary arterial hypertension (PAH)

KLF6 expression was increased during the early response to vascular stress induced by hypoxia and MCT in preclinical PAH. This is consistent with the established role of KLF6 as an early injury response factor (Gallardo-Vara et al., 2016; Garrido-Martín et al., 2013) as well as our observations described in chapter 3, Section 3.4.3. After an early increase, the mRNA levels of *KLF6* returned to control levels in the lungs of chronically hypoxic mice. *KLF6* expression

decreased even more dramatically in Sugen/hypoxia and MCT rats, possibly because endothelial damage in these two models was more severe compared with the hypoxia model (Chen et al., 2017b; Tada et al., 2008). Overall, the preclinical animal models of PAH showed an upregulation of *KLF6* expression in the early stages of the disease, which suggests that KLF6 may be involved in vascular repair. However, the downregulation of *KLF6* expression observed in the end stage of the disease may increase endothelial damage and potentially exacerbate vascular remodelling.

KLF6 expression was also significantly higher in ECFCs from PAH patients, compared with age- and sex-matched healthy controls. Consistent with our findings, increased *KLF6* expression was observed in PAH ECFCs in an organ-on-a-chip model of PAH (Ainscough et al., 2022b), and ECFCs are often used as endothelial surrogates in PAH and other cardiovascular diseases (Zhang, Cannavicci & Kutryk, 2022). Increasing evidence shows that the number of ECFCs increases in the end stages of PAH, suggesting a potential correlation between the number of these cells and the severity of the disease (Smits et al., 2018; Schiavon et al., 2012; Asosingh et al., 2008). However, the involvement of ECFCs in the pathogenesis of PAH is still open to debate. ECFCs can promote endothelial repair and help prevent endothelial dysfunction in PAH (Asosingh, Rose & Erzurum, 2015), but the increased pro-angiogenic potential of PAH ECFCs may also contribute to the formation of angio-obliterative vascular lesions and vascular remodelling (Banno & Yoder, 2018; Paschalaki & Randi, 2018; Duong et al., 2011). High *KLF6* expression levels in PAH ECFCs are consistent with the well-established pro-angiogenic characteristics of these cells. Future studies should be undertaken to establish the precise role of KLF6 in PAH development.

KLF6 increased the expression of genes associated with endothelial identity, repair and angiogenesis, such as *BMPR2*, *SOX17*, *KDR*, *ENG*, *CAV1*, *ACVRL1*, *SMAD1*, *CDH5*, and *PECAM1*. Interestingly, the expression and function of these genes is dysregulated in PAH (Wang et al., 2021a; Eyries et al., 2020; Nikitopoulou et al., 2016; Szulcek et al., 2016a; Han et al., 2013; Austin et al., 2012; Chaouat et al., 2004; Harrison et al., 2003; Atkinson et al., 2002). Loss of function mutations in *BMPR2* cause familial PAH, while BMPR2 expression is decreased in PAH pulmonary artery endothelial cells (Atkinson et al., 2002). Deficiencies in *BMPR2* enhance endothelial apoptosis and increase the release of proinflammatory cytokines and vasoconstrictors (Andruska & Spiekerkoetter, 2018). Our data suggest that KLF6 overexpression could potentially compensate for the loss of *BMPR2* in HPAECs. In addition

to its effects on *BMPR2* expression, KLF6 also significantly increased the expression of endothelial identity marker *SOX17* in HPAECs, which is consistent with effects reported in mouse embryonic stem cells (Zhao et al., 2010).

The transcriptional profiling of KLF6-overexpressing HPAECs revealed its involvement in critical PAH-linked signalling pathways such as FOXO, p53, TNF, NF-B, PI3K-Akt and Ras signalling pathways (Vigl et al., 2021; Wang et al., 2019b; Deng et al., 2017; Hurst et al., 2017; Garat et al., 2013; Price et al., 2013). Consistently, KLF6 DEGs also showed significant associations with PAH, IPAH and several other cardiovascular and lung disorders.

Having demonstrated that KLF6 upregulates the expression of PAH genes that regulate endothelial identity and survival, we then investigated the role of KLF6 in pulmonary vascular remodelling in PAH, particularly in plexiform lesions. These lesions, which represent a hallmark of severe PAH, are complex vascular structures that develop from remodelled pulmonary arteries (Jonigk et al., 2011; Abe et al., 2010), and there are significant associations between KLF6-dependent genes and DEGs in plexiform lesions. KLF6 affects key molecular pathways and biological processes that drive angiogenesis, including cell junction assembly, actin cytoskeleton and the structural organization of the extracellular matrix (ECM). KLF6 also influences several pathways related to PAH, including P53, cAMP and Hippo, as well as oestrogen signalling pathways (Jones et al., 2020; Wang et al., 2019b; Sassi et al., 2018; Kudryashova et al., 2016; Wright et al., 2015).

In severe PAH, the appearance of plexiform lesions indicates dysregulated angiogenesis in the advanced stage of the disease (Tuder et al., 2001b). Interestingly, the nuclear localization of KLF6 in the PAH endothelium was increased within PAH plexiform lesions. This suggests that certain subsets of endothelial cells that show a sustained activation of KLF6 may contribute to the exaggerated repair and exuberant angiogenesis that is seen in advanced human PAH.

The elevated expression of angiogenic marker VEGF has also been observed in plexiform lesions (Zhou et al., 2022; Voelkel & Gomez-Arroyo, 2014; Hirose et al., 2000b), and this increase in VEGF expression has been linked to the proliferation of PAECs and pulmonary vascular remodelling (Voelkel & Gomez-Arroyo, 2014). However, the exact cause-and-effect relationship between VEGF and pulmonary vascular remodelling remains unclear. VEGF plays a critical role in physiological angiogenesis from early embryonic development to adulthood,

but also in abnormal angiogenesis, as observed in cancer (Yang & Cao, 2022; Shibuya, 2011). Increasing evidence suggests that elevated VEGF levels in PAECs during the early stages of PAH may act as a protective response. However, as the disease progress, the persistent activation of VEGF may stimulate proliferation, migration and angiogenesis in PAECs, resulting in the formation of plexiform lesions (Kurakula et al., 2021; Budhiraja, Tuder & Hassoun, 2004).

Like VEGF, the impact of KLF6 activation may therefore vary depending on the stage of the disease. The activation of endothelial repair mechanisms and the prevention of apoptosis may be required to mitigate the effects of endothelial damage in the early stages of the disease, while the lack of inhibitory feedback mechanisms may result in exaggerated repair and accelerated vascular remodelling. Interestingly, elevated levels of KLF6 have been observed in PMVECs during advanced pulmonary angiogenesis and injury, and contribute to exacerbated lung dysfunction in hepatopulmonary syndrome (HPS) patients (Yang et al., 2019). KLF6 may therefore be regarded as an important regulator of both physiological and pathological angiogenesis in the pulmonary endothelium.

There is currently no selective pharmacological inhibitor or activator of endothelial KLF6 that can be used to investigate the functional significance of activity changes in KLF6 during PAH. However, in the context of cancer, KLF6 has been identified as a tumour suppressor in a variety of human cancers, including oral cancer, gastric cancer and lung cancer (Hsu et al., 2017; Sangodkar et al., 2009; Ito et al., 2004). The transcriptional activation of KLF6 has also been linked to elevated acetylation of histone H3 (Chen et al., 2011), although the acetylation of KLF6 and its ability to regulate gene expression are diminished by a single lysine-to-arginine point mutation (K209R) (Li et al., 2005a). Histone deacetylase 1 (HDAC1) inhibits KLF6 in clear cell renal cell carcinomas (ccRCC) (Jiang et al., 2020). Interestingly, treatment with trichostatin A (TSA), a histone deacetylase inhibitor (HDACI), enhances the acetylation of histone H3, which subsequently leads to the increased nuclear localization and transcriptional activity of KLF6 (Camolotto et al., 2013).

As well as epigenetic small molecule TSA treatment, microRNAs (MiRNAs) can modulate KLF6 expression in cells. For example, miR-191-5p has been found to induce epithelial-mesenchymal transition (EMT) in breast cancer by suppressing KLF6 (Pan et al., 2023). Like miR-191-5p, miR-200c-3p and miRNA-543 have been linked to the progression of gastric cell

carcinomas by inhibiting the expression of KLF6 (Wang et al., 2021b, 2020b). This suggests that these microRNAs act as effective regulators of KLF6 expression in late-stage PAH.

In addition to microRNAs, the long non-coding RNA lncRNA CR749391 was shown to interact with miR 181a to upregulate KLF6 expression in gastric cancer (Shi et al., 2020), suggesting that lncRNA-based therapy could be a promising approach to upregulating KLF6 expression in PAH.

Overall, there is still much work to be done to determine the precise role of KLF6 in PAH and to understand how it can be targeted *in vivo*. Ultimately, it is critical to investigate the mechanisms by which KLF6 influences gene expression in PAECs further during different stages of PAH. This could be accomplished using animal models with an inducible endothelial-specific deletion of KLF6 to focus on the effect of *KLF6* knockout at different stages of the disease.

8.2 Conclusion

In summary, this study was the first to demonstrate the dysregulation of KLF6 signalling in PAH. KLF6 triggers endothelial repair in response to stress conditions induced by hypoxia and inflammation. Its role in PAH will require further study, but it is likely that KLF6 de-activation following an early elevation in its activity may increase endothelial susceptibility to damage and dysregulate endothelial angiogenesis. The increased expression of KLF6 in PAH ECFCs and the accumulation of $KLF6^{+}$ Erg^{+} vWF^{+} cells in plexiform lesions suggest that it has a potential role in driving angiogenic responses in human PAH.

8.3 Study limitations

Endothelial cells are difficult to transfect, so adenoviral transduction was chosen as a way of manipulating the expression of KLF2, 4 and 6. However, this method has certain limitations. The overexpression of KLF6 by adenoviral infection is likely to exceed the physiological expression level of KLF6. However, as none of the 3 anti-KLF6 antibodies tested were suitable for western blot analysis, a semi-quantitative analysis of immunofluorescently-labelled KLF6 overexpressing cells was carried out, and the analysis of fluorescence intensity showed an approximately 5-fold physiological increase in KLF6 protein expression in HPAECs.

Adenoviral infection typically elicits a small degree of NF-κB activation under basal conditions, which may have an impact on the overall level of NF-κB activation in cells stimulated with TNF-α and hypoxia. It is therefore important to use an alternative method to validate these results. Here, the results were validated by RNA-seq analysis and qPCR.

In the spatial transcriptomics analysis, the chosen regions of interest (ROIs) comprised entire blood vessels incorporating endothelial cells and smooth muscle cells that were immunolabeled with specific antibodies (vWF was used to stain ECs and α-SMA was used to stain SMCs). In future, it would be useful to repeat the spatial transcriptomics using cell segmentation to identify unique transcriptomes of endothelial cells and smooth muscle cells in PAH. This could be achieved by creating masks for various stains within each ROI.

Using mice instead of rats in the chronic hypoxia induced PAH may also be a limitation, as mice exposed to hypoxia show a less severe PAH phenotype than rats (Wu et al., 2022). Meanwhile, KLF6 expression in the hypoxia/SU5416-induced PAH was only assessed on day 56. In future, it would be interesting to investigate the KLF6 expression at earlier time points in this model.

In this study, hypoxia was induced using 2% O_2. However, this level of oxygen may not accurately reflect actual physiological conditions, as the pulmonary artery receives deoxygenated blood at oxygen levels that range from 1-5% *in vivo* (Gutierrez et al., 2007). Future studies should include a wider range of oxygen concentrations, ranging from anoxia to 2% O_2, to represent oxygen levels in PAH lungs more accurately. In our study, the level of oxygen concentration acknowledged as normoxia was 21% O_2, while 2% O_2 was accepted as hypoxia. This assumption was established with the expectation that the HPAECs used in the experiments were sufficiently adapted to normoxic conditions following an extended period of culture, and that their transition to 2% O_2 would represent the processes that occur under hypoxic conditions *in vivo*. This is a constraint on the entire field of hypoxia research, as normoxic atmospheric conditions are commonly used as experimental controls regardless of the oxygen tensions encountered by cells *in vivo*.

8.4 Future work

Future studies should evaluate the role of endothelial KLF6 signalling in pathological alterations in PAH vasculature more fully, using the inducible endothelial-specific deletion of KLF6 animal models, and *KLF6* knockout should be induced at different time points of the disease. Although this study primarily focused on examining endothelial responses, it is equally important to understand how pulmonary artery smooth muscle cells (PASMCs) respond to the manipulation of KLF6 expression.

Loss of function mutations in *BMPR2* and *SOX17* cause familial PAH (Wang et al., 2021a; Lane et al., 2000), while their expression is decreased in PAH pulmonary artery endothelial cells (Yi et al., 2023; Atkinson et al., 2002). Meanwhile, KLF6 overexpression increases the expression of *BMPR2* and *SOX17*, suggesting that the activation of KLF6 may have a beneficial and compensatory effect. Future studies are needed to confirm the effect of the knockdown of BMPR2 and SOX17 on KLF6 expression.

Because of functional overlap and mutual regulation between the members of the KLF family (Eaton et al., 2008), it is crucial to fully understand the specific roles of different KLFs. This study only investigated the effect of KLF2 and KLF4 overexpression on KLF6. It would be valuable to examine the effect of KLF2 and KLF4 knockdown on KLF6. In addition to KLF2, KLF4 and KLF6, further investigation is needed to determine whether other members of the KLF family are implicated in endothelial dysfunction in PAH.

Altered shear stress in the pulmonary vasculature has been shown to be associated with PAH (Schäfer et al., 2016; Truong et al., 2013), and the reduction of wall shear stress in the proximal pulmonary arteries of PAH patients is believed to contribute to endothelial cell dysfunction and PAH development (Tang et al., 2012). This study only evaluated the effect of physiological shear stress on KLF6 expression, and it would be interesting to explore the effect of pathological shear stress (very low to high) as well as different flow patterns such as laminar, pulsatile and disturbed flow on KLF6 expression. It would also be beneficial to investigate the effects of shear stress on KLF6 expression in human microvascular endothelial cells (HMVECs), as PAH MVEC showed a delayed morphological adaptation to shear stress and cell injury in areas of nonuniform shear profiles. These are critical sites for vascular remodelling in PAH, although PAH PAEC from the same PAH lungs displayed no abnormalities (Szulcek et al., 2016b).

The increased permeability of endothelial cells is a key characteristic feature of PAH (Zhou et al., 2016). Because of time constraints, we were unable to examine the effect of KLF6 knockdown on endothelial permeability. It would be valuable to investigate the effect of KLF6 knockdown on endothelial barrier function using an organ-on-a-chip model containing 0.4 μm PET membrane to directly assess the influence of KLF6 knockdown on endothelial permeability under flow conditions. It would also be interesting to use an organ-on-a-chip model of the pulmonary artery with a PET membrane containing 8.0 μm pores and mimicking arterial basement membrane to observe the effect of KLF6 knockdown on endothelial cell migration in response to pro-angiogenic stimuli relevant to PAH, such as VEGF.

Oestrogen receptor-mediated signalling has also been linked to PAH pathogenesis (Lahm & Kawut, 2017; Austin et al., 2009a). Elevated levels of oestrogen receptor alpha (Erα) have been observed in female PAH PASMCs, which correlated with enhanced PASMC proliferation (Wright et al., 2015). KLF6 inhibits oestrogen receptor-mediated cell proliferation in ER-positive (ER^+) breast cancer cells by interrupting the interaction between Erα and c-Src, resulting in the inactivation of the c-Src-MAPK signalling pathway (Liu et al., 2010). Future studies should investigate the potential involvement of KLF6 in the sex-dependent regulation of pulmonary vascular remodelling in PAH.

Current approved therapies for PAH are not effective for all patients, and do not reverse the disease. Personalised medicine is an approach that tailors medical therapy to the specific characteristics of each patient, and this can be achieved by the integration of -omics studies to present a more comprehensive picture of a specific patient's condition. Improving our understanding of the molecular and genetic causes of the disease will therefore enable the development of more accurately tailored therapies. Connectivity map (CMap) is an online genetic signature database that uses cellular responses to perturbation to identify connections between compounds, diseases and genes (Lamb et al., 2006), and it would be interesting to utilise CMap to identify new compounds that may be linked to KLF6 dysfunction in HPAECs.

References

Abe, K., Toba, M., Alzoubi, A., Ito, M., Fagan, K.A., Cool, C.D., Voelkel, N.F., McMurtry, I.F. & Oka, M. (2010) Formation of Plexiform Lesions in Experimental Severe Pulmonary Arterial Hypertension. *Circulation*. 121 (25), 2747–2754. doi:10.1161/CIRCULATIONAHA.109.927681.

Abid, S., Marcos, E., Parpaleix, A., Amsellem, V., Breau, M., Houssaini, A., Vienney, N., Lefevre, M., Derumeaux, G., Evans, S., Hubeau, C., Delcroix, M., Quarck, R., Adnot, S. & Lipskaia, L. (2019) CCR2/CCR5-mediated macrophage–smooth muscle cell crosstalk in pulmonary hypertension. *European Respiratory Journal*. 54 (4). doi:10.1183/13993003.02308-2018.

Abman, S.H., Mullen, M.P., Sleeper, L.A., Austin, E.D., Rosenzweig, E.B., Kinsella, J.P., Ivy, D., Hopper, R.K., Raj, J.U., Fineman, J., Keller, R.L., Bates, A., Krishnan, U.S., Avitabile, C.M., Davidson, A., Natter, M.D. & Mandl, K.D. (2022) Characterisation of paediatric pulmonary hypertensive vascular disease from the PPHNet Registry. *The European respiratory journal*. 59 (1), 2003337. doi:10.1183/13993003.03337-2020.

Adams, T.S., Schupp, J.C., Poli, S., Ayaub, E.A., Neumark, N., Ahangari, F., Chu, S.G., Raby, B.A., DeIuliis, G., Januszyk, M., Duan, Q., Arnett, H.A., Siddiqui, A., Washko, G.R., Homer, R., Yan, X., Rosas, I.O. & Kaminski, N. (2020) Single-cell RNA-seq reveals ectopic and aberrant lung-resident cell populations in idiopathic pulmonary fibrosis. *Science Advances*. 6 (28), eaba1983. doi:10.1126/sciadv.aba1983.

Afshar, Y., Ma, F., Quach, A., Jeong, A., Sunshine, H.L., Freitas, V., Jami-Alahmadi, Y., Helaers, R., Li, X., Pellegrini, M., Wohlschlegel, J.A., Romanoski, C.E., Vikkula, M. & Iruela-Arispe, M.L. (2023) Transcriptional drifts associated with environmental changes in endothelial cells I.S. Daehn, A. Akhmanova, M. Civelek, & Z. Bouman Chen (eds.). *eLife*. 12, e81370. doi:10.7554/eLife.81370.

Aghajanian, A., Wittchen, E.S., Allingham, M.J., Garrett, T.A. & Burridge, K. (2008) Endothelial cell junctions and the regulation of vascular permeability and leukocyte transmigration. *Journal of thrombosis and haemostasis : JTH*. 6 (9), 1453–1460. doi:10.1111/j.1538-7836.2008.03087.x.

Ainscough, A.J., Smith, T.J., Haensel, M., Rhodes, C.J., Fellows, A., Whitwell, H.J., Vasilaki, E., Gray, K., Freeman, A., Howard, L.S., Wharton, J., Dunmore, B., Upton, P.D., Wilkins, M.R., Edel, J.B. & Wojciak-Stothard, B. (2022) An organ-on-chip model of pulmonary arterial hypertension identifies a BMPR2-SOX17-prostacyclin signalling axis. *Communications Biology*. 5 (1), 1–15. doi:10.1038/s42003-022-04169-z.

Ajalik, R.E., Alenchery, R.G., Cognetti, J.S., Zhang, V.Z., McGrath, J.L., Miller, B.L. & Awad, H.A. (2022) Human Organ-on-a-Chip Microphysiological Systems to Model Musculoskeletal Pathologies and Accelerate Therapeutic Discovery. *Frontiers in*

Bioengineering and Biotechnology. 10. https://www.frontiersin.org/articles/10.3389/fbioe.2022.846230.

Akimoto, S., Mitsumata, M., Sasaguri, T. & Yoshida, Y. (2000) Laminar shear stress inhibits vascular endothelial cell proliferation by inducing cyclin-dependent kinase inhibitor p21(Sdi1/Cip1/Waf1). *Circulation Research*. 86 (2), 185–190. doi:10.1161/01.res.86.2.185.

Al-Hilal, T.A., Keshavarz, A., Kadry, H., Lahooti, B., Al-Obaida, A., Ding, Z., Li, W., Kamm, R., McMurtry, I.F., Lahm, T., Nozik-Grayck, E., Stenmark, K.R. & Ahsan, F. (2020) Pulmonary-arterial-hypertension (PAH)-on-a-chip: fabrication, validation and application. *Lab on a Chip*. 20 (18), 3334–3345. doi:10.1039/D0LC00605J.

Alaiti, M.A., Orasanu, G., Tugal, D., Lu, Y. & Jain, M.K. (2012) Kruppel-Like Factors and Vascular Inflammation: Implications for Atherosclerosis. *Current atherosclerosis reports*. 14 (5), 438–449. doi:10.1007/s11883-012-0268-6.

Aldecoa, C., Llau, J.V., Nuvials, X. & Artigas, A. (2020) Role of albumin in the preservation of endothelial glycocalyx integrity and the microcirculation: a review. *Annals of Intensive Care*. 10 (1), 85. doi:10.1186/s13613-020-00697-1.

Alzaydi, M.M., Abdul-Salam, V.B., Whitwell, H.J., Russomanno, G., Glynos, A., Capece, D., Szabadkai, G., Wilkins, M.R. & Wojciak-Stothard, B. (2023) Intracellular Chloride Channels Regulate Endothelial Metabolic Reprogramming in Pulmonary Arterial Hypertension. *American Journal of Respiratory Cell and Molecular Biology*. 68 (1), 103–115. doi:10.1165/rcmb.2022-0111OC.

Ambade, A.S., Hassoun, P.M. & Damico, R.L. (2021) Basement Membrane Extracellular Matrix Proteins in Pulmonary Vascular and Right Ventricular Remodeling in Pulmonary Hypertension. *American Journal of Respiratory Cell and Molecular Biology*. 65 (3), 245–258. doi:10.1165/rcmb.2021-0091TR.

Ando, J. & Yamamoto, K. (2009) Vascular mechanobiology: endothelial cell responses to fluid shear stress. *Circulation Journal: Official Journal of the Japanese Circulation Society*. 73 (11), 1983–1992. doi:10.1253/circj.cj-09-0583.

Andreoli, V., Gehrau, R.C. & Bocco, J.L. (2010) Biology of Krüppel-like factor 6 transcriptional regulator in cell life and death. *IUBMB Life*. 62 (12), 896–905. doi:10.1002/iub.396.

Andruska, A. & Spiekerkoetter, E. (2018) Consequences of BMPR2 Deficiency in the Pulmonary Vasculature and Beyond: Contributions to Pulmonary Arterial Hypertension. *International Journal of Molecular Sciences*. 19 (9), 2499. doi:10.3390/ijms19092499.

Asosingh, K., Aldred, M.A., Vasanji, A., Drazba, J., Sharp, J., Farver, C., Comhair, S.A.A., Xu, W., Licina, L., Huang, L., Anand-Apte, B., Yoder, M.C., Tuder, R.M. & Erzurum, S.C. (2008) Circulating angiogenic precursors in idiopathic pulmonary

arterial hypertension. *The American Journal of Pathology*. 172 (3), 615–627. doi:10.2353/ajpath.2008.070705.

Asosingh, K., Rose, J. & Erzurum, S. (2015) *Endothelial Colony-Forming Cells in Pulmonary Arterial Hypertension*. In: pp. 183–192. doi:10.1007/978-3-319-16232-4_9.

Atkins, G.B. & Jain, M.K. (2007) Role of Krüppel-like transcription factors in endothelial biology. *Circulation Research*. 100 (12), 1686–1695. doi:10.1161/01.RES.0000267856.00713.0a.

Atkins, G.B., Wang, Y., Mahabeleshwar, G.H., Shi, H., Gao, H., Kawanami, D., Natesan, V., Lin, Z., Simon, D.I. & Jain, M.K. (2008) Hemizygous Deficiency of Kruppel-like Factor 2 Augments Experimental Atherosclerosis. *Circulation research*. 103 (7), 690–693. doi:10.1161/CIRCRESAHA.108.184663.

Atkinson, C., Stewart, S., Upton, P.D., Machado, R., Thomson, J.R., Trembath, R.C. & Morrell, N.W. (2002) Primary pulmonary hypertension is associated with reduced pulmonary vascular expression of type II bone morphogenetic protein receptor. *Circulation*. 105 (14), 1672–1678. doi:10.1161/01.cir.0000012754.72951.3d.

Austin, E.D., Cogan, J.D., West, J.D., Hedges, L.K., Hamid, R., Dawson, E.P., Wheeler, L.A., Parl, F.F., Loyd, J.E. & Phillips, J.A. (2009a) Alterations in oestrogen metabolism: implications for higher penetrance of familial pulmonary arterial hypertension in females. *The European respiratory journal*. 34 (5), 1093–1099. doi:10.1183/09031936.00010409.

Austin, E.D., Ma, L., LeDuc, C., Berman Rosenzweig, E., Borczuk, A., Phillips, J.A., Palomero, T., Sumazin, P., Kim, H.R., Talati, M.H., West, J., Loyd, J.E. & Chung, W.K. (2012) Whole exome sequencing to identify a novel gene (caveolin-1) associated with human pulmonary arterial hypertension. *Circulation. Cardiovascular Genetics*. 5 (3), 336–343. doi:10.1161/CIRCGENETICS.111.961888.

Austin, E.D., Phillips, J.A., Cogan, J.D., Hamid, R., Yu, C., Stanton, K.C., Phillips, C.A., Wheeler, L.A., Robbins, I.M., Newman, J.H. & Loyd, J.E. (2009b) Truncating and missense BMPR2 mutations differentially affect the severity of heritable pulmonary arterial hypertension. *Respiratory Research*. 10 (1), 87. doi:10.1186/1465-9921-10-87.

Avci-Adali, M., Ziemer, G. & Wendel, H.P. (2010) Induction of EPC homing on biofunctionalized vascular grafts for rapid in vivo self-endothelialization — A review of current strategies. *Biotechnology Advances*. 28 (1), 119–129. doi:10.1016/j.biotechadv.2009.10.005.

Baeyens, N., Bandyopadhyay, C., Coon, B.G., Yun, S. & Schwartz, M.A. (2016) Endothelial fluid shear stress sensing in vascular health and disease. *The Journal of Clinical Investigation*. 126 (3), 821–828. doi:10.1172/JCI83083.

Ball, M.K., Waypa, G.B., Mungai, P.T., Nielsen, J.M., Czech, L., Dudley, V.J., Beussink, L., Dettman, R.W., Berkelhamer, S.K., Steinhorn, R.H., Shah, S.J. & Schumacker, P.T. (2014) Regulation of Hypoxia-induced Pulmonary Hypertension by Vascular Smooth Muscle Hypoxia-Inducible Factor-1α. *American Journal of Respiratory and Critical Care Medicine*. 189 (3), 314–324. doi:10.1164/rccm.201302-0302OC.

Ban, Y., Liu, Y., Li, Y., Zhang, Y., Xiao, L., Gu, Y., Chen, S., Zhao, B., Chen, C. & Wang, N. (2019) S-nitrosation impairs KLF4 activity and instigates endothelial dysfunction in pulmonary arterial hypertension. *Redox Biology*. 21, 101099. doi:10.1016/j.redox.2019.101099.

Bannerman, D.D. & Goldblum, S.E. (2003) Mechanisms of bacterial lipopolysaccharide-induced endothelial apoptosis. *American Journal of Physiology. Lung Cellular and Molecular Physiology*. 284 (6), L899-914. doi:10.1152/ajplung.00338.2002.

Banno, K. & Yoder, M.C. (2018) Tissue regeneration using endothelial colony-forming cells: promising cells for vascular repair. *Pediatric Research*. 83 (1–2), 283–290. doi:10.1038/pr.2017.231.

Barker, A.J., Roldán-Alzate, A., Entezari, P., Shah, S.J., Chesler, N.C., Wieben, O., Markl, M. & François, C.J. (2015) Four-dimensional flow assessment of pulmonary artery flow and wall shear stress in adult pulmonary arterial hypertension: Results from two institutions. *Magnetic Resonance in Medicine*. 73 (5), 1904–1913. doi:10.1002/mrm.25326.

Barst, R.J., Rubin, L.J., Long, W.A., McGoon, M.D., Rich, S., et al. (1996) A comparison of continuous intravenous epoprostenol (prostacyclin) with conventional therapy for primary pulmonary hypertension. *The New England Journal of Medicine*. 334 (5), 296–301. doi:10.1056/NEJM199602013340504.

Bazan, I.S., Kim, S.-J., Ardito, T.A., Zhang, Y., Shan, P., Sauler, M. & Lee, P.J. (2022) Sex differences and altered mitophagy in experimental pulmonary hypertension. *American Journal of Physiology - Lung Cellular and Molecular Physiology*. 322 (5), L761–L769. doi:10.1152/ajplung.00019.2020.

Becker, L.M., Chen, S.-H., Rodor, J., de Rooij, L.P.M.H., Baker, A.H. & Carmeliet, P. (2023) Deciphering endothelial heterogeneity in health and disease at single-cell resolution: progress and perspectives. *Cardiovascular Research*. 119 (1), 6–27. doi:10.1093/cvr/cvac018.

Bell, R.D., White, R.J., Garcia-Hernandez, M.L., Wu, E., Rahimi, H., Marangoni, R.G., Slattery, P., Duemmel, S., Nuzzo, M., Huertas, N., Yee, M., O'Reilly, M.A., Morrell, C., Ritchlin, C.T., Schwarz, E.M. & Korman, B.D. (2020) TNF Induces Obliterative Pulmonary Vascular Disease in a Novel Model of Connective Tissue Disease Associated Pulmonary Arterial Hypertension (CTD-PAH). *Arthritis & rheumatology (Hoboken, N.J.)*. 72 (10), 1759–1770. doi:10.1002/art.41309.

Benincasa, G., Maron, B.A., Affinito, O., D'Alto, M., Franzese, M., Argiento, P., Schiano, C., Romeo, E., Bontempo, P., Golino, P., Berrino, L., Loscalzo, J. & Napoli, C.

(2023) Association Between Circulating CD4+ T Cell Methylation Signatures of Network-Oriented SOCS3 Gene and Hemodynamics in Patients Suffering Pulmonary Arterial Hypertension. *Journal of Cardiovascular Translational Research*. 16 (1), 17–30. doi:10.1007/s12265-022-10294-1.

Benzeno, S., Narla, G., Allina, J., Cheng, G.Z., Reeves, H.L., Banck, M.S., Odin, J.A., Diehl, J.A., Germain, D. & Friedman, S.L. (2004) Cyclin-dependent kinase inhibition by the KLF6 tumor suppressor protein through interaction with cyclin D1. *Cancer Research*. 64 (11), 3885–3891. doi:10.1158/0008-5472.CAN-03-2818.

Beppu, H., Ichinose, F., Kawai, N., Jones, R.C., Yu, P.B., Zapol, W.M., Miyazono, K., Li, E. & Bloch, K.D. (2004) BMPR-II heterozygous mice have mild pulmonary hypertension and an impaired pulmonary vascular remodeling response to prolonged hypoxia. *American Journal of Physiology. Lung Cellular and Molecular Physiology*. 287 (6), L1241-1247. doi:10.1152/ajplung.00239.2004.

Berghausen, E.M., Janssen, W., Vantler, M., Gnatzy-Feik, L.L., Krause, M., et al. (2021) Disrupted PI3K subunit p110α signaling protects against pulmonary hypertension and reverses established disease in rodents. *The Journal of Clinical Investigation*. 131 (19), e136939. doi:10.1172/JCI136939.

Bertrand, R., Solary, E., O'Connor, P., Kohn, K.W. & Pommier, Y. (1994) Induction of a common pathway of apoptosis by staurosporine. *Experimental Cell Research*. 211 (2), 314–321. doi:10.1006/excr.1994.1093.

Besnier, M., Finemore, M., Yu, C., Kott, K.A., Vernon, S.T., Seebacher, N.A., Genetzakis, E., Furman, A., Tang, O., Davis, R.L., Hansen, T., Psaltis, P.J., Bubb, K.J., Wise, S.G., Grieve, S.M., Di Bartolo, B.A. & Figtree, G.A. (2021) Patient Endothelial Colony-Forming Cells to Model Coronary Artery Disease Susceptibility and Unravel the Role of Dysregulated Mitochondrial Redox Signalling. *Antioxidants*. 10 (10), 1547. doi:10.3390/antiox10101547.

Best, D.H., Sumner, K.L., Smith, B.P., Damjanovich-Colmenares, K., Nakayama, I., Brown, L.M., Ha, Y., Paul, E., Morris, A., Jama, M.A., Dodson, M.W., Bayrak-Toydemir, P. & Elliott, C.G. (2017) EIF2AK4 Mutations in Patients Diagnosed With Pulmonary Arterial Hypertension. *Chest*. 151 (4), 821–828. doi:10.1016/j.chest.2016.11.014.

Bhargava, A., Kumar, A., Yuan, N., Gewitz, M.H. & Mathew, R. (1999) Monocrotaline induces interleukin-6 mRNA expression in rat lungs. *Heart Disease (Hagerstown, Md.)*. 1 (3), 126–132.

Bhattacharya, R., Senbanerjee, S., Lin, Z., Mir, S., Hamik, A., Wang, P., Mukherjee, P., Mukhopadhyay, D. & Jain, M.K. (2005) Inhibition of vascular permeability factor/vascular endothelial growth factor-mediated angiogenesis by the Kruppel-like factor KLF2. *The Journal of Biological Chemistry*. 280 (32), 28848–28851. doi:10.1074/jbc.C500200200.

Birukova, A.A., Burdette, D., Moldobaeva, N., Xing, J., Fu, P. & Birukov, K.G. (2010) RacGTPase is a hub for protein kinase A and Epac signaling in endothelial barrier

protection by cAMP. *Microvascular research*. 79 (2), 128–138. doi:10.1016/j.mvr.2009.11.007.

Blighe, K., Rana, S. & Lewis, M. (2019) EnhancedVolcano: Publication-ready volcano plots with enhanced colouring and labeling. *R package version. 1.4.0.* https://github.com/kevinblighe/EnhancedVolcano.

Bohnen, M.S., Ma, L., Zhu, N., Qi, H., McClenaghan, C., et al. (2018) Loss-of-Function ABCC8 Mutations in Pulmonary Arterial Hypertension. *Circulation. Genomic and Precision Medicine*. 11 (10), e002087. doi:10.1161/CIRCGEN.118.002087.

Bordenave, J., Tu, L., Berrebeh, N., Thuillet, R., Cumont, A., Le Vely, B., Fadel, E., Nadaud, S., Savale, L., Humbert, M., Huertas, A. & Guignabert, C. (2020) Lineage Tracing Reveals the Dynamic Contribution of Pericytes to the Blood Vessel Remodeling in Pulmonary Hypertension. *Arteriosclerosis, Thrombosis, and Vascular Biology*. 40 (3), 766–782. doi:10.1161/ATVBAHA.119.313715.

Botella, L.M., Sánchez-Elsner, T., Sanz-Rodriguez, F., Kojima, S., Shimada, J., Guerrero-Esteo, M., Cooreman, M.P., Ratziu, V., Langa, C., Vary, C.P.H., Ramirez, J.R., Friedman, S. & Bernabéu, C. (2002) Transcriptional activation of endoglin and transforming growth factor-beta signaling components by cooperative interaction between Sp1 and KLF6: their potential role in the response to vascular injury. *Blood*. 100 (12), 4001–4010. doi:10.1182/blood.V100.12.4001.

Boucherat, O., Agrawal, V., Lawrie, A. & Bonnet, S. (2022) The Latest in Animal Models of Pulmonary Hypertension and Right Ventricular Failure. *Circulation Research*. 130 (9), 1466–1486. doi:10.1161/CIRCRESAHA.121.319971.

Boucherat, O., Vitry, G., Trinh, I., Paulin, R., Provencher, S. & Bonnet, S. (2017) The cancer theory of pulmonary arterial hypertension. *Pulmonary Circulation*. 7 (2), 285–299. doi:10.1177/2045893217701438.

Bremnes, T., Paasche, J.D., Mehlum, A., Sandberg, C., Bremnes, B. & Attramadal, H. (2000) Regulation and intracellular trafficking pathways of the endothelin receptors. *The Journal of Biological Chemistry*. 275 (23), 17596–17604. doi:10.1074/jbc.M000142200.

Budhiraja, R., Tuder, R.M. & Hassoun, P.M. (2004) Endothelial Dysfunction in Pulmonary Hypertension. *Circulation*. 109 (2), 159–165. doi:10.1161/01.CIR.0000102381.57477.50.

Burton, V.J., Ciuclan, L.I., Holmes, A.M., Rodman, D.M., Walker, C. & Budd, D.C. (2011) Bone morphogenetic protein receptor II regulates pulmonary artery endothelial cell barrier function. *Blood*. 117 (1), 333–341. doi:10.1182/blood-2010-05-285973.

Cabral-Pacheco, G.A., Garza-Veloz, I., Castruita-De la Rosa, C., Ramirez-Acuña, J.M., Perez-Romero, B.A., Guerrero-Rodriguez, J.F., Martinez-Avila, N. & Martinez-Fierro, M.L. (2020) The Roles of Matrix Metalloproteinases and Their Inhibitors in

Human Diseases. *International Journal of Molecular Sciences*. 21 (24), 9739. doi:10.3390/ijms21249739.

Cao, G., Xuan, X., Hu, J., Zhang, R., Jin, H. & Dong, H. (2022) How vascular smooth muscle cell phenotype switching contributes to vascular disease. *Cell Communication and Signaling : CCS*. 20, 180. doi:10.1186/s12964-022-00993-2.

Carman, B.L., Predescu, D.N., Machado, R. & Predescu, S.A. (2019) Plexiform Arteriopathy in Rodent Models of Pulmonary Arterial Hypertension. *The American Journal of Pathology*. 189 (6), 1133–1144. doi:10.1016/j.ajpath.2019.02.005.

Carmeliet, P., Dor, Y., Herbert, J.M., Fukumura, D., Brusselmans, K., Dewerchin, M., Neeman, M., Bono, F., Abramovitch, R., Maxwell, P., Koch, C.J., Ratcliffe, P., Moons, L., Jain, R.K., Collen, D. & Keshert, E. (1998) Role of HIF-1alpha in hypoxia-mediated apoptosis, cell proliferation and tumour angiogenesis. *Nature*. 394 (6692), 485–490. doi:10.1038/28867.

Carreau, A., Hafny-Rahbi, B.E., Matejuk, A., Grillon, C. & Kieda, C. (2011) Why is the partial oxygen pressure of human tissues a crucial parameter? Small molecules and hypoxia. *Journal of Cellular and Molecular Medicine*. 15 (6), 1239–1253. doi:10.1111/j.1582-4934.2011.01258.x.

Chakraborty, R., Saddouk, F.Z., Carrao, A.C., Krause, D.S., Greif, D.M. & Martin, K.A. (2019) Promoters to Study Vascular Smooth Muscle. *Arteriosclerosis, Thrombosis, and Vascular Biology*. 39 (4), 603–612. doi:10.1161/ATVBAHA.119.312449.

Chan, S.Y. & Loscalzo, J. (2008) Pathogenic Mechanisms of Pulmonary Arterial Hypertension. *Journal of molecular and cellular cardiology*. 44 (1), 14–30. doi:10.1016/j.yjmcc.2007.09.006.

Chan, S.Y. & Rubin, L.J. (2017) Metabolic dysfunction in pulmonary hypertension: from basic science to clinical practice. *European Respiratory Review*. 26 (146). doi:10.1183/16000617.0094-2017.

Chandra, S.M., Razavi, H., Kim, J., Agrawal, R., Kundu, R.K., de Jesus Perez, V., Zamanian, R.T., Quertermous, T. & Chun, H.J. (2011) Disruption of the apelin-APJ system worsens hypoxia-induced pulmonary hypertension. *Arteriosclerosis, Thrombosis, and Vascular Biology*. 31 (4), 814–820. doi:10.1161/ATVBAHA.110.219980.

Chaouat, A., Coulet, F., Favre, C., Simonneau, G., Weitzenblum, E., Soubrier, F. & Humbert, M. (2004) Endoglin germline mutation in a patient with hereditary haemorrhagic telangiectasia and dexfenfluramine associated pulmonary arterial hypertension. *Thorax*. 59 (5), 446–448. doi:10.1136/thx.2003.11890.

Chen, F.E. & Ghosh, G. (1999) Regulation of DNA binding by Rel/NF-κB transcription factors: structural views. *Oncogene*. 18 (49), 6845–6852. doi:10.1038/sj.onc.1203224.

Chen, H., Liu, X., Lin, J., Chen, T., Feng, Q. & Zeng, Y. (2002) [Mutation analysis of KLF6 gene in human nasopharyngeal carcinomas]. *Ai Zheng = Aizheng = Chinese Journal of Cancer*. 21 (10), 1047–1050.

Chen, H., Yang, H., Yue, H., Strappe, P.M., Xia, P., Pan, L., Zhang, Y., Chai, S., Chen, S., Ma, L. & Wang, L. (2017a) Mesenchymal Stem Cells Expressing eNOS and a Cav1 Mutant Inhibit Vascular Smooth Muscle Cell Proliferation in a Rat Model of Pulmonary Hypertension. *Heart, Lung and Circulation*. 26 (5), 509–518. doi:10.1016/j.hlc.2016.08.002.

Chen, J., Wang, Y.-X., Dong, M.-Q., Zhang, B., Luo, Y., Niu, W. & Li, Z.-C. (2017b) Reoxygenation Reverses Hypoxic Pulmonary Arterial Remodeling by Inducing Smooth Muscle Cell Apoptosis via Reactive Oxygen Species-Mediated Mitochondrial Dysfunction. *Journal of the American Heart Association*. 6 (6), e005602. doi:10.1161/JAHA.117.005602.

Cheung, P., Xiol, J., Dill, M.T., Yuan, W.-C., Panero, R., Roper, J., Osorio, F.G., Maglic, D., Li, Q., Gurung, B., Calogero, R.A., Yilmaz, Ö.H., Mao, J. & Camargo, F.D. (2020) Regenerative Reprogramming of the Intestinal Stem Cell State via Hippo Signaling Suppresses Metastatic Colorectal Cancer. *Cell Stem Cell*. 27 (4), 590-604.e9. doi:10.1016/j.stem.2020.07.003.

Chida, A., Shintani, M., Nakayama, T., Furutani, Y., Hayama, E., Inai, K., Saji, T., Nonoyama, S. & Nakanishi, T. (2012) Missense mutations of the BMPR1B (ALK6) gene in childhood idiopathic pulmonary arterial hypertension. *Circulation Journal: Official Journal of the Japanese Circulation Society*. 76 (6), 1501–1508. doi:10.1253/circj.cj-11-1281.

Chiplunkar, A.R., Curtis, B.C., Eades, G.L., Kane, M.S., Fox, S.J., Haar, J.L. & Lloyd, J.A. (2013) The Krüppel-like factor 2 and Krüppel-like factor 4 genes interact to maintain endothelial integrity in mouse embryonic vasculogenesis. *BMC developmental biology*. 13, 40. doi:10.1186/1471-213X-13-40.

Chiu, J.-J. & Chien, S. (2011) Effects of Disturbed Flow on Vascular Endothelium: Pathophysiological Basis and Clinical Perspectives. *Physiological reviews*. 91 (1), 10.1152/physrev.00047.2009. doi:10.1152/physrev.00047.2009.

Cho, Y.G., Kim, C.J., Park, C.H., Yang, Y.M., Kim, S.Y., Nam, S.W., Lee, S.H., Yoo, N.J., Lee, J.Y. & Park, W.S. (2005) Genetic alterations of the KLF6 gene in gastric cancer. *Oncogene*. 24 (28), 4588–4590. doi:10.1038/sj.onc.1208670.

Christman, B.W., McPherson, C.D., Newman, J.H., King, G.A., Bernard, G.R., Groves, B.M. & Loyd, J.E. (1992) An imbalance between the excretion of thromboxane and prostacyclin metabolites in pulmonary hypertension. *The New England Journal of Medicine*. 327 (2), 70–75. doi:10.1056/NEJM199207093270202.

Chu, H.-R., Sun, Y.-C., Gao, Y., Guan, X.-M., Yan, H., Cui, X.-D., Zhang, X.-Y., Li, X., Li, H. & Cheng, M. (2019) Function of Krüppel-like factor 2 in the shear stress-induced

cell differentiation of endothelial progenitor cells to endothelial cells. *Molecular Medicine Reports*. 19 (3), 1739–1746. doi:10.3892/mmr.2019.9819.

Ciuclan, L., Bonneau, O., Hussey, M., Duggan, N., Holmes, A.M., Good, R., Stringer, R., Jones, P., Morrell, N.W., Jarai, G., Walker, C., Westwick, J. & Thomas, M. (2011) A Novel Murine Model of Severe Pulmonary Arterial Hypertension. *American Journal of Respiratory and Critical Care Medicine*. 184 (10), 1171–1182. doi:10.1164/rccm.201103-0412OC.

Claesson-Welsh, L., Dejana, E. & McDonald, D.M. (2021) Permeability of the endothelial barrier: identifying and reconciling controversies. *Trends in molecular medicine*. 27 (4), 314–331. doi:10.1016/j.molmed.2020.11.006.

Clapp, L.H., Finney, P., Turcato, S., Tran, S., Rubin, L.J. & Tinker, A. (2002) Differential effects of stable prostacyclin analogs on smooth muscle proliferation and cyclic AMP generation in human pulmonary artery. *American Journal of Respiratory Cell and Molecular Biology*. 26 (2), 194–201. doi:10.1165/ajrcmb.26.2.4695.

Clark, P.R., Jensen, T.J., Kluger, M.S., Morelock, M., Hanidu, A., Qi, Z., Tatake, R.J. & Pober, J.S. (2011) MEK5 is activated by shear stress, activates ERK5 and induces KLF4 to modulate TNF responses in human dermal microvascular endothelial cells. *Microcirculation (New York, N.Y.: 1994)*. 18 (2), 102–117. doi:10.1111/j.1549-8719.2010.00071.x.

Cober, N.D., VandenBroek, M.M., Ormiston, M.L. & Stewart, D.J. (2022) Evolving Concepts in Endothelial Pathobiology of Pulmonary Arterial Hypertension. *Hypertension*. 79 (8), 1580–1590. doi:10.1161/HYPERTENSIONAHA.122.18261.

Conway, D. & Schwartz, M.A. (2012) Lessons from the endothelial junctional mechanosensory complex. *F1000Prime Rep*. 4 (1). https://connect.h1.co$request.getParameter('target').

Coste, F., Guibert, C., Magat, J., Abell, E., Vaillant, F., Dubois, M., Courtois, A., Diolez, P., Quesson, B., Marthan, R., Savineau, J.-P., Muller, B. & Freund-Michel, V. (2017) Chronic hypoxia aggravates monocrotaline-induced pulmonary arterial hypertension: a rodent relevant model to the human severe form of the disease. *Respiratory Research*. 18 (1), 47. doi:10.1186/s12931-017-0533-x.

Courboulin, A., Tremblay, V.L., Barrier, M., Meloche, J., Jacob, M.H., Chapolard, M., Bisserier, M., Paulin, R., Lambert, C., Provencher, S. & Bonnet, S. (2011) Krüppel-like factor 5 contributes to pulmonary artery smooth muscle proliferation and resistance to apoptosis in human pulmonary arterial hypertension. *Respiratory Research*. 12 (1), 128. doi:10.1186/1465-9921-12-128.

Cowburn, A.S., Crosby, A., Macias, D., Branco, C., Colaço, R.D.D.R., Southwood, M., Toshner, M., Crotty Alexander, L.E., Morrell, N.W., Chilvers, E.R. & Johnson, R.S. (2016) HIF2α–arginase axis is essential for the development of pulmonary hypertension. *Proceedings of the National Academy of Sciences of the United States of America*. 113 (31), 8801–8806. doi:10.1073/pnas.1602978113.

Cracowski, J.-L., Chabot, F., Labarère, J., Faure, P., Degano, B., Schwebel, C., Chaouat, A., Reynaud-Gaubert, M., Cracowski, C., Sitbon, O., Yaici, A., Simonneau, G. & Humbert, M. (2014) Proinflammatory cytokine levels are linked to death in pulmonary arterial hypertension. *European Respiratory Journal*. 43 (3), 915–917. doi:10.1183/09031936.00151313.

Crosswhite, P. & Sun, Z. (2010) Nitric Oxide, Oxidative Stress and Inflammation in Pulmonary Arterial Hypertension. *Journal of hypertension*. 28 (2), 201–212. doi:10.1097/HJH.0b013e328332bcdb.

D'Astolfo, D.S., Gehrau, R.C., Bocco, J.L. & Koritschoner, N.P. (2008) Silencing of the transcription factor KLF6 by siRNA leads to cell cycle arrest and sensitizes cells to apoptosis induced by DNA damage. *Cell Death and Differentiation*. 15 (3), 613–616. doi:10.1038/sj.cdd.4402299.

Dai, G., Kaazempur-Mofrad, M.R., Natarajan, S., Zhang, Y., Vaughn, S., Blackman, B.R., Kamm, R.D., García-Cardeña, G. & Gimbrone, M.A. (2004) Distinct endothelial phenotypes evoked by arterial waveforms derived from atherosclerosis-susceptible and -resistant regions of human vasculature. *Proceedings of the National Academy of Sciences of the United States of America*. 101 (41), 14871–14876. doi:10.1073/pnas.0406073101.

Dai, J., Zhou, Q., Chen, J., Rexius-Hall, M.L., Rehman, J. & Zhou, G. (2018) Alpha-enolase regulates the malignant phenotype of pulmonary artery smooth muscle cells via the AMPK-Akt pathway. *Nature Communications*. 9, 3850. doi:10.1038/s41467-018-06376-x.

Damås, J.K., Otterdal, K., Yndestad, A., Aass, H., Solum, N.O., Frøland, S.S., Simonsen, S., Aukrust, P. & Andreassen, A.K. (2004) Soluble CD40 Ligand in Pulmonary Arterial Hypertension. *Circulation*. 110 (8), 999–1005. doi:10.1161/01.CIR.0000139859.68513.FC.

Danaher, P., Kim, Y., Nelson, B., Griswold, M., Yang, Z., Piazza, E. & Beechem, J.M. (2022) Advances in mixed cell deconvolution enable quantification of cell types in spatial transcriptomic data. *Nature Communications*. 13 (1), 385. doi:10.1038/s41467-022-28020-5.

Danku, A.E., Dulf, E.-H., Braicu, C., Jurj, A. & Berindan-Neagoe, I. (2022) Organ-On-A-Chip: A Survey of Technical Results and Problems. *Frontiers in Bioengineering and Biotechnology*. 10, 840674. doi:10.3389/fbioe.2022.840674.

Dannewitz Prosseda, S., Ali, M.K. & Spiekerkoetter, E. (2020) Novel Advances in Modifying BMPR2 Signaling in PAH. *Genes*. 12 (1), 8. doi:10.3390/genes12010008.

Dardik, A., Liu, A. & Ballermann, B.J. (1999) Chronic in vitro shear stress stimulates endothelial cell retention on prosthetic vascular grafts and reduces subsequent in vivo neointimal thickness. *Journal of Vascular Surgery*. 29 (1), 157–167. doi:10.1016/S0741-5214(99)70357-5.

Das, A., Fernandez-Zapico, M.E., Cao, S., Yao, J., Fiorucci, S., Hebbel, R.P., Urrutia, R. & Shah, V.H. (2006) Disruption of an SP2/KLF6 repression complex by SHP is required for farnesoid X receptor-induced endothelial cell migration. *The Journal of Biological Chemistry*. 281 (51), 39105–39113. doi:10.1074/jbc.M607720200.

Date, D., Das, R., Narla, G., Simon, D.I., Jain, M.K. & Mahabeleshwar, G.H. (2014) Kruppel-like Transcription Factor 6 Regulates Inflammatory Macrophage Polarization. *The Journal of Biological Chemistry*. 289 (15), 10318–10329. doi:10.1074/jbc.M113.526749.

Davies, P.F. (2009) Hemodynamic shear stress and the endothelium in cardiovascular pathophysiology. *Nature clinical practice. Cardiovascular medicine*. 6 (1), 16–26. doi:10.1038/ncpcardio1397.

Davies, P.F., Civelek, M., Fang, Y. & Fleming, I. (2013) The atherosusceptible endothelium: endothelial phenotypes in complex haemodynamic shear stress regions in vivo. *Cardiovascular Research*. 99 (2), 315–327. doi:10.1093/cvr/cvt101.

de Boer, S., Bowman, M., Notley, C., Mo, A., Lima, P., de Jong, A., Dirven, R., Weijers, E., Lillicrap, D., James, P. & Eikenboom, J. (2020) Endothelial characteristics in healthy endothelial colony forming cells; generating a robust and valid ex vivo model for vascular disease. *Journal of Thrombosis and Haemostasis*. 18 (10), 2721–2731. doi:10.1111/jth.14998.

de Man, F.S., Tu, L., Handoko, M.L., Rain, S., Ruiter, G., François, C., Schalij, I., Dorfmüller, P., Simonneau, G., Fadel, E., Perros, F., Boonstra, A., Postmus, P.E., van der Velden, J., Vonk-Noordegraaf, A., Humbert, M., Eddahibi, S. & Guignabert, C. (2012) Dysregulated renin-angiotensin-aldosterone system contributes to pulmonary arterial hypertension. *American Journal of Respiratory and Critical Care Medicine*. 186 (8), 780–789. doi:10.1164/rccm.201203-0411OC.

Dekker, R.J., Boon, R.A., Rondaij, M.G., Kragt, A., Volger, O.L., Elderkamp, Y.W., Meijers, J.C.M., Voorberg, J., Pannekoek, H. & Horrevoets, A.J.G. (2006) KLF2 provokes a gene expression pattern that establishes functional quiescent differentiation of the endothelium. *Blood*. 107 (11), 4354–4363. doi:10.1182/blood-2005-08-3465.

Dekker, R.J., van Soest, S., Fontijn, R.D., Salamanca, S., de Groot, P.G., VanBavel, E., Pannekoek, H. & Horrevoets, A.J.G. (2002) Prolonged fluid shear stress induces a distinct set of endothelial cell genes, most specifically lung Krüppel-like factor (KLF2). *Blood*. 100 (5), 1689–1698. doi:10.1182/blood-2002-01-0046.

Deng, C., Zhong, Z., Wu, D., Chen, Y., Lian, N., Ding, H., Zhang, Q., Lin, Q. & Wu, S. (2017) Role of FoxO1 and apoptosis in pulmonary vascular remolding in a rat model of chronic thromboembolic pulmonary hypertension. *Scientific Reports*. 7, 2270. doi:10.1038/s41598-017-02007-5.

Deng, Z., Morse, J.H., Slager, S.L., Cuervo, N., Moore, K.J., Venetos, G., Kalachikov, S., Cayanis, E., Fischer, S.G., Barst, R.J., Hodge, S.E. & Knowles, J.A. (2000) Familial primary pulmonary hypertension (gene PPH1) is caused by mutations in the bone

morphogenetic protein receptor-II gene. *American Journal of Human Genetics*. 67 (3), 737–744. doi:10.1086/303059.

Deshwal, H., Weinstein, T. & Sulica, R. (2021) Advances in the management of pulmonary arterial hypertension. *Journal of Investigative Medicine*. 69 (7), 1270–1280. doi:10.1136/jim-2021-002027.

Dewey, C.F., Bussolari, S.R., Gimbrone, M.A. & Davies, P.F. (1981) The dynamic response of vascular endothelial cells to fluid shear stress. *Journal of Biomechanical Engineering*. 103 (3), 177–185. doi:10.1115/1.3138276.

Dickinson, M.G., Bartelds, B., Borgdorff, M.A.J. & Berger, R.M.F. (2013) The role of disturbed blood flow in the development of pulmonary arterial hypertension: lessons from preclinical animal models. *American Journal of Physiology-Lung Cellular and Molecular Physiology*. 305 (1), L1–L14. doi:10.1152/ajplung.00031.2013.

DiFeo, A., Martignetti, J.A. & Narla, G. (2009) The role of KLF6 and its splice variants in cancer therapy. *Drug Resistance Updates: Reviews and Commentaries in Antimicrobial and Anticancer Chemotherapy*. 12 (1–2), 1–7. doi:10.1016/j.drup.2008.11.001.

DiFeo, A., Narla, G., Camacho-Vanegas, O., Nishio, H., Rose, S.L., Buller, R.E., Friedman, S.L., Walsh, M.J. & Martignetti, J.A. (2006a) E-cadherin is a novel transcriptional target of the KLF6 tumor suppressor. *Oncogene*. 25 (44), 6026–6031. doi:10.1038/sj.onc.1209611.

DiFeo, A., Narla, G., Hirshfeld, J., Camacho-Vanegas, O., Narla, J., Rose, S.L., Kalir, T., Yao, S., Levine, A., Birrer, M.J., Bonome, T., Friedman, S.L., Buller, R.E. & Martignetti, J.A. (2006b) Roles of KLF6 and KLF6-SV1 in ovarian cancer progression and intraperitoneal dissemination. *Clinical Cancer Research: An Official Journal of the American Association for Cancer Research*. 12 (12), 3730–3739. doi:10.1158/1078-0432.CCR-06-0054.

Dignam, J.P., Scott, T.E., Kemp-Harper, B.K. & Hobbs, A.J. (2022) Animal models of pulmonary hypertension: Getting to the heart of the problem. *British Journal of Pharmacology*. 179 (5), 811–837. doi:10.1111/bph.15444.

Dobin, A., Davis, C.A., Schlesinger, F., Drenkow, J., Zaleski, C., Jha, S., Batut, P., Chaisson, M. & Gingeras, T.R. (2013) STAR: ultrafast universal RNA-seq aligner. *Bioinformatics*. 29 (1), 15–21. doi:10.1093/bioinformatics/bts635.

Dong, R. & Yuan, G.-C. (2021) SpatialDWLS: accurate deconvolution of spatial transcriptomic data. *Genome Biology*. 22 (1), 145. doi:10.1186/s13059-021-02362-7.

Dorfmüller, P., Zarka, V., Durand-Gasselin, I., Monti, G., Balabanian, K., Garcia, G., Capron, F., Coulomb-Lherminé, A., Marfaing-Koka, A., Simonneau, G., Emilie, D. & Humbert, M. (2002) Chemokine RANTES in Severe Pulmonary Arterial Hypertension. *American Journal of Respiratory and Critical Care Medicine*. 165 (4), 534–539. doi:10.1164/ajrccm.165.4.2012112.

Duong, H.T., Comhair, S.A., Aldred, M.A., Mavrakis, L., Savasky, B.M., Erzurum, S.C. & Asosingh, K. (2011) Pulmonary Artery Endothelium Resident Endothelial Colony-Forming Cells in Pulmonary Arterial Hypertension. *Pulmonary Circulation*. 1 (4), 475–486. doi:10.4103/2045-8932.93547.

Durinck, S., Spellman, P.T., Birney, E. & Huber, W. (2009) Mapping Identifiers for the Integration of Genomic Datasets with the R/Bioconductor package biomaRt. *Nature protocols*. 4 (8), 1184–1191. doi:10.1038/nprot.2009.97.

Eaton, S.A., Funnell, A.P.W., Sue, N., Nicholas, H., Pearson, R.C.M. & Crossley, M. (2008) A Network of Krüppel-like Factors (Klfs): Klf8 IS REPRESSED BY Klf3 AND ACTIVATED BY Klf1 IN VIVO*. *Journal of Biological Chemistry*. 283 (40), 26937–26947. doi:10.1074/jbc.M804831200.

Ebong, E.E. & DePaola, N. (2013) Specificity in the participation of connexin proteins in flow-induced endothelial gap junction communication. *Pflügers Archiv - European Journal of Physiology*. 465 (9), 1293–1302. doi:10.1007/s00424-013-1245-9.

Eddahibi, S., Fabre, V., Boni, C., Martres, M.P., Raffestin, B., Hamon, M. & Adnot, S. (1999) Induction of Serotonin Transporter by Hypoxia in Pulmonary Vascular Smooth Muscle Cells. *Circulation Research*. 84 (3), 329–336. doi:10.1161/01.RES.84.3.329.

Eichstaedt, C.A., Song, J., Viales, R.R., Pan, Z., Benjamin, N., Fischer, C., Hoeper, M.M., Ulrich, S., Hinderhofer, K. & Grünig, E. (2017) First identification of Krüppel-like factor 2 mutation in heritable pulmonary arterial hypertension. *Clinical Science*. 131 (8), 689–698. doi:10.1042/CS20160930.

El Chami, H. & Hassoun, P.M. (2012) Immune and Inflammatory Mechanisms in Pulmonary Arterial Hypertension. *Progress in cardiovascular diseases*. 55 (2), 218–228. doi:10.1016/j.pcad.2012.07.006.

Enescu, D.M., Parasca, S.V., Badoiu, S.C., Miricescu, D., Ripszky Totan, A., Stanescu-Spinu, I.-I., Greabu, M. & Jinga, V. (2022) Hypoxia-Inducible Factors and Burn-Associated Acute Kidney Injury—A New Paradigm? *International Journal of Molecular Sciences*. 23 (5), 2470. doi:10.3390/ijms23052470.

Enevoldsen, F.C., Sahana, J., Wehland, M., Grimm, D., Infanger, M. & Krüger, M. (2020) Endothelin Receptor Antagonists: Status Quo and Future Perspectives for Targeted Therapy. *Journal of Clinical Medicine*. 9 (3), 824. doi:10.3390/jcm9030824.

Evans, C.E., Cober, N.D., Dai, Z., Stewart, D.J. & Zhao, Y.-Y. (2021) Endothelial cells in the pathogenesis of pulmonary arterial hypertension. *European Respiratory Journal*. 58 (3). doi:10.1183/13993003.03957-2020.

Ewels, P., Magnusson, M., Lundin, S. & Käller, M. (2016) MultiQC: summarize analysis results for multiple tools and samples in a single report. *Bioinformatics (Oxford, England)*. 32 (19), 3047–3048. doi:10.1093/bioinformatics/btw354.

Eyries, M., Montani, D., Girerd, B., Favrolt, N., Riou, M., Faivre, L., Manaud, G., Perros, F., Gräf, S., Morrell, N.W., Humbert, M. & Soubrier, F. (2020) Familial pulmonary arterial hypertension by KDR heterozygous loss of function. *European Respiratory Journal*. 55 (4). doi:10.1183/13993003.02165-2019.

Eyries, M., Montani, D., Nadaud, S., Girerd, B., Levy, M., et al. (2019) Widening the landscape of heritable pulmonary hypertension mutations in paediatric and adult cases. *European Respiratory Journal*. 53 (3). doi:10.1183/13993003.01371-2018.

Fan, Y., Lu, H., Liang, W., Hu, W., Zhang, J. & Chen, Y.E. (2017) Krüppel-like factors and vascular wall homeostasis. *Journal of Molecular Cell Biology*. 9 (5), 352–363. doi:10.1093/jmcb/mjx037.

Farha, S., Sharp, J., Asosingh, K., Park, M., Comhair, S.A.A., Tang, W.H.W., Thomas, J., Farver, C., Hsieh, F., Loyd, J.E. & Erzurum, S.C. (2012) Mast cell number, phenotype, and function in human pulmonary arterial hypertension. *Pulmonary Circulation*. 2 (2), 220–228. doi:10.4103/2045-8932.97609.

Faris, P., Negri, S., Perna, A., Rosti, V., Guerra, G. & Moccia, F. (2020) Therapeutic Potential of Endothelial Colony-Forming Cells in Ischemic Disease: Strategies to Improve their Regenerative Efficacy. *International Journal of Molecular Sciences*. 21 (19), 7406. doi:10.3390/ijms21197406.

Fels, B. & Kusche-Vihrog, K. (2020) It takes more than two to tango: mechanosignaling of the endothelial surface. *Pflugers Archiv*. 472 (4), 419–433. doi:10.1007/s00424-020-02369-2.

Fike, C.D., Aschner, J.L., Slaughter, J.C., Kaplowitz, M.R., Zhang, Y. & Pfister, S.L. (2011) Pulmonary Arterial Responses to Reactive Oxygen Species Are Altered in Newborn Piglets With Chronic Hypoxia-Induced Pulmonary Hypertension. *Pediatric Research*. 70 (2), 136–141. doi:10.1203/PDR.0b013e3182207ce7.

Frankish, A., Diekhans, M., Jungreis, I., Lagarde, J., Loveland, J.E., et al. (2020) GENCODE 2021. *Nucleic Acids Research*. 49 (D1), D916–D923. doi:10.1093/nar/gkaa1087.

Frump, A.L., Lai, Y.-C. & Lahm, T. (2020) Assessing the cancer hypothesis of pulmonary arterial hypertension: the devil is in the detail. *American Journal of Physiology - Lung Cellular and Molecular Physiology*. 318 (6), L1140–L1141. doi:10.1152/ajplung.00084.2020.

Fu, M., Luo, F., Wang, E., Jiang, Y., Liu, S., Peng, J. & Liu, B. (2021) Magnolol Attenuates Right Ventricular Hypertrophy and Fibrosis in Hypoxia-Induced Pulmonary Arterial Hypertensive Rats Through Inhibition of the JAK2/STAT3 Signaling Pathway. *Frontiers in Pharmacology*. 12, 755077. doi:10.3389/fphar.2021.755077.

Fujita, M., Mason, R.J., Cool, C., Shannon, J.M., Hara, N. & Fagan, K.A. (2002) Pulmonary hypertension in TNF-alpha-overexpressing mice is associated with decreased VEGF

gene expression. *Journal of Applied Physiology (Bethesda, Md.: 1985)*. 93 (6), 2162–2170. doi:10.1152/japplphysiol.00083.2002.

Fujiwara, M., Yagi, H., Matsuoka, R., Akimoto, K., Furutani, M., Imamura, S., Uehara, R., Nakayama, T., Takao, A., Nakazawa, M. & Saji, T. (2008) Implications of mutations of activin receptor-like kinase 1 gene (ALK1) in addition to bone morphogenetic protein receptor II gene (BMPR2) in children with pulmonary arterial hypertension. *Circulation Journal: Official Journal of the Japanese Circulation Society*. 72 (1), 127–133. doi:10.1253/circj.72.127.

Furuyama, T., Kitayama, K., Shimoda, Y., Ogawa, M., Sone, K., Yoshida-Araki, K., Hisatsune, H., Nishikawa, S., Nakayama, K., Nakayama, K., Ikeda, K., Motoyama, N. & Mori, N. (2004) Abnormal angiogenesis in Foxo1 (Fkhr)-deficient mice. *The Journal of Biological Chemistry*. 279 (33), 34741–34749. doi:10.1074/jbc.M314214200.

Galiè, N., Brundage, B.H., Ghofrani, H.A., Oudiz, R.J., Simonneau, G., Safdar, Z., Shapiro, S., White, R.J., Chan, M., Beardsworth, A., Frumkin, L. & Barst, R.J. (2009) Tadalafil Therapy for Pulmonary Arterial Hypertension. *Circulation*. 119 (22), 2894–2903. doi:10.1161/CIRCULATIONAHA.108.839274.

Galiè, N., Ghofrani, H.A., Torbicki, A., Barst, R.J., Rubin, L.J., Badesch, D., Fleming, T., Parpia, T., Burgess, G., Branzi, A., Grimminger, F., Kurzyna, M., Simonneau, G., & Sildenafil Use in Pulmonary Arterial Hypertension (SUPER) Study Group (2005) Sildenafil citrate therapy for pulmonary arterial hypertension. *The New England Journal of Medicine*. 353 (20), 2148–2157. doi:10.1056/NEJMoa050010.

Galiè, N., Müller, K., Scalise, A.-V. & Grünig, E. (2015) PATENT PLUS: a blinded, randomised and extension study of riociguat plus sildenafil in pulmonary arterial hypertension. *European Respiratory Journal*. 45 (5), 1314–1322. doi:10.1183/09031936.00105914.

Gallardo-Vara, E., Blanco, F.J., Roqué, M., Friedman, S.L., Suzuki, T., Botella, L.M. & Bernabeu, C. (2016) Transcription factor KLF6 upregulates expression of metalloprotease MMP14 and subsequent release of soluble endoglin during vascular injury. *Angiogenesis*. 19, 155–171. doi:10.1007/s10456-016-9495-8.

Gallego-Zazo, N., Cruz-Utrilla, A., del Cerro, M.J., Ochoa Parra, N., Blanco, J.N., Arias, P., Lapunzina, P., Escribano-Subias, P. & Tenorio-Castaño, J. (2022) Description of Two New Cases of AQP1 Related Pulmonary Arterial Hypertension and Review of the Literature. *Genes*. 13 (5), 927. doi:10.3390/genes13050927.

Garat, C.V., Crossno, J.T., Sullivan, T.M., Reusch, J.E.B. & Klemm, D.J. (2013) Inhibition of Phosphatidylinositol 3-kinase/Akt Signaling Attenuates Hypoxia-induced Pulmonary Artery Remodeling and Suppresses CREB Depletion in Arterial Smooth Muscle Cells. *Journal of cardiovascular pharmacology*. 62 (6), 539–548. doi:10.1097/FJC.0000000000000014.

Garrido-Martín, E.M., Blanco, F.J., Roquè, M., Novensà, L., Tarocchi, M., Lang, U.E., Suzuki, T., Friedman, S.L., Botella, L.M. & Bernabéu, C. (2013) Vascular injury triggers Krüppel-like factor 6 mobilization and cooperation with specificity protein 1 to promote endothelial activation through upregulation of the activin receptor-like kinase 1 gene. *Circulation Research*. 112 (1), 113–127. doi:10.1161/CIRCRESAHA.112.275586.

Garrison, A.T., Bignold, R.E., Wu, X. & Johnson, J.R. (2023) Pericytes: The lung-forgotten cell type. *Frontiers in Physiology*. 14, 1150028. doi:10.3389/fphys.2023.1150028.

Gerhold, K.A. & Schwartz, M.A. (2016) Ion Channels in Endothelial Responses to Fluid Shear Stress. *Physiology*. 31 (5), 359–369. doi:10.1152/physiol.00007.2016.

GHALEB, A.M., NANDAN, M.O., CHANCHEVALAP, S., DALTON, W.B., HISAMUDDIN, I.M. & YANG, V.W. (2005) Krüppel-like factors 4 and 5: the yin and yang regulators of cellular proliferation. *Cell research*. 15 (2), 92–96. doi:10.1038/sj.cr.7290271.

Ghofrani, H.-A., Galiè, N., Grimminger, F., Grünig, E., Humbert, M., Jing, Z.-C., Keogh, A.M., Langleben, D., Kilama, M.O., Fritsch, A., Neuser, D., Rubin, L.J., & PATENT-1 Study Group (2013) Riociguat for the treatment of pulmonary arterial hypertension. *The New England Journal of Medicine*. 369 (4), 330–340. doi:10.1056/NEJMoa1209655.

Ghosh, S., Gupta, M., Xu, W., Mavrakis, D.A., Janocha, A.J., Comhair, S.A.A., Haque, M.M., Stuehr, D.J., Yu, J., Polgar, P., Prasad, S.V.N. & Erzurum, S.C. (2016) Phosphorylation inactivation of endothelial nitric oxide synthesis in pulmonary arterial hypertension. *American Journal of Physiology - Lung Cellular and Molecular Physiology*. 310 (11), L1199. doi:10.1152/ajplung.00092.2016.

Giaid, A., Yanagisawa, M., Langleben, D., Michel, R.P., Levy, R., Shennib, H., Kimura, S., Masaki, T., Duguid, W.P. & Stewart, D.J. (1993) Expression of endothelin-1 in the lungs of patients with pulmonary hypertension. *The New England Journal of Medicine*. 328 (24), 1732–1739. doi:10.1056/NEJM199306173282402.

Giannotta, M., Trani, M. & Dejana, E. (2013) VE-cadherin and endothelial adherens junctions: active guardians of vascular integrity. *Developmental Cell*. 26 (5), 441–454. doi:10.1016/j.devcel.2013.08.020.

Goldblum, S.E., Ding, X. & Campbell-Washington, J. (1993) TNF-alpha induces endothelial cell F-actin depolymerization, new actin synthesis, and barrier dysfunction. *The American Journal of Physiology*. 264 (4 Pt 1), C894-905. doi:10.1152/ajpcell.1993.264.4.C894.

Goldthorpe, H., Jiang, J.-Y., Taha, M., Deng, Y., Sinclair, T., Ge, C.X., Jurasz, P., Turksen, K., Mei, S.H.J. & Stewart, D.J. (2015) Occlusive Lung Arterial Lesions in Endothelial-Targeted, Fas-Induced Apoptosis Transgenic Mice. *American Journal of Respiratory Cell and Molecular Biology*. 53 (5), 712–718. doi:10.1165/rcmb.2014-0311OC.

Gomez-Arroyo, J.G., Farkas, L., Alhussaini, A.A., Farkas, D., Kraskauskas, D., Voelkel, N.F. & Bogaard, H.J. (2012) The monocrotaline model of pulmonary hypertension in perspective. *American Journal of Physiology-Lung Cellular and Molecular Physiology*. 302 (4), L363–L369. doi:10.1152/ajplung.00212.2011.

Gorini, A., De Maria, B., Krasinska, P., Bussotti, M., Perego, F. & Dalla Vecchia, L.A. (2023) Physiological and Psychological Response to Acute Mental Stress in Female Patients Affected by Chronic Pulmonary Arterial Hypertension: An Explorative Controlled Pilot Trial. *Pharmaceuticals*. 16 (4), 493. doi:10.3390/ph16040493.

Gräf, S., Haimel, M., Bleda, M., Hadinnapola, C., Southgate, L., et al. (2018) Identification of rare sequence variation underlying heritable pulmonary arterial hypertension. *Nature Communications*. 9 (1), 1416. doi:10.1038/s41467-018-03672-4.

Groth, A., Vrugt, B., Brock, M., Speich, R., Ulrich, S. & Huber, L.C. (2014) Inflammatory cytokines in pulmonary hypertension. *Respiratory Research*. 15 (1), 47. doi:10.1186/1465-9921-15-47.

Gui, T., Wang, Y., Zhang, L., Wang, W., Zhu, H. & Ding, W. (2013) Krüppel-Like Factor 6 Rendered Rat Schwann Cell More Sensitive to Apoptosis via Upregulating FAS Expression. *PLoS ONE*. 8 (12), e82449. doi:10.1371/journal.pone.0082449.

Guo, D., Gu, J., Jiang, H., Ahmed, A., Zhang, Z. & Gu, Y. (2016) Inhibition of pyruvate kinase M2 by reactive oxygen species contributes to the development of pulmonary arterial hypertension. *Journal of Molecular and Cellular Cardiology*. 91, 179–187. doi:10.1016/j.yjmcc.2016.01.009.

Gutierrez, G., Venbrux, A., Ignacio, E., Reiner, J., Chawla, L. & Desai, A. (2007) The concentration of oxygen, lactate and glucose in the central veins, right heart, and pulmonary artery: a study in patients with pulmonary hypertension. *Critical Care*. 11 (2), R44. doi:10.1186/cc5739.

Haarman, M.G., Kerstjens-Frederikse, W.S., Vissia-Kazemier, T.R., Breeman, K.T.N., Timens, W., Vos, Y.J., Roofthooft, M.T.R., Hillege, H.L. & Berger, R.M.F. (2020) The Genetic Epidemiology of Pediatric Pulmonary Arterial Hypertension. *The Journal of Pediatrics*. 225, 65-73.e5. doi:10.1016/j.jpeds.2020.05.051.

Hahn, C. & Schwartz, M.A. (2009) Mechanotransduction in vascular physiology and atherogenesis. *Nature reviews. Molecular cell biology*. 10 (1), 53–62. doi:10.1038/nrm2596.

Hale, A.T., Tian, H., Anih, E., Recio, F.O., Shatat, M.A., Johnson, T., Liao, X., Ramirez-Bergeron, D.L., Proweller, A., Ishikawa, M. & Hamik, A. (2014) Endothelial Kruppel-like factor 4 regulates angiogenesis and the Notch signaling pathway. *The Journal of Biological Chemistry*. 289 (17), 12016–12028. doi:10.1074/jbc.M113.530956.

Hamik, A., Lin, Z., Kumar, A., Balcells, M., Sinha, S., Katz, J., Feinberg, M.W., Gerzsten, R.E., Edelman, E.R. & Jain, M.K. (2007) Kruppel-like factor 4 regulates endothelial

inflammation. *The Journal of Biological Chemistry*. 282 (18), 13769–13779. doi:10.1074/jbc.M700078200.

Harris, A.L. & Ashcroft, M. (2019) Oxygen and cancer: The response to hypoxia. In: F. Pezzella, M. Tavassoli, D.J. Kerr, F. Pezzella, M. Tavassoli, & D.J. Kerr (eds.). *Oxford Textbook of Cancer Biology*. Oxford University Press. p. 0. doi:10.1093/med/9780198779452.003.0018.

Hart, G.T., Hogquist, K.A. & Jameson, S.C. (2012) Kruppel-like factors in lymphocyte biology. *Journal of Immunology (Baltimore, Md. : 1950)*. 188 (2), 521–526. doi:10.4049/jimmunol.1101530.

Hashemi, S., Salma, J., Wales, S. & McDermott, J.C. (2015) Pro-survival function of MEF2 in cardiomyocytes is enhanced by β-blockers. *Cell Death Discovery*. 1 (1), 1–11. doi:10.1038/cddiscovery.2015.19.

Haslip, M., Dostanic, I., Huang, Y., Zhang, Y., Russell, K.S., Jurczak, M.J., Mannam, P., Giordano, F., Erzurum, S.C. & Lee, P.J. (2015) Endothelial Ucp2 regulates mitophagy and pulmonary hypertension during intermittent-hypoxia. *Arteriosclerosis, thrombosis, and vascular biology*. 35 (5), 1166–1178. doi:10.1161/ATVBAHA.114.304865.

Hayden, M.S. & Ghosh, S. (2014) Regulation of NF-κB by TNF Family Cytokines. *Seminars in immunology*. 26 (3), 253–266. doi:10.1016/j.smim.2014.05.004.

He, Y.-L., Li, J., Gong, S.-H., Cheng, X., Zhao, M., Cao, Y., Zhao, T., Zhao, Y.-Q., Fan, M., Wu, H.-T., Zhu, L.-L. & Wu, L.-Y. (2022) BNIP3 phosphorylation by JNK1/2 promotes mitophagy via enhancing its stability under hypoxia. *Cell Death & Disease*. 13 (11), 966. doi:10.1038/s41419-022-05418-z.

He, Z., He, J. & Xie, K. (2023) KLF4 transcription factor in tumorigenesis. *Cell Death Discovery*. 9 (1), 1–13. doi:10.1038/s41420-023-01416-y.

Heresi, G.A., Aytekin, M., Newman, J. & Dweik, R.A. (2010) CXC-Chemokine Ligand 10 in Idiopathic Pulmonary Arterial Hypertension: Marker of Improved Survival. *Lung*. 188 (3), 191–197. doi:10.1007/s00408-010-9232-9.

Hernandez, S., Lazcano, R., Serrano, A., Powell, S., Kostousov, L., Mehta, J., Khan, K., Lu, W. & Solis, L.M. (2022) Challenges and Opportunities for Immunoprofiling Using a Spatial High-Plex Technology: The NanoString GeoMx® Digital Spatial Profiler. *Frontiers in Oncology*. 12, 890410. doi:10.3389/fonc.2022.890410.

Heukels, P., Corneth, O.B.J., van Uden, D., van Hulst, J.A.C., van den Toorn, L.M., van den Bosch, A.E., Wijsenbeek, M.S., Boomars, K.A., Kool, M. & Hendriks, R.W. (2021) Loss of immune homeostasis in patients with idiopathic pulmonary arterial hypertension. *Thorax*. 76 (12), 1209–1218. doi:10.1136/thoraxjnl-2020-215460.

Hiepen, C., Jatzlau, J., Hildebrandt, S., Kampfrath, B., Goktas, M., Murgai, A., Camacho, J.L.C., Haag, R., Ruppert, C., Sengle, G., Cavalcanti-Adam, E.A., Blank, K.G. & Knaus, P. (2019) BMPR2 acts as a gatekeeper to protect endothelial cells from increased TGFβ responses and altered cell mechanics. *PLOS Biology*. 17 (12), e3000557. doi:10.1371/journal.pbio.3000557.

Hill, N.S., Gillespie, M.N. & McMurtry, I.F. (2017) Fifty Years of Monocrotaline-Induced Pulmonary Hypertension: What Has It Meant to the Field? *CHEST*. 152 (6), 1106–1108. doi:10.1016/j.chest.2017.10.007.

Hirata, T., Yamamoto, K., Ikeda, K. & Arita, M. (2021) Functional lipidomics of vascular endothelial cells in response to laminar shear stress. *FASEB journal: official publication of the Federation of American Societies for Experimental Biology*. 35 (2), e21301. doi:10.1096/fj.202002144R.

Hirose, S., Hosoda, Y., Furuya, S., Otsuki, T. & Ikeda, E. (2000) Expression of vascular endothelial growth factor and its receptors correlates closely with formation of the plexiform lesion in human pulmonary hypertension. *Pathology International*. 50 (6), 472–479. doi:10.1046/j.1440-1827.2000.01068.x.

Hong, K.-H., Lee, Y.J., Lee, E., Park, S.O., Han, C., Beppu, H., Li, E., Raizada, M.K., Bloch, K.D. & Oh, S.P. (2008) Genetic ablation of the BMPR2 gene in pulmonary endothelium is sufficient to predispose to pulmonary arterial hypertension. *Circulation*. 118 (7), 722–730. doi:10.1161/CIRCULATIONAHA.107.736801.

Hopper, R.K., Moonen, J.-R.A.J., Diebold, I., Cao, A., Rhodes, C.J., Tojais, N.F., Hennigs, J.K., Gu, M., Wang, L. & Rabinovitch, M. (2016) In Pulmonary Arterial Hypertension, Reduced BMPR2 Promotes Endothelial-to-Mesenchymal Transition via HMGA1 and Its Target Slug. *Circulation*. 133 (18), 1783–1794. doi:10.1161/CIRCULATIONAHA.115.020617.

Hsu, L.-S., Huang, R.-H., Lai, H.-W., Hsu, H.-T., Sung, W.-W., Hsieh, M.-J., Wu, C.-Y., Lin, Y.-M., Chen, M.-K., Lo, Y.-S. & Chen, C.-J. (2017) KLF6 inhibited oral cancer migration and invasion via downregulation of mesenchymal markers and inhibition of MMP-9 activities. *International Journal of Medical Sciences*. 14 (6), 530–535. doi:10.7150/ijms.19024.

Hu, Y., Chi, L., Kuebler, W.M. & Goldenberg, N.M. (2020) Perivascular Inflammation in Pulmonary Arterial Hypertension. *Cells*. 9 (11), 2338. doi:10.3390/cells9112338.

Huang, C.K., Sun, Y., Lv, L. & Ping, Y. (2022) ENO1 and Cancer. *Molecular Therapy - Oncolytics*. 24, 288–298. doi:10.1016/j.omto.2021.12.026.

Hubbard, A.K. & Rothlein, R. (2000) Intercellular adhesion molecule-1 (ICAM-1) expression and cell signaling cascades. *Free Radical Biology & Medicine*. 28 (9), 1379–1386. doi:10.1016/s0891-5849(00)00223-9.

Huertas, A., Tu, L., Humbert, M. & Guignabert, C. (2020) Chronic inflammation within the vascular wall in pulmonary arterial hypertension: more than a spectator. *Cardiovascular Research*. 116 (5), 885–893. doi:10.1093/cvr/cvz308.

Humbert, M., Guignabert, C., Bonnet, S., Dorfmüller, P., Klinger, J.R., Nicolls, M.R., Olschewski, A.J., Pullamsetti, S.S., Schermuly, R.T., Stenmark, K.R. & Rabinovitch, M. (2019) Pathology and pathobiology of pulmonary hypertension: state of the art and research perspectives. *The European Respiratory Journal*. 53 (1), 1801887. doi:10.1183/13993003.01887-2018.

Humbert, M., Kovacs, G., Hoeper, M.M., Badagliacca, R., Berger, R.M.F., et al. (2022) 2022 ESC/ERS Guidelines for the diagnosis and treatment of pulmonary hypertension. *European Heart Journal*. 43 (38), 3618–3731. doi:10.1093/eurheartj/ehac237.

Humbert, M., Morrell, N.W., Archer, S.L., Stenmark, K.R., MacLean, M.R., Lang, I.M., Christman, B.W., Weir, E.K., Eickelberg, O., Voelkel, N.F. & Rabinovitch, M. (2004) Cellular and molecular pathobiology of pulmonary arterial hypertension. *Journal of the American College of Cardiology*. 43 (12 Suppl S), 13S-24S. doi:10.1016/j.jacc.2004.02.029.

Hurst, L.A., Dunmore, B.J., Long, L., Crosby, A., Al-Lamki, R., Deighton, J., Southwood, M., Yang, X., Nikolic, M.Z., Herrera, B., Inman, G.J., Bradley, J.R., Rana, A.A., Upton, P.D. & Morrell, N.W. (2017) TNFα drives pulmonary arterial hypertension by suppressing the BMP type-II receptor and altering NOTCH signalling. *Nature Communications*. 8, 14079. doi:10.1038/ncomms14079.

Ingber, D.E. (2018) Developmentally inspired human 'organs on chips'. *Development (Cambridge, England)*. 145 (16), dev156125. doi:10.1242/dev.156125.

Ito, G., Uchiyama, M., Kondo, M., Mori, S., Usami, N., Maeda, O., Kawabe, T., Hasegawa, Y., Shimokata, K. & Sekido, Y. (2004) Krüppel-like factor 6 is frequently down-regulated and induces apoptosis in non-small cell lung cancer cells. *Cancer Research*. 64 (11), 3838–3843. doi:10.1158/0008-5472.CAN-04-0185.

Itoh, T., Nagaya, N., Ishibashi-Ueda, H., Kyotani, S., Oya, H., Sakamaki, F., Kimura, H. & Nakanishi, N. (2006) Increased plasma monocyte chemoattractant protein-1 level in idiopathic pulmonary arterial hypertension. *Respirology*. 11 (2), 158–163. doi:10.1111/j.1440-1843.2006.00821.x.

Jain, V., Bordes, S.J. & Bhardwaj, A. (2023) Physiology, Pulmonary Circulatory System. In: *StatPearls*. Treasure Island (FL), StatPearls Publishing. p. http://www.ncbi.nlm.nih.gov/books/NBK525948/.

Jandl, K., Marsh, L.M., Hoffmann, J., Mutgan, A.C., Baum, O., Bloch, W., Thekkekara-Puthenparampil, H., Kolb, D., Sinn, K., Klepetko, W., Heinemann, A., Olschewski, A., Olschewski, H. & Kwapiszewska, G. (2020) Basement Membrane Remodeling Controls Endothelial Function in Idiopathic Pulmonary Arterial Hypertension. *American Journal of Respiratory Cell and Molecular Biology*. 63 (1), 104–117. doi:10.1165/rcmb.2019-0303OC.

Jia, Z., Wang, S., Yan, H., Cao, Y., Zhang, X., Wang, L., Zhang, Z., Lin, S., Wang, X. & Mao, J. (2023) Pulmonary Vascular Remodeling in Pulmonary Hypertension. *Journal of Personalized Medicine*. 13 (2), 366. doi:10.3390/jpm13020366.

Jin, Q., Bhatta, A., Pagaduan, J.V., Chen, X., West-Foyle, H., Liu, J., Hou, A., Berkowitz, D., Kuo, S.C., Askin, F.B., Nguyen, T.D., Gracias, D.H. & Romer, L.H. (2020) Biomimetic human small muscular pulmonary arteries. *Science Advances*. 6 (13), eaaz2598. doi:10.1126/sciadv.aaz2598.

Jones, C., Bisserier, M., Bueno-Beti, C., Bonnet, G., Neves-Zaph, S., Lee, S.-Y., Milara, J., Dorfmüller, P., Humbert, M., Leopold, J.A., Hadri, L., Hajjar, R.J. & Sassi, Y. (2020) A novel secreted-cAMP pathway inhibits pulmonary hypertension via a feed-forward mechanism. *Cardiovascular Research*. 116 (8), 1500–1513. doi:10.1093/cvr/cvz244.

Jones, P.L., Cowan, K.N. & Rabinovitch, M. (1997) Tenascin-C, proliferation and subendothelial fibronectin in progressive pulmonary vascular disease. *The American Journal of Pathology*. 150 (4), 1349–1360.

Katoh, K. (2023) Effects of Mechanical Stress on Endothelial Cells In Situ and In Vitro. *International Journal of Molecular Sciences*. 24 (22), 16518. doi:10.3390/ijms242216518.

Kawanami, D., Mahabeleshwar, G.H., Lin, Z., Atkins, G.B., Hamik, A., Haldar, S.M., Maemura, K., Lamanna, J.C. & Jain, M.K. (2009) Kruppel-like factor 2 inhibits hypoxia-inducible factor 1alpha expression and function in the endothelium. *The Journal of Biological Chemistry*. 284 (31), 20522–20530. doi:10.1074/jbc.M109.025346.

Kendall, R.T. & Feghali-Bostwick, C.A. (2014) Fibroblasts in fibrosis: novel roles and mediators. *Frontiers in Pharmacology*. 5, 123. doi:10.3389/fphar.2014.00123.

Kerstjens-Frederikse, W.S., Bongers, E.M.H.F., Roofthooft, M.T.R., Leter, E.M., Douwes, J.M., Van Dijk, A., Vonk-Noordegraaf, A., Dijk-Bos, K.K., Hoefsloot, L.H., Hoendermis, E.S., Gille, J.J.P., Sikkema-Raddatz, B., Hofstra, R.M.W. & Berger, R.M.F. (2013) TBX4 mutations (small patella syndrome) are associated with childhood-onset pulmonary arterial hypertension. *Journal of Medical Genetics*. 50 (8), 500–506. doi:10.1136/jmedgenet-2012-101152.

Kierans, S.J. & Taylor, C.T. (2021) Regulation of glycolysis by the hypoxia-inducible factor (HIF): implications for cellular physiology. *The Journal of Physiology*. 599 (1), 23–37. doi:10.1113/JP280572.

Kim, G.-D., Ng, H.P., Chan, E.R. & Mahabeleshwar, G.H. (2020) Kruppel-like factor 6 promotes macrophage inflammatory and hypoxia response. *FASEB journal: official publication of the Federation of American Societies for Experimental Biology*. 34 (2), 3209–3223. doi:10.1096/fj.201902221R.

Kim, M., Kim, S., Lim, J.H., Lee, C., Choi, H.C. & Woo, C.-H. (2012) Laminar Flow Activation of ERK5 Protein in Vascular Endothelium Leads to Atheroprotective

Effect via NF-E2-related Factor 2 (Nrf2) Activation. *The Journal of Biological Chemistry*. 287 (48), 40722–40731. doi:10.1074/jbc.M112.381509.

Kim, Y., Ratziu, V., Choi, S.G., Lalazar, A., Theiss, G., Dang, Q., Kim, S.J. & Friedman, S.L. (1998) Transcriptional activation of transforming growth factor beta1 and its receptors by the Kruppel-like factor Zf9/core promoter-binding protein and Sp1. Potential mechanisms for autocrine fibrogenesis in response to injury. *The Journal of Biological Chemistry*. 273 (50), 33750–33758. doi:10.1074/jbc.273.50.33750.

Klouda, T. & Yuan, K. (2021) Inflammation in Pulmonary Arterial Hypertension. In: Y.-X. Wang (ed.). *Lung Inflammation in Health and Disease, Volume I*. Advances in Experimental Medicine and Biology. Cham, Springer International Publishing. pp. 351–372. doi:10.1007/978-3-030-63046-1_19.

Koehler, R., Grünig, E., Pauciulo, M.W., Hoeper, M.M., Olschewski, H., Wilkens, H., Halank, M., Winkler, J., Ewert, R., Bremer, H., Kreuscher, S., Janssen, B. & Nichols, W.C. (2004) Low frequency of BMPR2 mutations in a German cohort of patients with sporadic idiopathic pulmonary arterial hypertension. *Journal of Medical Genetics*. 41 (12), e127–e127. doi:10.1136/jmg.2004.023101.

Kojima, S., Hayashi, S., Shimokado, K., Suzuki, Y., Shimada, J., Crippa, M.P. & Friedman, S.L. (2000) Transcriptional activation of urokinase by the Krüppel-like factor Zf9/COPEB activates latent TGF-beta1 in vascular endothelial cells. *Blood*. 95 (4), 1309–1316.

Kolde, R. (2019) pheatmap: Pretty Heatmaps. *R package version 1.0.12*. https://cran.r-project.org/web/packages/pheatmap/index.html.

Kolton Schneider, L., Ali, Y.S. & Agnew, J.D. (2023) Scleroderma-Associated Pulmonary Arterial Hypertension: Early Detection for Better Outcomes. In: *StatPearls*. Treasure Island (FL), StatPearls Publishing. p. http://www.ncbi.nlm.nih.gov/books/NBK576387/.

Kondo, T., Okumura, N., Adachi, S. & Murohara, T. (2019) Pulmonary Hypertension: Diagnosis, Management, and Treatment. *Nagoya Journal of Medical Science*. 81 (1), 19–30. doi:10.18999/nagjms.81.1.19.

Koritschoner, N.P., Bocco, J.L., Panzetta-Dutari, G.M., Dumur, C.I., Flury, A. & Patrito, L.C. (1997) A novel human zinc finger protein that interacts with the core promoter element of a TATA box-less gene. *The Journal of Biological Chemistry*. 272 (14), 9573–9580. doi:10.1074/jbc.272.14.9573.

Kourdova, L.T., Miranda, A.L., Racca, A.C., Rojas, M.L., Del Puerto, M.C., Castro, C., Genti-Raimondi, S. & Panzetta-Dutari, G.M. (2022) Downregulation of krüppel-like factor 6 expression modulates extravillous trophoblast cell behavior by increasing reactive oxygen species. *Placenta*. 127, 62–72. doi:10.1016/j.placenta.2022.08.002.

Kourembanas, S., Hannan, R.L. & Faller, D.V. (1990) Oxygen tension regulates the expression of the platelet-derived growth factor-B chain gene in human endothelial cells. *The Journal of Clinical Investigation*. 86 (2), 670–674. doi:10.1172/JCI114759.

Kourembanas, S., Marsden, P.A., McQuillan, L.P. & Faller, D.V. (1991) Hypoxia induces endothelin gene expression and secretion in cultured human endothelium. *The Journal of Clinical Investigation*. 88 (3), 1054–1057. doi:10.1172/JCI115367.

Krassowski, M., Arts, M., Lagger, C. & Max (2022) *krassowski/complex-upset: v1.3.5*. doi:10.5281/zenodo.7314197.

Kudryashova, T.V., Goncharov, D.A., Pena, A., Kelly, N., Vanderpool, R., et al. (2016) HIPPO-Integrin-linked Kinase Cross-Talk Controls Self-Sustaining Proliferation and Survival in Pulmonary Hypertension. *American Journal of Respiratory and Critical Care Medicine*. 194 (7), 866–877. doi:10.1164/rccm.201510-2003OC.

Kumar, A., Lin, Z., SenBanerjee, S. & Jain, M.K. (2005) Tumor necrosis factor alpha-mediated reduction of KLF2 is due to inhibition of MEF2 by NF-kappaB and histone deacetylases. *Molecular and Cellular Biology*. 25 (14), 5893–5903. doi:10.1128/MCB.25.14.5893-5903.2005.

Kuo, C.T., Veselits, M.L., Barton, K.P., Lu, M.M., Clendenin, C. & Leiden, J.M. (1997) The LKLF transcription factor is required for normal tunica media formation and blood vessel stabilization during murine embryogenesis. *Genes & Development*. 11 (22), 2996–3006. doi:10.1101/gad.11.22.2996.

Kurakula, K., Smolders, V.F.E.D., Tura-Ceide, O., Jukema, J.W., Quax, P.H.A. & Goumans, M.-J. (2021) Endothelial Dysfunction in Pulmonary Hypertension: Cause or Consequence? *Biomedicines*. 9 (1), 57. doi:10.3390/biomedicines9010057.

Kutikhin, A.G., Tupikin, A.E., Matveeva, V.G., Shishkova, D.K., Antonova, L.V., Kabilov, M.R. & Velikanova, E.A. (2020) Human Peripheral Blood-Derived Endothelial Colony-Forming Cells Are Highly Similar to Mature Vascular Endothelial Cells yet Demonstrate a Transitional Transcriptomic Signature. *Cells*. 9 (4), 876. doi:10.3390/cells9040876.

Lahm, T. & Kawut, S.M. (2017) Inhibiting oestrogen signalling in pulmonary arterial hypertension: sex, drugs and research. *The European Respiratory Journal*. 50 (2), 1700983. doi:10.1183/13993003.00983-2017.

Laitman, B.M., Asp, L., Mariani, J.N., Zhang, J., Liu, J., et al. (2016) The Transcriptional Activator Krüppel-like Factor-6 Is Required for CNS Myelination. *PLoS Biology*. 14 (5), e1002467. doi:10.1371/journal.pbio.1002467.

Lamb, J., Crawford, E.D., Peck, D., Modell, J.W., Blat, I.C., et al. (2006) The Connectivity Map: using gene-expression signatures to connect small molecules, genes, and disease. *Science (New York, N.Y.)*. 313 (5795), 1929–1935. doi:10.1126/science.1132939.

Lane, K.B., Machado, R.D., Pauciulo, M.W., Thomson, J.R., Phillips, J.A., Loyd, J.E., Nichols, W.C. & Trembath, R.C. (2000) Heterozygous germline mutations in BMPR2, encoding a TGF-β receptor, cause familial primary pulmonary hypertension. *Nature Genetics*. 26 (1), 81–84. doi:10.1038/79226.

Lau, E.M.T., Giannoulatou, E., Celermajer, D.S. & Humbert, M. (2017) Epidemiology and treatment of pulmonary arterial hypertension. *Nature Reviews Cardiology*. 14 (10), 603–614. doi:10.1038/nrcardio.2017.84.

Le Hiress, M., Tu, L., Ricard, N., Phan, C., Thuillet, R., Fadel, E., Dorfmüller, P., Montani, D., de Man, F., Humbert, M., Huertas, A. & Guignabert, C. (2015) Proinflammatory Signature of the Dysfunctional Endothelium in Pulmonary Hypertension. Role of the Macrophage Migration Inhibitory Factor/CD74 Complex. *American Journal of Respiratory and Critical Care Medicine*. 192 (8), 983–997. doi:10.1164/rccm.201402-0322OC.

Lee, J.S., Yu, Q., Shin, J.T., Sebzda, E., Bertozzi, C., Chen, M., Mericko, P., Stadtfeld, M., Zhou, D., Cheng, L., Graf, T., MacRae, C.A., Lepore, J.J., Lo, C.W. & Kahn, M.L. (2006) Klf2 is an essential regulator of vascular hemodynamic forces in vivo. *Developmental Cell*. 11 (6), 845–857. doi:10.1016/j.devcel.2006.09.006.

Lee, M.Y., Luciano, A.K., Ackah, E., Rodriguez-Vita, J., Bancroft, T.A., Eichmann, A., Simons, M., Kyriakides, T.R., Morales-Ruiz, M. & Sessa, W.C. (2014) Endothelial Akt1 mediates angiogenesis by phosphorylating multiple angiogenic substrates. *Proceedings of the National Academy of Sciences of the United States of America*. 111 (35), 12865–12870. doi:10.1073/pnas.1408472111.

Lei, W., He, Y., Shui, X., Li, G., Yan, G., Zhang, Y., Huang, S., Chen, C. & Ding, Y. (2016) Expression and analyses of the HIF-1 pathway in the lungs of humans with pulmonary arterial hypertension. *Molecular Medicine Reports*. 14 (5), 4383–4390. doi:10.3892/mmr.2016.5752.

Leopold, J.A. (2021) Inhibiting Jak2 Ameliorates Pulmonary Hypertension: Fulfilling the Promise of Precision Medicine. *American Journal of Respiratory Cell and Molecular Biology*. 64 (1), 12–13. doi:10.1165/rcmb.2020-0384ED.

Leung, C.M., de Haan, P., Ronaldson-Bouchard, K., Kim, G.-A., Ko, J., Rho, H.S., Chen, Z., Habibovic, P., Jeon, N.L., Takayama, S., Shuler, M.L., Vunjak-Novakovic, G., Frey, O., Verpoorte, E. & Toh, Y.-C. (2022) A guide to the organ-on-a-chip. *Nature Reviews Methods Primers*. 2 (1), 1–29. doi:10.1038/s43586-022-00118-6.

Levy, M., Eyries, M., Szezepanski, I., Ladouceur, M., Nadaud, S., Bonnet, D. & Soubrier, F. (2016) Genetic analyses in a cohort of children with pulmonary hypertension. *European Respiratory Journal*. 48 (4), 1118–1126. doi:10.1183/13993003.00211-2016.

Lévy, M., Maurey, C., Celermajer, D.S., Vouhé, P.R., Danel, C., Bonnet, D. & Israël-Biet, D. (2007) Impaired apoptosis of pulmonary endothelial cells is associated with intimal proliferation and irreversibility of pulmonary hypertension in congenital heart disease.

Journal of the American College of Cardiology. 49 (7), 803–810. doi:10.1016/j.jacc.2006.09.049.

Li, B., Teng, C., Yu, H., Jiang, X., Xing, X., Jiang, Q., Lin, C., Zhao, Z., Zhang, R. & He, W. (2023a) Alleviating experimental pulmonary hypertension via co-delivering FoxO1 stimulus and apoptosis activator to hyperproliferating pulmonary arteries. *Acta Pharmaceutica Sinica B*. 13 (6), 2369–2382. doi:10.1016/j.apsb.2022.12.002.

Li, D., Yea, S., Li, S., Chen, Z., Narla, G., Banck, M., Laborda, J., Tan, S., Friedman, J.M., Friedman, S.L. & Walsh, M.J. (2005) Krüppel-like Factor-6 Promotes Preadipocyte Differentiation through Histone Deacetylase 3-dependent Repression of DLK1*. *Journal of Biological Chemistry*. 280 (29), 26941–26952. doi:10.1074/jbc.M500463200.

Li, H., Zhou, W.-Y., Xia, Y.-Y. & Zhang, J.-X. (2022) Endothelial Mechanosensors for Atheroprone and Atheroprotective Shear Stress Signals. *Journal of Inflammation Research*. 15, 1771–1783. doi:10.2147/JIR.S355158.

Li, J., Yu, D., He, C., Yu, Q., Huo, Z., Zhang, Y. & Zhang, S. (2023b) KLF6 alleviates hepatic ischemia-reperfusion injury by inhibiting autophagy. *Cell Death & Disease*. 14 (7), 393. doi:10.1038/s41419-023-05872-3.

Li, P. & Fan, H. (2023) Pericyte Loss in Diseases. *Cells*. 12 (15), 1931. doi:10.3390/cells12151931.

Li, X. & Wang, C.-Y. (2021) From bulk, single-cell to spatial RNA sequencing. *International Journal of Oral Science*. 13 (1), 36. doi:10.1038/s41368-021-00146-0.

Li, Y., Li, Y., Li, L., Yin, M., Wang, J. & Li, X. (2021) PKR deficiency alleviates pulmonary hypertension via inducing inflammasome adaptor ASC inactivation. *Pulmonary Circulation*. 11 (4), 20458940211046156. doi:10.1177/20458940211046156.

Liang, S., Desai, A.A., Black, S.M. & Tang, H. (2021) Cytokines, Chemokines, and Inflammation in Pulmonary Arterial Hypertension. In: Y.-X. Wang (ed.). *Lung Inflammation in Health and Disease, Volume I*. Advances in Experimental Medicine and Biology. Cham, Springer International Publishing. pp. 275–303. doi:10.1007/978-3-030-63046-1_15.

Liang, X., Arullampalam, P., Yang, Z. & Ming, X.-F. (2019) Hypoxia Enhances Endothelial Intercellular Adhesion Molecule 1 Protein Level Through Upregulation of Arginase Type II and Mitochondrial Oxidative Stress. *Frontiers in Physiology*. 10, 1003. doi:10.3389/fphys.2019.01003.

Liao, Y., Wang, J., Jaehnig, E.J., Shi, Z. & Zhang, B. (2019) WebGestalt 2019: gene set analysis toolkit with revamped UIs and APIs. *Nucleic Acids Research*. 47 (W1), W199–W205. doi:10.1093/nar/gkz401.

Lin, K., Hsu, P.-P., Chen, B.P., Yuan, S., Usami, S., Shyy, J.Y.-J., Li, Y.-S. & Chien, S. (2000) Molecular mechanism of endothelial growth arrest by laminar shear stress.

Proceedings of the National Academy of Sciences. 97 (17), 9385–9389. doi:10.1073/pnas.170282597.

Liu, J., Du, T., Yuan, Y., He, Y., Tan, Z. & Liu, Z. (2010) KLF6 inhibits estrogen receptor-mediated cell growth in breast cancer via a c-Src-mediated pathway. *Molecular and Cellular Biochemistry*. 335 (1–2), 29–35. doi:10.1007/s11010-009-0237-8.

Long, L., Ormiston, M.L., Yang, X., Southwood, M., Gräf, S., Machado, R.D., Mueller, M., Kinzel, B., Yung, L.M., Wilkinson, J.M., Moore, S.D., Drake, K.M., Aldred, M.A., Yu, P.B., Upton, P.D. & Morrell, N.W. (2015) Selective enhancement of endothelial BMPR-II with BMP9 reverses pulmonary arterial hypertension. *Nature Medicine*. 21 (7), 777–785. doi:10.1038/nm.3877.

Looney, A.P., Han, R., Stawski, L., Marden, G., Iwamoto, M. & Trojanowska, M. (2017) Synergistic Role of Endothelial ERG and FLI1 in Mediating Pulmonary Vascular Homeostasis. *American Journal of Respiratory Cell and Molecular Biology*. 57 (1), 121–131. doi:10.1165/rcmb.2016-0200OC.

Love, M.I., Huber, W. & Anders, S. (2014) Moderated estimation of fold change and dispersion for RNA-seq data with DESeq2. *Genome Biology*. 15 (12), 550. doi:10.1186/s13059-014-0550-8.

Lunt, S.Y., Muralidhar, V., Hosios, A.M., Israelsen, W.J., Gui, D.Y., et al. (2015) Pyruvate kinase isoform expression alters nucleotide synthesis to impact cell proliferation. *Molecular Cell*. 57 (1), 95–107. doi:10.1016/j.molcel.2014.10.027.

Luo, H., Liu, B., Zhao, L., He, J., Li, T., Zha, L., Li, X., Qi, Q., Liu, Y. & Yu, Z. (2017) Galectin-3 mediates pulmonary vascular remodeling in hypoxia-induced pulmonary arterial hypertension. *Journal of the American Society of Hypertension: JASH*. 11 (10), 673-683.e3. doi:10.1016/j.jash.2017.07.009.

Ma, L., Roman-Campos, D., Austin, E.D., Eyries, M., Sampson, K.S., Soubrier, F., Germain, M., Trégouët, D.-A., Borczuk, A., Rosenzweig, E.B., Girerd, B., Montani, D., Humbert, M., Loyd, J.E., Kass, R.S. & Chung, W.K. (2013) A novel channelopathy in pulmonary arterial hypertension. *The New England Journal of Medicine*. 369 (4), 351–361. doi:10.1056/NEJMoa1211097.

Maarman, G., Lecour, S., Butrous, G., Thienemann, F. & Sliwa, K. (2013) A comprehensive review: the evolution of animal models in pulmonary hypertension research; are we there yet? *Pulmonary Circulation*. 3 (4), 739–756. doi:10.1086/674770.

Machado, R.D., Pauciulo, M.W., Thomson, J.R., Lane, K.B., Morgan, N.V., et al. (2001) BMPR2 haploinsufficiency as the inherited molecular mechanism for primary pulmonary hypertension. *American Journal of Human Genetics*. 68 (1), 92–102. doi:10.1086/316947.

Machado, R.D., Southgate, L., Eichstaedt, C.A., Aldred, M.A., Austin, E.D., et al. (2015) Pulmonary Arterial Hypertension: A Current Perspective on Established and

Emerging Molecular Genetic Defects. *Human mutation*. 36 (12), 1113–1127. doi:10.1002/humu.22904.

Mahmoud, M., Upton, P.D. & Arthur, H.M. (2011) Angiogenesis regulation by TGFβ signalling: clues from an inherited vascular disease. *Biochemical Society Transactions*. 39 (6), 1659–1666. doi:10.1042/BST20110664.

Mahmoud, M.M., Serbanovic-Canic, J., Feng, S., Souilhol, C., Xing, R., Hsiao, S., Mammoto, A., Chen, J., Ariaans, M., Francis, S.E., Van der Heiden, K., Ridger, V. & Evans, P.C. (2017) Shear stress induces endothelial-to-mesenchymal transition via the transcription factor Snail. *Scientific Reports*. 7, 3375. doi:10.1038/s41598-017-03532-z.

Mahomed, A.S., Burke-Gaffney, A., Moledina, S. & Wort, S.J. (2019) S98 The effects of BMPRII loss on endothelial shear adaptation in the pulmonary vascular endothelium. *Thorax*. 74 (Suppl 2), A61–A61. doi:10.1136/thorax-2019-BTSabstracts2019.104.

Malhotra, R., Paskin-Flerlage, S., Zamanian, R.T., Zimmerman, P., Schmidt, J.W., Deng, D.Y., Southwood, M., Spencer, R., Lai, C.S., Parker, W., Channick, R.N., Morrell, N.W., Elliott, C.G. & Yu, P.B. (2013) Circulating angiogenic modulatory factors predict survival and functional class in pulmonary arterial hypertension. *Pulmonary Circulation*. 3 (2), 369–380. doi:10.4103/2045-8932.110445.

Mandras, S., Kovacs, G., Olschewski, H., Broderick, M., Nelsen, A., Shen, E. & Champion, H. (2021) Combination Therapy in Pulmonary Arterial Hypertension—Targeting the Nitric Oxide and Prostacyclin Pathways. *Journal of Cardiovascular Pharmacology and Therapeutics*. 26 (5), 453–462. doi:10.1177/10742484211006531.

Marcu, R., Choi, Y.J., Xue, J., Fortin, C.L., Wang, Y., Nagao, R.J., Xu, J., MacDonald, J.W., Bammler, T.K., Murry, C.E., Muczynski, K., Stevens, K.R., Himmelfarb, J., Schwartz, S.M. & Zheng, Y. (2018) Human Organ-Specific Endothelial Cell Heterogeneity. *iScience*. 4, 20–35. doi:10.1016/j.isci.2018.05.003.

Maron, B.A. (2023) Revised Definition of Pulmonary Hypertension and Approach to Management: A Clinical Primer. *Journal of the American Heart Association*. 12 (8), e029024. doi:10.1161/JAHA.122.029024.

Marsh, L.M., Jandl, K., Grünig, G., Foris, V., Bashir, M., Ghanim, B., Klepetko, W., Olschewski, H., Olschewski, A. & Kwapiszewska, G. (2018) The inflammatory cell landscape in the lungs of patients with idiopathic pulmonary arterial hypertension. *The European Respiratory Journal*. 51 (1), 1701214. doi:10.1183/13993003.01214-2017.

Masilamani, A.P., Ferrarese, R., Kling, E., Thudi, N.K., Kim, H., Scholtens, D.M., Dai, F., Hadler, M., Unterkircher, T., Platania, L., Weyerbrock, A., Prinz, M., Gillespie, G.Y., Harsh IV, G.R., Bredel, M. & Carro, M.S. (2017) KLF6 depletion promotes NF-κB signaling in glioblastoma. *Oncogene*. 36 (25), 3562–3575. doi:10.1038/onc.2016.507.

Masri, F.A., Xu, W., Comhair, S.A.A., Asosingh, K., Koo, M., Vasanji, A., Drazba, J., Anand-Apte, B. & Erzurum, S.C. (2007) Hyperproliferative apoptosis-resistant endothelial cells in idiopathic pulmonary arterial hypertension. *American Journal of Physiology. Lung Cellular and Molecular Physiology*. 293 (3), L548-554. doi:10.1152/ajplung.00428.2006.

Mastej, V., Axen, C., Wary, A., Minshall, R.D. & Wary, K.K. (2022) A requirement for Krüppel Like Factor-4 in the maintenance of endothelial cell quiescence. *Frontiers in Cell and Developmental Biology*. 10, 1003028. doi:10.3389/fcell.2022.1003028.

Matsui, K., Takano, Y., Yu, Z.-X., Hi, J.E.S., Stetler-Stevenson, W.G., Travis, W.D. & Ferrans, V.J. (2002) Immunohistochemical study of endothelin-1 and matrix metalloproteinases in plexogenic pulmonary arteriopathy. *Pathology, Research and Practice*. 198 (6), 403–412. doi:10.1078/0344-0338-00273.

Matsumoto, N., Kubo, A., Liu, H., Akita, K., Laub, F., Ramirez, F., Keller, G. & Friedman, S.L. (2006) Developmental regulation of yolk sac hematopoiesis by Krüppel-like factor 6. *Blood*. 107 (4), 1357–1365. doi:10.1182/blood-2005-05-1916.

McConnell, B.B. & Yang, V.W. (2010) Mammalian Krüppel-like factors in health and diseases. *Physiological Reviews*. 90 (4), 1337–1381. doi:10.1152/physrev.00058.2009.

Medina, R.J., O'Neill, C.L., O'Doherty, T.M., Wilson, S.E.J. & Stitt, A.W. (2012) Endothelial Progenitors as Tools to Study Vascular Disease. *Stem Cells International*. 2012, 346735. doi:10.1155/2012/346735.

Melero-Martin, J.M. (2022) Human Endothelial Colony-Forming Cells. *Cold Spring Harbor Perspectives in Medicine*. 12 (12), a041154. doi:10.1101/cshperspect.a041154.

Michelakis, E.D., Gurtu, V., Webster, L., Barnes, G., Watson, G., et al. (2017) Inhibition of pyruvate dehydrogenase kinase improves pulmonary arterial hypertension in genetically susceptible patients. *Science Translational Medicine*. 9 (413), eaao4583. doi:10.1126/scitranslmed.aao4583.

Mironov, A.A., Mironov, A., Sanavio, B., Krol, S. & Beznoussenko, G.V. (2023) Intracellular Membrane Transport in Vascular Endothelial Cells. *International Journal of Molecular Sciences*. 24 (6), 5791. doi:10.3390/ijms24065791.

Mitra, R., O'Neil, G.L., Harding, I.C., Cheng, M.J., Mensah, S.A. & Ebong, E.E. (2017) Glycocalyx in Atherosclerosis-Relevant Endothelium Function and as a Therapeutic Target. *Current Atherosclerosis Reports*. 19 (12), 63. doi:10.1007/s11883-017-0691-9.

Miyata, M., Sakuma, F., Yoshimura, A., Ishikawa, H., Nishimaki, T. & Kasukawa, R. (2009) Pulmonary Hypertension in Rats 2.: Role of lnterleukin-6. *International Archives of Allergy and Immunology*. 108 (3), 287–291. doi:10.1159/000237166.

Mizuno, S., Bogaard, H.J., Kraskauskas, D., Alhussaini, A., Gomez-Arroyo, J., Voelkel, N.F. & Ishizaki, T. (2011) p53 Gene deficiency promotes hypoxia-induced pulmonary hypertension and vascular remodeling in mice. *American Journal of Physiology-Lung Cellular and Molecular Physiology*. 300 (5), L753–L761. doi:10.1152/ajplung.00286.2010.

Mochizuki, S., Vink, H., Hiramatsu, O., Kajita, T., Shigeto, F., Spaan, J.A.E. & Kajiya, F. (2003) Role of hyaluronic acid glycosaminoglycans in shear-induced endothelium-derived nitric oxide release. *American Journal of Physiology-Heart and Circulatory Physiology*. 285 (2), H722–H726. doi:10.1152/ajpheart.00691.2002.

Morello, F., Perino, A. & Hirsch, E. (2009) Phosphoinositide 3-kinase signalling in the vascular system. *Cardiovascular Research*. 82 (2), 261–271. doi:10.1093/cvr/cvn325.

Morisaki, H., Nakanishi, N., Kyotani, S., Takashima, A., Tomoike, H. & Morisaki, T. (2004) BMPR2 mutations found in Japanese patients with familial and sporadic primary pulmonary hypertension. *Human Mutation*. 23 (6), 632–632. doi:10.1002/humu.9251.

Mukhopadhyay, D., Tsiokas, L., Zhou, X.M., Foster, D., Brugge, J.S. & Sukhatme, V.P. (1995) Hypoxic induction of human vascular endothelial growth factor expression through c-Src activation. *Nature*. 375 (6532), 577–581. doi:10.1038/375577a0.

Murata, T., Kinoshita, K., Hori, M., Kuwahara, M., Tsubone, H., Karaki, H. & Ozaki, H. (2005) Statin protects endothelial nitric oxide synthase activity in hypoxia-induced pulmonary hypertension. *Arteriosclerosis, Thrombosis, and Vascular Biology*. 25 (11), 2335–2342. doi:10.1161/01.ATV.0000186184.33537.48.

Mushaben, E.M., Hershey, G.K., Pauciulo, M.W., Nichols, W.C. & Cras, T.D.L. (2012) Chronic Allergic Inflammation Causes Vascular Remodeling and Pulmonary Hypertension in Bmpr2 Hypomorph and Wild-Type Mice. *PLOS ONE*. 7 (3), e32468. doi:10.1371/journal.pone.0032468.

Nagel, T., Resnick, N., Dewey, C.F. & Gimbrone, M.A. (1999) Vascular endothelial cells respond to spatial gradients in fluid shear stress by enhanced activation of transcription factors. *Arteriosclerosis, Thrombosis, and Vascular Biology*. 19 (8), 1825–1834. doi:10.1161/01.atv.19.8.1825.

Nakajima, H. & Mochizuki, N. (2017) Flow pattern-dependent endothelial cell responses through transcriptional regulation. *Cell Cycle*. 16 (20), 1893–1901. doi:10.1080/15384101.2017.1364324.

Napetschnig, J. & Wu, H. (2013) Molecular Basis of NF-κB Signaling. *Annual review of biophysics*. 42, 443–468. doi:10.1146/annurev-biophys-083012-130338.

Narla, G., Difeo, A., Reeves, H.L., Schaid, D.J., Hirshfeld, J., et al. (2005) A germline DNA polymorphism enhances alternative splicing of the KLF6 tumor suppressor gene and is associated with increased prostate cancer risk. *Cancer Research*. 65 (4), 1213–1222. doi:10.1158/0008-5472.CAN-04-4249.

Narla, G., Heath, K.E., Reeves, H.L., Li, D., Giono, L.E., Kimmelman, A.C., Glucksman, M.J., Narla, J., Eng, F.J., Chan, A.M., Ferrari, A.C., Martignetti, J.A. & Friedman, S.L. (2001) KLF6, a candidate tumor suppressor gene mutated in prostate cancer. *Science (New York, N.Y.)*. 294 (5551), 2563–2566. doi:10.1126/science.1066326.

Nasim, M.T., Ogo, T., Ahmed, M., Randall, R., Chowdhury, H.M., et al. (2011) Molecular genetic characterization of SMAD signaling molecules in pulmonary arterial hypertension. *Human Mutation*. 32 (12), 1385–1389. doi:10.1002/humu.21605.

Nave, A.H., Mižíková, I., Niess, G., Steenbock, H., Reichenberger, F., Talavera, M.L., Veit, F., Herold, S., Mayer, K., Vadász, I., Weissmann, N., Seeger, W., Brinckmann, J. & Morty, R.E. (2014) Lysyl oxidases play a causal role in vascular remodeling in clinical and experimental pulmonary arterial hypertension. *Arteriosclerosis, Thrombosis, and Vascular Biology*. 34 (7), 1446–1458. doi:10.1161/ATVBAHA.114.303534.

Nayak, L., Lin, Z. & Jain, M.K. (2011) "Go With the Flow": How Krüppel-Like Factor 2 Regulates the Vasoprotective Effects of Shear Stress. *Antioxidants & Redox Signaling*. 15 (5), 1449–1461. doi:10.1089/ars.2010.3647.

Ni, S., Ji, T., Dong, J., Chen, F., Feng, H., Zhao, H., Chen, D. & Ma, W. (2022) Immune Cells in Pulmonary Arterial Hypertension. *Heart, Lung and Circulation*. 31 (7), 934–943. doi:10.1016/j.hlc.2022.02.007.

Nicoleau, S., Fellows, A. & Wojciak-Stothard, B. (2021) Role of Krüppel-like factors in pulmonary arterial hypertension. *The International Journal of Biochemistry & Cell Biology*. 134, 105977. doi:10.1016/j.biocel.2021.105977.

Nicolls, M.R., Mizuno, S., Taraseviciene-Stewart, L., Farkas, L., Drake, J.I., Al Husseini, A., Gomez-Arroyo, J.G., Voelkel, N.F. & Bogaard, H.J. (2012) New models of pulmonary hypertension based on VEGF receptor blockade-induced endothelial cell apoptosis. *Pulmonary Circulation*. 2 (4), 434–442. doi:10.4103/2045-8932.105031.

Nikitopoulou, I., Orfanos, S.E., Kotanidou, A., Maltabe, V., Manitsopoulos, N., Karras, P., Kouklis, P., Armaganidis, A. & Maniatis, N.A. (2016) Vascular endothelial-cadherin downregulation as a feature of endothelial transdifferentiation in monocrotaline-induced pulmonary hypertension. *American Journal of Physiology. Lung Cellular and Molecular Physiology*. 311 (2), L352-363. doi:10.1152/ajplung.00156.2014.

Noria, S., Xu, F., McCue, S., Jones, M., Gotlieb, A.I. & Langille, B.L. (2004) Assembly and Reorientation of Stress Fibers Drives Morphological Changes to Endothelial Cells Exposed to Shear Stress. *The American Journal of Pathology*. 164 (4), 1211–1223.

O'Neill, C.L., McLoughlin, K.J., Chambers, S.E.J., Guduric-Fuchs, J., Stitt, A.W. & Medina, R.J. (2018) The Vasoreparative Potential of Endothelial Colony Forming Cells: A Journey Through Pre-clinical Studies. *Frontiers in Medicine*. 5, 273. doi:10.3389/fmed.2018.00273.

Oh, S.P., Seki, T., Goss, K.A., Imamura, T., Yi, Y., Donahoe, P.K., Li, L., Miyazono, K., ten Dijke, P., Kim, S. & Li, E. (2000) Activin receptor-like kinase 1 modulates transforming growth factor-beta 1 signaling in the regulation of angiogenesis. *Proceedings of the National Academy of Sciences of the United States of America*. 97 (6), 2626–2631. doi:10.1073/pnas.97.6.2626.

Ohnesorge, N., Viemann, D., Schmidt, N., Czymai, T., Spiering, D., Schmolke, M., Ludwig, S., Roth, J., Goebeler, M. & Schmidt, M. (2010) Erk5 Activation Elicits a Vasoprotective Endothelial Phenotype via Induction of Krüppel-like Factor 4 (KLF4). *The Journal of Biological Chemistry*. 285 (34), 26199–26210. doi:10.1074/jbc.M110.103127.

Oishi, Y. & Manabe, I. (2018) Krüppel-Like Factors in Metabolic Homeostasis and Cardiometabolic Disease. *Frontiers in Cardiovascular Medicine*. 5, 69. doi:10.3389/fcvm.2018.00069.

Oliveira, S.D.S., Chen, J., Castellon, M., Mao, M., Raj, J.U., Comhair, S., Erzurum, S., Silva, C.L.M., Machado, R.F., Bonini, M.G. & Minshall, R.D. (2019) Injury-Induced Shedding of Extracellular Vesicles Depletes Endothelial Cells of Cav-1 (Caveolin-1) and Enables TGF-β (Transforming Growth Factor-β)–Dependent Pulmonary Arterial Hypertension. *Arteriosclerosis, thrombosis, and vascular biology*. 39 (6), 1191–1202. doi:10.1161/ATVBAHA.118.312038.

Ormiston, M.L., Toshner, M.R., Kiskin, F.N., Huang, C.J.Z., Groves, E., Morrell, N.W. & Rana, A.A. (2015) Generation and Culture of Blood Outgrowth Endothelial Cells from Human Peripheral Blood. *Journal of Visualized Experiments : JoVE*. (106), 53384. doi:10.3791/53384.

Ortogero, N., Yang, Z., Vitancol, R., Griswold, M. & Henderson, D. (2023) *GeomxTools: NanoString GeoMx Tools*. doi:10.18129/B9.bioc.GeomxTools.

Pak, O., Aldashev, A., Welsh, D. & Peacock, A. (2007) The effects of hypoxia on the cells of the pulmonary vasculature. *European Respiratory Journal*. 30 (2), 364–372. doi:10.1183/09031936.00128706.

Papandreou, I., Cairns, R.A., Fontana, L., Lim, A.L. & Denko, N.C. (2006) HIF-1 mediates adaptation to hypoxia by actively downregulating mitochondrial oxygen consumption. *Cell Metabolism*. 3 (3), 187–197. doi:10.1016/j.cmet.2006.01.012.

Park, C.S., Kim, S.H., Yang, H.Y., Kim, J.-H., Schermuly, R.T., Cho, Y.S., Kang, H., Park, J.-H., Lee, E., Park, H., Yang, J.M., Noh, T.W., Lee, S.-P., Bae, S.S., Han, J., Ju, Y.S., Park, J.-B. & Kim, I. (2022) Sox17 Deficiency Promotes Pulmonary Arterial Hypertension via HGF/c-Met Signaling. *Circulation Research*. 131 (10), 792–806. doi:10.1161/CIRCRESAHA.122.320845.

Park, D.-W., Song, J.-M., Han, K.-H., Lee, C.W., Kang, D.-H., Lee, S.-D., Joo, S.-J., Song, H., Lee, J.W. & Song, J.-K. (2008) Different Gene Expression Patterns in the Lungs of Patients with Secondary Pulmonary Hypertension. *Korean Circulation Journal*. 38 (1), 51–59. doi:10.4070/kcj.2008.38.1.51.

Parmar, K.M., Larman, H.B., Dai, G., Zhang, Y., Wang, E.T., Moorthy, S.N., Kratz, J.R., Lin, Z., Jain, M.K., Gimbrone, M.A. & García-Cardeña, G. (2006) Integration of flow-dependent endothelial phenotypes by Kruppel-like factor 2. *Journal of Clinical Investigation*. 116 (1), 49–58. doi:10.1172/JCI24787.

Paschalaki, K.E. & Randi, A.M. (2018) Recent Advances in Endothelial Colony Forming Cells Toward Their Use in Clinical Translation. *Frontiers in Medicine*. 5, 295. doi:10.3389/fmed.2018.00295.

Patel, N.M., Kawut, S.M., Jelic, S., Arcasoy, S.M., Lederer, D.J. & Borczuk, A.C. (2013) Pulmonary arteriole gene expression signature in idiopathic pulmonary fibrosis. *The European respiratory journal*. 41 (6), 1324–1330. doi:10.1183/09031936.00084112.

Patro, R., Duggal, G., Love, M.I., Irizarry, R.A. & Kingsford, C. (2017) Salmon provides fast and bias-aware quantification of transcript expression. *Nature Methods*. 14 (4), 417–419. doi:10.1038/nmeth.4197.

Paudel, R., Fusi, L. & Schmidt, M. (2021) The MEK5/ERK5 Pathway in Health and Disease. *International Journal of Molecular Sciences*. 22 (14), 7594. doi:10.3390/ijms22147594.

Paulin, R., Meloche, J. & Bonnet, S. (2012) STAT3 signaling in pulmonary arterial hypertension. *JAK-STAT*. 1 (4), 223–233. doi:10.4161/jkst.22366.

Penaloza, D. & Arias-Stella, J. (2007) The Heart and Pulmonary Circulation at High Altitudes. *Circulation*. 115 (9), 1132–1146. doi:10.1161/CIRCULATIONAHA.106.624544.

Perros, F., Dorfmüller, P., Souza, R., Durand-Gasselin, I., Mussot, S., Mazmanian, M., Hervé, P., Emilie, D., Simonneau, G. & Humbert, M. (2007) Dendritic cell recruitment in lesions of human and experimental pulmonary hypertension. *European Respiratory Journal*. 29 (3), 462–468. doi:10.1183/09031936.00094706.

Petsophonsakul, P., Furmanik, M., Forsythe, R., Dweck, M., Schurink, G.W., Natour, E., Reutelingsperger, C., Jacobs, M., Mees, B. & Schurgers, L. (2019) Role of Vascular Smooth Muscle Cell Phenotypic Switching and Calcification in Aortic Aneurysm Formation. *Arteriosclerosis, Thrombosis, and Vascular Biology*. 39 (7), 1351–1368. doi:10.1161/ATVBAHA.119.312787.

Piñero, J., Bravo, À., Queralt-Rosinach, N., Gutiérrez-Sacristán, A., Deu-Pons, J., Centeno, E., García-García, J., Sanz, F. & Furlong, L.I. (2017) DisGeNET: a comprehensive platform integrating information on human disease-associated genes and variants. *Nucleic Acids Research*. 45 (Database issue), D833–D839. doi:10.1093/nar/gkw943.

Piñero, J., Ramírez-Anguita, J.M., Saüch-Pitarch, J., Ronzano, F., Centeno, E., Sanz, F. & Furlong, L.I. (2020) The DisGeNET knowledge platform for disease genomics: 2019 update. *Nucleic Acids Research*. 48 (D1), D845–D855. doi:10.1093/nar/gkz1021.

Piva, R., Deaglio, S., Famà, R., Buonincontri, R., Scarfò, I., et al. (2015) The Krüppel-like factor 2 transcription factor gene is recurrently mutated in splenic marginal zone lymphoma. *Leukemia*. 29 (2), 503–507. doi:10.1038/leu.2014.294.

Price, L.C., Caramori, G., Perros, F., Meng, C., Gambaryan, N., et al. (2013) Nuclear Factor κ-B Is Activated in the Pulmonary Vessels of Patients with End-Stage Idiopathic Pulmonary Arterial Hypertension. *PLoS ONE*. 8 (10), e75415. doi:10.1371/journal.pone.0075415.

Privratsky, J.R. & Newman, P.J. (2014) PECAM-1: regulator of endothelial junctional integrity. *Cell and Tissue Research*. 355 (3), 607–619. doi:10.1007/s00441-013-1779-3.

Pugliese, S.C., Poth, J.M., Fini, M.A., Olschewski, A., El Kasmi, K.C. & Stenmark, K.R. (2015) The role of inflammation in hypoxic pulmonary hypertension: from cellular mechanisms to clinical phenotypes. *American Journal of Physiology - Lung Cellular and Molecular Physiology*. 308 (3), L229–L252. doi:10.1152/ajplung.00238.2014.

Puigdevall, P., Piccari, L., Blanco, I., Barberà, J.A., Geiger, D., Badenas, C., Milà, M., Castelo, R. & Madrigal, I. (2019) Genetic linkage analysis of a large family identifies FIGN as a candidate modulator of reduced penetrance in heritable pulmonary arterial hypertension. *Journal of Medical Genetics*. 56 (7), 481–490. doi:10.1136/jmedgenet-2018-105669.

Pullamsetti, S.S., Mamazhakypov, A., Weissmann, N., Seeger, W. & Savai, R. (2020) Hypoxia-inducible factor signaling in pulmonary hypertension. *The Journal of Clinical Investigation*. 130 (11), 5638–5651. doi:10.1172/JCI137558.

Qin, X., Wang, X., Wang, Y., Tang, Z., Cui, Q., Xi, J., J. Li, Y.-S., Chien, S. & Wang, N. (2010) MicroRNA-19a mediates the suppressive effect of laminar flow on cyclin D1 expression in human umbilical vein endothelial cells. *Proceedings of the National Academy of Sciences*. 107 (7), 3240–3244. doi:10.1073/pnas.0914882107.

Quillard, T., Devallière, J., Coupel, S. & Charreau, B. (2010) Inflammation dysregulates Notch signaling in endothelial cells: Implication of Notch2 and Notch4 to endothelial dysfunction. *Biochemical Pharmacology*. 80 (12), 2032–2041. doi:10.1016/j.bcp.2010.07.010.

Rabiet, M.J., Plantier, J.L., Rival, Y., Genoux, Y., Lampugnani, M.G. & Dejana, E. (1996) Thrombin-induced increase in endothelial permeability is associated with changes in cell-to-cell junction organization. *Arteriosclerosis, Thrombosis, and Vascular Biology*. 16 (3), 488–496. doi:10.1161/01.atv.16.3.488.

Rabinovitch, M., Guignabert, C., Humbert, M. & Nicolls, M.R. (2014) Inflammation and Immunity in the Pathogenesis of Pulmonary Arterial Hypertension. *Circulation research*. 115 (1), 165–175. doi:10.1161/CIRCRESAHA.113.301141.

Racca, A.C., Ridano, M.E., Bandeira, C.L., Bevilacqua, E., Avvad Portari, E., Genti-Raimondi, S., Graham, C.H. & Panzetta-Dutari, G.M. (2016) Low oxygen tension

induces Krüppel-Like Factor 6 expression in trophoblast cells. *Placenta*. 45, 50–57. doi:10.1016/j.placenta.2016.07.006.

Rajagopal, S., Ruetzler, K., Ghadimi, K., Horn, E.M., Kelava, M., Kudelko, K.T., Moreno-Duarte, I., Preston, I., Rose Bovino, L.L., Smilowitz, N.R., Vaidya, A. & null, null (2023) Evaluation and Management of Pulmonary Hypertension in Noncardiac Surgery: A Scientific Statement From the American Heart Association. *Circulation*. 147 (17), 1317–1343. doi:10.1161/CIR.0000000000001136.

Ranchoux, B., Antigny, F., Rucker-Martin, C., Hautefort, A., Péchoux, C., et al. (2015) Endothelial-to-mesenchymal transition in pulmonary hypertension. *Circulation*. 131 (11), 1006–1018. doi:10.1161/CIRCULATIONAHA.114.008750.

Ratziu, V., Lalazar, A., Wong, L., Dang, Q., Collins, C., Shaulian, E., Jensen, S. & Friedman, S.L. (1998) Zf9, a Kruppel-like transcription factor up-regulated in vivo during early hepatic fibrosis. *Proceedings of the National Academy of Sciences of the United States of America*. 95 (16), 9500–9505.

Reeves, H.L., Narla, G., Ogunbiyi, O., Haq, A.I., Katz, A., Benzeno, S., Hod, E., Harpaz, N., Goldberg, S., Tal-Kremer, S., Eng, F.J., Arthur, M.J.P., Martignetti, J.A. & Friedman, S.L. (2004) Kruppel-like factor 6 (KLF6) is a tumor-suppressor gene frequently inactivated in colorectal cancer. *Gastroenterology*. 126 (4), 1090–1103. doi:10.1053/j.gastro.2004.01.005.

Reiter, G., Reiter, U., Kovacs, G., Kainz, B., Schmidt, K., Maier, R., Olschewski, H. & Rienmueller, R. (2008) Magnetic Resonance–Derived 3-Dimensional Blood Flow Patterns in the Main Pulmonary Artery as a Marker of Pulmonary Hypertension and a Measure of Elevated Mean Pulmonary Arterial Pressure. *Circulation: Cardiovascular Imaging*. 1 (1), 23–30. doi:10.1161/CIRCIMAGING.108.780247.

Reitsma, S., Slaaf, D.W., Vink, H., van Zandvoort, M.A.M.J. & oude Egbrink, M.G.A. (2007) The endothelial glycocalyx: composition, functions, and visualization. *Pflügers Archiv - European Journal of Physiology*. 454 (3), 345–359. doi:10.1007/s00424-007-0212-8.

Remillard, C.V., Tigno, D.D., Platoshyn, O., Burg, E.D., Brevnova, E.E., Conger, D., Nicholson, A., Rana, B.K., Channick, R.N., Rubin, L.J., O'connor, D.T. & Yuan, J.X.-J. (2007) Function of Kv1.5 channels and genetic variations of KCNA5 in patients with idiopathic pulmonary arterial hypertension. *American Journal of Physiology. Cell Physiology*. 292 (5), C1837-1853. doi:10.1152/ajpcell.00405.2006.

Reyes-Palomares, A., Gu, M., Grubert, F., Berest, I., Sa, S., Kasowski, M., Arnold, C., Shuai, M., Srivas, R., Miao, S., Li, D., Snyder, M.P., Rabinovitch, M. & Zaugg, J.B. (2020) Remodeling of active endothelial enhancers is associated with aberrant gene-regulatory networks in pulmonary arterial hypertension. *Nature Communications*. 11, 1673. doi:10.1038/s41467-020-15463-x.

Rhodes, C.J., Wharton, J., Boon, R.A., Roexe, T., Tsang, H., et al. (2013) Reduced MicroRNA-150 Is Associated with Poor Survival in Pulmonary Arterial

Hypertension. *American Journal of Respiratory and Critical Care Medicine*. 187 (3), 294–302. doi:10.1164/rccm.201205-0839OC.

Ricard, N., Tu, L., Le Hiress, M., Huertas, A., Phan, C., Thuillet, R., Sattler, C., Fadel, E., Seferian, A., Montani, D., Dorfmüller, P., Humbert, M. & Guignabert, C. (2014) Increased Pericyte Coverage Mediated by Endothelial-Derived Fibroblast Growth Factor-2 and Interleukin-6 Is a Source of Smooth Muscle–Like Cells in Pulmonary Hypertension. *Circulation*. 129 (15), 1586–1597. doi:10.1161/CIRCULATIONAHA.113.007469.

Roger, I., Milara, J., Montero, P. & Cortijo, J. (2021) The Role of JAK/STAT Molecular Pathway in Vascular Remodeling Associated with Pulmonary Hypertension. *International Journal of Molecular Sciences*. 22 (9), 4980. doi:10.3390/ijms22094980.

Rosenberg, H.C. & Rabinovitch, M. (1988) Endothelial injury and vascular reactivity in monocrotaline pulmonary hypertension. *The American Journal of Physiology*. 255 (6 Pt 2), H1484-1491. doi:10.1152/ajpheart.1988.255.6.H1484.

Roth, R.A. & Reindel, J.F. (1991) Lung vascular injury from monocrotaline pyrrole, a putative hepatic metabolite. *Advances in Experimental Medicine and Biology*. 283, 477–487. doi:10.1007/978-1-4684-5877-0_64.

Rubinstein, M., Idelman, G., Plymate, S.R., Narla, G., Friedman, S.L. & Werner, H. (2004) Transcriptional activation of the insulin-like growth factor I receptor gene by the Kruppel-like factor 6 (KLF6) tumor suppressor protein: potential interactions between KLF6 and p53. *Endocrinology*. 145 (8), 3769–3777. doi:10.1210/en.2004-0173.

Ryan, J., Bloch, K. & Archer, S.L. (2011) Rodent models of pulmonary hypertension: harmonisation with the world health organisation's categorisation of human PH. *International Journal of Clinical Practice*. 65 (s172), 15–34. doi:10.1111/j.1742-1241.2011.02710.x.

Ryan, J., Dasgupta, A., Huston, J., Chen, K.-H. & Archer, S.L. (2015) Mitochondrial dynamics in pulmonary arterial hypertension. *Journal of Molecular Medicine (Berlin, Germany)*. 93 (3), 229–242. doi:10.1007/s00109-015-1263-5.

Ryan, J.J. & Archer, S.L. (2015) Emerging concepts in the molecular basis of pulmonary arterial hypertension (PAH): Part I: Metabolic plasticity and mitochondrial dynamics in the pulmonary circulation and right ventricle in PAH. *Circulation*. 131 (19), 1691–1702. doi:10.1161/CIRCULATIONAHA.114.006979.

Sakao, S., Taraseviciene-Stewart, L., Lee, J.D., Wood, K., Cool, C.D. & Voelkel, N.F. (2005) Initial apoptosis is followed by increased proliferation of apoptosis-resistant endothelial cells. *FASEB journal: official publication of the Federation of American Societies for Experimental Biology*. 19 (9), 1178–1180. doi:10.1096/fj.04-3261fje.

Sakao, S., Taraseviciene-Stewart, L., Wood, K., Cool, C.D. & Voelkel, N.F. (2006) Apoptosis of pulmonary microvascular endothelial cells stimulates vascular smooth

muscle cell growth. *American Journal of Physiology. Lung Cellular and Molecular Physiology*. 291 (3), L362-368. doi:10.1152/ajplung.00111.2005.

Sakao, S., Tatsumi, K. & Voelkel, N.F. (2009) Endothelial cells and pulmonary arterial hypertension: apoptosis, proliferation, interaction and transdifferentiation. *Respiratory Research*. 10 (1), 95. doi:10.1186/1465-9921-10-95.

Salibe-Filho, W., Araujo, T.L.S., G. Melo, E., B. C. T. Coimbra, L., Lapa, M.S., Acencio, M.M.P., Freitas-Filho, O., Capelozzi, V.L., Teixeira, L.R., Fernandes, C.J.C.S., Jatene, F.B., Laurindo, F.R.M. & Terra-Filho, M. (2020) Shear stress-exposed pulmonary artery endothelial cells fail to upregulate HSP70 in chronic thromboembolic pulmonary hypertension. *PLoS ONE*. 15 (12), e0242960. doi:10.1371/journal.pone.0242960.

Sanchez, O., Marcos, E., Perros, F., Fadel, E., Tu, L., Humbert, M., Dartevelle, P., Simonneau, G., Adnot, S. & Eddahibi, S. (2007) Role of Endothelium-derived CC Chemokine Ligand 2 in Idiopathic Pulmonary Arterial Hypertension. *American Journal of Respiratory and Critical Care Medicine*. 176 (10), 1041–1047. doi:10.1164/rccm.200610-1559OC.

Sangodkar, J., Dhawan, N.S., Melville, H., Singh, V.J., Yuan, E., et al. (2012) Targeting the FOXO1/KLF6 axis regulates EGFR signaling and treatment response. *The Journal of Clinical Investigation*. 122 (7), 2637–2651. doi:10.1172/JCI62058.

Sangodkar, J., Shi, J., DiFeo, A., Schwartz, R., Bromberg, R., Choudhri, A., McClinch, K., Hatami, R., Scheer, E., Kremer-Tal, S., Martignetti, J.A., Hui, A., Leung, W.K., Friedman, S.L. & Narla, G. (2009) Functional role of the KLF6 tumour suppressor gene in gastric cancer. *European Journal of Cancer (Oxford, England: 1990)*. 45 (4), 666–676. doi:10.1016/j.ejca.2008.11.009.

Sangwung, P., Zhou, G., Nayak, L., Chan, E.R., Kumar, S., Kang, D.-W., Zhang, R., Liao, X., Lu, Y., Sugi, K., Fujioka, H., Shi, H., Lapping, S.D., Ghosh, C.C., Higgins, S.J., Parikh, S.M., Jo, H. & Jain, M.K. (n.d.) KLF2 and KLF4 control endothelial identity and vascular integrity. *JCI Insight*. 2 (4), e91700. doi:10.1172/jci.insight.91700.

Sarah, B., Ashrith, G. & Sandeep, S. (2021) Evaluation, Diagnosis, and Classification of Pulmonary Hypertension. *Methodist DeBakey Cardiovascular Journal*. 17 (2), 86–91. doi:10.14797/OCDF4453.

Sarfstein, R., Belfiore, A. & Werner, H. (2010) Identification of Insulin-Like Growth Factor-I Receptor (IGF-IR) Gene Promoter-Binding Proteins in Estrogen Receptor (ER)-Positive and ER-Depleted Breast Cancer Cells. *Cancers*. 2 (2), 233–261. doi:10.3390/cancers2020233.

Sato, M. & Ohashi, T. (2005) Biorheological views of endothelial cell responses to mechanical stimuli. *Biorheology*. 42 (6), 421–441.

Savai, R., Al-Tamari, H.M., Sedding, D., Kojonazarov, B., Muecke, C., Teske, R., Capecchi, M.R., Weissmann, N., Grimminger, F., Seeger, W., Schermuly, R.T. & Pullamsetti,

S.S. (2014) Pro-proliferative and inflammatory signaling converge on FoxO1 transcription factor in pulmonary hypertension. *Nature Medicine*. 20 (11), 1289–1300. doi:10.1038/nm.3695.

Savale, L., Tu, L., Rideau, D., Izziki, M., Maitre, B., Adnot, S. & Eddahibi, S. (2009) Impact of interleukin-6 on hypoxia-induced pulmonary hypertension and lung inflammation in mice. *Respiratory Research*. 10 (1), 6. doi:10.1186/1465-9921-10-6.

Sayedyahossein, S., Thines, L. & Sacks, D.B. (2023) Ca2+ signaling and the Hippo pathway: Intersections in cellular regulation. *Cellular Signalling*. 110, 110846. doi:10.1016/j.cellsig.2023.110846.

Schäfer, M., Kheyfets, V.O., Schroeder, J.D., Dunning, J., Shandas, R., Buckner, J.K., Browning, J., Hertzberg, J., Hunter, K.S. & Fenster, B.E. (2016) Main pulmonary arterial wall shear stress correlates with invasive hemodynamics and stiffness in pulmonary hypertension. *Pulmonary Circulation*. 6 (1), 37–45. doi:10.1086/685024.

Schiavon, M., Fadini, G.P., Lunardi, F., Agostini, C., Boscaro, E., Calabrese, F., Marulli, G. & Rea, F. (2012) Increased tissue endothelial progenitor cells in end-stage lung diseases with pulmonary hypertension. *The Journal of Heart and Lung Transplantation: The Official Publication of the International Society for Heart Transplantation*. 31 (9), 1025–1030. doi:10.1016/j.healun.2012.06.005.

Schwiening, M., Swietlik, E.M., Pandya, D., Burling, K., Barker, P., Feng, O.Y., Treacy, C.M., Abreu, S., Wort, S.J., Pepke-Zaba, J., Graf, S., Marciniak, S.J., Morrell, N.W. & Soon, E. (2022) Different Cytokine Patterns in BMPR2-Mutation-Positive Patients and Patients With Pulmonary Arterial Hypertension Without Mutations and Their Influence on Survival. *Chest*. 161 (6), 1651. doi:10.1016/j.chest.2022.01.019.

Semenza, G.L., Roth, P.H., Fang, H.M. & Wang, G.L. (1994) Transcriptional regulation of genes encoding glycolytic enzymes by hypoxia-inducible factor 1. *The Journal of Biological Chemistry*. 269 (38), 23757–23763.

SenBanerjee, S., Lin, Z., Atkins, G.B., Greif, D.M., Rao, R.M., Kumar, A., Feinberg, M.W., Chen, Z., Simon, D.I., Luscinskas, F.W., Michel, T.M., Gimbrone, M.A., García-Cardeña, G. & Jain, M.K. (2004) KLF2 Is a Novel Transcriptional Regulator of Endothelial Proinflammatory Activation. *The Journal of Experimental Medicine*. 199 (10), 1305–1315. doi:10.1084/jem.20031132.

Sharmin, N., Nganwuchu, C.C. & Nasim, M.T. (2021) Targeting the TGF-β signaling pathway for resolution of pulmonary arterial hypertension. *Trends in Pharmacological Sciences*. 42 (7), 510–513. doi:10.1016/j.tips.2021.04.002.

Shatat, M.A., Tian, H., Zhang, R., Tandon, G., Hale, A., Fritz, J.S., Zhou, G., Martínez-González, J., Rodríguez, C., Champion, H.C., Jain, M.K. & Hamik, A. (2014) Endothelial Krüppel-Like Factor 4 Modulates Pulmonary Arterial Hypertension. *American Journal of Respiratory Cell and Molecular Biology*. 50 (3), 647–653. doi:10.1165/rcmb.2013-0135OC.

Shen, B., Smith, R.S., Hsu, Y.-T., Chao, L. & Chao, J. (2009) Kruppel-like factor 4 is a novel mediator of Kallistatin in inhibiting endothelial inflammation via increased endothelial nitric-oxide synthase expression. *The Journal of Biological Chemistry*. 284 (51), 35471–35478. doi:10.1074/jbc.M109.046813.

Shen, L. (2016) *GeneOverlap: An R package to test and visualize gene overlaps*. In: 2016 p. https://www.semanticscholar.org/paper/GeneOverlap%3A-An-R-package-to-test-and-visualize-Shen/117e12840af966176bbc348db6edf034b0ea479c.

Shi, Y., Liu, J., Zhang, R., Zhang, M., Cui, H., Wang, L., Cui, Y., Wang, W., Sun, Y. & Wang, C. (2023) Targeting Endothelial ENO1 (Alpha-Enolase) -PI3K-Akt-mTOR Axis Alleviates Hypoxic Pulmonary Hypertension. *Hypertension*. 80 (5), 1035–1047. doi:10.1161/HYPERTENSIONAHA.122.19857.

Shintani, M., Yagi, H., Nakayama, T., Saji, T. & Matsuoka, R. (2009) A new nonsense mutation of SMAD8 associated with pulmonary arterial hypertension. *Journal of Medical Genetics*. 46 (5), 331–337. doi:10.1136/jmg.2008.062703.

Shiojima, I. & Walsh, K. (2002) Role of Akt Signaling in Vascular Homeostasis and Angiogenesis. *Circulation Research*. 90 (12), 1243–1250. doi:10.1161/01.RES.0000022200.71892.9F.

Shyam P. Reddy, E. (2019) ETS-Related Gene (ERG) and Friend leukemia integration – 1 (FLI-1) Transcription Factors in the Precision Treatment of Pulmonary Arterial Hypertension and Pulmonary Fibrosis. *Journal of Cancer Epidemiology & Treatment*. 3 (1), 1–4. doi:10.24218/jcet.2019.21.

Sindi, H.A., Russomanno, G., Satta, S., Abdul-Salam, V.B., Jo, K.B., Qazi-Chaudhry, B., Ainscough, A.J., Szulcek, R., Jan Bogaard, H., Morgan, C.C., Pullamsetti, S.S., Alzaydi, M.M., Rhodes, C.J., Piva, R., Eichstaedt, C.A., Grünig, E., Wilkins, M.R. & Wojciak-Stothard, B. (2020) Therapeutic potential of KLF2-induced exosomal microRNAs in pulmonary hypertension. *Nature Communications*. 11 (1), 1185. doi:10.1038/s41467-020-14966-x.

Slavin, D.A., Koritschoner, N.P., Prieto, C.C., López-Díaz, F.J., Chatton, B. & Bocco, J.L. (2004) A new role for the Kruppel-like transcription factor KLF6 as an inhibitor of c-Jun proto-oncoprotein function. *Oncogene*. 23 (50), 8196–8205. doi:10.1038/sj.onc.1208020.

Smits, J., Tasev, D., Andersen, S., Szulcek, R., Botros, L., Ringgaard, S., Andersen, A., Vonk-Noordegraaf, A., Koolwijk, P. & Bogaard, H.J. (2018) Blood Outgrowth and Proliferation of Endothelial Colony Forming Cells are Related to Markers of Disease Severity in Patients with Pulmonary Arterial Hypertension. *International Journal of Molecular Sciences*. 19 (12), 3763. doi:10.3390/ijms19123763.

Smolders, V.F.E.D., Rodríguez, C., Blanco, I., Szulcek, R., Timens, W., et al. (2022) Metabolic profile in endothelial cells of chronic thromboembolic pulmonary hypertension and pulmonary arterial hypertension. *Scientific Reports*. 12 (1), 2283. doi:10.1038/s41598-022-06238-z.

Sommer, N., Ghofrani, H.A., Pak, O., Bonnet, S., Provencher, S., Sitbon, O., Rosenkranz, S., Hoeper, M.M. & Kiely, D.G. (2021) Current and future treatments of pulmonary arterial hypertension. *British Journal of Pharmacology*. 178 (1), 6–30. doi:10.1111/bph.15016.

Song, S., Yamamura, A., Yamamura, H., Ayon, R.J., Smith, K.A., Tang, H., Makino, A. & Yuan, J.X.-J. (2014) Flow shear stress enhances intracellular Ca2+ signaling in pulmonary artery smooth muscle cells from patients with pulmonary arterial hypertension. *American Journal of Physiology - Cell Physiology*. 307 (4), C373–C383. doi:10.1152/ajpcell.00115.2014.

Soon, E., Holmes, A.M., Treacy, C.M., Doughty, N.J., Southgate, L., Machado, R.D., Trembath, R.C., Jennings, S., Barker, L., Nicklin, P., Walker, C., Budd, D.C., Pepke-Zaba, J. & Morrell, N.W. (2010) Elevated Levels of Inflammatory Cytokines Predict Survival in Idiopathic and Familial Pulmonary Arterial Hypertension. *Circulation*. 122 (9), 920–927. doi:10.1161/CIRCULATIONAHA.109.933762.

Soubrier, F., Chung, W.K., Machado, R., Grünig, E., Aldred, M., Geraci, M., Loyd, J.E., Elliott, C.G., Trembath, R.C., Newman, J.H. & Humbert, M. (2013) Genetics and genomics of pulmonary arterial hypertension. *Journal of the American College of Cardiology*. 62 (25 Suppl), D13-21. doi:10.1016/j.jacc.2013.10.035.

Sprague, A.H. & Khalil, R.A. (2009) Inflammatory cytokines in vascular dysfunction and vascular disease. *Biochemical Pharmacology*. 78 (6), 539–552. doi:10.1016/j.bcp.2009.04.029.

Stacher, E., Graham, B.B., Hunt, J.M., Gandjeva, A., Groshong, S.D., McLaughlin, V.V., Jessup, M., Grizzle, W.E., Aldred, M.A., Cool, C.D. & Tuder, R.M. (2012) Modern Age Pathology of Pulmonary Arterial Hypertension. *American Journal of Respiratory and Critical Care Medicine*. 186 (3), 261–272. doi:10.1164/rccm.201201-0164OC.

Steiner, M.K., Syrkina, O.L., Kolliputi, N., Mark, E.J., Hales, C.A. & Waxman, A.B. (2009) Interleukin-6 Overexpression Induces Pulmonary Hypertension. *Circulation Research*. 104 (2), 236–244. doi:10.1161/CIRCRESAHA.108.182014.

Stenmark, K.R., Frid, M.G., Graham, B.B. & Tuder, R.M. (2018) Dynamic and diverse changes in the functional properties of vascular smooth muscle cells in pulmonary hypertension. *Cardiovascular Research*. 114 (4), 551–564. doi:10.1093/cvr/cvy004.

Stenmark, K.R., Meyrick, B., Galie, N., Mooi, W.J. & McMurtry, I.F. (2009) Animal models of pulmonary arterial hypertension: the hope for etiological discovery and pharmacological cure. *American Journal of Physiology-Lung Cellular and Molecular Physiology*. 297 (6), L1013–L1032. doi:10.1152/ajplung.00217.2009.

Steward, R., Tambe, D., Hardin, C.C., Krishnan, R. & Fredberg, J.J. (2015) Fluid shear, intercellular stress, and endothelial cell alignment. *American Journal of Physiology - Cell Physiology*. 308 (8), C657–C664. doi:10.1152/ajpcell.00363.2014.

Strowitzki, M.J., Cummins, E.P. & Taylor, C.T. (2019) Protein Hydroxylation by Hypoxia-Inducible Factor (HIF) Hydroxylases: Unique or Ubiquitous? *Cells*. 8 (5), 384. doi:10.3390/cells8050384.

Suh, K.S., Mutoh, M., Nagashima, K., Fernandez-Salas, E., Edwards, L.E., Hayes, D.D., Crutchley, J.M., Marin, K.G., Dumont, R.A., Levy, J.M., Cheng, C., Garfield, S. & Yuspa, S.H. (2004) The Organellular Chloride Channel Protein CLIC4/mtCLIC Translocates to the Nucleus in Response to Cellular Stress and Accelerates Apoptosis *. *Journal of Biological Chemistry*. 279 (6), 4632–4641. doi:10.1074/jbc.M311632200.

Sun, S., Chen, H., Sun, L., Wang, M., Wu, X. & Xiao, Z.-X.J. (2020) Hotspot mutant p53-R273H inhibits KLF6 expression to promote cell migration and tumor metastasis. *Cell Death & Disease*. 11 (7), 595. doi:10.1038/s41419-020-02814-1.

Suske, G., Bruford, E. & Philipsen, S. (2005) Mammalian SP/KLF transcription factors: Bring in the family. *Genomics*. 85 (5), 551–556. doi:10.1016/j.ygeno.2005.01.005.

Suzuki, T., Carrier, E.J., Talati, M.H., Rathinasabapathy, A., Chen, X., Nishimura, R., Tada, Y., Tatsumi, K. & West, J. (2018) Isolation and characterization of endothelial-to-mesenchymal transition cells in pulmonary arterial hypertension. *American Journal of Physiology. Lung Cellular and Molecular Physiology*. 314 (1), L118–L126. doi:10.1152/ajplung.00296.2017.

Sweet, D.R., Fan, L., Hsieh, P.N. & Jain, M.K. (2018) Krüppel-Like Factors in Vascular Inflammation: Mechanistic Insights and Therapeutic Potential. *Frontiers in Cardiovascular Medicine*. 5, 6. doi:10.3389/fcvm.2018.00006.

Sweet, D.R., Lam, C. & Jain, M.K. (2021) Evolutionary Protection of Krüppel-Like Factors 2 and 4 in the Development of the Mature Hemovascular System. *Frontiers in Cardiovascular Medicine*. 8, 645719. doi:10.3389/fcvm.2021.645719.

Sweet, D.R., Padmanabhan, R., Liao, X., Dashora, H.R., Tang, X., Nayak, L., Jain, R., Val, S.D., Vinayachandran, V. & Jain, M.K. (2023) Krüppel-Like Factors Orchestrate Endothelial Gene Expression Through Redundant and Non-Redundant Enhancer Networks. *Journal of the American Heart Association: Cardiovascular and Cerebrovascular Disease*. 12 (4). doi:10.1161/JAHA.121.024303.

Syafruddin, S.E., Mohtar, M.A., Wan Mohamad Nazarie, W.F. & Low, T.Y. (2020) Two Sides of the Same Coin: The Roles of KLF6 in Physiology and Pathophysiology. *Biomolecules*. 10 (10), 1378. doi:10.3390/biom10101378.

Sydykov, A., Mamazhakypov, A., Maripov, A., Kosanovic, D., Weissmann, N., Ghofrani, H.A., Sarybaev, A.Sh. & Schermuly, R.T. (2021) Pulmonary Hypertension in Acute and Chronic High Altitude Maladaptation Disorders. *International Journal of Environmental Research and Public Health*. 18 (4), 1692. doi:10.3390/ijerph18041692.

Szulcek, R., Happé, C.M., Rol, N., Fontijn, R.D., Dickhoff, C., et al. (2016) Delayed Microvascular Shear Adaptation in Pulmonary Arterial Hypertension. Role of Platelet Endothelial Cell Adhesion Molecule-1 Cleavage. *American Journal of Respiratory and Critical Care Medicine*. 193 (12), 1410–1420. doi:10.1164/rccm.201506-1231OC.

Tada, Y., Laudi, S., Harral, J., Carr, M., Ivester, C., Tanabe, N., Takiguchi, Y., Tatsumi, K., Kuriyama, T., Nichols, W.C. & West, J. (2008) MURINE PULMONARY RESPONSE TO CHRONIC HYPOXIA IS STRAIN SPECIFIC. *Experimental lung research*. 34 (6), 313–323. doi:10.1080/01902140802093204.

Tajeddin, A. & Mustafaoglu, N. (2021) Design and Fabrication of Organ-on-Chips: Promises and Challenges. *Micromachines*. 12 (12), 1443. doi:10.3390/mi12121443.

Tamm, M., Bihl, M., Eickelberg, O., Stulz, P., Perruchoud, A.P. & Roth, M. (1998) Hypoxia-induced interleukin-6 and interleukin-8 production is mediated by platelet-activating factor and platelet-derived growth factor in primary human lung cells. *American Journal of Respiratory Cell and Molecular Biology*. 19 (4), 653–661. doi:10.1165/ajrcmb.19.4.3058.

Tang, B.T., Pickard, S.S., Chan, F.P., Tsao, P.S., Taylor, C.A. & Feinstein, J.A. (2012) Wall shear stress is decreased in the pulmonary arteries of patients with pulmonary arterial hypertension: An image-based, computational fluid dynamics study. *Pulmonary Circulation*. 2 (4), 470–476. doi:10.4103/2045-8932.105035.

Tang, C., Luo, Y., Li, S., Huang, B., Xu, S. & Li, L. (2021) Characteristics of inflammation process in monocrotaline-induced pulmonary arterial hypertension in rats. *Biomedicine & Pharmacotherapy*. 133, 111081. doi:10.1016/j.biopha.2020.111081.

Tang, H., Babicheva, A., McDermott, K.M., Gu, Y., Ayon, R.J., et al. (2018) Endothelial HIF-2α contributes to severe pulmonary hypertension due to endothelial-to-mesenchymal transition. *American Journal of Physiology-Lung Cellular and Molecular Physiology*. 314 (2), L256–L275. doi:10.1152/ajplung.00096.2017.

Tang, W., Li, M., Yangzhong, X., Zhang, X., Zu, A., Hou, Y., Li, L. & Sun, S. (2022) Hippo signaling pathway and respiratory diseases. *Cell Death Discovery*. 8, 213. doi:10.1038/s41420-022-01020-6.

Taraseviciene-Stewart, L., Kasahara, Y., Alger, L., Hirth, P., Mc Mahon, G., Waltenberger, J., Voelkel, N.F. & Tuder, R.M. (2001) Inhibition of the VEGF receptor 2 combined with chronic hypoxia causes cell death-dependent pulmonary endothelial cell proliferation and severe pulmonary hypertension. *FASEB journal: official publication of the Federation of American Societies for Experimental Biology*. 15 (2), 427–438. doi:10.1096/fj.00-0343com.

Terragni, J., Graham, J.R., Adams, K.W., Schaffer, M.E., Tullai, J.W. & Cooper, G.M. (2008) Phosphatidylinositol 3-kinase signaling in proliferating cells maintains an anti-apoptotic transcriptional program mediated by inhibition of FOXO and non-canonical

activation of NFκB transcription factors. *BMC Cell Biology*. 9, 6. doi:10.1186/1471-2121-9-6.

Tettey, A., Jiang, Y., Li, X. & Li, Y. (2021) Therapy for Pulmonary Arterial Hypertension: Glance on Nitric Oxide Pathway. *Frontiers in Pharmacology*. 12, 767002. doi:10.3389/fphar.2021.767002.

Thenappan, T., Chan, S.Y. & Weir, E.K. (2018) Role of extracellular matrix in the pathogenesis of pulmonary arterial hypertension. *American Journal of Physiology - Heart and Circulatory Physiology*. 315 (5), H1322–H1331. doi:10.1152/ajpheart.00136.2018.

Thompson, C.L., Fu, S., Heywood, H.K., Knight, M.M. & Thorpe, S.D. (2020) Mechanical Stimulation: A Crucial Element of Organ-on-Chip Models. *Frontiers in Bioengineering and Biotechnology*. 8. https://www.frontiersin.org/articles/10.3389/fbioe.2020.602646.

Thompson, J.E., Phillips, R.J., Erdjument-Bromage, H., Tempst, P. & Ghosh, S. (1995) I kappa B-beta regulates the persistent response in a biphasic activation of NF-kappa B. *Cell*. 80 (4), 573–582. doi:10.1016/0092-8674(95)90511-1.

Tian, W., Jiang, X., Sung, Y.K., Shuffle, E., Wu, T.-H., et al. (2019) Phenotypically-Silent Bone Morphogenetic Protein Receptor 2 (Bmpr2) Mutations Predispose Rats to Inflammation-Induced Pulmonary Arterial Hypertension by Enhancing The Risk for Neointimal Transformation. *Circulation*. 140 (17), 1409–1425. doi:10.1161/CIRCULATIONAHA.119.040629.

Tinajero, M.G. & Gotlieb, A.I. (2020) Recent Developments in Vascular Adventitial Pathobiology: The Dynamic Adventitia as a Complex Regulator of Vascular Disease. *The American Journal of Pathology*. 190 (3), 520–534. doi:10.1016/j.ajpath.2019.10.021.

Tobal, R., Potjewijd, J., van Empel, V.P.M., Ysermans, R., Schurgers, L.J., Reutelingsperger, C.P., Damoiseaux, J.G.M.C. & van Paassen, P. (2021) Vascular Remodeling in Pulmonary Arterial Hypertension: The Potential Involvement of Innate and Adaptive Immunity. *Frontiers in Medicine*. 8, 806899. doi:10.3389/fmed.2021.806899.

Toshner, M., Voswinckel, R., Southwood, M., Al-Lamki, R., Howard, L.S.G., Marchesan, D., Yang, J., Suntharalingam, J., Soon, E., Exley, A., Stewart, S., Hecker, M., Zhu, Z., Gehling, U., Seeger, W., Pepke-Zaba, J. & Morrell, N.W. (2009) Evidence of Dysfunction of Endothelial Progenitors in Pulmonary Arterial Hypertension. *American Journal of Respiratory and Critical Care Medicine*. 180 (8), 780–787. doi:10.1164/rccm.200810-1662OC.

Trembath, R.C., Thomson, J.R., Machado, R.D., Morgan, N.V., Atkinson, C., Winship, I., Simonneau, G., Galie, N., Loyd, J.E., Humbert, M., Nichols, W.C., Morrell, N.W., Berg, J., Manes, A., McGaughran, J., Pauciulo, M. & Wheeler, L. (2001) Clinical and molecular genetic features of pulmonary hypertension in patients with hereditary

hemorrhagic telangiectasia. *The New England Journal of Medicine*. 345 (5), 325–334. doi:10.1056/NEJM200108023450503.

Truong, U., Fonseca, B., Dunning, J., Burgett, S., Lanning, C., Ivy, D.D., Shandas, R., Hunter, K. & Barker, A.J. (2013) Wall shear stress measured by phase contrast cardiovascular magnetic resonance in children and adolescents with pulmonary arterial hypertension. *Journal of Cardiovascular Magnetic Resonance*. 15 (1), 81. doi:10.1186/1532-429X-15-81.

Tu, L., Dewachter, L., Gore, B., Fadel, E., Dartevelle, P., Simonneau, G., Humbert, M., Eddahibi, S. & Guignabert, C. (2011) Autocrine fibroblast growth factor-2 signaling contributes to altered endothelial phenotype in pulmonary hypertension. *American Journal of Respiratory Cell and Molecular Biology*. 45 (2), 311–322. doi:10.1165/rcmb.2010-0317OC.

Tuder, R.M. (2017) Pulmonary Vascular Remodeling in Pulmonary Hypertension. *Cell and tissue research*. 367 (3), 643–649. doi:10.1007/s00441-016-2539-y.

Tuder, R.M., Ponticos, M. & Holmes, A. (2017) Pathogenesis of Pulmonary Arterial Hypertension. In: J. Varga, C.P. Denton, F.M. Wigley, Y. Allanore, & M. Kuwana (eds.). *Scleroderma: From Pathogenesis to Comprehensive Management*. Cham, Springer International Publishing. pp. 385–401. doi:10.1007/978-3-319-31407-5_26.

Tzima, E., Irani-Tehrani, M., Kiosses, W.B., Dejana, E., Schultz, D.A., Engelhardt, B., Cao, G., DeLisser, H. & Schwartz, M.A. (2005) A mechanosensory complex that mediates the endothelial cell response to fluid shear stress. *Nature*. 437 (7057), 426–431. doi:10.1038/nature03952.

Umar, S., Iorga, A., Matori, H., Nadadur, R.D., Li, J., Maltese, F., van der Laarse, A. & Eghbali, M. (2011) Estrogen rescues preexisting severe pulmonary hypertension in rats. *American Journal of Respiratory and Critical Care Medicine*. 184 (6), 715–723. doi:10.1164/rccm.201101-0078OC.

Umar, S., Rabinovitch, M. & Eghbali, M. (2012) Estrogen Paradox in Pulmonary Hypertension. *American Journal of Respiratory and Critical Care Medicine*. 186 (2), 125–131. doi:10.1164/rccm.201201-0058PP.

Vigl, B., Trubacova, S., Poglitsch, M., Domenig, O., Balis, P., Barta, A., Valovic, P., Liskova, S., Simko, F. & Paulis, L. (2021) PHARMACOLOGIC ACTIVATION OF THE ALTERNATIVE RAS ATTENUATES DEVELOPMENT OF PULMONARY ARTERIAL HYPERTENSION IN MONOCROTALINE TREATED RATS. *Journal of Hypertension*. 39, e348. doi:10.1097/01.hjh.0000748560.08337.80.

Voelkel, N.F., Tuder, R.M., Bridges, J. & Arend, W.P. (1994) Interleukin-1 receptor antagonist treatment reduces pulmonary hypertension generated in rats by monocrotaline. *American Journal of Respiratory Cell and Molecular Biology*. 11 (6), 664–675. doi:10.1165/ajrcmb.11.6.7946395.

Wakasugi, T., Shimizu, I., Yoshida, Y., Hayashi, Y., Ikegami, R., Suda, M., Katsuumi, G., Nakao, M., Hoyano, M., Kashimura, T., Nakamura, K., Ito, H., Nojiri, T., Soga, T. & Minamino, T. (2019) Role of smooth muscle cell p53 in pulmonary arterial hypertension. *PLoS ONE*. 14 (2), e0212889. doi:10.1371/journal.pone.0212889.

Wang, G., Fan, R., Ji, R., Zou, W., Penny, D.J., Varghese, N.P. & Fan, Y. (2016) Novel homozygous BMP9 nonsense mutation causes pulmonary arterial hypertension: a case report. *BMC Pulmonary Medicine*. 16 (1), 17. doi:10.1186/s12890-016-0183-7.

Wang, H., Yang, G., Zhang, Q., Liang, X., Liu, Y., Gao, M., Guo, Y. & Chen, L. (2020a) Apremilast ameliorates ox-LDL-induced endothelial dysfunction mediated by KLF6. *Aging*. 12 (19), 19012–19021. doi:10.18632/aging.103665.

Wang, Q., Zuo, X., Wang, Y., Xie, W., Wang, H. & Zhang, M. (2013) Monocrotaline-induced pulmonary arterial hypertension is attenuated by TNF-α antagonists via the suppression of TNF-α expression and NF-κB pathway in rats. *Vascular Pharmacology*. 58 (1), 71–77. doi:10.1016/j.vph.2012.07.006.

Wang, T.-M., Wang, S.-S., Xu, Y.-J., Zhao, C.-M., Qiao, X.-H., Yang, C.-X., Liu, X.-Y. & Yang, Y.-Q. (2021) SOX17 Loss-of-Function Mutation Underlying Familial Pulmonary Arterial Hypertension. *International Heart Journal*. 62 (3), 566–574. doi:10.1536/ihj.20-711.

Wang, W.Y., Lin, D., Jarman, E.H., Polacheck, W.J. & Baker, B.M. (2020b) Functional angiogenesis requires microenvironmental cues balancing endothelial cell migration and proliferation. *Lab on a chip*. 20 (6), 1153–1166. doi:10.1039/c9lc01170f.

Wang, X.-J., Lian, T.-Y., Jiang, X., Liu, S.-F., Li, S.-Q., et al. (2019a) Germline BMP9 mutation causes idiopathic pulmonary arterial hypertension. *European Respiratory Journal*. 53 (3). doi:10.1183/13993003.01609-2018.

Wang, Y., Yang, C., Gu, Q., Sims, M., Gu, W., Pfeffer, L.M. & Yue, J. (2015) KLF4 Promotes Angiogenesis by Activating VEGF Signaling in Human Retinal Microvascular Endothelial Cells. *PloS One*. 10 (6), e0130341. doi:10.1371/journal.pone.0130341.

Wang, Z., Mehra, V., Simpson, M.T., Maunze, B., Chakraborty, A., Holan, L., Eastwood, E., Blackmore, M.G. & Venkatesh, I. (2018) KLF6 and STAT3 co-occupy regulatory DNA and functionally synergize to promote axon growth in CNS neurons. *Scientific Reports*. 8 (1), 12565. doi:10.1038/s41598-018-31101-5.

Wang, Z., Yang, K., Zheng, Q., Zhang, C., Tang, H., et al. (2019b) Divergent changes of p53 in pulmonary arterial endothelial and smooth muscle cells involved in the development of pulmonary hypertension. *American Journal of Physiology - Lung Cellular and Molecular Physiology*. 316 (1), L216–L228. doi:10.1152/ajplung.00538.2017.

Wani, M.A., Means, R.T. & Lingrel, J.B. (1998) Loss of LKLF function results in embryonic lethality in mice. *Transgenic Research*. 7 (4), 229–238. doi:10.1023/a:1008809809843.

Wani, M.A., Wert, S.E. & Lingrel, J.B. (1999) Lung Kruppel-like factor, a zinc finger transcription factor, is essential for normal lung development. *The Journal of Biological Chemistry*. 274 (30), 21180–21185. doi:10.1074/jbc.274.30.21180.

Wechezak, A.R., Viggers, R.F. & Sauvage, L.R. (1985) Fibronectin and F-actin redistribution in cultured endothelial cells exposed to shear stress. *Laboratory Investigation; a Journal of Technical Methods and Pathology*. 53 (6), 639–647.

Wei, G., Zhu, D., Sun, Y., Zhang, L., Liu, X., Li, M. & Gu, J. (2021) The protective effects of azilsartan against oscillatory shear stress-induced endothelial dysfunction and inflammation are mediated by KLF6. *Journal of Biochemical and Molecular Toxicology*. 35 (6), 1–8. doi:10.1002/jbt.22766.

Weisel, F.C., Kloepping, C., Pichl, A., Sydykov, A., Kojonazarov, B., et al. (2014) Impact of S-Adenosylmethionine Decarboxylase 1 on Pulmonary Vascular Remodeling. *Circulation*. 129 (14), 1510–1523. doi:10.1161/CIRCULATIONAHA.113.006402.

Welch, C.L., Aldred, M.A., Balachandar, S., Dooijes, D., Eichstaedt, C.A., et al. (2023) Defining the clinical validity of genes reported to cause pulmonary arterial hypertension. *Genetics in Medicine*. 25 (11). doi:10.1016/j.gim.2023.100925.

Welsh, D.J., Peacock, A.J., MacLean, M. & Harnett, M. (2001) Chronic hypoxia induces constitutive p38 mitogen-activated protein kinase activity that correlates with enhanced cellular proliferation in fibroblasts from rat pulmonary but not systemic arteries. *American Journal of Respiratory and Critical Care Medicine*. 164 (2), 282–289. doi:10.1164/ajrccm.164.2.2008054.

Welsh, D.J., Scott, P., Plevin, R., Wadsworth, R. & Peacock, A.J. (1998) Hypoxia enhances cellular proliferation and inositol 1,4, 5-triphosphate generation in fibroblasts from bovine pulmonary artery but not from mesenteric artery. *American Journal of Respiratory and Critical Care Medicine*. 158 (6), 1757–1762. doi:10.1164/ajrccm.158.6.9706054.

Welsh, D.J., Scott, P.H. & Peacock, A.J. (2006) p38 MAP kinase isoform activity and cell cycle regulators in the proliferative response of pulmonary and systemic artery fibroblasts to acute hypoxia. *Pulmonary Pharmacology & Therapeutics*. 19 (2), 128–138. doi:10.1016/j.pupt.2005.04.008.

White, S.J., Hayes, E.M., Lehoux, S., Jeremy, J.Y., Horrevoets, A.J. & Newby, A.C. (2011) Characterization of the Differential Response of Endothelial Cells Exposed to Normal and Elevated Laminar Shear Stress. *Journal of Cellular Physiology*. 226 (11), 2841–2848. doi:10.1002/jcp.22629.

Witt, K.E. & Huerta-Sánchez, E. (2019) Convergent evolution in human and domesticate adaptation to high-altitude environments. *Philosophical Transactions of the Royal Society B: Biological Sciences*. 374 (1777), 20180235. doi:10.1098/rstb.2018.0235.

Wojciak-Stothard, B. (2011) Endothelial Cell Migration Under Flow. In: C.M. Wells & M. Parsons (eds.). *Cell Migration: Developmental Methods and Protocols*. Methods in Molecular Biology. Totowa, NJ, Humana Press. pp. 137–147. doi:10.1007/978-1-61779-207-6_10.

Wojciak-Stothard, B., Abdul-Salam, V.B., Lao, K.H., Tsang, H., Irwin, D.C., Lisk, C., Loomis, Z., Stenmark, K.R., Edwards, J.C., Yuspa, S.H., Howard, L.S., Edwards, R.J., Rhodes, C.J., Gibbs, J.S.R., Wharton, J., Zhao, L. & Wilkins, M.R. (2014) Aberrant Chloride Intracellular Channel 4 Expression Contributes to Endothelial Dysfunction in Pulmonary Arterial Hypertension. *Circulation*. 129 (17), 1770–1780. doi:10.1161/CIRCULATIONAHA.113.006797.

Wojciak-Stothard, B., Tsang, L.Y.F. & Haworth, S.G. (2005) Rac and Rho play opposing roles in the regulation of hypoxia/reoxygenation-induced permeability changes in pulmonary artery endothelial cells. *American Journal of Physiology. Lung Cellular and Molecular Physiology*. 288 (4), L749-760. doi:10.1152/ajplung.00361.2004.

Wright, A.F., Ewart, M.-A., Mair, K., Nilsen, M., Dempsie, Y., Loughlin, L. & Maclean, M.R. (2015) Oestrogen receptor alpha in pulmonary hypertension. *Cardiovascular Research*. 106 (2), 206–216. doi:10.1093/cvr/cvv106.

Wu, D. & Yotnda, P. (2011) Induction and Testing of Hypoxia in Cell Culture. *Journal of Visualized Experiments : JoVE*. (54), 2899. doi:10.3791/2899.

Wu, D., Huang, R.-T., Hamanaka, R.B., Krause, M., Oh, M.-J., Kuo, C.-H., Nigdelioglu, R., Meliton, A.Y., Witt, L., Dai, G., Civelek, M., Prabhakar, N.R., Fang, Y. & Mutlu, G.M. (2017) HIF-1α is required for disturbed flow-induced metabolic reprogramming in human and porcine vascular endothelium K. Alitalo (ed.). *eLife*. 6, e25217. doi:10.7554/eLife.25217.

Wu, X., Ma, J., Ding, D., Ma, Y., Wei, Y. & Jing, Z. (2022) Experimental animal models of pulmonary hypertension: Development and challenges. *Animal Models and Experimental Medicine*. 5 (3), 207–216. doi:10.1002/ame2.12220.

Wu, Y., Hao, R., Lan, B., Mu, Y., Dang, F. & Wang, R. (2021) The protective effects of naproxen against interleukin-1β (IL-1β)- induced damage in human umbilical vein endothelial cells (HUVECs). *Bioengineered*. 12 (1), 5361–5372. doi:10.1080/21655979.2021.1955560.

Xie, X., Wang, F., Zhu, L., Yang, H., Pan, D., Liu, Y., Qu, X., Gu, Y., Li, X. & Chen, S. (2020) Low shear stress induces endothelial cell apoptosis and monocyte adhesion by upregulating PECAM-1 expression. *Molecular Medicine Reports*. 21 (6), 2580–2588. doi:10.3892/mmr.2020.11060.

Xu, J., Li, X., Zhou, S., Wang, R., Wu, M., Tan, C., Chen, J. & Wang, Z. (2021) Inhibition of CXCR4 ameliorates hypoxia-induced pulmonary arterial hypertension in rats. *American Journal of Translational Research*. 13 (3), 1458–1470.

Xu, W., Janocha, A.J. & Erzurum, S.C. (2021) Metabolism in Pulmonary Hypertension. *Annual review of physiology*. 83, 551–576. doi:10.1146/annurev-physiol-031620-123956.

Xu, W., Kaneko, F.T., Zheng, S., Comhair, S.A.A., Janocha, A.J., Goggans, T., Thunnissen, F.B.J.M., Farver, C., Hazen, S.L., Jennings, C., Dweik, R.A., Arroliga, A.C. & Erzurum, S.C. (2004) Increased arginase II and decreased NO synthesis in endothelial cells of patients with pulmonary arterial hypertension. *FASEB journal: official publication of the Federation of American Societies for Experimental Biology*. 18 (14), 1746–1748. doi:10.1096/fj.04-2317fje.

Yan, D., Li, G., Zhang, Y. & Liu, Y. (2019) Angiotensin-converting enzyme 2 activation suppresses pulmonary vascular remodeling by inducing apoptosis through the Hippo signaling pathway in rats with pulmonary arterial hypertension. *Clinical and Experimental Hypertension (New York, N.Y.: 1993)*. 41 (6), 589–598. doi:10.1080/10641963.2019.1583247.

Yang, F., Zhang, Y., Zhu, J., Wang, J., Jiang, Z., Zhao, C., Yang, Q., Huang, Y., Yao, W., Pang, W., Han, L. & Zhou, J. (2020) Laminar Flow Protects Vascular Endothelial Tight Junctions and Barrier Function via Maintaining the Expression of Long Non-coding RNA MALAT1. *Frontiers in Bioengineering and Biotechnology*. 8, 647. doi:10.3389/fbioe.2020.00647.

Yang, J., Zhou, R., Zhang, M., Tan, H. & Yu, J. (2018) Betaine Attenuates Monocrotaline-Induced Pulmonary Arterial Hypertension in Rats via Inhibiting Inflammatory Response. *Molecules*. 23 (6), 1274. doi:10.3390/molecules23061274.

Yang, L., Wan, N., Gong, F., Wang, X., Feng, L. & Liu, G. (2023) Transcription factors and potential therapeutic targets for pulmonary hypertension. *Frontiers in Cell and Developmental Biology*. 11, 1132060. doi:10.3389/fcell.2023.1132060.

Yang, Y., Yu, H., Yang, C., Zhang, Y., Ai, X., Wang, X., Lu, K. & Yi, B. (2019) Krüppel-like factor 6 mediates pulmonary angiogenesis in rat experimental hepatopulmonary syndrome and is aggravated by bone morphogenetic protein 9. *Biology Open*. 8 (6), bio040121. doi:10.1242/bio.040121.

Yi, D., Liu, B., Ding, H., Li, S., Li, R., Pan, J., Ramirez, K., Xia, X., Kala, M., Ye, Q., Lee, W.H., Frye, R.E., Wang, T., Zhao, Y., Knox, K.S., Glembotski, C.C., Fallon, M.B. & Dai, Z. (2023) E2F1 Mediates SOX17 Deficiency–Induced Pulmonary Hypertension. *Hypertension*. 80 (11), 2357–2371. doi:10.1161/HYPERTENSIONAHA.123.21241.

Young, A., Wu, W., Sun, W., Larman, H.B., Wang, N., Li, Y.-S., Shyy, J.Y., Chien, S. & García-Cardeña, G. (2009) Flow Activation of AMP-Activated Protein Kinase in Vascular Endothelium Leads to Krüppel-Like Factor 2 Expression. *Arteriosclerosis,*

Thrombosis, and Vascular Biology. 29 (11), 1902–1908. doi:10.1161/ATVBAHA.109.193540.

Young, J.M., Williams, D.R. & Thompson, A.A.R. (2019) Thin Air, Thick Vessels: Historical and Current Perspectives on Hypoxic Pulmonary Hypertension. *Frontiers in Medicine*. 6, 93. doi:10.3389/fmed.2019.00093.

Yu, A.Y., Shimoda, L.A., Iyer, N.V., Huso, D.L., Sun, X., McWilliams, R., Beaty, T., Sham, J.S.K., Wiener, C.M., Sylvester, J.T. & Semenza, G.L. (1999) Impaired physiological responses to chronic hypoxia in mice partially deficient for hypoxia-inducible factor 1α. *Journal of Clinical Investigation*. 103 (5), 691. doi:10.1172/JCI5912.

Yu, X., Chen, X., Zheng, X.D., Zhang, J., Zhao, X., Liu, Y., Zhang, H., Zhang, L., Yu, H., Zhang, M., Ma, C., Hao, X. & Zhu, D. (2018) Growth Differentiation Factor 11 Promotes Abnormal Proliferation and Angiogenesis of Pulmonary Artery Endothelial Cells. *Hypertension (Dallas, Tex.: 1979)*. 71 (4), 729–741. doi:10.1161/HYPERTENSIONAHA.117.10350.

Yuan, J.X.-J. & Rubin, L.J. (2005) Pathogenesis of Pulmonary Arterial Hypertension. *Circulation*. 111 (5), 534–538. doi:10.1161/01.CIR.0000156326.48823.55.

Yuan, K., Shao, N.-Y., Hennigs, J.K., Discipulo, M., Orcholski, M.E., Shamskhou, E., Richter, A., Hu, X., Wu, J.C. & de Jesus Perez, V.A. (2016) Increased Pyruvate Dehydrogenase Kinase 4 Expression in Lung Pericytes Is Associated with Reduced Endothelial-Pericyte Interactions and Small Vessel Loss in Pulmonary Arterial Hypertension. *The American Journal of Pathology*. 186 (9), 2500–2514. doi:10.1016/j.ajpath.2016.05.016.

Zeng, B., Lin, J., Cai, X., Che, L., Zeng, W. & Liu, S. (2022) Krüppel-Like Factor 6 Downregulation Is Connected with a Poor Prognosis and Tumor Growth in Non-Small-Cell Lung Cancer. *Computational and Mathematical Methods in Medicine*. 2022, 3193553. doi:10.1155/2022/3193553.

Zeng, X.-Q., Li, N., Pan, D.-Y., Miao, Q., Ma, G.-F., Liu, Y.-M., Tseng, Y.-J., Li, F., Xu, L.-L. & Chen, S.-Y. (2015) Kruppel-like factor 2 inhibit the angiogenesis of cultured human liver sinusoidal endothelial cells through the ERK1/2 signaling pathway. *Biochemical and Biophysical Research Communications*. 464 (4), 1241–1247. doi:10.1016/j.bbrc.2015.07.113.

Zha, B., Qiu, P., Zhang, C., Li, X. & Chen, Z. (2020) GPR30 Promotes the Phenotypic Switching of Vascular Smooth Muscle Cells via Activating the AKT and ERK Pathways. *OncoTargets and therapy*. 13, 3801–3808. doi:10.2147/OTT.S244128.

Zhang, H.-S., Liu, Q., Piao, C.-M., Zhu, Y., Li, Q.-Q., Du, J. & Gu, H. (2019a) Genotypes and Phenotypes of Chinese Pediatric Patients With Idiopathic and Heritable Pulmonary Arterial Hypertension—A Single-Center Study. *Canadian Journal of Cardiology*. 35 (12), 1851–1856. doi:10.1016/j.cjca.2019.07.628.

Zhang, J., Tang, X., Zhang, X., Zhou, C. & Yin, K.-J. (2019b) *Krüppel-like transcription factors in vascular biology and cerebrovascular diseases*.

Zhang, K., Sun, L. & Kang, Y. (2023) Regulation of phosphoglycerate kinase 1 and its critical role in cancer. *Cell Communication and Signaling : CCS*. 21, 240. doi:10.1186/s12964-023-01256-4.

Zhang, Q., Cannavicci, A. & Kutryk, M.J.B. (2022) Exploring Endothelial Colony-Forming Cells to Better Understand the Pathophysiology of Disease: An Updated Review. *Stem Cells International*. 2022, 4460041. doi:10.1155/2022/4460041.

Zhang, R., Wang, X.-J., Zhang, H.-D., Sun, X.-Q., Zhao, Q.-H., Wang, L., He, J., Jiang, X., Liu, J.-M. & Jing, Z.-C. (2016) Profiling nitric oxide metabolites in patients with idiopathic pulmonary arterial hypertension. *European Respiratory Journal*. 48 (5), 1386–1395. doi:10.1183/13993003.00245-2016.

Zhang, X., Zhang, C., Li, Q., Piao, C., Zhang, H. & Gu, H. (2021) Clinical characteristics and prognosis analysis of idiopathic and hereditary pulmonary hypertension patients with ACVRL1 gene mutations. *Pulmonary Circulation*. 11 (4), 20458940211044577. doi:10.1177/20458940211044577.

Zhang, Z., Zhu, S., Wang, M., Wang, X., Tong, X., Wan, J. & Ding, J. (2022) New progress in diagnosis and treatment of pulmonary arterial hypertension. *Journal of Cardiothoracic Surgery*. 17, 216. doi:10.1186/s13019-022-01947-y.

Zhao, L., Long, L., Morrell, N.W. & Wilkins, M.R. (1999) NPR-A-Deficient mice show increased susceptibility to hypoxia-induced pulmonary hypertension. *Circulation*. 99 (5), 605–607. doi:10.1161/01.cir.99.5.605.

Zhao, X., Monson, C., Gao, C., Gouon-Evans, V., Matsumoto, N., Sadler, K.C. & Friedman, S.L. (2010) Klf6/copeb is required for hepatic outgrowth in zebrafish and for hepatocyte specification in mouse ES cells. *Developmental Biology*. 344 (1), 79–93. doi:10.1016/j.ydbio.2010.04.018.

Zhao, Y.D., Courtman, D.W., Deng, Y., Kugathasan, L., Zhang, Q. & Stewart, D.J. (2005) Rescue of Monocrotaline-Induced Pulmonary Arterial Hypertension Using Bone Marrow–Derived Endothelial-Like Progenitor Cells. *Circulation Research*. 96 (4), 442–450. doi:10.1161/01.RES.0000157672.70560.7b.

Zheng, X., Li, A., Zhao, L., Zhou, T., Shen, Q., Cui, Q. & Qin, X. (2013) Key role of microRNA-15a in the KLF4 suppressions of proliferation and angiogenesis in endothelial and vascular smooth muscle cells. *Biochemical and Biophysical Research Communications*. 437 (4), 625–631. doi:10.1016/j.bbrc.2013.07.017.

Zhou, C., Townsley, M.I., Alexeyev, M., Voelkel, N.F. & Stevens, T. (2016) Endothelial hyperpermeability in severe pulmonary arterial hypertension: role of store-operated calcium entry. *American Journal of Physiology. Lung Cellular and Molecular Physiology*. 311 (3), L560-569. doi:10.1152/ajplung.00057.2016.

Zhou, G., Hamik, A., Nayak, L., Tian, H., Shi, H., et al. (2012) Endothelial Kruppel-like factor 4 protects against atherothrombosis in mice. *The Journal of Clinical Investigation*. 122 (12), 4727–4731. doi:10.1172/JCI66056.

Zhou, Y., Niu, W., Luo, Y., Li, H., Xie, Y., Wang, H., Liu, Y., Fan, S., Li, Z., Xiong, W., Li, X., Ren, C., Tan, M., Li, G. & Zhou, M. (2019a) p53/Lactate dehydrogenase A axis negatively regulates aerobic glycolysis and tumor progression in breast cancer expressing wild-type p53. *Cancer Science*. 110 (3), 939–949. doi:10.1111/cas.13928.

Zhou, Y., Zhou, B., Pache, L., Chang, M., Khodabakhshi, A.H., Tanaseichuk, O., Benner, C. & Chanda, S.K. (2019b) Metascape provides a biologist-oriented resource for the analysis of systems-level datasets. *Nature Communications*. 10 (1), 1523. doi:10.1038/s41467-019-09234-6.

Zhu, L., Yang, X.-P., Janic, B., Rhaleb, N.-E., Harding, P., Nakagawa, P., Peterson, E.L. & Carretero, O.A. (2016) Ac-SDKP suppresses TNF-α-induced ICAM-1 expression in endothelial cells via inhibition of IκB kinase and NF-κB activation. *American Journal of Physiology - Heart and Circulatory Physiology*. 310 (9), H1176–H1183. doi:10.1152/ajpheart.00252.2015.

Zhu, N., Gonzaga-Jauregui, C., Welch, C., Ma, L., Qi, H., et al. (2018a) Exome Sequencing in Children with Pulmonary Arterial Hypertension Demonstrates Differences Compared to Adults. *Circulation. Genomic and precision medicine*. 11 (4), e001887. doi:10.1161/CIRCGEN.117.001887.

Zhu, N., Pauciulo, M.W., Welch, C.L., Lutz, K.A., Coleman, A.W., et al. (2019) Novel risk genes and mechanisms implicated by exome sequencing of 2572 individuals with pulmonary arterial hypertension. *Genome Medicine*. 11 (1), 69. doi:10.1186/s13073-019-0685-z.

Zhu, N., Welch, C.L., Wang, J., Allen, P.M., Gonzaga-Jauregui, C., et al. (2018b) Rare variants in SOX17 are associated with pulmonary arterial hypertension with congenital heart disease. *Genome Medicine*. 10 (1), 56. doi:10.1186/s13073-018-0566-x.

Zou, Z., Long, X., Zhao, Q., Zheng, Y., Song, M., Ma, S., Jing, Y., Wang, S., He, Y., Esteban, C.R., Yu, N., Huang, J., Chan, P., Chen, T., Belmonte, J.C.I., Zhang, W., Qu, J. & Liu, G.-H. (2021) A Single-Cell Transcriptomic Atlas of Human Skin Aging. *Developmental Cell*. 56 (3), 383-397.e8. doi:10.1016/j.devcel.2020.11.002.

Zuo, W., Liu, N., Zeng, Y., Xiao, Z., Wu, K., Yang, F., Li, B., Song, Q., Xiao, Y. & Liu, Q. (2021) Luteolin Ameliorates Experimental Pulmonary Arterial Hypertension via Suppressing Hippo-YAP/PI3K/AKT Signaling Pathway. *Frontiers in Pharmacology*. 12, 663551. doi:10.3389/fphar.2021.663551.

Appendices

Appendix 1: Supplementary figures and tables

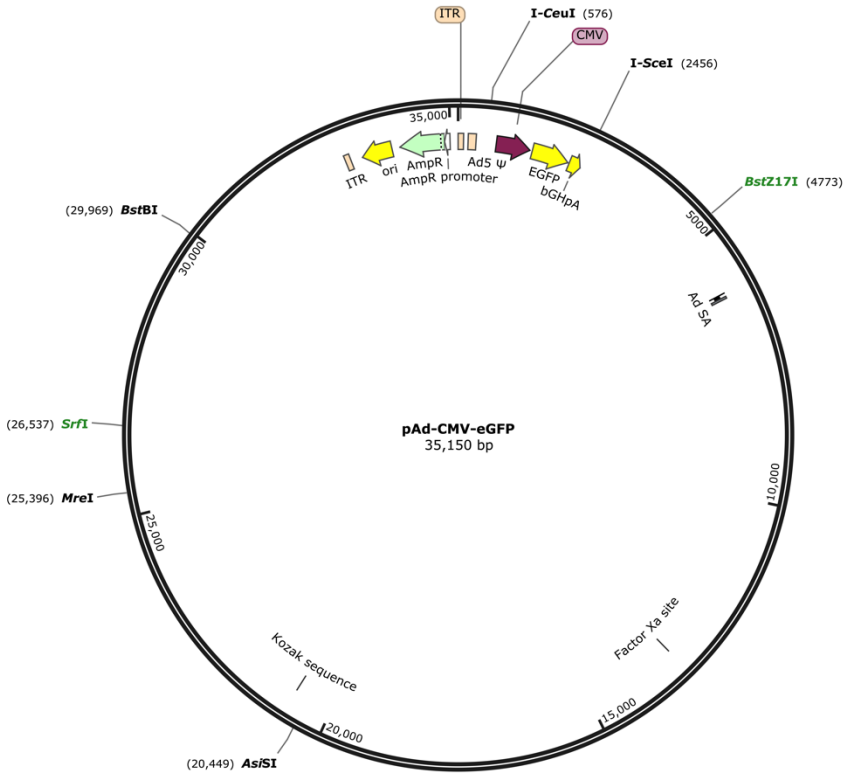

Figure S1: Adenoviral vector map Ad-GFP.
Backbone: recombinant human adenovirus Type5 (dE1/E3); promoter: CMV; reporter: enhanced green fluorescent protein (eGFP). Map obtained from (Vector Biolabs,1060).

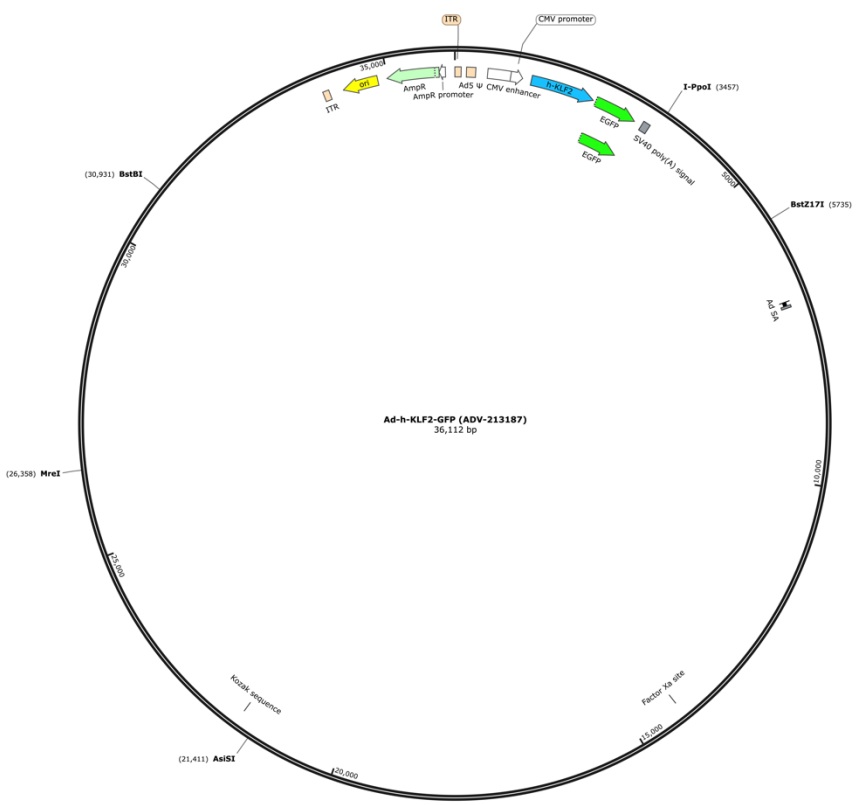

Figure S2: Adenoviral vector map human KLF2.
Backbone: Human Adenovirus Type5 (dE1/E3); promoter: CMV; transgene: human KLF2; marker/tag: GFP (fused to C-terminal); RefSeq# BC071983. Map obtained from (Vector Biolabs, ADV-213187).

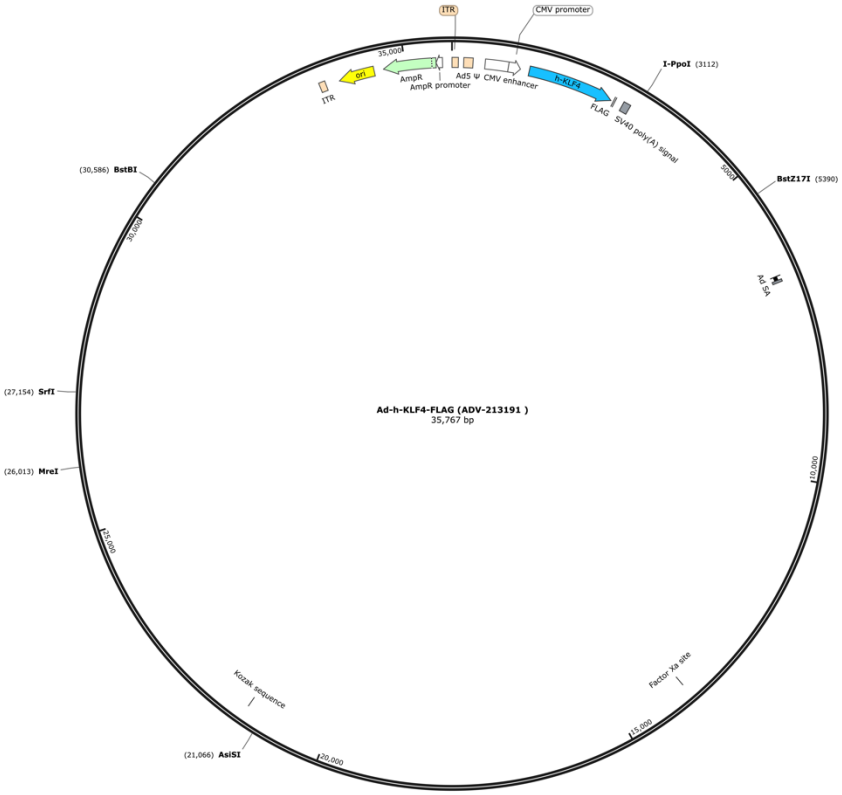

Figure S3: Adenoviral vector map human KLF4.
Backbone: recombinant adeno-associated virus (AAV); promoter: CMV; transgene: human KLF4; marker/tag: FLAG (fused to C-terminal); RefSeq# BC029923. Map obtained from (Vector Biolabs, ADV-213191).

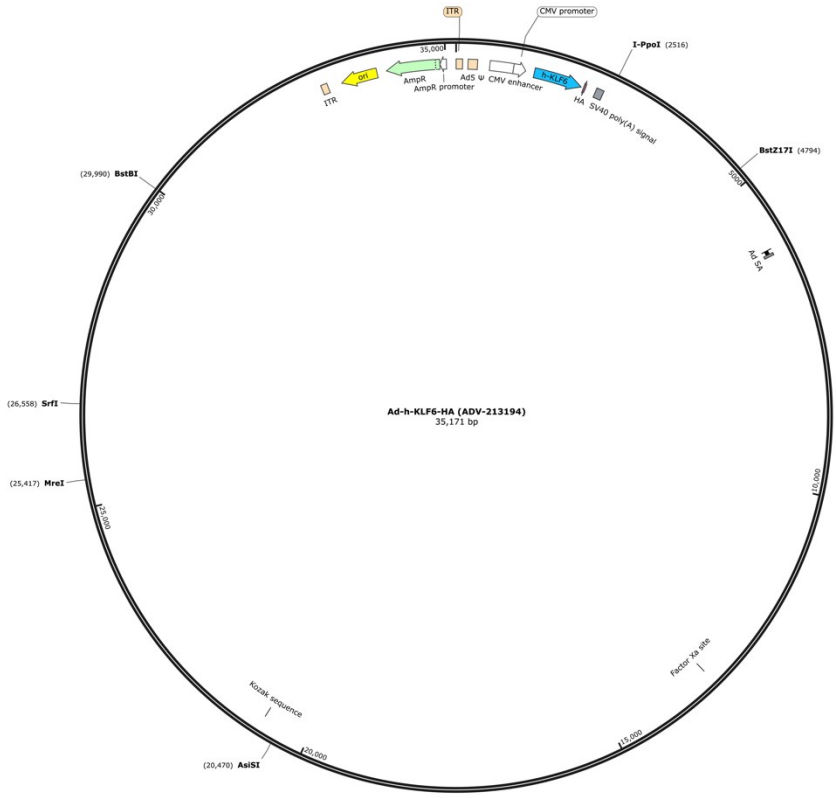

Figure S4: Adenoviral vector map human KLF6.
Backbone: recombinant adeno-associated virus (AAV); promoter: CMV; transgene: human KLF6; marker/tag: HA (fused to C-terminal); RefSeq# BC000311. Map obtained from (Vector Biolabs, ADV-213194).

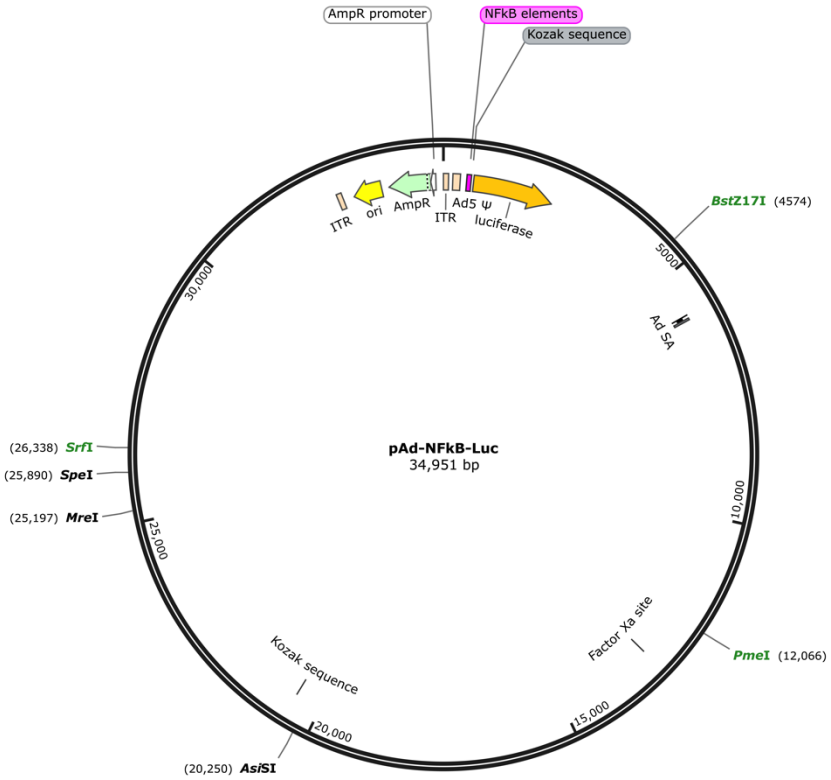

Figure S5: Adenoviral vector map Ad-NFKb-Luc.
Backbone: recombinant human adenovirus Type5 (dE1/E3); promoter: direct repeats of nuclear factor-κB (NF-κB) response elements; reporter: luciferase. Map obtained from (Vector Biolabs,1740).

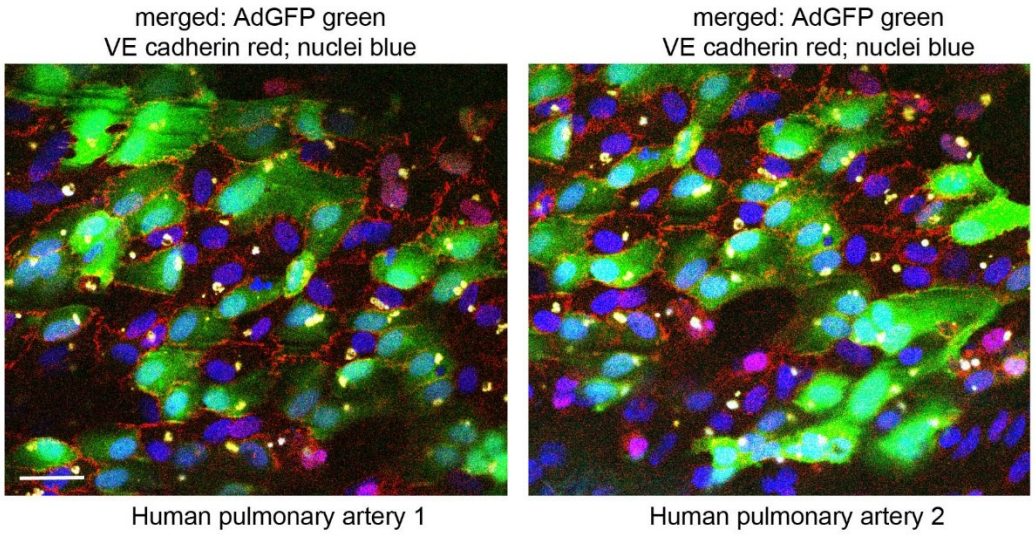

Figure S6: Adenoviral transduction efficiency in the endothelium of human pulmonary artery explants. Surgically removed pulmonary arteries were opened up and the endothelial side was incubated with AdGFP for 24 hours. Following a 24-hour incubation, the tissues were fixed and stained for endothelial adherens junctions marker VE-cadherin. In the merged image, VE-cadherin is red, nuclei are blue (DAPI), and AdGFP-overexpressing cells are green; n=2. Scale bar = 20µm.

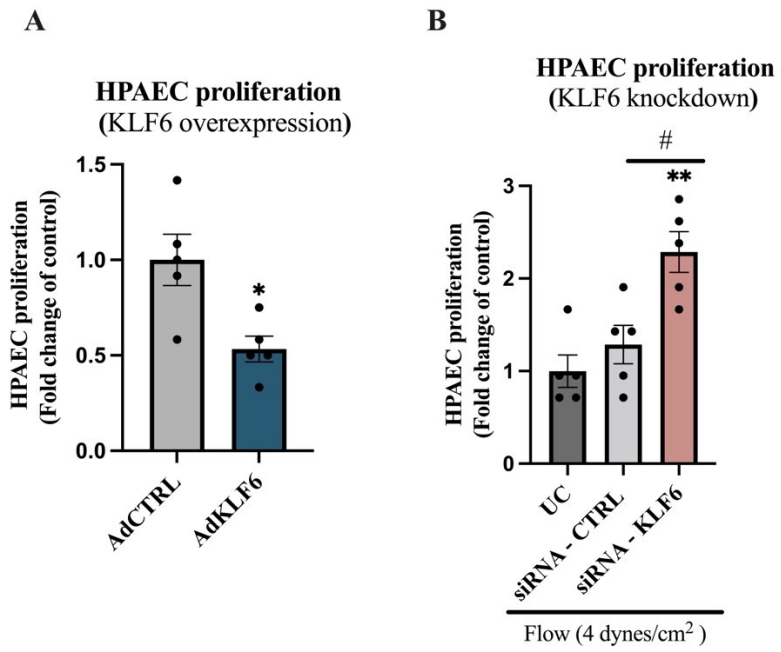

Figure S7: Effect of KLF6 overexpression and knockdown on HPAEC proliferation.
HPAEC proliferation was assessed by EdU incorporation assay in **(A)** HPAECs infected with AdCTRL or AdKLF6. **(B)** HPAECs transfected with KLF6 siRNA or siRNA-CTRL. 24h or 48 h post-transfection, the cells were cultured in serum-reduced (0.2% FBS) and growth factor-free medium. After 6h, EdU nucleotides were added directly to cell culture medium at a final concentration of 10 µM. CTRL-siRNA and KLF6-siRNA-transfected cells were subjected to laminar flow of 4 dynes/cm^2 for 24h. 24 hours later, EdU-positive cells were observed under a fluorescent Zeiss Axio Observer widefield microscope (Carl Zeiss AG, Germany) with a 10x objective. Percentage of EdU-positive cells out of total number of cells was quantified with ImageJ software. $^{*}P<0.05$, comparison with adenoviral controls using unpaired t-test or $^{**}P<0.01$, comparison with untreated control; $^{\#\#}P<0.01$, comparison with siRNA negative control using one-way ANOVA with Tukey's post-hoc test; n=5. Error bars indicate mean ±SEM.

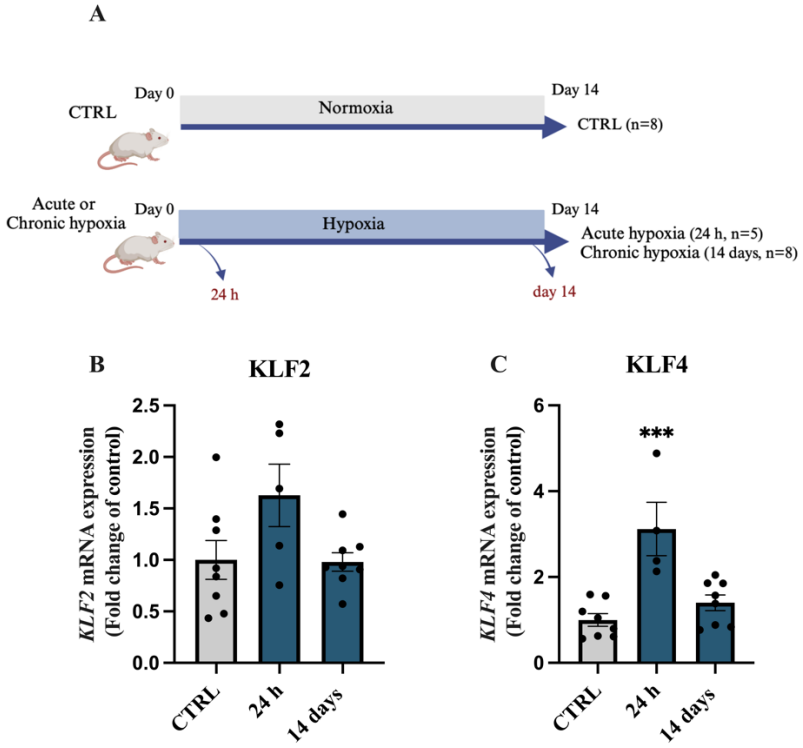

Figure S8: *KLF2* and *KLF4* mRNA expression levels in lungs of chronic hypoxia mouse model of PAH.
(A) Schematic diagram of experimental timeline. **(B)** *KLF2* mRNA expression levels in lung tissues of chronic hypoxia mouse at 14 hours and 14 days after hypoxia exposure. **(C)** *KLF4* mRNA expression levels in lung tissues of chronic hypoxia mouse at 14 hours and 14 days after hypoxia exposure. Data were normalized to the reference gene (*B2M*). ***P<0.001, comparison with normoxic control rats using one-way ANOVA with Tukey's post-hoc test; n=4-8. Error bars indicate mean ±SEM.

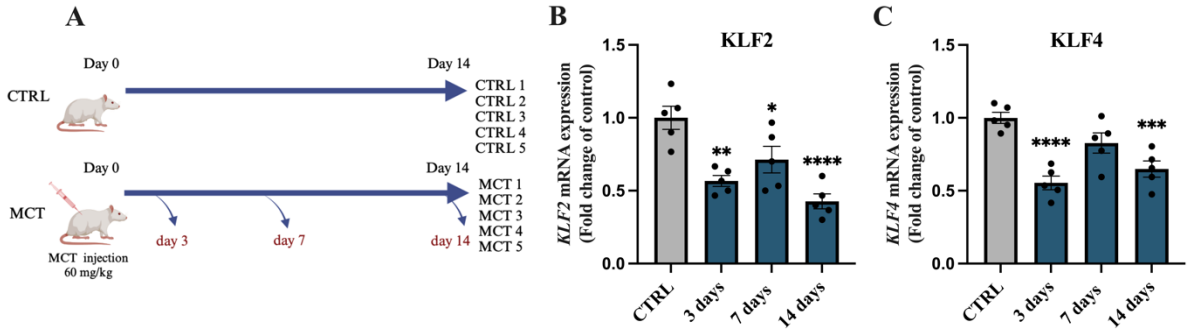

Figure S9: *KLF2* and *KLF4* mRNA expression levels in lungs of MCT rat model of PAH.
(A) Schematic diagram of experimental timeline. **(B)** *KLF2* mRNA expression levels in lung tissues of MCT rats at day 3, 7 and 14 after MCT injection. **(C)** *KLF4* mRNA expression levels in lung tissues of MCT rats at day 3, 7 and 14 after MCT injection. Data were normalized to the reference gene (*ACTB*). CTRL: healthy control; MCT: MCT PAH model. *P<0.05, **P<0.01, ***P<0.001, ****P<0.0001, comparison with control rats using one-way ANOVA with Tukey's post-hoc test; n=5. Error bars indicate mean ±SEM.

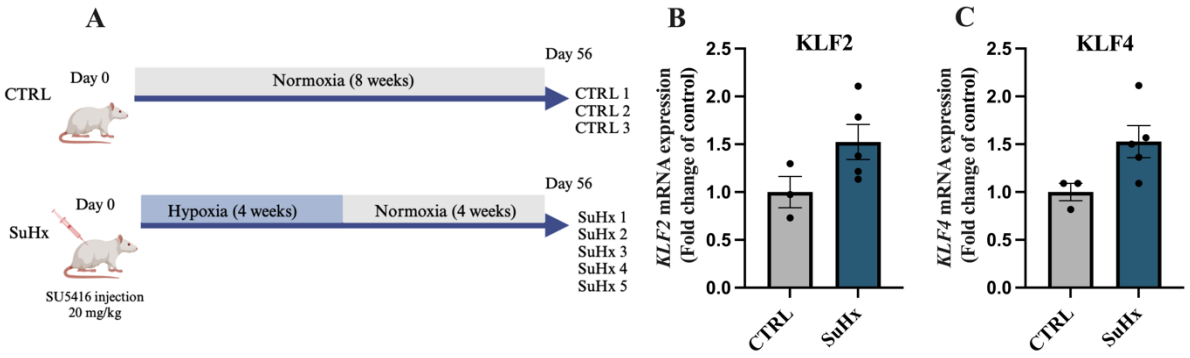

Figure S10: *KLF2* and *KLF4* mRNA expression levels in lungs of Sugen/hypoxia rat model of PAH.
(A) Schematic diagram of experimental design**. (B)** *KLF2* mRNA expression levels in lung tissues of Sugen/hypoxia rats at day 56. **(C)** *KLF4* mRNA expression levels in lung tissues of Sugen/hypoxia rats at day 56. Data were normalized to the reference gene (*ACTB*). CTRL: healthy control; SuHx: SuHx PAH model. Error bars indicate mean ±SEM; n=3-5.

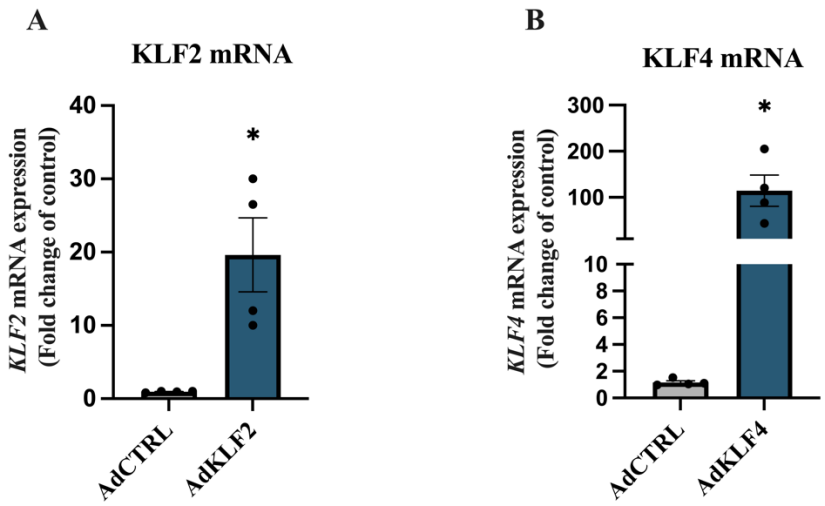

Figure S11: *KLF2* and *KLF4* overexpression in HPAECs.
(A) *KLF2* mRNA expression in HPAECs transfected with AdCTRL-GFP or AdKLF2-GFP. Data were normalized to the reference gene (β-Actin). *P<0.05, comparison with AdCTRL-GFP; unpaired t-test. Error bars indicate mean ±SEM; n=4. **(B)** *KLF4* mRNA expression in HPAECs transfected with AdCTRL or AdKLF4. Data were normalized to the reference gene (*ACTB*). *P<0.05, comparison with AdCTRL-GFP; unpaired t-test. Error bars indicate mean ±SEM; n=4.

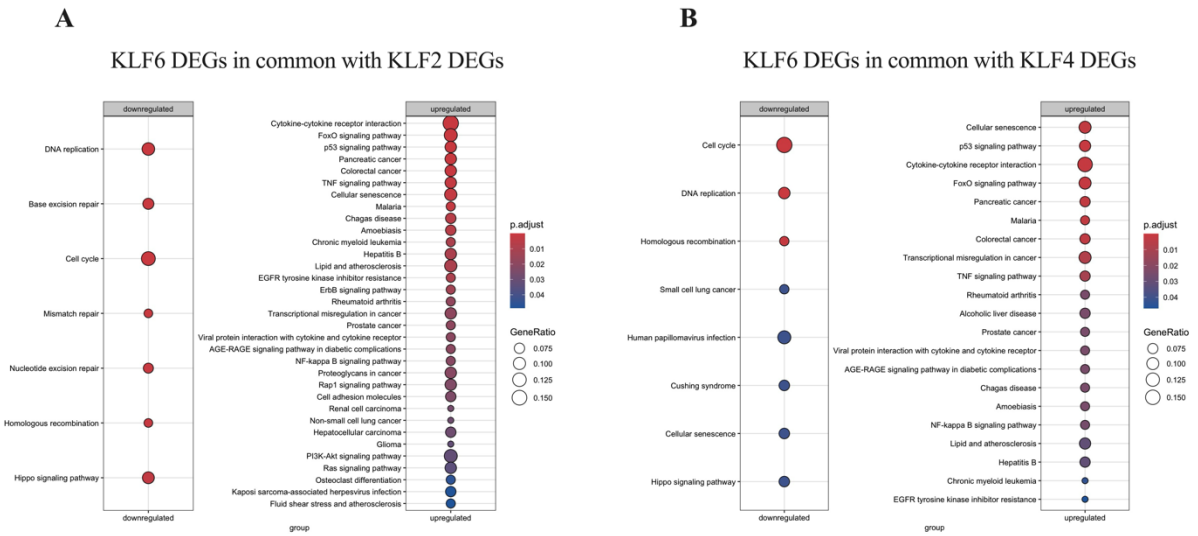

Figure S12: KEGG pathway analysis for KLF6 DEGs in common with KLF2 and KLF4 DEGs in HPAECs.

(A) Dot plot showing the enriched KEGG pathways of KLF6 DEGs (left, down-regulated genes; right, up -regulated genes) in common with KLF2 DEGs in HPAECs. n= 490 DEGs. **(B)** Dot plot showing the enriched KEGG pathways of KLF6 DEGs (left, down-regulated genes; right, up -regulated genes) in common with KLF4 DEGs in HPAECs. n= 400 DEGs. The colour of the dots represents the adjusted P-value, and the size of the dots represents the number of DEGs in the pathway.

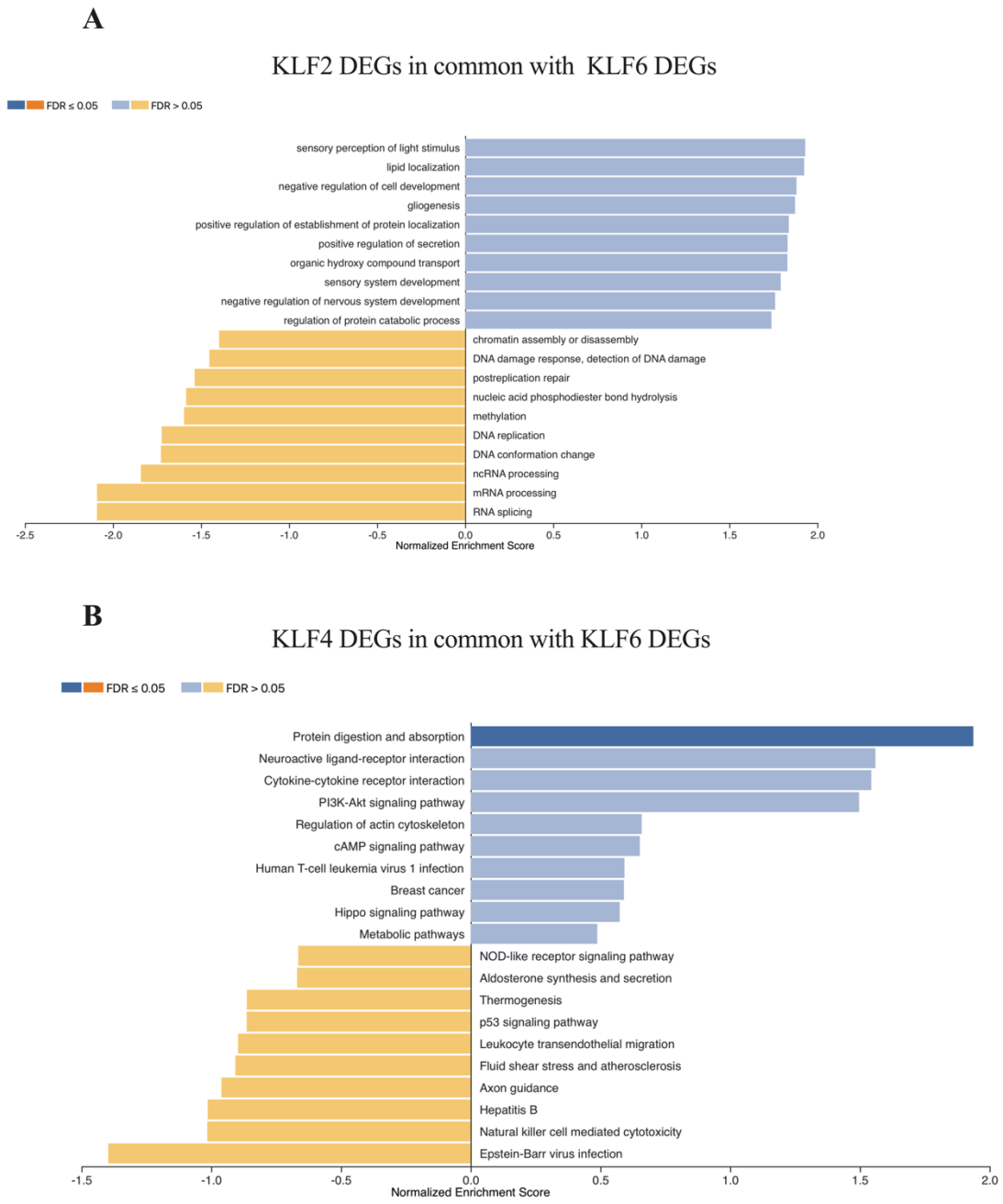

Figure S13: WebGestalt KEGG pathway analysis for KLF2 DEGs and KLF4 DEGs in common with KLF6 DEGs in HPAECs.
(A) WebGestalt KEGG pathway enrichment analysis of KLF2 DEGs in common with KLF6 DEGs in HPAECs. **(B)** WebGestalt KEGG pathway enrichment analysis of KLF2 DEGs in common with KLF6 DEGs in HPAECs. The x-axis represents normalized enrichment score. Darker colours = FDR ≤ 0.05; Lighter colours = FDR > 0.05.

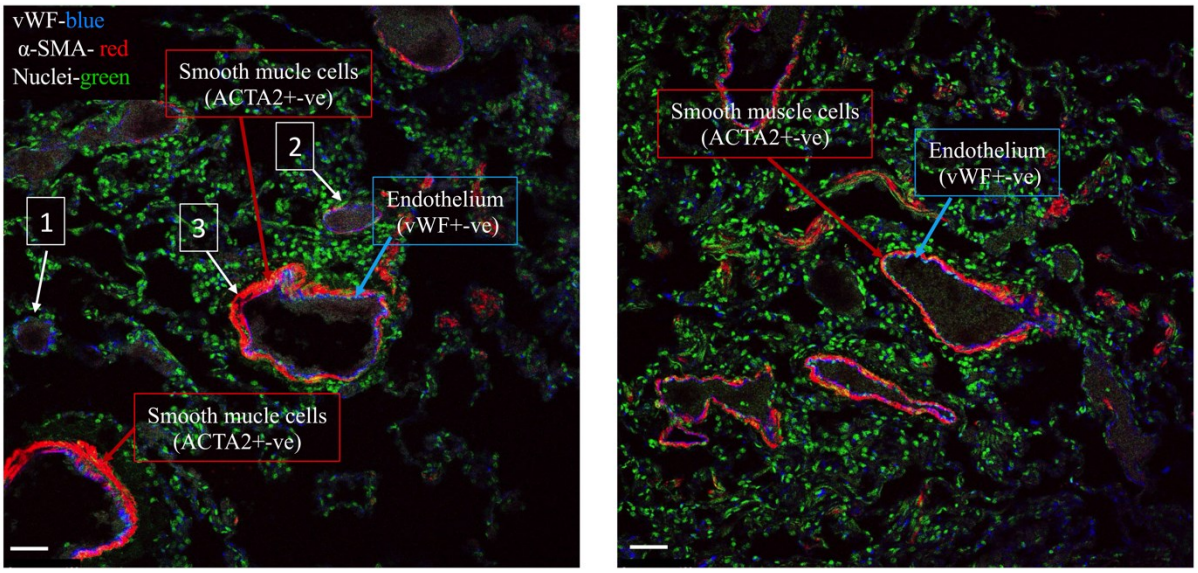

Figure S14: Optimization of immunofluorescence staining for spatial transcriptomics analysis. Representative confocal images of human lung sections immunostained for endothelial cells marker (vWF; blue) and smooth muscle cells marker (α-SMA; red) and nuclei were stained with DAPI (pseudocolor in green). Arrows point to a (1) small non-muscularised (2) larger partially muscularised and (3) muscularised intrapulmonary arteries. Scale bar=50µm

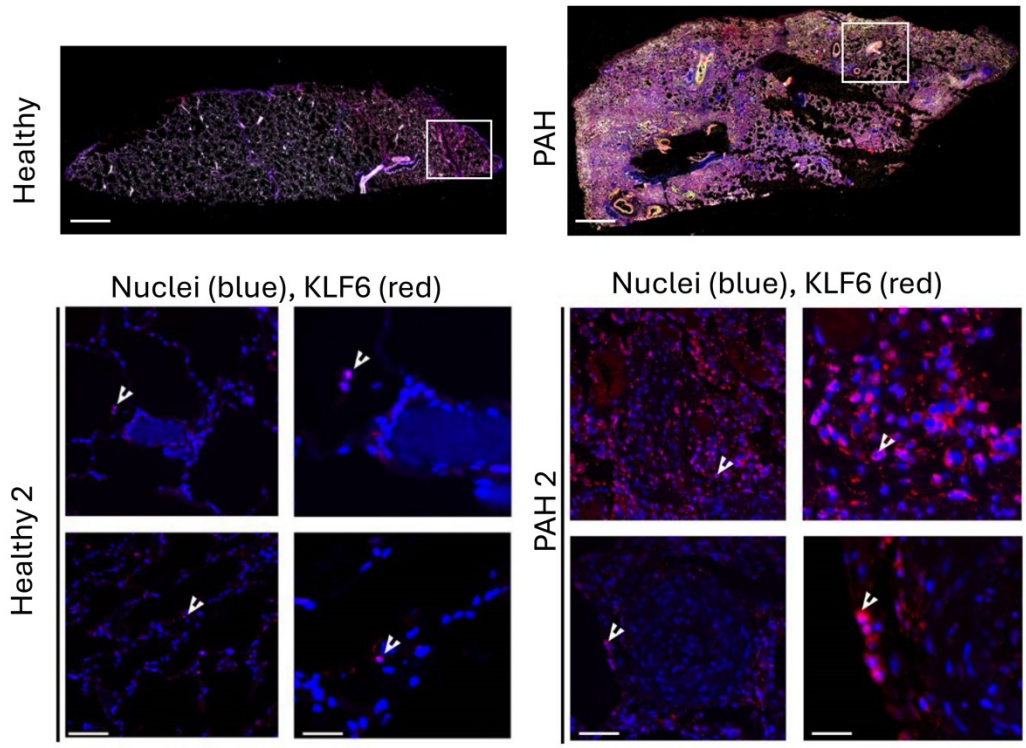

Figure S15: Representative images of tissue sections used for spatial transcriptomic and KLF6 localization. (A) Human healthy and PAH lung, immunofluorescence: vWF (red), α-SMA (yellow), nuclei (blue). Scale bar =600 µm. Boxed areas indicate regions illustrated in (Healthy 2) and (PAH 2) images below. KLF6 localization in **(B)** lung tissues from healthy control 2 and PAH patient 2; immunofluorescence: KLF6 (red) and nuclei (blue). Scale bar=50 µm. Enlarged corresponding images are shown in the right panel. Arrows point to nuclear localization of KLF6 (pink). Scale bar =20 µm

Gene Name	Log Fold Change	P value (p)	FDR (q)
Top 50 Up-regulated genes (ranked by FDR)			
ADAMTSL1	2.26	2.69E-40	5.27E-36
CD82	2.39	2.11E-39	4.13E-35
PIK3R3	2.56	3.07E-37	6.00E-33
EMCN	2.10	1.24E-35	2.42E-31
CDKN1A	2.08	1.53E-35	2.99E-31
LNCOG	2.61	1.46E-30	2.84E-26
LY96	2.29	6.18E-30	1.20E-25
APLN	3.28	2.46E-29	4.78E-25
CD34	2.19	3.88E-29	7.53E-25
PLAU	3.06	5.91E-29	1.15E-24
TSC22D3	2.09	6.06E-29	1.18E-24
BTG2	2.63	1.50E-28	2.91E-24
C1QTNF6	2.95	2.01E-28	3.90E-24
TGFBR2	2.43	2.15E-28	4.17E-24
FOXO1	2.35	3.25E-28	6.30E-24
ADAM19	2.34	1.46E-26	2.82E-22
RALA	2.01	5.92E-26	1.14E-21
KLF6	7.50	9.16E-26	1.77E-21
ROBO4	2.14	3.09E-25	5.95E-21
FAM107A	2.73	7.70E-25	1.48E-20
CREB3L1	2.45	2.41E-24	4.64E-20
ZNF24TR	2.07	3.23E-24	6.21E-20
ACVRL1	2.29	4.54E-24	8.73E-20
MGAT4A	2.06	5.21E-24	1.00E-19
PRAG1	2.47	7.26E-24	1.39E-19
VWA5A	2.50	1.04E-23	2.00E-19
BCL6	2.45	2.48E-23	4.76E-19
FOSL2	2.21	2.77E-23	5.31E-19
ZMAT3	2.19	5.45E-23	1.04E-18
TSC22D1	2.04	2.85E-22	5.45E-18
CFAP54	2.31	2.86E-22	5.47E-18
ST8SIA4	2.42	3.34E-22	6.38E-18
LGR4	2.09	1.07E-21	2.04E-17
INKA2	2.61	2.13E-21	4.06E-17
FLRT3	5.22	3.00E-21	5.72E-17
CUBN	2.75	3.17E-21	6.04E-17
AQP5	3.14	4.78E-21	9.10E-17
HMGA2	2.68	7.20E-21	1.37E-16
PRRG1	2.23	1.11E-20	2.11E-16
TNIK	2.06	1.20E-20	2.28E-16

TNFSF4	3.58	1.51E-20	2.87E-16
GADD45A	2.33	1.98E-20	3.76E-16
PHEX	2.78	2.65E-20	5.03E-16
KDR	2.66	3.27E-20	6.21E-16
TIGAR	2.03	3.53E-20	6.70E-16
RNF152	2.22	4.08E-20	7.74E-16
FILIP1L	3.02	4.08E-20	7.74E-16
CXCL1	2.78	5.47E-20	1.04E-15
SESN2	2.20	6.31E-20	1.20E-15
MIR100HG	2.02	9.87E-20	1.87E-15
Top 50 down-regulated genes (ranked by FDR)			
H2BC12	-3.53	7.77E-157	1.53E-152
ENSG00000290032	-3.53	1.69E-122	3.33E-118
CHAF1B	-3.89	3.93E-90	7.74E-86
CLN6	-2.63	1.78E-88	3.51E-84
SLC25A19	-3.38	3.40E-85	6.70E-81
TOR3A	-2.29	6.44E-84	1.27E-79
CCNE1	-5.25	6.76E-84	1.33E-79
MYO19	-2.99	1.07E-82	2.11E-78
NR2C2AP	-3.47	2.32E-81	4.57E-77
CKB	-5.43	5.80E-74	1.14E-69
E2F1	-4.58	4.98E-73	9.81E-69
PPIF	-2.77	1.86E-72	3.66E-68
RFC2	-2.60	1.03E-71	2.03E-67
MCM3	-2.72	1.24E-69	2.44E-65
DSCC1	-4.25	2.20E-67	4.33E-63
PAQR4	-3.90	1.35E-66	2.66E-62
TUBA4A	-3.05	1.06E-63	2.09E-59
CHAF1A	-2.80	3.12E-62	6.14E-58
FANCA	-3.76	6.43E-60	1.27E-55
NCKIPSD	-2.49	1.45E-59	2.85E-55
FANCI	-2.77	2.32E-59	4.57E-55
SFMBT1	-2.96	2.53E-59	4.98E-55
DPH2	-2.32	3.74E-59	7.36E-55
CHRNA5	-3.37	4.02E-59	7.91E-55
ATAD3A	-2.23	1.99E-58	3.92E-54
KHK	-5.19	5.44E-58	1.07E-53
FEN1	-3.25	9.06E-58	1.78E-53
SPAG1	-2.24	2.51E-57	4.94E-53
POLR3K	-2.08	9.28E-57	1.83E-52
PSMC3IP	-4.04	2.09E-54	4.11E-50
DERL3	-5.42	2.04E-53	4.01E-49
PKMYT1	-4.13	4.86E-53	9.56E-49
DONSON	-2.66	5.80E-53	1.14E-48

SLC47A1	-3.60	3.64E-52	7.16E-48
SLC1A5	-2.05	1.04E-51	2.04E-47
POLD1	-2.65	1.38E-51	2.71E-47
FOXRED2	-2.83	1.39E-51	2.73E-47
MCM5	-2.90	3.20E-50	6.29E-46
MCM2	-3.71	3.62E-50	7.12E-46
MTHFD	-2.14	4.22E-50	8.29E-46
SLC25A22	-2.44	1.23E-49	2.42E-45
SKP2	-2.23	1.24E-49	2.44E-45
SLC43A3	-2.62	4.93E-49	9.69E-45
WDR4	-2.03	1.13E-48	2.22E-44
ADCY3	-2.86	1.44E-48	2.83E-44
FSD1	-3.30	2.36E-48	4.64E-44
RRM1	-2.78	2.81E-48	5.52E-44
ZDHHC23	-3.62	1.41E-47	2.77E-43
TONSL	-3.39	1.90E-47	3.73E-43
POLD3	-2.30	2.48E-47	4.87E-43

Table S1: Top 50 up- and down-regulated differentially expressed genes following KLF6 overexpression in HPAECs. All have gene symbols except *ENSG00000290032*, which has an Ensemble ID.

Comparison lists	Genes shared
KLF6 HPAECs and PAH HPAECs	*ACVRL1, ADAMTS4, ANGPTL4, APC2, ARHGDIG, BMX, BRI3BP, BTBD19, BTN1A1, CALCRL, CCDC116, CCL2, CCN1, CCNE1, CD34, CDC45, CDCP1, CDKN1A, CENPK, CENPU, CIP2A, CLUH, COCH, COL2A1 CRABP2, DNAJB4, DOCK11, EXOSC5, FANCI, FOXRED2, GJA5, GLB1L2, HOMER1, IL17RB, INSYN2B, KCNH3, KDR, KLF6, LDB2, LINC00641, LRRC34, MCM7, MIR22HG, MYBL2, MYOM3, NCAPG2, NKAIN1 NUP210, ORC1, PCLAF, PLCXD1, POLQ, RAD18, RET, RGS4, ROBO4, RRM2, SCX, SH2D3C, SLC19A1, SLC38A3, SLC47A1, SPINT1, TCAM1P, TCIM, TGFBR2, THBS1, TMEM100, TNFSF4, TNIK ,TOX, YPEL2 ZNF561, ZNF608*
KLF6 HPAECs and PAH ECFCs	*ADAM19, ADAMTS4, ADCK2, ANGPTL4, APLN, ARHGAP45, ARID5B, ARRDC3, AURKB, B3GNT7, BCL2, BCL6, BIRC5, BTBD19, BTG2, C9orf40, CA12, CAV1, CD82, CDC25A, CDCA5, CDCP1, CDT1, CENPV, CFAP54, CLSPN, CMSS1, CUBN, CXCL1, CXCL2, DDIT4, DNAJB4, DTL, EEF1AKMT4, ENO2, FANCG, GREM1, H2AX, HAGHL, HES4, HSPD1, IER5L, IGFBP5, IL33, IL6, INKA2, KLF6, KSR2, L2HGDH, LINC01013, LINC01235, LRP3, MCM5, MCRIP2, MIR22HG, MMS22L, MN1, MOCOS, MTHFD1, MYBL2, NCAPH2, NEDD9, NRG1, PAICS, PASK, PPIF, PPP1R3C, RAC3, RALA ,RGS4, RNF144B, RNF208, RRM2, SAMD1, SAPCD2, SDC1, SESN2, SKA3, SLC1A5, SLC43A3, SOX4, SPNS2, ST8SIA4, TCF19, TFRC, TMOD1, TNFSF18, TNIK, TP53INP1, TRIP13, TSC22D1, TSC22D3, TUBA4A, TYMS, TYRO3, WDR4 ZGRF1 ZMAT3, ZNF19, ZNF561*
KLF6 HPAECs and IPAH PAECs	*ABCG2, ADAM19, ADAMTSL1, ADGRF5, B3GNT7, BDH1, BRCA1, CCL2, CENPP, CHPF, CHSY3, DSP, FZD9, HES4, IER5L, IGSF3, INHBB, KCNQ5, LINC00472, MAP2K6, NTN1, PRRG4, PTPN3, RASGRP3, RET, SH2D3C, SH3GL2, SPNS2, SPTBN5, THBS2, TSC22D1, TSPAN33, VWA1*
KLF6 HPAECs and known PAH genes	*ACKR3, ACVRL1, ADGRF5, BDH1, CAV1, CERS1, CREB3L1, DSP, FGFR3, GRIN1, HIF3A, IRF5, NKX2-5, PDSS1, PHEX, SNX10, STOX1, THBS1*

Table S2: List of differentially expressed genes in common between KLF6 HPAECs, PAH HPAECs, PAH ECFCs (Ainscough et al., 2022a)**, IPAH PAECs** (Rhodes et al., 2015) **and known PAH genes** (Reyes-Palomares et al., 2020).

Gene Name	Log Fold Change	P value (p)	FDR (q)
Top 50 Up-regulated genes (ranked by FDR)			
CD82	2.85	6.64E-56	1.32E-51
CDKN1A	2.33	9.19E-44	1.81E-39
PIK3R3	2.81	3.93E-43	7.75E-39
ADAMTSL1	2.21	3.77E-38	7.40E-34
RNASE1	2.15	8.08E-37	1.58E-32
CD34	2.41	9.99E-35	1.95E-30
BTG2	2.93	1.45E-34	2.84E-30
LNCOG	2.81	3.12E-34	6.10E-30
HBP1	2.07	1.92E-33	3.75E-29
LY96	2.43	5.81E-33	1.13E-28
PHLDB2	2.17	1.91E-31	3.71E-27
ZMAT3	2.61	4.65E-31	9.03E-27
KLF6	8.42	9.42E-31	1.83E-26
ZNF24TR	2.36	1.93E-30	3.75E-26
NEDD9	3.13	2.04E-30	3.96E-26
PRAG1	2.84	3.31E-30	6.42E-26
PRKCE	2.16	5.37E-30	1.04E-25
RAB30	2.10	8.85E-30	1.71E-25
DAB2	2.08	1.63E-29	3.16E-25
MDM2	2.23	2.18E-29	4.22E-25
ADAM19	2.49	5.21E-29	1.01E-24
TGFBR2	2.45	7.82E-29	1.51E-24
UGCG	2.46	7.94E-29	1.54E-24
FNDC3B	2.06	2.45E-28	4.73E-24
PDE3A	2.09	3.01E-28	5.81E-24
SESN2	2.71	3.24E-28	6.26E-24
TSC22D1	2.32	6.74E-28	1.30E-23
PGF	2.17	9.75E-28	1.88E-23
FGD6	2.15	1.22E-27	2.35E-23
PIR	2.16	1.61E-27	3.10E-23
PLAU	2.95	1.84E-27	3.54E-23
TIGAR	2.41	2.02E-27	3.89E-23
CDH11	2.25	2.11E-27	4.06E-23
ERRFI1	2.54	2.12E-27	4.08E-23
CGNL1	2.18	3.97E-27	7.64E-23
LGR4	2.38	6.05E-27	1.16E-22
ANKS1A	2.07	8.28E-27	1.59E-22
SMURF2	2.12	1.46E-26	2.81E-22
CREB3L1	2.55	1.55E-26	2.98E-22
PPM1D	2.05	1.76E-26	3.38E-22
RALA	2.03	2.61E-26	5.01E-22
MGAT4A	2.18	2.96E-26	5.68E-22
APLN	3.06	4.26E-26	8.17E-22

ACVRL1	2.39	4.52E-26	8.67E-22
CFAP54	2.59	6.48E-26	1.24E-21
KDM4A	2.18	6.85E-26	1.31E-21
INKA2	2.93	6.98E-26	1.34E-21
ZSCAN31	3.02	4.79E-25	9.16E-21
FAM107A	2.73	6.27E-25	1.20E-20
PNRC2	2.07	6.53E-25	1.25E-20
Top 50 down-regulated genes (ranked by FDR)			
H2BC12	-3.20	4.04E-132	8.06E-128
CLN6	-3.27	3.68E-126	7.34E-122
CHAF1B	-4.73	2.18E-120	4.35E-116
RFC2	-3.45	4.25E-119	8.48E-115
TUBA4A	-4.22	9.35E-114	1.86E-109
E2F1	-6.14	5.66E-112	1.13E-107
TOR3A	-2.68	1.04E-110	2.07E-106
FANCI	-3.92	2.96E-110	5.90E-106
MTHFD1	-3.24	7.01E-109	1.40E-104
ENSG00000290032	-3.21	1.85E-106	3.69E-102
SNRPA1	-2.60	1.99E-99	3.97E-95
NR2C2AP	-3.95	4.36E-99	8.69E-95
PAQR4	-4.97	1.39E-98	2.77E-94
MCM3	-3.28	2.16E-98	4.31E-94
DSCC1	-5.57	3.80E-93	7.57E-89
ATAD3A	-2.87	2.59E-92	5.16E-88
PKMYT1	-6.11	1.07E-90	2.13E-86
WDR4	-2.94	1.24E-90	2.47E-86
SLC25A19	-3.61	3.00E-90	5.98E-86
CCNE1	-5.60	9.02E-90	1.80E-85
MCM5	-3.94	2.07E-88	4.12E-84
PPIF	-3.08	3.86E-88	7.69E-84
MYO19	-3.09	7.70E-88	1.53E-83
TIMELESS	-2.51	1.28E-84	2.55E-80
MYBL2	-5.97	3.00E-84	5.98E-80
FEN1	-4.02	3.33E-84	6.63E-80
C8orf33	-2.05	3.37E-83	6.71E-79
RBM19	-2.12	2.35E-82	4.68E-78
TRIP13	-4.62	2.40E-82	4.78E-78
TK1	-3.98	1.76E-81	3.51E-77
FANCA	-4.66	1.32E-79	2.63E-75
ZWINT	-4.14	1.34E-79	2.67E-75
RNASEH2B	-2.66	8.52E-79	1.70E-74
PSMC3IP	-5.08	1.43E-78	2.85E-74
POLD1	-3.34	4.30E-78	8.56E-74
MCM2	-4.68	5.89E-77	1.17E-72
CHAF1A	-3.20	7.17E-77	1.43E-72
ADCY3	-3.67	9.96E-77	1.98E-72
CDC45	-5.18	1.32E-76	2.63E-72

RAD51	-4.87	1.66E-76	3.30E-72
CHRNA5	-3.93	2.50E-76	4.98E-72
SMC1A	-2.20	2.68E-76	5.33E-72
RRM2	-4.87	1.10E-74	2.19E-70
POLR3K	-2.43	1.3E-74	2.59E-70
RRM1	-3.49	2.03E-73	4.04E-69
CLSPN	-5.54	2.29E-73	4.56E-69
C20orf27	-2.55	3.42E-73	6.81E-69
TUBG1	-2.11	6.33E-73	1.26E-68
SIGMAR1	-2.23	2.35E-72	4.68E-68
NCKIPSD	-2.78	5.40E-72	1.07E-67

Table S3: Top 50 up- and down-regulated differentially expressed genes following exposure of KLF6 overexpressing HPAECs to hypoxia. All have gene symbols except *ENSG00000290032* which has an Ensemble ID and is annotated as a lncRNA.

Gene Name	Log Fold Change	P value (p)	FDR (q)
Top 50 Up-regulated genes (ranked by FDR)			
ADAMTSL1	2.89	5.04E-63	1.02E-58
LNCOG	2.93	8.75E-34	1.75E-29
SLC22A4	2.39	9.69E-33	1.93E-28
LY96	2.34	6.33E-31	1.26E-26
TOX	2.99	4.09E-30	8.14E-26
LRRC17	3.69	2.11E-29	4.19E-25
ANK3	2.93	1.46E-28	2.90E-24
PLAU	3.01	7.30E-28	1.45E-23
GDF15	3.53	9.55E-28	1.89E-23
EMCN	2.18	1.14E-27	2.26E-23
CPA4	2.56	3.55E-27	7.03E-23
VWA5A	3.07	7.45E-23	7.45E-23
RALA	2.05	5.88E-27	1.16E-22
ZNF24TR	2.44	1.31E-26	2.59E-22
MYLK	2.69	2.72E-26	5.38E-22
DIPK2B	3.94	1.17E-25	2.31E-21
CFAP54	2.55	2.18E-25	4.31E-21
C1QTNF6	2.75	3.58E-25	7.07E-21
MDM2	2.03	5.87E-25	1.16E-20
ITGA2	2.13	2.04E-24	4.02E-20
STXBP5-AS1	4.04	2.30E-24	4.54E-20
BTG2	2.38	1.88E-23	3.70E-19
TSC22D1	2.09	8.92E-19	8.92E-19
TGFBR2	2.16	4.59E-23	9.02E-19
KLF6	7.08	8.69E-23	1.71E-18
GADD45A	2.45	1.80E-22	3.53E-18
DCUN1D3	2.13	2.52E-22	4.94E-18

ZMAT3	2.15	6.41E-22	1.26E-17
ADAM19	2.09	7.55E-22	1.48E-17
ARL4C	2.31	1.95E-21	3.81E-17
MAP3K1	2.12	2.74E-21	5.36E-17
IRAK2	2.10	2.97E-21	5.80E-17
FBXL13	2.23	3.51E-21	6.86E-17
GASK1B	2.85	3.53E-21	6.90E-17
CCDC85A	2.47	6.63E-21	1.29E-16
PTGS1	2.02	1.12E-20	2.18E-16
APLN	2.67	2.59E-20	5.05E-16
SESN2	2.21	4.59E-20	8.94E-16
ACVRL1	2.05	6.08E-20	1.18E-15
CITED4	2.57	7.12E-20	1.39E-15
ENSG00000261468	3.21	1.42E-18	2.75E-14
MARCHF4	2.10	1.65E-18	3.19E-14
HMGA2	2.43	5.50E-18	1.06E-13
MIR31HG	2.03	1.01E-17	1.95E-13
ADTRP	2.12	1.27E-17	2.45E-13
FAM107A	2.23	1.38E-17	2.66E-13
SLC7A14	4.09	1.82E-17	3.50E-13
SPRED3	2.23	1.97E-17	3.79E-13
ARID5B	2.66	2.62E-17	5.04E-13
MN1	3.03	2.70E-17	5.19E-13
Top 50 down-regulated genes (ranked by FDR)			
H2BC12	-2.96	5.61E-116	1.13E-111
SLC25A19	-3.77	7.65E-101	1.54E-96
TOR3A	-2.47	1.32E-95	2.66E-91
ENSG00000290032	-2.99	7.39E-95	1.49E-90
CKB	-6.67	1.35E-87	2.72E-83
SKP2	-3.07	6.76E-87	1.36E-82
TUBA4A	-3.60	2.07E-85	4.18E-81
CCNE1	-5.31	8.04E-84	1.62E-79
DSCC1	-4.62	1.72E-73	3.47E-69
AIF1L	-2.86	4.39E-72	8.86E-68
TMEM106C	-3.54	6.32E-72	1.27E-67
E2F1	-4.57	1.43E-70	2.88E-66
CHAF1B	-3.32	6.60E-68	1.33E-63
POLR3K	-2.30	6.77E-67	1.37E-62
CLN6	-2.24	1.08E-66	2.18E-62
SLC47A1	-4.29	3.18E-66	6.41E-62
NCKIPSD	-2.68	1.18E-64	2.38E-60
PAQR4	-3.81	9.26E-63	1.87E-58
SDC1	-3.72	2.46E-62	4.96E-58
DPH2	-2.36	1.36E-61	2.74E-57
MCM3	-2.55	4.32E-61	8.71E-57
ENO2	-3.58	4.60E-60	9.27E-56

CHRNA5	-3.37	4.41E-59	8.89E-55
TSEN54	-2.98	6.55E-58	1.32E-53
RBBP8	-3.40	7.61E-58	1.53E-53
CHAF1A	-2.71	7.98E-58	1.61E-53
XRCC3	-2.86	1.09E-57	2.20E-53
MYO19	-2.46	1.20E-57	2.42E-53
TFDP1	-2.33	3.70E-56	7.46E-52
FAM136A	-2.00	5.85E-55	1.18E-50
RRM1	-2.99	6.48E-55	1.31E-50
PIGX	-2.33	1.34E-54	2.70E-50
DONSON	-2.70	5.21E-54	1.05E-49
C9orf40	-3.17	1.14E-53	2.30E-49
CAMK1	-2.28	1.33E-51	2.68E-47
NR2C2AP	-2.66	1.48E-51	2.98E-47
ENTPD1-AS1	-2.20	5.67E-51	1.14E-46
EMP2	-3.89	6.82E-51	1.37E-46
RFC2	-2.16	6.91E-51	1.39E-46
FGFRL1	-3.49	8.30E-51	1.67E-46
KHK	-5.63	3.37E-50	6.79E-46
CCDC14	-2.34	4.96E-49	9.99E-45
UNG	-3.78	1.92E-48	3.87E-44
PRPS1	-2.23	3.59E-47	7.23E-43
MCRIP2	-2.74	1.85E-46	3.72E-42
RRM2	-3.78	2.08E-46	4.19E-42
GAL	-5.98	2.49E-46	5.01E-42
TCOF1	-2.35	7.41E-45	1.49E-40
DUSP9	-9.12	1.59E-44	3.20E-40
CEP78	-2.69	1.98E-44	3.98E-40

Table S4: Top 50 up- and down-regulated differentially expressed genes following treatment of KLF6 overexpressing HPAECs with TNF-α. All have gene symbols except *ENSG00000261468*, *ENSG00000290032* which have an Ensemble ID.

Gene Name	Log Fold Change	P value (p)	FDR (q)
Top 50 Up-regulated genes (ranked by FDR)			
CKB	7.71	1.58E-163	3.17E-159
H2BC12	3.33	1.54E-142	3.09E-138
ENSG00000290032	3.39	7.28E-117	1.46E-112
CCNE1	5.57	4.98E-95	1.00E-90
NR2C2AP	3.58	9.79E-90	1.97E-85
CDC25A	5.18	2.76E-85	5.54E-81
CHAF1B	3.76	2.49E-84	5.00E-80
MYO19	2.97	4.08E-82	8.19E-78
ZGRF1	4.62	2.03E-81	4.08E-77
UHRF1	4.75	9.25E-78	1.86E-73
E2F1	4.71	1.21E-76	2.43E-72
ICAM1	4.70	1.39E-75	2.79E-71
ARC	5.78	2.36E-72	4.74E-68
MCM3	2.75	5.50E-71	1.10E-66
CHAF1A	2.97	1.81E-69	3.63E-65
WDR76	4.88	6.23E-69	1.25E-64
DERL3	6.46	1.11E-68	2.23E-64
ASS1	3.37	1.28E-67	2.57E-63
PSMC3IP	4.44	1.86E-67	3.73E-63
POLD3	2.72	1.31E-65	2.63E-61
ZNF367	5.68	1.91E-65	3.83E-61
SFMBT1	2.94	6.16E-64	1.24E-59
FEN1	3.40	3.80E-63	7.62E-59
SCML1	2.52	1.21E-62	2.43E-58
RFC2	2.42	1.59E-62	3.19E-58
EMP2	4.22	4.43E-62	8.89E-58
PRPS2	3.10	5.80E-62	1.16E-57
BTG3	3.82	1.05E-61	2.11E-57
MCM4	3.96	2.22E-61	4.45E-57
RBBP8	3.43	2.27E-60	4.55E-56
PPIF	2.50	7.17E-60	1.44E-55
CDC6	4.43	8.77E-60	1.76E-55
RRAD	7.05	3.39E-59	6.80E-55
DTL	4.63	6.67E-59	1.34E-54
DONSON	2.80	6.95E-59	1.39E-54
TMEM38B	3.10	9.77E-57	1.96E-52
KLF2	5.45	1.06E-56	2.13E-52
GMNN	3.02	1.95E-54	3.91E-50
CDK2	3.24	2.75E-54	5.51E-50
XRCC2	4.51	6.40E-54	1.28E-49
CCNE2	5.39	7.45E-54	1.49E-49
MSH2	2.66	1.47E-53	2.95E-49
BRME1	6.49	2.36E-53	4.73E-49

SLC25A19	2.63	2.46E-53	4.93E-49
MCM10	4.42	5.32E-53	1.07E-48
FANCA	3.47	8.25E-53	1.65E-48
SLC47A1	3.63	7.91E-52	1.59E-47
GAL	6.32	4.40E-51	8.82E-47
SLC6A8	2.33	1.39E-50	2.79E-46
ATAD2	3.87	6.38E-50	1.28E-45
Top 50 down-regulated genes (ranked by FDR)			
CLIC1	-3.79	5.72E-106	1.15E-101
EMCN	-2.40	2.74E-44	5.48E-40
TP53I11	-2.69	9.09E-40	1.82E-35
RALA	-2.21	1.70E-30	3.37E-26
ZNF24TR	-2.49	7.71E-30	1.53E-25
NRP1	-2.04	2.56E-29	5.07E-25
CD93	-2.42	2.33E-28	4.61E-24
PIK3R3	-2.21	3.60E-28	7.13E-24
FOXO1	-2.34	3.12E-27	6.17E-23
APLN	-3.14	8.51E-27	1.68E-22
RGS3	-2.37	5.42E-26	1.07E-21
TGFBR2	-2.27	4.35E-25	8.57E-21
EVA1A	-2.02	4.63E-24	9.11E-20
TNIK	-2.23	1.41E-23	2.77E-19
SPRY2	-2.31	4.39E-23	8.61E-19
JUP	-2.41	6.10E-23	1.20E-18
MYRIP	-2.21	8.81E-23	1.73E-18
KDR	-2.87	8.99E-23	1.76E-18
LINC01235	-3.08	1.19E-22	2.33E-18
TCF4	-2.10	4.30E-22	8.42E-18
ARHGEF37	-2.18	1.22E-21	2.38E-17
NREP	-2.85	1.53E-21	2.99E-17
CFAP54	-2.46	1.72E-21	3.36E-17
CYRIA	-2.22	3.51E-21	6.85E-17
SOX4	-2.43	4.57E-21	8.91E-17
RNF152	-2.35	7.42E-21	1.45E-16
ZNF521	-2.70	7.87E-21	1.53E-16
APH1B	-2.14	3.91E-20	7.61E-16
PRRG1	-2.22	4.37E-20	8.50E-16
PPFIBP2	-2.97	9.88E-20	1.92E-15
NR2F2	-2.26	1.26E-19	2.45E-15
MILR1	-2.51	1.34E-18	2.59E-14
PDE7B	-2.72	2.06E-18	3.98E-14
LINC00205	-2.03	2.59E-18	5.00E-14
TM4SF1	-2.23	7.41E-18	1.43E-13
TMEM187	-2.02	9.38E-18	1.81E-13
PDE4B	-2.82	1.00E-17	1.93E-13
MARCKS	-2.17	2.38E-17	4.58E-13

FRMD6	-2.52	3.29E-17	6.32E-13
VWA5A	-2.25	3.35E-17	6.44E-13
PCDH17	-4.06	8.40E-17	1.61E-12
LDB2	-2.77	1.18E-16	2.26E-12
CSGALNACT1	-2.86	1.23E-16	2.36E-12
PHLDA1	-2.35	1.56E-16	2.99E-12
MAST4	-2.02	1.65E-16	3.16E-12
ERG	-2.06	2.25E-16	4.30E-12
TRIM5	-2.26	2.38E-16	4.55E-12
PHEX	-3.07	2.41E-16	4.61E-12
RBM43	-2.54	2.66E-16	5.08E-12
ZNF189	-2.07	2.91E-16	5.56E-12

Table S5: Top 50 up- and down-regulated differentially expressed genes following KLF2 overexpression in HPAECs. All have gene symbols except *ENSG00000290032* which has an Ensemble ID.

Gene Name	Log Fold Change	P value (p)	FDR (q)
Top 50 Up-regulated genes (ranked by FDR)			
PTP4A3	7.85	8.85E-274	1.88E-269
ADIRF	4.06	2.72E-273	5.78E-269
KLF4	9.60	3.88E-266	8.25E-262
SQSTM1	3.13	7.21E-264	1.53E-259
PLCD1	5.51	4.22E-259	8.97E-255
MKNK2	4.08	3.03E-247	6.44E-243
S100A2	6.86	3.17E-244	6.74E-240
VASN	6.24	3.90E-209	8.29E-205
IGFBP6	6.75	8.86E-195	1.88E-190
FSTL3	5.69	1.94E-187	4.12E-183
MARCKSL1	3.31	2.03E-186	4.31E-182
TIMP1	4.32	4.67E-181	9.92E-177
KRT18	3.77	1.16E-178	2.46E-174
CLIC3	7.13	5.96E-171	1.27E-166
SLC6A8	4.29	9.56E-167	2.03E-162
PTHLH	6.79	1.22E-157	2.59E-153
ASS1	4.94	3.77E-152	8.01E-148
ARC	7.93	8.51E-152	1.81E-147
TNFAIP2	6.18	5.47E-150	1.16E-145
MMP15	4.82	3.32E-148	7.05E-144
RCOR1	4.29	4.49E-144	9.53E-140
CLCN2	5.46	5.65E-141	1.20E-136
COL9A3	8.82	1.10E-140	2.34E-136
DNASE1L1	2.56	2.53E-139	5.37E-135
CD82	4.60	1.92E-137	4.08E-133
NOS3	4.87	6.84E-137	1.45E-132
VSIG10L	8.12	1.81E-136	3.84E-132
LAMB3	3.92	2.83E-126	6.01E-122
PLAUR	3.33	3.55E-125	7.54E-121
CDC42EP4	2.86	1.70E-123	3.61E-119
TNFSF9	6.97	1.31E-121	2.78E-117
DDAH2	3.98	1.79E-121	3.80E-117
ECM1	4.62	1.36E-103	2.89E-99
TNK2	3.23	2.73E-102	5.79E-98
CKB	5.34	5.04E-100	1.07E-95
ADAMTS4	5.46	5.39E-99	1.14E-94
UNC13D	3.70	8.73E-98	1.85E-93
BBLN	3.43	5.67E-94	1.20E-89
TAMALIN	3.13	3.31E-93	7.02E-89
GPC1	2.25	2.06E-92	4.37E-88
NPTXR	4.35	5.76E-92	1.22E-87
PLEKHO2	4.46	2.18E-91	4.62E-87
SMTN	2.99	6.22E-91	1.32E-86
SLC9A3R1	2.52	4.57E-90	9.69E-86

OSGIN1	5.05	6.23E-90	1.32E-85
RHOF	4.08	2.19E-88	4.64E-84
SYNC	5.31	6.25E-88	1.33E-83
DGAT1	2.81	1.04E-85	2.21E-81
CRABP2	7.32	3.04E-85	6.45E-81
CPAMD8	8.53	1.93E-84	4.09E-80
Top 50 down-regulated genes (ranked by FDR)			
H2BC12	-2.86	3.63E-107	7.70E-103
CLN6	-2.84	8.46E-101	1.80E-96
CHAF1B	-4.12	5.96E-99	1.26E-94
MYO19	-3.29	8.75E-98	1.86E-93
NCKIPSD	-3.31	5.53E-95	1.17E-90
FOXRED2	-3.68	1.16E-81	2.46E-77
POLD1	-3.42	2.33E-81	4.94E-77
MCM3	-2.92	5.89E-79	1.25E-74
NME4	-2.50	5.59E-77	1.18E-72
LPIN1	-2.38	1.05E-76	2.22E-72
ENSG00000290032	-2.67	1.04E-75	2.20E-71
DSCC1	-4.60	3.86E-75	8.17E-71
MCM2	-4.61	7.80E-75	1.65E-70
PM20D2	-3.51	1.83E-74	3.87E-70
MCM5	-3.58	6.25E-74	1.32E-69
CAD	-2.78	4.14E-73	8.76E-69
MBD3	-2.21	6.32E-73	1.34E-68
NR2C2AP	-3.22	6.66E-72	1.41E-67
FSD1	-4.17	1.41E-71	2.98E-67
SIGMAR1	-2.21	7.29E-71	1.54E-66
CDK2	-3.78	8.44E-71	1.79E-66
RFC2	-2.59	9.06E-71	1.92E-66
SLC25A19	-3.02	3.69E-70	7.81E-66
JPT2	-2.36	2.63E-65	5.56E-61
TMEM97	-3.61	1.03E-63	2.18E-59
WDR5	-2.40	3.08E-63	6.51E-59
UNG	-4.35	6.28E-63	1.33E-58
ZDHHC23	-4.47	7.16E-63	1.51E-58
PFAS	-2.62	7.97E-63	1.68E-58
C19orf48	-2.30	6.59E-62	1.39E-57
PAICS	-2.92	1.38E-61	2.91E-57
SFXN4	-2.57	2.38E-61	5.03E-57
WDHD1	-2.54	2.69E-61	5.68E-57
PSMG1	-2.07	2.20E-60	4.65E-56
ATIC	-2.56	4.39E-60	9.27E-56
FANCI	-2.78	3.93E-59	8.29E-55
DPH2	-2.32	6.43E-59	1.36E-54
TCOF1	-2.72	1.33E-58	2.81E-54
B3GAT3	-2.44	1.94E-58	4.09E-54

FEN1	-3.27	3.40E-58	7.17E-54
SKP2	-2.42	1.98E-57	4.17E-53
PARP1	-2.16	2.87E-57	6.05E-53
SFXN2	-3.76	4.35E-57	9.17E-53
SPTBN2	-3.43	2.41E-56	5.08E-52
CC2D1A	-2.00	3.96E-56	8.34E-52
SNX8	-2.05	2.77E-54	5.83E-50
IRAK1	-2.22	3.49E-54	7.35E-50
YDJC	-2.97	7.13E-54	1.50E-49
ADCK2	-2.80	1.22E-53	2.57E-49
XRCC2	-4.79	1.78E-53	3.75E-49

Table S6: Top 50 up- and down-regulated differentially expressed genes following KLF4 overexpression in HPAECs. All have gene symbols except *ENSG00000290032* which has an Ensemble ID.

Comparison lists	Overlapping genes
KLF2, KLF4 and KLF6	*ADAM11, ADCY1, AGMAT, ANKLE1, ARHGEF4, ASF1B, ASTL, ATAD2, ATAD3B, ATAD5, AUNIP, BATF3, BIRC5, BLM, BRI3BP, BRME1, BTN1A1, C1QTNF2, C2orf88, C9orf40, CAMK4, CCDC116, CCDC138, CCDC150, CCDC181, CCL2, CCNE1, CDC25A, CDC45, CDC6, CDC7, CDCA5, CDCA7, CDK2, CENPK, CENPM, CENPP, CENPQ, CENPU, CENPV, CFAP91, CHAF1B, CHDH, CHST6, CIB2, CKB, CLGN, CLSPN, CMSS1, CNIH2, COCH, COL2A1, CRABP2, CSPG5, DDN, DDX12P, DERL3, DMC1, DNA2, DNMT1, DONSON, DSCC1, DSP, DTL, DUSP2, DUSP9, E2F2, EMILIN3, EMP2, ENSG00000234160, ENSG00000251131, ENSG00000260196, ENSG00000266680, ENSG00000273342, ENSG00000289298, ENSG00000289635, ENSG00000290032, ENSG00000291224, ERFE, ERVMER34-1, ESCO2, EXO1, EXOSC5, FAM111B, FAM184A, FANCB, FANCI, FAXC, FEN1, FERMT1, FGFR3, FGFR4, FHDC1, FIBCD1, FLRT3, FOXRED2, FSD1, FUT3, FZD3, FZD9, GALNT16, GINS2, GINS4, GMNN, GNG4, GPR3, GREM1, GRM2, H2BC12, H2BC17, H3C10, HADH, HAUS5, HELLS, HPDL, HS6ST2, HSD11B2, HSD17B6, ICA1L, ICAM5, IGFBPL1, IL12RB2, ISM2, ITPRIPL1, JPH1, KCNH2, KCNQ5, KHDC1, KHK, KIF24, KISS1R, KLHL23, LAMA3, LAMC3, LINC00641, LINGO1, LRP3, LRRCC1, MANEAL, MCM10, MCM2, MCM3, MCM4, MCM5, MCM6, MCM7, MCM8, MDGA1, MESP1, MFSD2A, MGAT3, MNS1, MSH2, MTARC1, MYBL1, MYBL2, MYO19, MYRF, NAT8L, NCAPG2, NCAPH2, NCR3LG1, NETO2, NPTX1, NR2C2AP, NR4A1, NTN1, NUP210, NXPH4, OLFM1, OLFM2, OR2B6, ORC1, P2RX5, PAK6, PCDHGC4, PCLAF, PKMYT1, POLA1, POLE2, POLQ, PRRT4, PSMC3IP, PTPN3, RAD18, RAD51, RAD51AP1, RAD54L, RADIL, RASL10B, RBBP8, RECQL4, RFC2, RFC3, RFC4, RFC5, RHEBL1, RIBC2, RNF157, RRM1, RRM2, RTN4R, SAMD1, SDC1, SEPTIN3, SH3GL3, SHROOM1, SKA3, SLC1A4, SLC25A19, SLC27A2, SLC39A8, SLC47A1, SLC6A17 SLCO2B1, SLFN13, SMKR1, SNX10, STOX1, SYT7, TCF19, TCOF1, TEDC2, TESC, TFDP1, TFR2, TIPIN, TMEM106C, TMEM200B, TMEM38B, TONSL, TRABD2A, TSPAN33, TUB, TXNDC16, TYMS, UHRF1, UNG, USP2-AS1, VASN, VSTM4, WDR62, WDR76, XRCC2, XYLB, ZGRF1, ZNF367, ZWINT*
KLF2 and KLF4	ABTB2, AKAP5, ANKDD1A, APOE, AQP1, AQP3, ARC, ARL9, ASS1, BCYRN1, BEND3, C11orf96, C15orf62, CA2, CABLES2, CBFA2T3, CCN3, CD52, CD55, CEBPA, CHRM4, CLEC3B, CLIC3, CMKLR1, COL6A1, COL9A3, CPLX1, CSGALNACT1, CSPG4, DDIAS, DEPP1, DOC2B, DUSP8, ECM1, EEF1A2, ELFN1, ELN, EML5, ENSG00000261526, ENTPD2, FGF18, GDF3, GFPT2, GINS3, GKAP1, GLRB, GPR137C, HBA2, HR, IGF2, IGF2BP1, IGFBP6, IMMP1L,

	IRX3, ITGA9, KLK10, KRT13, LYPD5, MAFA, MISP3, MMP28, MRAS, NGEF, NGFR, NKX6-2, NOS3, PCNA, PDGFB, PI16, PIM1, PLVAP, POLR1E, PPAT, PRRX2, RASD2, RASL10A, RELT, RNF125, RRAD, RRP7BP, S100P, SCNN1D, SEMA7A, SLC17A7, SLC6A3, SLC6A8, TMEM198B, TNFAIP2, TNPO2, TNXB, TRIM36, ULBP1, WNT11, ZBTB7C, ZNF425
KLF2 and KLF6	*AADAT, ABCG2, ABHD3, ADAMTS17, ADAMTS18, ADCY3, ADGRB2, ADGRF5, ADPRHL1, ANKRD35, ANKRD50, ANO1, APC2, APLN, ARHGAP45, ARHGEF16, ARID5B, B3GNT7, B4GALNT3, BAIAP2L2, BCL2, BHLHA15, BMP8B, BMX, BRSK2, BTG3, C1QL1, C2orf72, C3orf80, CALCRL, CCNE2, CCNG2, CD274, CD83, CDCP1, CDT1, CEND1, CEP72, CERS1, CFAP54, CGAS, CHAF1A, CHRNA5, CHSY3, CORO1A, CSRP2, CUBN, DIO2, DIPK1A, DNAJB4, DOCK11, DPF1, E2F1, EBF4, EID3, ELOVL7, EMCN, ENO2, ENSG00000232949, ENSG00000233461, ENSG00000248187, ENSG00000272405, ENSG00000275632, ENSG00000286320, ENSG00000287853, ENSG00000289327, EPCAM, ESYT3, FAM117A, FAM162B, FAM169A, FAM222A, FAM81A, FANCA, FAT1, FGFRL1, FILIP1L, FLRT2, FNDC5, FOXA3, FOXE3, FOXO1, FRMD6, GAL, GALNT14, GJA3, GJA5, GJB2, GLB1L2, GNAL, GNAZ, GREB1L, GRM8, HAS3, HAUS2, HES4, HES6, HOMER1, HS3ST1, IFNA22P, IL17RB, INA, INKA1, INKA2, INSYN2B, ISM1, ITPKA, KCNH3, KCNJ2, KDR, KIF26A, KIF5C, KLRG1, KREMEN1, LDB2, LHX2, LINC01013, LINC01235, LINC02915, LLGL2, LPL, LRP4, LRTM2, LYPD1, MANCR, MAP2K6, MAP3K21, MAP7, MAP7D2, MAP9, MATCAP2, MIR503HG, MMS22L, MTHFD2, MYB, NCAPD3, NECAB2, NEO1, NEURL1, NIBAN1, NKX2-5, NPC1L1, NPW, NREP, NSUN5, ORC6, OTOGL, OXCT2, PAQR4, PARM1, PASK, PCDH17, PCDH9, PCED1B, PDE3B, PDE4B, PDE7B, PDSS1, PGBD5, PHEX, PHGDH, PHLDA1, PIK3R3, PITX3, PLCXD1, PLK2, POLD3, POLE, PPFIBP2, PPIF, PRPS2, PRRG1, PTCHD4, PUSL1, RAB3IL1, RALA, RASD1, RASGRP3, RASL11A, RBL1, RBPMS2, RGS7BP, RHBDL3, RNF144B, RNF152, RPRML, RPS6KA1, RRAGD, S1PR1-DT, SCML2, SCUBE2, SCX, SERPINB9P1, SFMBT1, SH2D4A, SH3GL2, SHISA8, SIRPB2, SLC2A4, SLC30A3, SLC38A3, SLC43A3, SLC7A14, SLC7A5, SLCO4A1, SMCO4, SOX4, SPINT1, SPTBN4, STEAP1B-AS1, STK26, SYNGR3, TAF4B, TCAM1P, TCF7, TCIM, TELO2, TFEC, TFRC, TGFBR2, THBS1, THBS2, TK1, TMEM201, TMEM30B, TMEM52, TNFSF4, TNIK, TP53INP1, TP73, TSEN54, TTBK1, TTYH2, TUBGCP4, TYRO3, UGT8, VWA5A, ZNF24TR, ZNF296, ZNF561, ZNF608, ZSCAN31*
KLF4 and KLF6	*ACKR3, ADAM19, ADAMTS4, ADCK2, ALDH5A1, ALKBH2, ANGPTL4, AQP5, ARHGAP44, ARSI, ATAD3A, ATP2A1-AS1, AURKB, BCAS4, BEGAIN, BRCA1, BRCA2, BRIP1, C1QTNF6,*

	CAD, CCDC136, CCIN, CCNI2, CD24, CD82, CDHR3, CELSR2, CENPH, CEP78, CGREF1, CHPF, CILP2, CIP2A, CLDN14, CLDN23, CLN6, COL17A1, CREB3L1, CXCL1, CXCL2, DDN-AS1, DGAT2, DGUOK-AS1, DHFR, DHRS13, DNAH14, DNM1, DPH2, DTYMK, ELFN1-AS1, ENHO, ESRP2, FAM107A, FAM161A, FAM216A, FAM3D, FANCD2, FANCG, FNDC10, FOSL2, GDF15, GSDMC, H2AC13, H4C8, HAGHL, HSPD1, IER5L, IGFBP5, IGSF3, IL6, IMPA2, INHBB, KCNAB3, KCNS1, KIF1A, KLF6, KRT15, LOXL3, LRFN1, LRRC3, MAD2L1, MAP6, MAPK8IP2, MELK, MIR22HG, MN1, MRE11, MRTO4, MT1A, MYEOV, MYOM3, NARF-AS2, NCKIPSD, NDP, NIPAL4, NKPD1, NMNAT2, NT5M, OIP5, PACSIN3, PAICS, PALM3, PARD6A, PBK, PEG10, PIMREG, PLAU, PM20D2, POLD1, POLR1G, PPP1R3C, PPP2R3B, PRAG1, PRELP, PRIM1, PSAT1, PTPRU, RAC3, REEP2, REM1, RGS4, SCLY, SHMT1, SKP2, SLC17A9, SLC19A1, SLC25A10, SLC46A1, SLC5A6, SMIM10, SNAI2, SNX25P1, SPNS2, SPRED3, SRM, STXBP6, TAFA5, TEX15, TMEM217, TMEM97, TPD52, TPD52L1, TRIP13, TSC22D1, VPS9D1-AS1, VRK1, WDFY4, WNT5B, YDJC, YPEL2, ZDHHC23, ZNF423

Table S7: List of differentially expressed genes in common between KLF2, KLF4 and KLF6. All have gene symbols except *ENSG00000234160, ENSG00000251131, ENSG00000260196, ENSG00000266680, ENSG00000273342, ENSG00000289298, ENSG00000289635, ENSG00000290032, ENSG00000291224,* ENSG00000261526, *ENSG00000232949, ENSG00000233461, ENSG00000248187, ENSG00000272405, ENSG00000275632, ENSG00000286320, ENSG00000287853, ENSG00000289327* which have an Ensemble ID.

Name	Unique genes
KLF2	*TFPI, DBF4, ANOS1, RUNX3, DEPDC1B, TLL1, PHLPP2, SCML1, PER3, RRP12, PDZD4, IFI35, MAST4, SEMA3A, PLD1, ACACB, MAP2, EDN1, TXLNG, SRRT, TRMT6, KCNH4, ICAM1, RAPGEF4, CCDC80, NRP1, RANBP1, PNN, ZMYND8, RPRD1B, LIPG, KLF5, FLT1, ACD, USP31, NFKBIB, DOT1L, LYL1, BBC3, ICAM4, KLF1, NPTX2, EZH2, GIMAP2, DTX4, CHKA, CLEC2B, BCL7A, CYP27B1, OAS2, NT5DC3, GCNT2, GABRR2, FBXO5, TRIM38, IRX4, EVA1A, STAT1, SRSF7, MSH6, DNAJC6, KIF21B, SERPINC1, COLEC11, SGIP1, ONECUT2, SPART-AS1, EGR1, RDH10, TBX2, TNFSF10, INHBA, DDX39A, STIL, SDC4, CPNE5, BMP4, CD93, IFI6, HSPA2, KLF2, SPECC1, APOC1, HAUS8, TRIM5, PER2, LARGE1, PIWIL4, ARHGAP32, SP110, USP37, SPRY2, ZNF189, CTSV, CASP1, SIX3, RBP4, APH1B, LEF1, RGS3, AMIGO2, DUSP6, SUOX, N4BP2L1, DNAJA4, TICRR, SLC39A6, RGS16, DLX1, MED12L, LYAR, NKD2, OTULINL, PIK3R1, MLIP, ARHGAP18, AGBL3, TMEM140, GCNA, VLDLR, NR6A1, HNMT, ANK3, POU4F1, BCL2L11, NR4A2, LURAP1L, GRAP, ANGPT1, CXADR, SUPV3L1, ERG, MX1, CNNM4, RRP1B, SH2B2, LRWD1, IKZF3, USP1, GBP2, RBM15, TM4SF18, SPDYA, GASK1B, HHIP, F2RL2, TLR3, KCNK5, GPR146, ALDH1A1, WNK2, DDX21, BTNL9, PRTG, NKX3-1, SPATA33, TLCD3A, KRT80, TRANK1, ATOH8, LETM1, EFNA1, CXCL11, ARL13B, TM4SF1, MYRIP, SIX2, STAT2, PYGO1, INSR, KCNG3, DSEL, SLC25A33, ENC1, C3AR1, TLN2, KLF11, CERS6, ZNF483, PPP1R3B, JUP, RNF213, KLHL15, TP53I11, NRIP3, CLEC14A, CDK5R1, FAM210A, TOP3A, SAMD9L, HASPIN, CD163L1, TMEM187, RNF227, ANKRD18A, ZNF792, OXTR, DDX60L, ATG9B, SYNM, DCAF4L1, KCNJ14, GLUD2, ARHGEF37, ZNRF3, RFLNB, MAML2, IRS3P, RBM43, ROBO2, FAM43A, NR2F2, TRIM69, C3orf70, HSPA14, ISG15, NANOS1, FAM221A, CFAP119, FAT4, TCF4, MAML3, ENPP1, CYRIA, C2CD4A, RASSF9, ZNF521, ZNF525, MIR1915HG, LIN52, FTH1P3, CLIC1, EML6, MIR17HG, H3C9P, PPP3CB-AS1, RPL23AP53, LINC00205, HSP90AA2P, BAIAP2-DT, PROB1, LINC01128, EMC1-AS1, DDX3ILA1, ENSG00000233251, GAS6-AS1, CLDN14-AS1, ZNF37BP, MIR155HG, ENSG00000236255, LINC02984, APOBEC3G, PTPRG-AS1, CNTF, RN7SL832P, ENSG00000245025, SNHG10, NR2F2-AS1, ENSG00000249631, OSMR-DT, LINC02762, LINC01094, FOXD1, CCDC71L, FLJ20021, SNHG9, SNHG1, LINC02454, SALL3, ENSG00000256663, GLIPR1-AS1, INAFM1, CHMP4BP1, CAPN10-DT, ZNNT1, LINC02188, ENSG00000261889, ENSG00000266490, FMNL1-DT, ENSG00000267405, HEATR6-DT, ICAM4-AS1, EML2-AS1, ENSG00000269399, MIRLET7A1HG, ENSG00000270681, MILR1, CASC15, ENSG00000272275, ENSG00000272512, ENSG00000272941, PAXIP1-DT, EPOP, ENSG00000275185, ENSG00000276900, MARCKS, ENSG00000278727, ENSG00000278903, ENSG00000279696, ENSG00000280239, SNHG4, ENSG00000282988, ENSG00000283635, ENSG00000284607, ENSG00000284946, ENSG00000285589, ENSG00000287001, ENSG00000289092*
KLF4	*FGR, SEMA3F, LASP1, ATOSB, SOX8, CRLF1, OSBPL7, CX3CL1, CACNA1G, ALDH3B1, TBXA2R, MATK, CACNA2D2, TEAD3, ST3GAL1, MMP25, IL32, GIPR, PHF7, SEMA3G, PLAUR, SEMA3B, LTF, DNASE1L1, SERPINB1, OSBPL5, SLC45A4, TIMP2, VCAN, ATOSA, RRM2B, EPN3,*

	TNIP3, COL23A1, TRAF3IP2, ATP2B4, SLC2A3, PSD, TNK2, GPC1, DLX3, DGKA, ERBB3, MYLK, SLC9A3, ELOVL1, RASGRP2, PPP2R5B, BCL3, MAPK6, FSTL3, ST6GALNAC1, GBA2, SPEG, STK10, CRMP1, GSDMB, ATP2A3, ARHGEF10L, CELSR1, FSCN1, RAP1GAP, LRCH4, NEBL, ADCYAP1R1, TP53INP2, TNS1, RAPGEF3, CEACAM1, SLC4A4, SESN1, CHRNA3, ZNF324, APOB, BCORL1, WDR47, OVGP1, AQP6, ACHE, PTHLH, PPP1R13B, SMOX, SLC8B1, LAG3, RCOR1, CHRD, EFNB1, MYO15A, JPH4, SLC7A8, TGM1, UNC13D, TBC1D2, CRTAC1, IL11, SMIM24, HIVEP1, CATSPERG, CBARP, IZUMO4, PALM, MKNK2, OSM, TBC1D10A, PLA2G3, SH3BP1, TIMP3, SUN2, BIK, CABP7, APOL4, APOL1, GSKIP, NFATC2, DOK5, NTSR1, ZNF516, RENBP, ELF4, TIMP1, KLF8, SGCG, RGCC, MEDAG, ELMO3, MMP15, NDRG4, CRISPLD2, FOXF1, SALL1, CORO2B, CEMIP, SFRP1, NDRG1, NEFM, KCNN4, TUBB4A, CKM, IL4I1, NOVA2, SNAPC2, TNNT1, EBI3, MYH14, CD79A, CNFN, CYTH2, CLEC11A, CAPS, COMP, RASA4, WDR91, DNAH11, HOXA1, LFNG, EPHB6, CORO2A, AKNA, CREB3, GLIS3, UNC5B, VSIR, KAZALD1, RGS9, SLC6A4, ALDH3A1, COL1A1, SLC9A3R1, CDR2L, PMP22, ALDOC, INPP4B, KLF3, UGDH, NRXN2, SLC15A3, SLC22A18, CD81, PITPNM1, SELPLG, KRT18, GLI1, SCNN1A, MGP, RAB5B, ADTRP, TFEB, VEGFA, SEMA5A, PCDH12, CPEB4, NPHP3, COL7A1, HES1, HYAL1, EFCC1, KLHL24, TNNC1, CLCN2, OTOF, PDE1A, TLX2, KDM3A, WNT6, IL1RL1, MLPH, ID2, GRIN3B, TRIM62, MEF2D, FBXO2, SWT1, NCF2, MYCL, KCNQ4, ETV3, PADI2, GBP3, TSPAN1, PROX1, APOA1, USP35, CNR1, TNFAIP3, VAMP8, PPL, KLF9, GALNT12, GPR68, FKBP1B, MSX2, TEK, PTK2B, PDLIM2, NPPB, FABP3, CCRL2, CXCR4, PTGFR, GLIPR2, LRP1, SARDH, DNPEP, SNAI1, PMEPA1, IQSEC2, GRM4, PACSIN1, LRRFIP1, CXCL6, EREG, MT1G, DOK4, IRF1, IL1B, PAX8, PSD4, TNFSF9, C3, RTN2, ZNF436, MMP24, ID1, AMOT, NR1D1, AHDC1, EDN2, FBXL12, ADGRE2, FBXL16, ZFP36, ADM2, APOL2, RAC2, KRT17, RNF112, VGF, FLNC, DLL4, CHAC1, LOXL1, SOX15, KLK14, SIGLEC9, ADCY4, EPB41L4A, CDKN1C, CDH15, STARD8, NALF2, CNN1, GADD45G, ATP8B3, ZSWIM6, FCHO1, UNC13A, ZBTB46, HELZ2, LSP1, H19, PNPLA7, ULBP2, EPS8L1, LILRB2, ACSS2, GFAP, GSE1, SLC6A6, KCNC3, KREMEN2, MAP1B, WDR44, RARA, RAI2, PODNL1, DNAJB1, RAMP1, PTPRE, MATN2, HSPA12B, CRP, CASP9, LGR6, CCNA1, PLAAT4, MYH11, GIMAP6, BHLHE40, WNT2B, MYCN, EMP1, DAGLA, APLNR, C5AR2, SLC37A2, ITGA7, AGAP2, FAIM2, RNASEL, TMEM127, PLXNC1, NACAD, ZFHX2, IL1RN, BIN1, KLF4, DNAJB5, IRF4, TUBB2A, TUBB2B, IER3, CPEB2, MYO7A, FCHSD2, IL18BP, LRRC32, SORL1, SQOR, PLCB2, CYP1B1, DUSP5, SHF, SHISAL1, PARVG, SLC46A3, CERS5, ITGB7, RHOF, SLC25A47, BAHD1, DISP2, PSTPIP1, NTRK3, ITGAX, MARVELD3, OSGIN1, SLC14A1, CBX4, GRB7, STAC2, COL6A2, SIK1, LMTK3, ARHGEF19, FCN3, ATP1B1, NECTIN4, EFNA3, HCN3, ACTA1, WNT9A, PLEKHA6, PTPN7, SYT2, GPR17, CSRNP1, PLA1A, MUC4, CAMK2D, KCNMB1, DOK3, IGFBP1, DENND2A, SLC16A2, FAM83A, SLC25A25, PTGES, LCN2, ADIRF, TNKS1BP1, CAPN5, ADAM33, TAGLN, ADRA2A, THRB, ADAM8, GFRA1, HSPB8, ZFP36L2, ING1, JPH3, FAM167A, OBSCN, TRIM11, CCSAP, ADAMTS1, KLF10, TTC39B, PIK3AP1, PPARGC1B, FAM161B, KCNMA1, CFAP161, PCDH1, SAMD8,

	RAB11FIP1, MAPK13, FBRS, IL34, MYO1E, TMEM164, CABP1, TRIM63, TENT5B, CLSTN2, CDA, WNT9B, STC1, SPON2, FAM131B, CPAMD8, CFAP157, MPZL3, ZBTB7B, LMNA, FOXH1, SQSTM1, SCGB3A1, FBXO27, GRIN2C, CYGB, SIGLEC11, SIGLEC16, SHANK1, PLCD3, TAMALIN, BCL6B, PRR35, DRAXIN, LAPTM5, SYNC, KIAA1522, ALPL, WNT4, VCAM1, FCRLB, ATF3, IER5, KIF26B, PKDCC, SGPP2, CTSS, NPPC, ALPP, CRYBA2, IHH, EOMES, FBLN2, SERPINI1, ADAMTS9, TGM4, LIPH, MELTF, DUSP7, FHIP1A, EDIL3, CSF2, CITED2, TBX20, BMPER, COL1A2, CA3, INTS6L, HSPA12A, PLEKHF1, TMEM130, BEAN1, NYAP1, TSC22D4, PIP5KL1, TMEM92, FAM102A, GOLGA2, CA4, MIDN, KLHL26, SERTAD3, CYP2S1, PSCA, PLIN4, RILP, KLK1, RCOR2, SPRYD3, TMC8, DNASE1L2, KCNJ4, CCDC110, GFRA2, NSG1, LGALS9, ASMTL, PCSK9, SH3TC2, PTAFR, NPR1, CXCL8, SCN9A, HIC2, OTUD7A, KLF13, IFFO2, MYO7B, GPR37L1, SLC16A5, FOS, CST1, KRT8, CD14, KISS1, PFKFB3, SERPINB9, RASA4B, HTRA3, TRH, ZNF160, SOX7, BBLN, JUNB, TMEM37, KRT19, TPPP, KCND3, ZNF562, CXXC5, ZNF274, SPSB1, P2RY6, LGALS4, ZNF57, MAL, ORMDL3, LRRC15, ISG20, CEBPB, IL16, PRSS27, CARNS1, CTSW, RAB37, OVOL1, RARG, HSPA6, KCNK7, SNX33, HEG1, WFIKKN2, CD7, HAP1, PHOSPHO1, TLR6, PHLDA3, SLCO2A1, CD248, BTC, DES, MARCKSL1, TMEM51-AS1, DDIT3, CHST1, CST6, TBC1D10C, CLCF1, P2RY2, BAIAP2, DENND2C, PLEKHD1, TPRN, LPCAT4, IRX5, ACER2, EPS8L2, ULK1, B3GNT8, CASKIN2, LINC02904, MIEF2, GPR4, PNPLA2, CRACR2B, CCDC184, MLF1, ZFAND2A, KLHL11, MAF, ERN1, THBD, ZBTB7A, EXOC3L1, HES7, ALOXE3, GGN, TMEM151A, ALOX12B, CDC42EP4, ZBTB42, FOXS1, TDRP, SHISA2, WDFY3-AS2, SLC26A11, PJA1, ZNF467, TMIE, PHLDA2, ADGRB1, SPACA6, ZSCAN22, FBXL6, TSKU, LCK, GALNT9, ABAT, AFMID, TMEM121B, RP1L1, BMP8A, SMTN, TBX1, CLDN5, KCNJ12, OAF, ALDH1A3, SRPK3, MRGPRE, PKP3, FOXO4, PTP4A3, SOCS3, APOBR, DGAT1, MAFF, ADSS1, SIGIRR, NOTUM, IL3RA, SOCS1, IRF7, LMNTD2, AHNAK2, IRS2, SPACDR, NDUFA13, BCL9L, ZNF555, ARHGAP30, ARAP1, PDE2A, CARMIL3, PRR5, VSIG10L, KRT16, HEXIM1, KRT14, RTN4RL2, ESPN, PLCD1, MT1X, BCAM, SAMD11, SPRY4, GABRD, SEMA4D, PEAR1, LCN10, S100A3, WNT7B, CCDC9B, TMEM198, NHLRC3, ENSG00000188897, INSYN2A, SBSN, SP6, CLDN4, ZNF600, ALKAL2, S100A14, KAZN, TOGARAM2, ZNF699, S100A4, HRCT1, GREB1, NTNG2, ELAVL3, INCA1, SLC6A9, S100A2, SCN8A, LAMB3, PDLIM7, SERTAD1, SIGLEC15, ATP6AP1-DT, CYSRT1, SYNGAP1, DACT3, STMN3, GALP, SSPOP, EOLA1, SERPINB2, SLC22A20P, ZNF823, AKAP17A, ODAD3, ZNF442, NTRK1, TPM2, ATL1, DLL1, PLXNB3, APCDD1L, L1CAM, FOXO6, MAFB, COL11A2, SMIM5, SLC44A4, HSPA1B, VWA7, PSORS1C2, CDSN, PSORS1C1, LILRB3, RNF39, AKT1S1, GABBR1, SMPD5, MROH6, ADGRG1, MT1M, KRT81, EXOC3L4, RGL3, ZDHHC11B, VGLL3, GPX3, ACKR1, LTC4S, LCAT, ZBTB9, LBH, DDAH2, PPM1N, MEG3, PPP1R3G, NPTXR, APOL6, LINC01133, PLEKHM1, HSPA7, MIAT, C14orf132, LINC01537, LINC02575, TFAP2A-AS1, ZNF341-AS1, ANKRD63, KLF3-AS1, ENSG00000231811, ENSG00000232855, ZC3H12A-DT, KRTAP5-AS1, PINLYP, SSR4P1, SAPCD1-AS1, KIAA0040, CLCA4-AS1, UNC5B-AS1, KMT2E-AS1, PNMA2, CBLL1-AS1, PLEKHO2, MUC20-OT1,

	IFITM10, ENSG00000244310, LILRA6, MSANTD2-AS1, NEAT1, PICART1, ENSG00000248896, EDIL3-DT, GPR162, GASAL1, PCDHGA10, LMNTD2-AS1, SLC22A18AS, USP30-AS1, ENSG00000257086, NHLRC4, LBX2-AS1, LINC01629, LINC00520, ENSG00000258982, SH3RF3-AS1, ZNRD2-DT, ENSG00000260273, CEROX1, ENSG00000260877, ENSG00000260912, WFDC21P, EPPK1, ENSG00000261168, DSP-AS1, FIGNL2, ENSG00000261512, ENSG00000261578, SCRT1, ENSG00000262160, RARA-AS1, MYO15B, LCN6, LINC02594, DNAAF3-AS1, ERFL, GABRQ, ZNF818P, SPIB, ENSG00000270001, SRGAP2D, ENSG00000270972, GOLPH3-DT, ENSG00000272106, ILRUN-AS1, ENSG00000272768, ENSG00000273066, ENSG00000273145, ENSG00000273174, ENSG00000274422, ENSG00000275202, ENSG00000275880, ENSG00000275993, FUT8-AS1, SUNO1, ENSG00000277182, SSTR3, EPB41L4A-DT, ENSG00000278997, ENSG00000279086, ENSG00000279227, ENSG00000279821, EXOC3L2, ENSG00000285517, ENSG00000285867, ENSG00000287170, ENSG00000287200, ENSG00000287356, RENO1, C3orf36, ENSG00000288934, ENSG00000288947, ENSG00000289089, ENSG00000289987, SDHAP4, ENSG00000291117, SARM1, ADAM22, SCMH1, BID, SLC38A5, PLEKHB1, METTL1, GPM6B, PDE4A, PHKA1, MBD3, HLTF, UBE2T, PAFAH1B3, DOCK3, P2RX7, NAT14, PRTFDC1, YPEL1, GINS1, SUV39H1, SMS, TAF7L, SLC25A15, DHODH, NME4, BCAT2, SNX8, NCS1, NPM3, DNAJC12, RND2, NEIL3, CCDC34, FOXM1, PTK7, LMNB1, HRH2, OGG1, GPX7, MREG, DYNC2I2, TMEM131L, CLCC1, OBSL1, CSE1L, ATP8A1, BFSP1, TCF15, PDCD2L, BCL2L12, PRRG2, TRAP1, SRD5A3, SMO, DUT, GAMT, EXOSC2, CC2D1A, ENOSF1, TESMIN, NASP, ZBED3, PATJ, MORC4, MACROD1, LPIN1, ECHDC3, DZIP1, CARS2, MRAP2, GDF11, CDK4, AHI1, SEMA4F, SLC19A3, USP44, RNASEH2B, EDNRB, MDC1, SLC37A4, CEP55, ATIC, PARP16, SORD, PRELID3A, ARRB2, TNFRSF11A, ITGB3BP, PARP1, FAHD2B, CAND2, ANO7, PRPS1, RADX, SIGMAR1, GBGT1, SH3GLB2, PGAP2, B3GAT3, TMEM25, DSN1, GXYLT1, CCL28, SPC25, SUV39H2, ADGRA3, EME1, AGPAT5, NDUFAF6, SFXN2, BUB1B, TMEM268, LRRC43, FANCC, SV2A, CCDC24, NAE1, SPC24, AMDHD2, SDC3, RPL39L, CDCA7L, ZNF704, FABP5, KIAA1958, COMTD1, HPRT1, CLMP, DIS3L, C19orf48, ODAD2, REPS2, CDK1, FABP4, EPHX4, SUSD5, C11orf80, SPTBN2, FAM53A, PELI3, CCDC14, RMI2, SPHK1, LRRC75B, OPLAH, PFAS, WSCD1, PLD6, DCTPP1, RCC1, MTURN, AMIGO1, IDH2, OGFRP1, PSMG1, SFXN4, TRAIP, IRAK1, TOP1MT, COL14A1, TMEM120B, HACD4, DHFRP1, WDR5, NUDT11, ASB13, H2AC11, WDHD1, GK, SERTAD4-AS1, RANBP17, ATP6V0E2-AS1, TMEM240, JPT2, LINC01357, SLC25A34-AS1, BOLA3-DT, FTCDNL1, HAGLROS, SLC16A1-AS1, ZNF883, HMGN2P3, DLEU2, LINC00665, GBX2-AS1, H2BC15, RNASEH1-DT, KDM4A-AS1, B3GNT9, PRKCQ-AS1, ST3GAL6-AS1, ARHGEF25, ARPIN, CCDC169, SBF2-AS1, MOCS2-DT, ENSG00000254682, B4GAT1-DT, TMPO-AS1, BOP1, ENSG00000262413, MIR924HG, FBXO17, CISD3, ENSG00000280079, ENSG00000280202, ENSG00000288018, ENSG00000291079, ENSG00000291133, DPY19L2P2
KLF6	*ADAMTS6, DCBLD2, MGAT4A, LNX1, NUAK1, TIGAR, MPP4, TGFB2, SH2D3C, PALMD, PIK3IP1, CCM2L, ITGB8, CAV1, SULT1E1, NEDD9,*

	ARRDC3, ST8SIA4, BCL6, CBLB, VIPR1, ST3GAL5, GADD45A, OLFML3, TNFSF18, HIF3A, CDKN1A, GDF5, TMEM35A, LRRC17, SESN2, PIK3C2B, BMAL1, LYVE1, HTR2B, RAPGEF5, IL33, SPTBN5, PRICKLE1, ACVRL1, CCN1, DIPK2B, ST8SIA6, HMGA2, ROBO4, LY96, GNA14, NRG1, ZNF19, TSC22D3, BTG2, GAB3, TGFA, MAMDC2, TMEM100, ZNF610, DDIT4, KCNAB1, KSR2, ZMAT3, CD34, SELP, CCDC121, ADAMTSL1, IL6-AS1, ZBTB18, CITED4, MEX3B, FAM167B, ZFP36L1, EVI2B, DCUN1D3, FAM110D, PDCD1LG2, TOX, LGR4, GIMAP1, BTBD19, DNMBP-AS1, INKA2-AS1, MIR34AHG, DIRC3-AS1, LINC00472, STXBP5-AS1, SPAAR, LINC00607, RBMS3-AS3, DIAPH2-AS1, ENSG00000237870, LINC01119, GASK1B-AS1, LINC02057, LINC01091, RMEL3, ENSG00000251095, MIR100HG, LNCOG, TSPAN5-DT, ENSG00000261468, GAPLINC, ENSG00000267745, MIR222HG, RAB33B-AS1, TRAC, ENSG00000286062, BAIAP2L1, PLEKHG6, SH2D2A, CA12, MOCOS, IGSF9B, NKAIN1, L2HGDH, DLL3, CDKL1, MTHFD1, SNTA1, HOMER2, SPAG1, IL27RA, SLC1A5, ADAP1, GCK, MPP2, ENSG00000111788, FANCE, WWC1, KCNIP3, EFHD1, DLGAP3, PLS1, UTP20, TNFRSF8, H2BC11, TMEM74B, XRCC3, TUBA4A, GAL3ST1, IRF5, TOMM40, SMPDL3B, F12, CLUH, MYBBP1A, CYP2J2, PRRG4, B4GALNT1, TMOD1, PLCE1, CYP11A1, ULK3, PCSK6, GFRA3, MTFR2, SLC39A4, SLC43A1, PAK1, ST14, TEX30, CCDC74B, RETREG1, SRSF12, PXYLP1, ADAMTS3, MPV17L, WDR4, PTGER1, BDH1, POLR3K, AKR7A3, CHCHD4, CAMK2N2, RET, TRMT61A, GPD1, P2RY1, WNT10B, FAM241B, LRRC34, GATM, MBOAT1, MCRIP2, PRR18, GRIN1, SLC25A22, VWA1, FAM83H, B4GALNT4, ACP7, ADAP2, TMEM121, FAM131C, SAPCD2, TOR3A, H2AX, SH2D5, CFD, NUP62CL, SPIRE2, ELOA2, RNF208, KRT18P17, EMSLR, FOXP4-AS1, ZNF853, PDXP, ARHGDIG, TMEM179, TGFBR3L, ENSG00000274276, ENSG00000276529, EEF1AKMT4, NPBWR1, ENSG00000288749

Table S8: List of unique differentially expressed genes for KLF2, KLF4 and KLF6.

Gene Name	Log Fold Change	P value (p)	FDR (q)
GABARAPL2	0.46	2.41E-08	1.17E-04
ENSA	0.33	8.84E-07	2.14E-03
GTF2I	0.40	5.72E-06	9.25E-03
AKT1	0.52	1.28E-05	1.55E-02
RAN	0.63	6.18E-05	5.99E-02
UFC1	0.37	1.04E-04	7.27E-02
MGLL	0.36	1.05E-04	7.27E-02
BZW1	0.38	1.51E-04	8.25E-02
IRS2	0.98	1.53E-04	8.25E-02
COX6C	0.37	2.54E-04	1.14E-01
CNOT11	-0.36	2.59E-04	1.14E-01
FARP2	-0.36	2.85E-04	1.15E-01
DIPK2A	-0.33	3.33E-04	1.17E-01
TUBE1	-0.31	3.39E-04	1.17E-01
KLF9	1.24	5.65E-04	1.52E-01
BCAR1	0.42	6.04E-04	1.52E-01
ERCC1	-0.33	6.05E-04	1.52E-01
CDH11	0.32	6.06E-04	1.52E-01
CDC42EP4	0.54	6.12E-04	1.52E-01
HSPB8	-0.31	6.28E-04	1.52E-01
ELOC	0.30	7.32E-04	1.69E-01
MTHFS	-0.35	8.24E-04	1.82E-01
FKBP1A	0.53	9.37E-04	1.97E-01
ATP13A3	0.37	1.03E-03	2.08E-01
MECP2	-0.29	1.08E-03	2.10E-01
RPL7	0.90	1.16E-03	2.12E-01
TOB2	0.34	1.18E-03	2.12E-01
PPA1	0.30	1.37E-03	2.25E-01
OST4	0.40	1.39E-03	2.25E-01
PPP1R2	0.40	1.39E-03	2.25E-01
ECHDC2	0.29	1.55E-03	2.34E-01
ERP29	0.43	1.55E-03	2.34E-01
MAZ	0.96	1.60E-03	2.35E-01
BRK1	0.76	1.80E-03	2.46E-01
RFC1	-0.32	1.84E-03	2.46E-01
RPL21	0.85	1.84E-03	2.46E-01
NIPAL2	-0.46	1.90E-03	2.46E-01
RPL7A	1.01	2.03E-03	2.46E-01
RPS10	0.99	2.05E-03	2.46E-01
GIMAP7	-0.47	2.17E-03	2.46E-01
RPL22	0.91	2.26E-03	2.46E-01
ARL6IP1	0.30	2.28E-03	2.46E-01
HNRNPA1	1.01	2.41E-03	2.46E-01

ANXA5	0.90	2.49E-03	2.46E-01
PLSCR1	0.31	2.49E-03	2.46E-01
MPZL1	0.44	2.51E-03	2.46E-01
RPL17	0.90	2.51E-03	2.46E-01
TOMM7	0.66	2.57E-03	2.46E-01
VWF	1.00	2.67E-03	2.46E-01
PCLO	-0.41	2.76E-03	2.46E-01
MICOS10	0.28	2.80E-03	2.46E-01
CDK11A	0.47	2.81E-03	2.46E-01
DCAF11	-0.30	2.83E-03	2.46E-01
RPS2	1.28	2.90E-03	2.46E-01
SH3BGRL3	0.56	3.00E-03	2.50E-01
BTF3	0.77	3.09E-03	2.54E-01
UQCR11	0.40	3.26E-03	2.61E-01
LAMB1	0.89	3.35E-03	2.61E-01
MICAL1	0.54	3.39E-03	2.61E-01
RPL32	0.88	3.47E-03	2.61E-01
RETREG3	-0.35	3.49E-03	2.61E-01
MAP1LC3B	0.32	3.52E-03	2.61E-01
RPL35A	0.82	3.56E-03	2.61E-01
ATP5F1D	0.44	3.65E-03	2.64E-01
PKD2	0.45	3.93E-03	2.80E-01
DLAT	-0.30	4.02E-03	2.82E-01
FDX1	-0.30	4.07E-03	2.82E-01
RPL26	0.90	4.29E-03	2.90E-01
MADD	-0.29	4.39E-03	2.90E-01
ZFAND5	1.15	4.41E-03	2.90E-01
PPFIBP2	-0.26	4.47E-03	2.90E-01
RPL13	0.92	4.72E-03	2.93E-01
RPS15A	0.97	4.73E-03	2.93E-01
TFPI	0.59	4.87E-03	2.93E-01
SUMO3	0.29	4.88E-03	2.93E-01
MYH9	0.98	5.02E-03	2.93E-01
EEF1B2	0.60	5.05E-03	2.93E-01
PDLIM1	0.84	5.13E-03	2.93E-01
PPP6C	0.26	5.34E-03	2.93E-01
TNFSF10	-0.78	5.45E-03	2.93E-01
ILVBL	-0.26	5.49E-03	2.93E-01
PSMB3	0.28	5.51E-03	2.93E-01
AKIRIN2	0.28	5.60E-03	2.93E-01
CHTOP	-0.28	5.63E-03	2.93E-01
MRPS25	-0.37	5.72E-03	2.93E-01
SUMO1	0.25	5.81E-03	2.93E-01
PIK3R1	0.71	5.85E-03	2.93E-01

PABPC4	0.38	5.86E-03	2.93E-01
GDI2	0.37	5.88E-03	2.93E-01
TMED10	0.28	6.12E-03	2.93E-01
RPL39	0.75	6.17E-03	2.93E-01
NFKBIA	0.98	6.18E-03	2.93E-01
RPL34	0.88	6.26E-03	2.93E-01
NMD3	-0.30	6.33E-03	2.93E-01
RNASEK	0.50	6.33E-03	2.93E-01
FOXO3	0.87	6.44E-03	2.93E-01
SLIT2	-0.29	6.45E-03	2.93E-01
FGL2	0.59	6.49E-03	2.93E-01
MRFAP1L1	-0.36	6.52E-03	2.93E-01
PER1	0.90	6.58E-03	2.93E-01

Table S9: Top 100 up- and down-regulated differentially expressed genes between control and PAH vessels.

Gene Name	Log Fold Change	P value (p)	FDR (q)
MYH9	0.53	1.56E-07	7.55E-04
CAPZB	0.57	4.56E-05	1.10E-01
FBLIM1	0.73	8.39E-05	1.36E-01
PDLIM3	0.67	2.17E-04	1.48E-01
MICAL2	0.64	2.44E-04	1.48E-01
EMP3	0.50	4.63E-04	1.87E-01
PLEKHG5	0.50	6.15E-04	2.01E-01
COL8A1	0.60	9.15E-04	2.19E-01
NES	0.61	1.05E-03	2.19E-01
HES4	0.55	1.67E-03	2.54E-01
ANO1	0.66	1.78E-03	2.54E-01
AIF1L	0.61	1.98E-03	2.55E-01
IGF1	0.51	2.03E-03	2.55E-01
PDLIM4	0.58	2.08E-03	2.55E-01
SOD3	0.68	2.57E-03	2.73E-01
FHL3	0.50	2.60E-03	2.73E-01
ITGA8	0.54	3.16E-03	2.73E-01
FBXO32	0.75	3.38E-03	2.73E-01
PHLDA1	0.57	4.01E-03	3.04E-01
PDE3A	0.52	4.77E-03	3.21E-01
LGALS1	0.62	8.03E-03	3.59E-01
CRIP1	0.58	1.01E-02	3.59E-01
LTBP1	0.75	1.13E-02	3.73E-01
MAP1B	0.55	1.17E-02	3.73E-01
ITGA7	0.56	1.18E-02	3.73E-01
SYNPO	0.71	1.18E-02	3.73E-01
SH3BGRL3	0.55	1.19E-02	3.73E-01
MFGE8	1.02	1.38E-02	3.95E-01
PRSS23	0.57	1.39E-02	3.95E-01
JAM2	0.52	1.41E-02	3.95E-01
NOTCH3	0.92	1.41E-02	3.95E-01
FBN1	0.57	1.51E-02	3.98E-01
HYAL2	0.52	1.60E-02	4.05E-01
VIM	0.59	1.60E-02	4.05E-01
COL18A1	0.78	1.90E-02	4.17E-01
LTBP2	0.50	2.16E-02	4.21E-01
TPM4	0.54	2.25E-02	4.21E-01
COL5A2	0.56	2.31E-02	4.21E-01
AQP1	0.59	2.36E-02	4.21E-01
HTRA1	0.58	2.38E-02	4.21E-01
MYL9	0.60	2.50E-02	4.21E-01
SLC16A3	0.51	2.51E-02	4.21E-01

ECE1	0.64	2.63E-02	4.21E-01
SERPINE1	0.74	2.65E-02	4.21E-01
EFHD1	0.54	2.67E-02	4.21E-01
GJA5	0.53	2.71E-02	4.21E-01
ANKH	0.51	3.05E-02	4.21E-01
FRZB	0.81	3.23E-02	4.21E-01
IRAG1	0.54	3.46E-02	4.21E-01
SPARC	0.62	4.08E-02	4.31E-01
SFRP2	0.87	4.14E-02	4.35E-01
ACTN1	0.58	4.44E-02	4.37E-01
TPM1	0.62	4.52E-02	4.37E-01
SFRP4	0.57	4.70E-02	4.42E-01
ITGA10	0.59	4.83E-02	4.45E-01

Table S10: List of differentially expressed genes in non-plexiform and Plexiform lesions.

Comparison Lists	Overlapping genes
KLF6 and PAH vessels	*ABHD2, ABI1, ADA2, ADAM9, AKIRIN2, AKT1, ALS2CL, ANAPC5, APOE, ARF3, ARHGAP29, ARHGDIB, ARID5B, ARL13B, ARL6IP5, BCAR1, BCL2L1, BCL9L, BGN, BTG1, CCT4, CCT8, CD63, CD83, CDC42EP4, CDH11, CDK2AP1, CDV3, CHIC2, CIAO2B, CLU, CNOT8, COA4, CST3, DAPK3, DAZAP1, DAZAP2, DDR2, DIPK2A, DLAT, DLST, DVL1, ECHDC2, EFEMP1, EGFR, EHD4, EIF4B, EIF5A, ELK4, ENO1, ERCC1, ESD, FAM43A, FDX1, FGL2, FKBP11, FKBP1A, FKTN, FNDC3B, FOSL2, GIMAP2, GOLGB1, GPI, GPR108, GSN, HIGD1A, HMGN2, HNRNPA3, HNRNPAB, HNRNPDL, HNRNPF, HSPA8, IARS1, ID1, IFNGR1, IGFBP4, IGFBP7, IL13RA1, ILF3, ILVBL, ING5, IRF2BP2, KLC2, KLF9, LAMB1, LAMC1, LASP1, MALL, MAP1B, MAP3K6, MAPK9, MAZ, MGAT4B, MGLL, MORF4L1, MPZL2, MRPS25, MRPS26, MT1A, MVP, MXD4, MYCT1, NASP, NCL, NEK7, NEXN, NFIX, NFKBIA, NNMT, NPM1, PABPC1, PARM1, PIK3IP1, PIK3R1, PKD2, PLEC, PLK2, POGLUT3, POLR2E, PPA1, PPFIBP2, PPP1CB, PRMT5, PRRC1, PSAT1, PSMD3, PTDSS1, PTMA, PTMS, PTPN1, PXDC1, PYCR3, QSOX1, RAB14, RAB1A, RAN, RETREG3, RHOC, RND3, RNF115, RPS27L, RPS6KA2, RRAS, RTN4, S1PR1, SAMD4A, SDHB, SGK1, SHC1, SKIL, SLC25A13, SLC25A5, SMARCA2, SNRPG, SOX13, SPARC, SRPRA, STOML2, STX2, SUMF2, SYNGR2, TAF15, TBC1D15, TEAD2, TET2, TFPI, THBS1, THOC1, TIMP1, TMED10, TNKS1BP1, TNPO1, TNS2, TOB2, TRAM1, TRIM22, TRIM28, TSN, TUBA1C, TUBE1, TXNIP, TXNRD1, U2AF2, UBXN8, UQCRC1, VAPA, VIM, VWF, XRCC6, YAP1, YIPF3, YWHAZ, ZFAND5*
KLF6 and Plexiform lesions	*ABLIM3, ACVRL1, AFF1, ANKH, ANKRD39, ANO1, ANP32B, ANTXR1, ARF1, ARHGAP19, ARHGEF15, ARHGEF7, ATP8B1, AXL, BTBD6, C5orf24, CALM3, CAPNS1, CAVIN1, CBX6, CD276, CD59, CENPB, CLIC4, COL5A2, COL8A1, COPA, COPG1, CREB3L2, CSRP2, CTNNB1, DARS1, DIPK2A, DPP7, EFHD1, EFTUD2, ELAVL1, ELK4, ENO2, ERCC1, ESD, FBLIM1, FBXO11, FGL2, FHL2, FHL3, FMNL3, FNDC3B, FUS, FZD9, GADD45A, GBE1, GDI1, GJA5, GLG1, GOLGB1, GPR4, GRK2, GSN, H1-0, H2BC5, H4C8, HBP1, HES4, HIGD1A, HMGB2, HNRNPUL1, HTRA1, ICAM2, ICMT, ILVBL, INF2, IPO5, ISM1, IST1, ITGA1, ITGA10, ITGA5, ITM2C, KIAA2013, KLHDC3, LAMA4, LIMS2, LOX, LTBP1, LTBP2, LZTS2, MAP1B, MAP3K11, MARCHF7, MICA, MICAL2, MMP14, MORF4L1, MORF4L2, MRPL3, MSN, MTCH2, MTHFD2, MYL12B, MYO1D, NCL, NFIC, NLRP1, NPM1, NPTN, NSMF, NUBP2, PAPSS2, PCDH1,*

	PCIF1, PDE3A, PDE8A, PDLIM5, PHLDA1, PHLDA3, PKD2, PKMYT1, PLEC, PLS3, PMEPA1, PPP1CB, PPP1R18, PRKACA, PRSS23, PRXL2B, PTDSS1, PTK2, PTMA, PTP4A3, PTTG1IP, RAB13, RAB6A, RANBP1, RAPGEF5, RARA, RER1, RHOC, RNF115, RRAGA, RRAS, RUFY1, S100A16, SARAF, SCARA3, SEC24D, SESN2, SFT2D2, SH3BP5, SH3GLB1, SH3PXD2A, SHROOM4, SIVA1, SLC16A3, SLC2A4RG, SOCS5, SPARC, SPTAN1, SRSF2, SSB, SSU72, ST3GAL1, SUN1, SYNPO, TACSTD2, TBCA, TCEAL9, TLE1, TMF1, TNS2, TPI1, TRIB2, TUBB, TUFM, UBE2H, UBL3, VIM, WBP1L, WWTR1, ZBTB38

Table S11: List of differentially expressed genes in common between KLF6, PAH vessels and plexiform lesions.

Appendix 2: Figure permissions

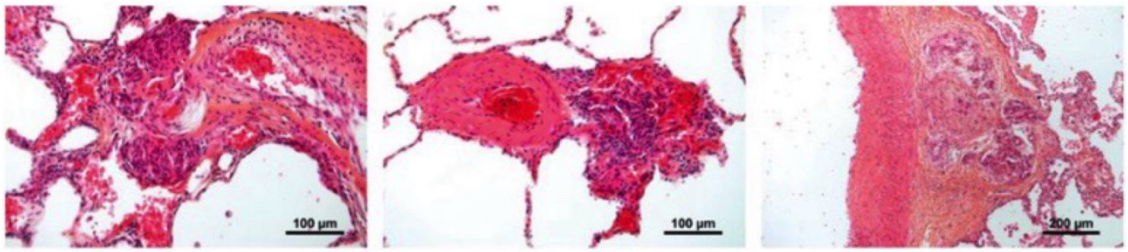

Pathology and pathobiology of pulmonary hypertension: state of the art and research perspectives.

Humbert, Marc; Guignabert, Christophe; Bonnet, Sébastien; Dorfmüller, Peter; Klinger, ...More *The European respiratory journal : official journal of the European Society for Clinical Respiratory Physiology*, 24 Jan 2019, Vol. 53, Issue 1,

ISSN: 09031936
DOI: 10.1183/13993003.01887-2018
PMID: 30545970
PMCID: PMC6351340

Publisher: European Respiratory Society; EUROPEAN RESPIRATORY SOCIETY
Language: English
Country: United Kingdom of Great Britain and Northern Ireland

Details >

Request Reprints/ePrints | Request Single Copy | Request Permission | Open Access - Creative Commons CC BY-NC 4.0

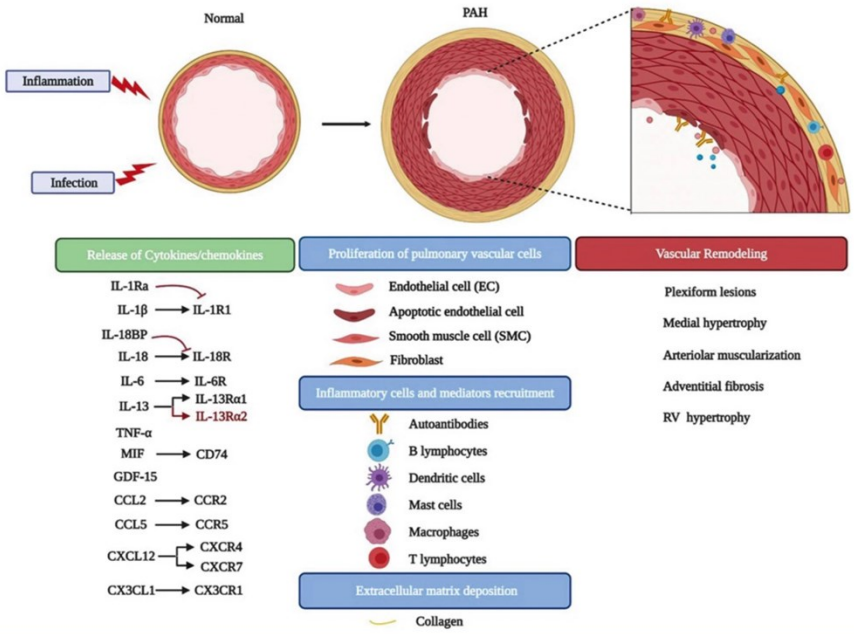

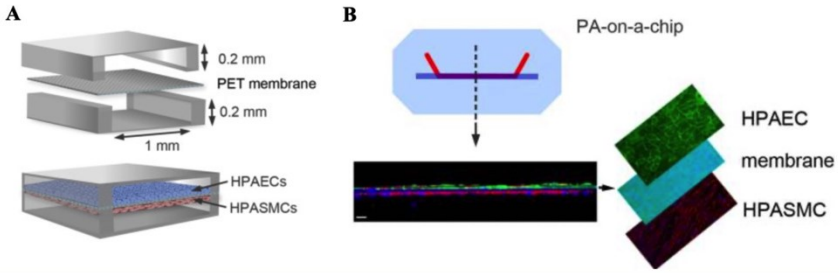

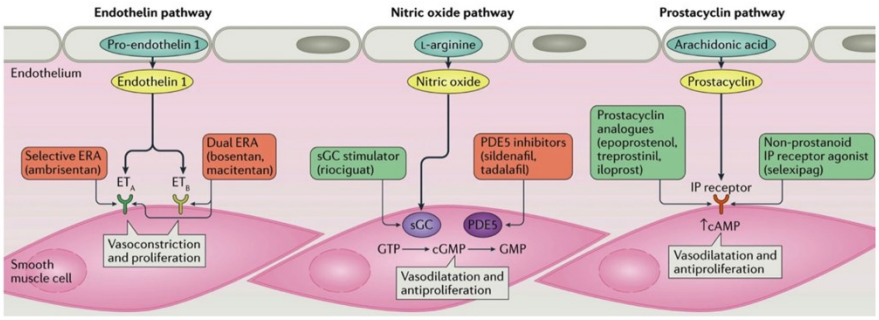

Order Date	26-Feb-2024	**Type of Use**	Republish in a thesis/dissertation
Order License ID	1454349-1	**Publisher**	Nature Research
ISSN	1759-5010	**Portion**	Chart/graph/table/figure

LICENSED CONTENT

Publication Title	Nature Reviews Cardiology	**Publication Type**	e-Journal
Article Title	Epidemiology and treatment of pulmonary arterial hypertension.	**Start Page**	603
		End Page	614
Author/Editor	World Heart Federation.	**Issue**	10
Date	01/01/2009	**Volume**	14
Language	English	**URL**	http://www.nature.com/nrcardio/index.ht...
Country	United States of America		
Rightsholder	Springer Nature BV		

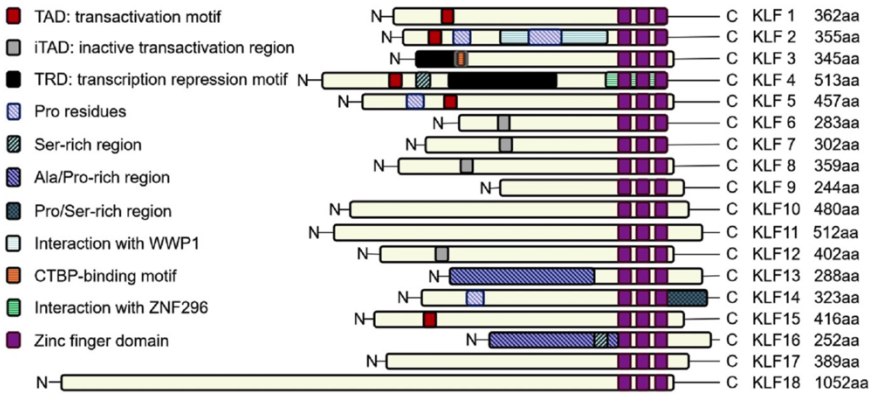

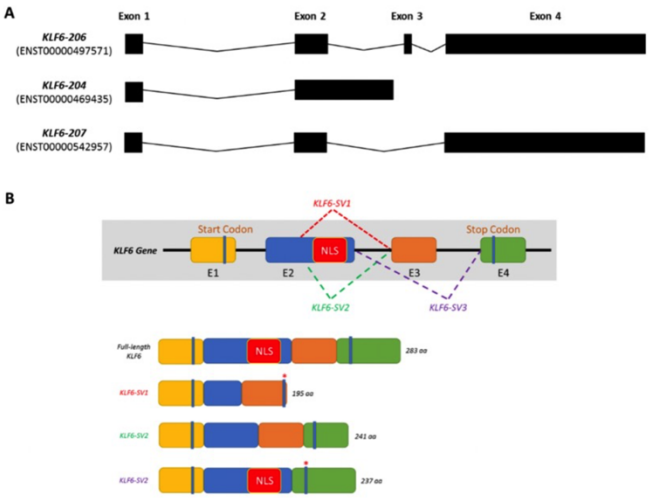

Two Sides of the Same Coin: The Roles of KLF6 in Physiology and Pathophysiology.

Syafruddin, Saiful E.; Mohtar, M. Aiman; Wan Mohamad Nazarie, ...More *Biomolecules*, 01 Oct 2020, Vol. 10, Issue 10, pages 1378 - ...

ISSN: 2218273X
DOI: 10.3390/biom10101378
PMID: 32998281
PMCID: PMC7601070

Publisher: MDPI AG; MDPI
Language: English
Country: Switzerland
URL: https://www.mdpi.com/2218-273X/10/10/1378

Details >

Request Reprints/ePrints | Request Single Copy | Request Permission | Open Access - Creative Commons CC BY 4.0

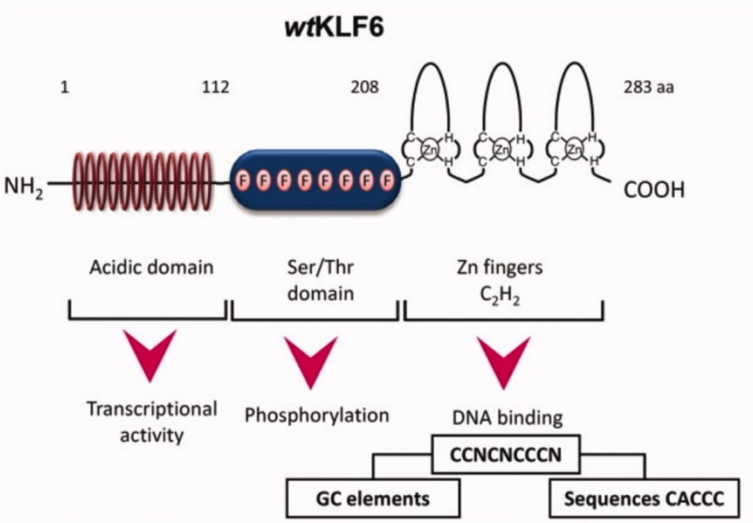

Order Date	26-Feb-2024	**Type of Use**	Republish in a thesis/dissertation
Order License ID	1454463-1	**Publisher**	TAYLOR & FRANCIS LTD
ISSN	15216543	**Portion**	Chart/graph/table/figure

LICENSED CONTENT

Publication Title	IUBMB life	**Rightsholder**	John Wiley & Sons - Books
Article Title	Biology of Krüppel-like factor 6 transcriptional regulator in cell life and death.	**Publication Type**	Journal
		Start Page	896
Author/Editor	INTERNATIONAL UNION OF BIOCHEMISTRY AND MOLECULAR BIOLOGY	**End Page**	905
		Issue	12
Date	01/01/1999	**Volume**	62
Language	English		
Country	United Kingdom of Great Britain and Northern Ireland		

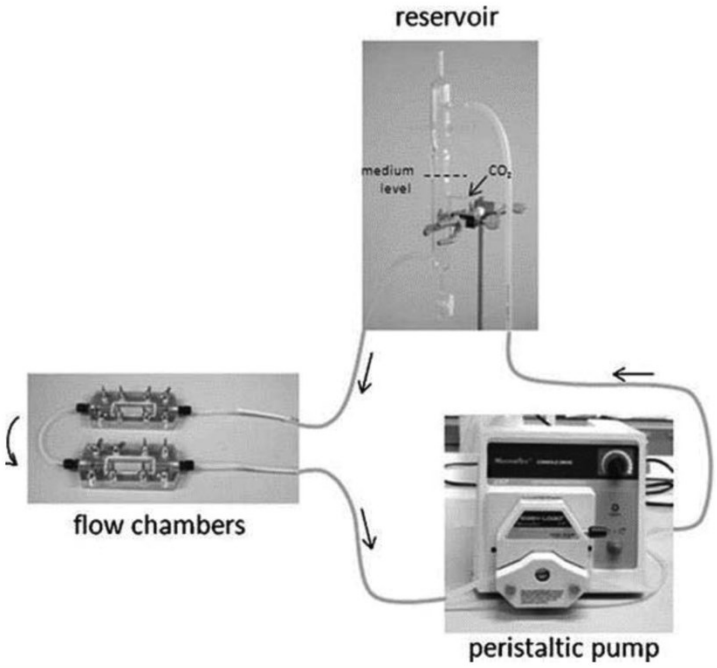

Order Date	14-Mar-2024	**Type of Use**	Republish in a thesis/dissertation
Order License ID	1461492-1	**Publisher**	Springer
ISSN	1940-6029	**Portion**	Image/photo/illustration

LICENSED CONTENT

Publication Title	METHODS IN MOLECULAR BIOLOGY. ONLINE	**Rightsholder**	Springer Nature BV
Article Title	Endothelial cell migration under flow.	**Publication Type**	e-Journal
Date	01/01/1984	**Start Page**	137
Language	English	**End Page**	147
Country	United States of America	**Volume**	769